CONTRACTOR REPORT

Hydrogen Generation by Metal Corrosion in Simulated Waste Isolation Pilot Plant Environments:

Progress Report for the Period November 1989 through December 1992

M. R. Telander and R. E. Westerman
Pacific Northwest Laboratory
Operated for the US Department of Energy
by Battelle Memorial Institute

Hydrogen Generation by Metal Corrosion in Simulated Waste Isolation Pilot Plant Environments:

Progress Report for the Period November 1989 through December 1992[a]

M. R. Telander and R. E. Westerman
Pacific Northwest Laboratory
Operated for the US Department of Energy
by Battelle Memorial Institute

ABSTRACT

The corrosion and gas-generation characteristics of three material types: low-carbon steel (the current waste packaging material for the Waste Isolation Pilot Plant), Cu-base materials, and Ti-base materials were determined in both the liquid and vapor phase of Brine A, a brine representative of an intergranular Salado Formation brine. Test environments included anoxic brine and anoxic brine with overpressures of CO_2, H_2S, and H_2. Low-carbon steel reacted at a slow, measurable rate with anoxic brine, liberating H_2 on an equimolar basis with Fe reacted. Presence of CO_2 caused the initial reaction to proceed more rapidly, but CO_2-induced passivation stopped the reaction if the CO_2 were present in sufficient quantities. Low-carbon steel immersed in brine with H_2S showed no reaction, apparently because of passivation of the steel by formation of a protective iron sulfide reaction product. Cu- and Ti-base materials showed essentially no corrosion when exposed to brine and overpressures of N_2, CO_2, and H_2S except for the rapid and complete reaction between Cu-base materials and H_2S. No significant reaction took place on any material in any environment in the vapor-phase exposures.

ACKNOWLEDGMENTS

CONTENTS

CONTENTS (Continued)

CONTENTS (Continued)

CONTENTS (Continued)

Figures

CONTENTS (Continued)

Tables

CONTENTS (Continued)

EXECUTIVE SUMMARY

A mined geologic repository site for demonstrating the safe management and disposal of defense-related transuranic (TRU) waste is being developed by the US Department of Energy near Carlsbad, New Mexico. The site, designated the Waste Isolation Pilot Plant (WIPP), is located in the bedded salt of the Salado Formation, at a depth of 655 m (2150 ft) below the land surface.

If brine should enter the repository and contact the low-carbon steel waste containers (and metallic items in the waste), the possibility exists that corrosion product H_2 could pressurize the facility. The rate of H_2 formation and the ultimate H_2 pressure attained would be dependent on the amount of brine available, the corrosion products formed, the kinetics of the specific corrosion reactions involved, and the available storage volume.

Sandia National Laboratories (SNL), WIPP Gas Generation Program, issued a subcontract to Pacific Northwest Laboratory (PNL)[a] authorizing the performance of laboratory experiments to assist in resolving the gas generation and performance assessment-related questions. The present report summarizes the laboratory corrosion results obtained through December 1992.

The experimental work has focused on the corrosion/gas generation characteristics of three material types: low-carbon steel (the current packaging material); Cu-base materials; and Ti-base materials. The latter two classes are considered to be alternative packaging materials should low-carbon steels prove unusable. Four basic test environments are being used in the tests: Brine A (a Na, Mg, K chloride-sulfate brine simulating a WIPP intergranular Salado Formation brine) with a N_2 overpressure; Brine A with a CO_2 overpressure; Brine A with an H_2S overpressure; and Brine A with an H_2 overpressure.

Test specimens of low-carbon steel have been exposed to the test environments in the entirely immersed condition as well as the vapor-phase-only condition. Limited testing has been done with steel specimens embedded in nearly pure particulate halite (NaCl) obtained from the WIPP site. All testing has been done at 30°C. The experimental work has involved a determination of the rate at which pressure (H_2 gas) builds in test containers; the gravimetric determination of the metal lost from the test specimens because of the corrosion reaction; correlation between H_2 formed and metal reacted, where possible; identification of the corrosion products formed; and post-test determination of the compositions of gases and brines in the test containers.

It has been shown that the long-term (last 12 months of 24-month corrosion tests) corrosion rate of steel in anoxic Brine A is 0.71 μm/yr, producing 0.10 mol H_2/m^2-steel-yr. The corrosion product is not adherent and not identifiable by x-ray diffraction analysis (XRD). The long-term corrosion rate is approximately linear. Increasing the pressure of N_2 increases the corrosion rate.

A dichotomy exists in the case of CO_2 overpressures, in that increasing the gas overpressure increases the initial corrosion rate and also increases the probability of passivation due to the formation of an impermeable corrosion product film, either $FeCO_3$ or a close relative.

In the low-carbon steel corrosion studies, the molar equivalency between Fe reacted and H_2 formed was satisfactory in both the N_2/immersed and the CO_2/immersed tests. Steel exposed to the vapor phase over Brine A only, with either N_2 or CO_2 present, showed essentially no evidence of corrosion.

Steel specimens exposed to a H_2S pressure of 5 atm, either immersed in Brine A or suspended in Brine A vapor, showed essentially no reaction. This is attributed to the passivating effect of pyrite (FeS_2) or a similar protective higher-sulfide corrosion product.

Limited anoxic corrosion studies were performed in which steel specimens were embedded in particulate salt (halite) that had been obtained from the Salado Formation in the WIPP underground workings. The particulate salt was either (a) contacting a pool of Brine A in a test autoclave (a "wicking" test) or (b) suspended above the Brine A (an attempt to form a "vapor transport" test). The corrosion rates observed in the former test were similar to those observed in tests in which steel specimens were immersed in Brine A with a N_2 overpressure. In the latter test, the intended vapor-transport process was compromised by an unexpected condensation-drip process from the underside of the autoclave head. The corrosion rates were relatively low, because of (a) lack of reactant H_2O, or (b) the low-Mg test environment resulting from the condensed-H_2O drip.

Alternative packaging materials (Cu-base and Ti-base alloys) showed essentially no corrosion when exposed to environments of Brine A and overpressures of N_2, CO_2, and H_2S, except for the rapid and complete reaction between the Cu-base materials and H_2S. Cu-base materials would appear to be a poor choice for use in the WIPP repository if H_2S is expected to be present in the environment, for example, through generation by microbial sulfate-reduction processes. It appears as though Ti-base materials could be used without concern for significant gas production.

1.0 INTRODUCTION

A mined geologic repository for demonstrating the safe management and disposal of defense-related transuranic (TRU) waste is being developed by the US Department of Energy near Carlsbad, New Mexico. The site, designated the Waste Isolation Pilot Plant (WIPP), is located in the bedded salt of the Salado Formation, at a depth of 655 m (2150 ft) below the land surface. Eight storage panels of seven rooms each will be mined. The panels, access ways, and shafts will be sealed before the site is decommissioned.

At the present time, a large quantity of transuranic (TRU) wastes are being temporarily stored in steel drums and steel waste boxes at waste generator sites. Under current plans, these wastes would be transported to and emplaced within the WIPP site without additional modification of the original packaging. Additional metal pieces (Fe- and Al-based alloys, for example) are contained within the waste containers as contaminated waste materials.

A number of scenarios have been advanced whereby brine could intrude into the repository (Guzowski, 1990). Should brine contact the metallic waste containers (and certain of the metallic wastes within the containers), anoxic corrosion product H_2 would be expected to form (Lappin et al., 1989; Brush et al., 1991b; Brush et al., 1991a). The amount of H_2 and the ultimate H_2 pressure attained would be dependent on the amount of brine available for reaction, the corrosion products formed, and the kinetics of the corrosion reactions involved. The effect of microbes in the brine/ waste repository environment and the possible formation of CO_2 and/or H_2S by microbial activity have also been cited as being potentially important gas-generation processes.

Butcher (1990) has discussed the potential negative effects of gas pressure on the WIPP site. This pressure will tend to retard room closure; it can contribute to fractures within the disturbed rock zone; it has the potential of leaking from the site, possibly causing perceptual, technical, or regulatory concerns; it can contribute to two-phase gas-driven flow from the repository; and it could possibly degrade the repository sealing system.

The site-pressurization concerns led to a selection of alternative container materials; that is, materials that would not be expected to generate significant quantities of gas in the WIPP repository environment. A Waste Container Materials Panel was convened by the WIPP Project in 1990 (EATF, 1991) to make a preliminary selection of alternative packaging materials. Of the metallic

container materials considered, copper-base and titanium-base alloys were judged to offer the best combination of properties when fabricability, availability, technology status, cost, and gas-generation potential were taken into account. Though no programmatic decision has yet been made regarding the use of these alternative materials, verification of their corrosion and gas-generating characteristics has been considered to be an important task in support of the WIPP Project so that their use could be invoked if deemed necessary.

Past studies have not permitted an unambiguous resolution of the WIPP gas generation and repository pressurization question, because of 1) use of test temperatures different from those expected in WIPP disposal rooms, 2) inadequate test durations, 3) inadequate backpressure of corrosion product gases, and 4) an inadequate simulation of the brine chemistry specific to the WIPP site. For these reasons, the Sandia National Laboratories (SNL) WIPP Gas Generation Program, on behalf of the WIPP Project, issued a subcontract to Pacific Northwest Laboratory (PNL) authorizing the performance of laboratory experiments to assist in resolving the gas-generation question as it relates to low-carbon steel and alternative material corrosion. This report summarizes all available results obtained since the receipt of work authorization at PNL in November 1989 through the end of calendar year 1992.

2.0 OBJECTIVE

The major objective of the present WIPP-PNL project is to determine the rate of hydrogen generation and the hydrogen pressurization potential associated with the reaction of steel drum and waste box materials, alternative packaging materials, and metal wastes contained in drums and waste boxes with simulated, repository-relevant WIPP environments.

3.0 SCOPE OF WORK

The initial (and major) effort in the present project has been directed toward characterizing the behavior of low-carbon steels in simulated WIPP environments: namely, environments consisting of liquid Brine A or water vapor in equilibrium with Brine A, with overpressures of N_2, CO_2, H_2, or H_2S gas. Four lots (heats) of steel have been included in the tests: two lots of ASTM Grade A366, representative of 55-gallon steel waste drums, and two lots of ASTM Grade A570, representative of steel waste boxes and steel waste components. The N_2 overpressure is used in the anoxic test environments in which only the brine constituents are to react with the metal specimens. Because microbial degradation activity on organic-matrix waste materials isolated in the WIPP repository may produce significant quantities of CO_2 and H_2S, these species have been included in selected tests. This is an important focus of this laboratory program. The test matrix describing the gas-generation studies performed to date involving low-carbon steel is presented in Table 3-1. Discussions of specific low-carbon-steel tests and test results in the present report will be keyed to this matrix by test environment (i.e., gas, brine or vapor, overpressure) and container (test) identification.

The scope of work of the present study was extended beyond low-carbon-steel studies in 1991 to include an assessment of the anoxic corrosion and gas-generation behavior of four alternative WIPP metal packaging materials. These materials are unalloyed copper, cupronickel 90-10, Ti Grade 2 (a grade of commercial-purity Ti), and Ti Grade 12 (a crevice-corrosion-resistant Ti-base alloy containing 0.7-0.9% Ni and 0.2-0.4% Mo). As in the case of the low-carbon-steel studies, the corrosion rates of these materials are being investigated in brine environments with overpressures of N_2, CO_2, and H_2S. The test matrix describing the gas-generation studies performed to date on alternative materials is presented in Table 3-2.

Throughout this report, "psig" refers to psi gauge and "psia" refers to psi absolute, where psig + 14.7 is equivalent to psia. The term "atm" always refers to atmospheres pressure absolute. In describing pressure differences "psi" is used.

The "brine" environment referred to in the test matrices refers to a saturated Na-Mg-K chloride-sulfate brine designated "Brine A." This brine simulates intergranular Salado Formation brines at or near the stratigraphic horizon of the WIPP repository (Molecke, 1983). It is discussed in detail in Section 5.2.3 of this report.

Table 3-1. Test Matrix, Low-Carbon Steel Tests. Pressures given in table are approximate.
Test temperature = 30 ±5°C

Test Type	Overpressure Gas	Container (or Test) Identification	Test Time, Months Aim	Actual	Initial Gas Overpressure or Amount	Steel Lot(s)[a] in Test	Remarks
Specimens immersed in Brine A	N_2	1, 2	3	3	10 atm	J, K, L, M	Tests concluded, specimens examined
		9, 10	6	6			
		17, 18	12	12			
		25, 26	24	24			
SWC[b]	CO_2	3,[c]4[c]	3	3	12 atm		
		11,[c] 12[c]	6	6			
		19,[c] 20[c]	12	12			
		27,[c] 28[c]	24	24			
		33	Open		0.32 mol/m^2 steel		Test duration not defined, to be based on observed results
		34			0.16 mol/m^2 steel		
		35			0.063 mol/m^2 steel		
		36			0.032 mol/m^2 steel		
		37			0.016 mol/m^2 steel		
		38[e]			0.00 mol/m^2 steel		
	H_2S	40[c]			5 atm		
		41[c]					
Specimens in vapor phase	N_2	5, 6	3	3	10 atm		Tests concluded, specimens examined
		13, 14	6	6			
		21, 22	12	12			
SWC		29, 30	24	24			
	CO_2	7, 8	3	3			
		15, 16	6	6			
		23, 24	12	12			
		31, 32	24	24			
	H_2S	42	Open		5 atm		Test duration not defined
		43					
Specimens immersed in Brine A	H_2	AUT-1	3	6	70 atm	J, K	Tests concluded, specimens examined
		AUT-3	6	12	36 atm		
		AUT-4			70 atm		
AUT[d]	N_2	AUT-2	3	6	73 atm		
	CO_2	AUT-7	6	6	36 atm	J, K, L, M	
		AUT-8	12	Open			In progress
Specimens embedded in salt	N_2	AUT-5	3	3	10 atm	J	Salt mass contacting brine - concluded
AUT		AUT-6					Salt mass above brine - concluded

[a] J = ASTM A366; K = ASTM A366; L = ASTM A570; M = ASTM A570.

[b] SWC = seal-welded test containers.

[c] Containers equipped with 300-psig full-range gauges. All other SWC tests equipped with 200-psig full-range gauges.

[d] AUT = high-pressure autoclave system.

[e] Part of test series directed toward determining the effect of CO_2, but contains only N_2 as a control.

Table 3-2. Test Matrix, Alternative Packaging Materials Tests. Specimens immersed in brine in seal-welded test containers. Temperature = 30 ±5°C

Material	Overpres- sure Gas	Container (or Test) Identification	Test Time, Months Aim	Actual	Remarks
Copper and cupronickel 90-10	N₂, 10 atm	1A	6	10	Tests concluded, specimens examined
		7A	12	15	
		13A	24	Open	Aim test duration not yet attained
	CO₂, 10 atm	2A	6	10	Tests concluded, specimens examined
		8A*	12	15	
		14A*	24	Open	Aim test duration not yet attained
	H₂S, 5 atm	3A	6	9	Tests concluded, specimens examined
		9A*	12	15	H₂ vented, container re-pressurized with H₂S at 9 months
		15A*	24	Open	Aim test duration not yet attained (H₂ vented, container re-pressurized with H₂S at 9 months)
Ti Grade 2 and Ti Grade 12	N₂, 10 atm	4A	6	10	Tests concluded, specimens examined
		10A	12	15	
		16A	24	Open	Aim test duration not yet attained
	CO₂, 10 atm	5A	6	10	Tests concluded, specimens examined
		11A	12	15	
		17A*	24	Open	Aim test duration not yet attained
	H₂S, 5 atm	6A	6	9	Tests concluded, specimens examined
		12A	12	15	
		18A*	24	Open	Aim test duration not yet attained
None	H₂S, 5 atm	19A	Open		"Control" container

* Tests equipped with 300-psig full-range gauges. All others equipped with 200-psig full-range gauges.

The principal metal wastes contained within the existing TRU waste receptacles capable of participating in H_2-generating reactions are alloys of Fe and Al. The gas-generating behavior of Fe alloys is currently being investigated because of the obvious potential importance of the low-carbon-steel drums and waste boxes currently in use. The behavior of Al alloys has not yet been addressed. Initiation of Al alloy investigations is planned for CY 1993.

4.0 TECHNICAL BACKGROUND

The present study has focused on the corrosion and gas-generation characteristics of low-carbon steel, Cu-base materials, and Ti-base materials in simulated WIPP environments consisting of brine with overpressures of N_2, CO_2, H_2, and H_2S. Relevant background information obtained from the literature will be presented in this section of the report, in the following order:

- Fe-anoxic brine

- Fe-CO_2

- Fe-H_2S

- Cu-anoxic brine

- Cu-CO_2

- Cu-H_2S

- Ti-anoxic brine

- Ti-CO_2

- Ti-H_2S

4.1 Fe-Anoxic Brine

On a thermodynamic basis, iron is capable of reacting with water to form high hydrogen overpressures. Brush et al. (1991a; 1991b) have estimated the hydrogen fugacities to be ~ 400 atm in equilibrium with an Fe_3O_4 reaction product and ~ 60 atm in equilibrium with an $Fe(OH)_2$ reaction product. Simpson and Schenk (1989) presented similar thermodynamic conclusions. Brush et al. noted that the $Fe(OH)_2$ product is unstable compared to the Fe_3O_4 product. The high potential pressures predicted by such thermodynamic calculations provided the WIPP Project incentive for laboratory studies (such as the present PNL study) designed to determine the kinetics of the corrosion

and gas-generation reactions and the nature of the reaction products formed. Also, such calculations have provided the incentive for investigating the potential replacement of low-carbon steels with alternative packaging materials.

The tendency for steels to corrode in anoxic brine at significant rates with concomitant production of hydrogen has been documented in recent studies. For example, Haberman and Frydrych (1988) investigated the corrosion of cast low-carbon steels in synthetic anoxic Permian Basin brines at temperatures of 90, 150, and 200°C. They found significant corrosion rates and reported that the corrosion rates increased with the Mg concentration in the brine. Simpson and Schenk (1989) studied the corrosion of low-carbon steel in natural and synthetic granitic ground waters and NaCl solutions at 25, 50, and 80°C over a pH range of 7-10 and concluded that the resulting reactions could produce H_2 at a rate faster than it could diffuse through the compacted bentonite backfill proposed for a Swiss nuclear repository. They reported a corrosion (penetration) rate of 3.6 μm/yr (0.14 mil/yr, or "mpy") for a low-carbon steel in a neutral (pH 7) anoxic NaCl brine containing 8000 ppm Cl^- (0.23 $\underline{M}$) at 50°C; the corresponding rate in 800 ppm Cl^- (0.023 $\underline{M}$) brine is 1.4 μm/yr (0.055 mpy). The test duration was described only as that required to reach a steady-state corrosion rate, with a minimum test duration of 16 days. By contrast, Braithwaite and Molecke (1980) reported the linearized corrosion rate of low-carbon steel (AISI 1018) in both Brine A, a concentrated Na-Mg-K brine, and Brine B, a nearly saturated NaCl brine, under anoxic test conditions at 25°C, to be 30 μm/yr (1.2 mpy). The test duration was 28 days. The relatively high corrosion rate reported by Braithwaite and Molecke (1980) was apparently due either to the relatively corrosive brine media used in their tests or to the possibility that the test duration used by Simpson and Schenk (1989) was much longer than 28 days, allowing the corrosion rate to decrease to a relatively low level due to the formation of a corrosion product film on the surface of the steel specimens that retarded the corrosion rate.

Grauer et al. (1991) investigated the corrosion/gas generation of steel under anoxic conditions in aqueous cementitious (alkaline) environments. Their work clearly demonstrates the profound effect of pH on steel corrosion under anoxic conditions. The low-temperature data of Grauer et al. (1991)

and Simpson and Schenk (1989) illustrate the effect of pH on the corrosion rate of steel over a range of anoxic aqueous environments:

pH	Approximate Relative Corrosion Rate
7	1
10 - 11	0.1 - 0.01
12	0.01 - 0.001
13	< 0.001

Although these conclusions are approximate, they provide some guidance in evaluating the potential beneficial effect of additions of alkaline reagents to the WIPP backfill material to decrease the corrosion rate of steel containers.

4.2 Fe-CO_2

The corrosive effects of aqueous solutions of CO_2 on low-carbon and low-alloy steels have been well known and have been the subject of many research investigations over the past 50 years. Most of the work has been sponsored by oil and gas producers. The subject has received increased attention in recent years with the increased use of CO_2 pressurization in enhanced oil recovery techniques, and with the occurrence of CO_2 in deep gas-producing wells. The nature of the research sponsorship explains the general nature of the work found in the literature: corrosion studies done under flowing conditions at elevated temperature over short test durations, frequently with the aqueous solutions not saturated with corrosion products. The objective of such work is, of course, to improve the economics of gas and oil production by determining optimal alloys for tubular products and developing effective corrosion inhibition methods. These conditions are not generally relevant to expected WIPP conditions, so only a small fraction of the large body of research results available in the literature are directly applicable to or comparable with the present PNL studies.

4.2.1 General Mechanisms of Corrosion

Aqueous O_2-free solutions of CO_2 are corrosive to iron and low-carbon steels because they form weak acids:

$$CO_2 + H_2O = H_2CO_3 = H^+ + HCO_3^- \tag{1}$$

$$HCO_3^- = H^+ + CO_3^{2-} \tag{2}$$

$$Fe = Fe^{2+} + 2e^- \tag{3}$$

$$2H^+ + 2e^- = H_2 \tag{4}$$

$$H_2CO_{3ads} + 1e^- = H_{ads} + HCO_{3ads}^- \tag{5}$$
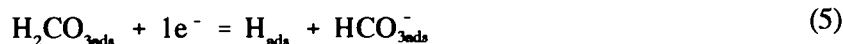
The corrosion rate of bare steel in carbonic acid solutions is controlled by the kinetics of the H_2 evolution at the cathode [Equations (4) and (5)]. It has been determined that the hydrogen evolution from steel surfaces in contact with CO_2 solutions can occur by the two fundamentally different mechanisms shown in Equations (4) and (5). One mechanism involves the electrochemical reduction of H^+ ions that diffuse to the surface of the steel, in common with general acid corrosion phenomena [Equation (4)]. The other mechanism involves the direct reduction of adsorbed H_2CO_3 molecules, as shown in Equation (5) (Schmitt, 1983a). The relative rapidity of the hydrogen reduction by the two parallel mechanisms makes corrosion in aqueous CO_2 solutions relatively rapid compared to corrosion in other acids, such as HCl, at the same pH (Schmitt, 1983a; Hausler and Stegmann, 1988).

The increase generally found in steel corrosion rates (prior to stable corrosion product film formation) in aqueous CO_2 solutions with increasing pressure of CO_2 (see Section 4.2.3.2 of this report) is consistent with Equations (4) and (5). The pH decreases with increasing CO_2 pressure, attaining values as low as 4.3 at 0.1 atm, 3.9 at 1 atm, and 3.4 at 10 atm CO_2 over a 0.5 M NaCl solution at

25°C (Crolet and Bonis, 1984). Seki et al. (1982) report pH values of 5.1 and 4.3 at CO_2 pressures of 0.1 atm and 1 atm, respectively, using an artificial seawater solution. These results are consistent with an increase in the rate of Equation (4) with increased CO_2 pressure. The increasing concentration of H_2CO_3 with CO_2 pressure, according to the Henry's Law constant for the specific solution involved, would of course be consistent with an increase in the rate of Equation (5) with increasing CO_2 pressure. As the reaction of the iron or steel surface in aqueous CO_2 solutions proceeds, the corrosion product $FeCO_3$ (siderite) will form if the solubility of Fe^{2+} in the solution near the metal surface has attained the saturation concentration:

$$Fe^{2+} + CO_3^{2-} = FeCO_3 \qquad (6)$$

by the overall reaction

$$Fe + CO_2 + H_2O = FeCO_3 + H_2 \qquad (7)$$
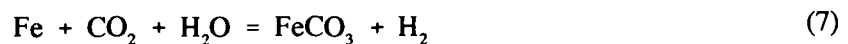
Formation of an $FeCO_3$ film on a given low-carbon or low-alloy steel is favored by static or low-flow-rate conditions. These conditions permit the concentration of Fe^{2+} ions to increase near the corroding steel surface and eventually attain the saturation concentration. Other conditions that favor $FeCO_3$ deposition are alkaline conditions from addition of alkaline corrosion inhibitors, for example, and increased temperature due to the retrograde solubility of $FeCO_3$. On the other hand, increasing CO_2 partial pressure and the concentration of calcium or magnesium ions in the brine increases the iron carbonate solubility (Hausler, 1983).

It has been generally found that chloride ion concentration is not an important factor in the corrosion of steels in aqueous CO_2 environments (Ikeda et al., 1984).

Another possible corrosion product in the corrosion of steels in aqueous CO_2 environments is Fe_3O_4. Its formation is favored by low CO_2 and H_2 fugacities and elevated temperatures. Dunlop et al. (1983) have computed the stability fields of $FeCO_3$ and Fe_3O_4 as a function of the CO_2 and H_2

fugacities and temperature. Also, Ca can be found in siderite films when the environment contains Ca salts. Murata et al. (1983) suggested the possibility that this is due to codeposition of $CaCO_3$ with $FeCO_3$.

Conditions in the WIPP (i.e., essentially static conditions, limited brine volume, and high Fe^{2+} availability) are consistent with a rapid formation of corrosion product film on the surface of corroding steel. The corrosion product is expected to exert ultimate rate control through the control of reactant transport kinetics. Hausler (1983) postulated that the transport processes through the siderite film involved simultaneous migration of Fe^{2+} ions, by an interstitial diffusion process, and electron transport via protonation of carbonate ions in the siderite lattice. After testing the model with experimental results, he concluded that the model was overly simple and could not readily explain all of the complex corrosion processes observed. The detailed corrosion-product-layer transport processes that control the corrosion rates of steel in static aqueous environments containing CO_2 remain largely undefined.

4.2.2 Thermodynamic Considerations

The overall reaction of Fe with H_2O and CO_2 to form $FeCO_3$ and H_2 [Equation (7)] is strongly favored thermodynamically. If the $\Delta G°$ values for H_2O, CO_2, and $FeCO_3$ at 25°C are assigned (Rossini et al., 1952), and if the fugacity of H_2O is assigned the value 0.03 atm (Brush, 1991b), the following equilibrium constant results:

$$\frac{f_{H_2}}{f_{CO_2}} = 6 \times 10^5 \qquad (8)$$

Equation (8) shows that, under equilibrium conditions, the fugacity of H_2 could equal 6×10^5 times the fugacity of CO_2. This information provides incentive for a study of the kinetic processes involved, as a CO_2 fugacity of less than 0.001 atm could, in theory, produce an H_2 pressure sufficient to affect the integrity of the repository.

4.2.3 Corrosion Kinetics, Experimental Studies

As previously mentioned, the major part of the reported research work performed to date has been done at temperatures higher than the expected WIPP operating temperature of ~30°C and has also utilized flowing systems and short-term (typically 1-7 days) test durations. A great deal of work has been done under test conditions that do not permit formation of adherent corrosion product films. And, of course, no corrosion investigations have been performed by others in test media equivalent to Brine A with CO_2 overpressures. In spite of these obvious problems of relevance of results, that experimental work which appears to be in some way related to the WIPP site conditions or that would tend to augment the PNL investigations will be described here.

4.2.3.1 EFFECT OF TEMPERATURE ON THE CORROSION PRODUCT FILM

A profound effect of temperature has been observed on the nature of the corrosion product film formed on steel in aqueous CO_2 solutions. In corrosion tests utilizing a flowing 5% NaCl brine with a 30 atm overpressure of CO_2 (equilibrated with the brine at 25°C in a different portion of the loop), Ikeda et al. (1983) found that at temperatures <60°C the $FeCO_3$ that formed on the steel surface was "soft and not adhesive." The corrosion observed was uniform. At temperatures in the vicinity of 100°C, the film was "thick and not tight," and deep pitting attack was observed. At temperatures >150°C, the $FeCO_3$ film was "fine, tight, and adhesive," and uniform corrosion was again observed. According to Schmitt (1983b), "considering the present knowledge on CO_2 corrosion, it appears that the temperature is obviously the most important parameter." Schmitt (1983b), in an admittedly overly simplified analysis, characterized CO_2 corrosion of steels at temperatures <60°C as forming non-protective films, with the rate of corrosion being dependent on H_2 evolution and independent of flow rate. He went on to state that the corrosion rate under these low-temperature circumstances would be expected to be predicted by the relation

$$\log \text{ rate} = 0.67 \log P_{CO_2} + C \tag{9}$$

where P_{CO_2} is the pressure of CO_2 in atmospheres and C is a constant. This relation was first described by de Waard and Milliams (1975a; 1975b) and has been shown to predict corrosion rates reasonably well under a variety of CO_2-charged-brine conditions *that essentially preclude formation of an adherent $FeCO_3$ film* (Schmitt, 1983a; Videm and Dugstad, 1987; Ikeda et al., 1983). In a separate review of low-temperature corrosion, Schmitt (1983a) stated that the corrosion dependence on CO_2 pressure [per Equation (9)] has been shown to be reliable to low partial pressures of CO_2 (<2 atm) and temperatures up to 60°C "under laminar flow conditions."

It should be further noted that de Waard and Milliams (1975b) were forced to reject data from a significant number of tests in developing their corrosion rate-CO_2 pressure relationship [Equation (9)] because of an $FeCO_3$ film forming on their corrosion specimens and yielding corrosion-rate results that were too low. This generally occurred at temperatures >60°C in their "vigorously stirred" solutions, but also happened at 40°C if the solution (0.1 or 1.0% NaCl) was stagnant. Based on the results of the work performed by the investigators cited, and bearing in mind the inherent WIPP-relevance questions already described, it appears that the corrosion product films expected to form on steel under CO_2-charged repository conditions will have protective characteristics, but that they may not be as protective as films formed at higher temperatures, i.e., temperatures >60°C.

4.2.3.2 CORROSION RATES

Summaries of the corrosion kinetics observed in a large number of steel corrosion studies in aqueous CO_2 systems were presented by Videm and Dugstad (1987), Burke (1984), and DeBerry and Clark (1984).

The corrosion rates in flowing environments at 25°C and CO_2 pressures >1 atm [one study only, due to A. A. Abramyan, reported by DeBerry and Clark (1984)] show steel corrosion rates of >5 mm/yr (>200 mpy) at 10 atm pressure of CO_2, and a rate of >10 mm/yr (>400 mpy) at 35 atm pressure of CO_2. These data were obtained in an aqueous environment (unspecified by DeBerry and Clark) flowing at 1 cm/s. The tests were only 12 h in duration. The corrosion rate

versus P_{CO_2} plot is in excellent agreement with Equation (9), suggesting that the metal surfaces were unencumbered by corrosion product films. This could be due to the flow rate, the very-short-term nature of the tests, or both.

Loop test results at higher temperatures and more rapid flow rates show even higher corrosion rates than those of Abramyan. The grouping (60 to 100°C, 1 m/s to 20 m/s, variable pH, variable Fe^{2+} concentrations) of loop data presented by Videm and Dugstad (1987) shows a range of corrosion rates from 4 mm/yr (160 mpy) to 20 mm/yr (800 mpy) at 1 atm CO_2 pressure; from 20 mm/yr (800 mpy) to 60 mm/yr (2400 mpy) at 10 atm CO_2 pressure; and from 40 mm/yr (1600 mpy) to $\sim$ 100 mm/yr ($\sim$ 4000 mpy) at 35 atm CO_2 pressure.

It appears that only two quantitative, low-temperature (20 to 30°C) static (unstirred, unflowing) studies have been reported on steel corrosion in aqueous CO_2 environments wherein corrosion product films have been obviously permitted to form on the corrosion specimens. In one study, Rhodes and Clark (1936) exposed specimens of two lots of steel (0.18 C, 0.39 Mn; 0.22 C, 0.66 Mn) to distilled water at various pressures of CO_2 at 22.5°C. Test durations were $\sim$ 3 days. The penetration rates observed ranged from 1.2 mm/yr (47 mpy) at 10 atm CO_2 pressure to 1.5 mm/yr (60 mpy) at 31 atm (450 psia). These rates are only about one-fourth as high as the rates determined by Abramyan under flowing conditions, consistent with the formation of a partially protective film on the specimens in the static test. Rhodes and Clark did report a "loose black coating" on their specimens that was easily removed by "wiping with cloth." The corrosion rates obtained in the low-CO_2-pressure range agreed well with Equation (9). The high-CO_2-pressure data showed lower-than-expected rates, suggesting a higher degree of corrosion product film integrity at the higher CO_2 concentrations. The second static-environment, film-forming study was performed by Greco and Wright (1962). They used a somewhat lower range of CO_2 pressures than Rhodes and Clark (0.25-4.5 atm), a 400-ppm NaCl solution, a test duration of 2 days, and a test temperature of 30°C. The test material is described as "shim stock," as "mild steel," and as "iron"; its exact composition is not clear. Greco and Wright reported corrosion rates of 0.25 mm/yr (9.9 mpy) at 0.25 atm CO_2; 0.35 mm/yr (14 mpy) at 1 atm CO_2; and 0.93 mm/yr (37 mpy) at 5 atm CO_2. These data provide a very satisfactory continuation (extrapolation) of the data of Rhodes and Clark to lower CO_2 pressures. The corrosion-rate data of Greco and Wright exhibit the CO_2 pressure dependency shown in Equation (9) over the entire pressure range, consistent with only partial protection from the "extremely slight and gray in color" film that formed on the specimens in the course of the short (2-day) test periods.

Three additional autoclave studies deserve mention here. Murata et al. (1983) described the results obtained from autoclave studies using a simulated seawater environment, temperatures of 25° and 60°C, a 5-day test duration, a low-carbon steel (0.12% C, 1.28% Mn, 0.021% Nb, 0.03% Al) test material, and a CO_2 pressure range of 10^{-2} to 10^2 atm. Unfortunately, it was not reported whether the specimens were covered with corrosion product during the test exposure, and a lack of description of the degree of agitation of the test medium makes it difficult to determine. The authors imply clean specimen surfaces during the 25°C test to explain the test results because they refer to the presence of a $CaCO_3$ layer on the specimens during the 60°C test, when the pressure of CO_2 was above 1 atm. However, the corrosion rates presented are similar to those of Rhodes and Clark (1936), which strongly suggests presence of a corrosion product film.

The second study, by Masamura et al. (1983), involved exposure of a low-carbon steel to water at 40°C with a CO_2 pressure of approximately 30 atm in a refreshed autoclave system. The water was equilibrated with CO_2 before entering the autoclave. The duration of the test was 4 days. The corrosion rate observed (5.6 mm/yr, or 220 mpy) lies between the filmed-specimen data of Rhodes and Clark (1936) and the bare-specimen-data of Abramyan (DeBerry and Clark, 1984). This intermediate rate suggests that specimen filming occurred and that it occurred partway through the test. However, no detailed description of the specimen(s) after the test is given, so relevant inferences are not possible.

In the third study (Seki et al., 1982), truly static conditions were apparently employed. Specimens of two low-carbon steels were immersed in synthetic seawater at 25°C for 4 days, using CO_2 pressures ranging from 1 to 10 atm. The corrosion rates observed under these conditions ranged from 0.47 mm/yr (19 mpy) at 1.0 atm CO_2 pressure to 0.76 mm/yr (30 mpy) at 10 atm CO_2 pressure, in reasonably good agreement with the filmed-specimen corrosion rate results of Greco and Wright. Nothing is mentioned in the paper, however, about the nature of the specimen surfaces when the test was concluded, though the results are consistent with transport control through semi-protective corrosion product layers. The limited data of Seki et al. (1982) do not show the same degree of CO_2 pressure dependence as the data of Greco and Wright, though there is plainly an increase in corrosion rate with increasing CO_2 pressure.

4.3 Fe-H$_2$S

As in the case of the Fe-CO$_2$ studies described in the previous section of this report, existing Fe-H$_2$S corrosion data derive primarily from work sponsored by oil and gas producers. The primary focus has been on sulfide-induced cracking of steels; however, some corrosion data exist, and those considered relevant to the WIPP site will be presented in this section of the report.

4.3.1 General Mechanism of Corrosion

Weak acid solutions are formed when H$_2$S gas is dissolved in aqueous solutions:

$$H_2S + H_2O = H^+ + HS^- + H_2O \qquad (10)$$

$$HS^- + H_2O = H^+ + S^{2-} + H_2O \qquad (11)$$

Crolet and Bonis (1984) and Seki et al. (1982) determined the relationship between the pressure of H$_2$S gas and the resultant pH in water, 0.5 M NaCl, and simulated seawater solutions. The acidifying effect of H$_2$S is similar to, but slightly less than, the acidifying effect of CO$_2$ at equivalent pressures. For example, for a 0.5 M NaCl solution at 25°C, Crolet and Bonis give pH values of 4.0 and 3.9 for H$_2$S and CO$_2$ at 1 atm, respectively. At 10 atm H$_2$S and CO$_2$, the pH values are 3.6 and 3.4, respectively.

The corrosion of iron or steel in aqueous H$_2$S solutions can be described by combining the anodic reaction

$$Fe = Fe^{2+} + 2e^- \qquad (12)$$
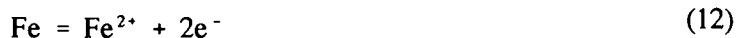
with the cathodic reaction

$$2H^+ + 2e^- = H_2 \qquad (13)$$
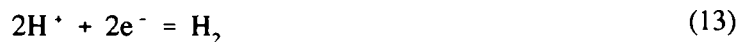
which utilizes the H^+ produced in Equations (10) and (11). The overall reaction is

$$Fe + H_2S = FeS + H_2 \qquad (14)$$

or

$$Fe + 2H_2S = FeS_2 + 2H_2 \qquad (15)$$

The reaction product H_2 is, of course, a matter of concern to the WIPP Project.

A wide range of iron sulfide reaction products can form depending on factors such as pressure of H_2S, temperature, and time of exposure. Equation (14) represents the formation of iron sulfides that are approximated by the composition FeS; namely, mackinawite (FeS_{1-x}), troilite (FeS), and pyrrhotite ($Fe_{1-x}S$), whereas Equation (15) describes the formation of either marcasite or pyrite (FeS_2).[a]

Wikjord et al. (1980) have presented a much more complete description of the sulfides that can form on steels.

In a static environment, the expected corrosion product formation sequence in the reaction of steels with aqueous H_2S solutions is mackinawite[b] (FeS_{1-x}) → troilite (FeS) → pyrrhotite ($Fe_{1-x}S$) → pyrite/marcasite (FeS_2). Mackinawite, the lowest sulfide, is considered to be the least protective of the sulfide corrosion products; pyrrhotite and pyrite are considered to offer the most protection to the metal substrate (Meyer et al., 1958; Wikjord et al., 1980; Tewari et al., 1979; Tapping et al., 1983; Thomason, 1978).

---

[a] Marcasite and pyrite have the same stoichiometry, but different crystal structures. Marcasite is orthorhombic, pyrite is cubic.

[b] Mackinawite is frequently referred to as "kansite" in older publications. Milton (1966) demonstrated the equivalence of mackinawite and kansite, and recommended that the term "kansite" be dropped.

The sulfide corrosion product formation sequence shown is logical, as the corrosion product layer would be expected to exhibit a greater proportion of higher sulfides as the cation concentration gradient became slower due to film thickening. Differences in system conditions and uncertainty regarding the corrosion product formation kinetics make a prediction of corrosion product(s) difficult, if a specific system has not been previously studied experimentally.

Sardisco et al. (1963) and Sardisco and Pitts (1965) have reported the only data (known to the authors of this report) that tend to contradict the corrosion product sequence noted. In the course of tests of short (3-day) duration in an aqueous environment at 24°C, they observed the formation of a relatively protective film of marcasite/pyrite and troilite, with some mackinawite, at a low H_2S partial pressure (0.0068 atm) in CO_2. At greater partial pressures of H_2S (to 0.22 atm), a relatively non-protective film formed, consisting primarily of mackinawite. They found that the best mathematical description of the metal reacted as a function of time could be made, in general, using a mixed-parabolic kinetic expression

$$Ay^2 + By + C = t \qquad (16)$$

where   A, B, and C are constants

   y = metal reacted

   t = time

The mixed-parabolic expression is consistent with the overall reaction being controlled partially by an interface reaction and partially by the passage of ions and electrons across the reaction product film. At the lowest H_2S pressure employed (0.00065 atm, or 0.00958 psia), the reaction kinetics tended toward parabolic, expected in the case of protective films. A troilite + pyrite/marcasite film was present on the specimen surfaces. At the highest H_2S pressures employed (0.22 atm, or 3.25 psia), the kinetic expression tended toward linear, consistent with the lack of protectiveness expected from the predominantly mackinawite film.

Meyer et al. (1958) noted an initial protective mackinawite "tarnish film" on steel specimens exposed at room temperature to moist H_2S at ~ 1 atm pressure. After a time period of 5 to 10 days

the tarnish film changed to a "rough flaky scale" of mackinawite and lost its original highly protective character. When the H_2S was humidified by a 5% NaCl brine, or when CO_2 was present in the system, the mackinawite remained the predominant phase. In experiments in which the H_2S was humidified with water alone the initial mackinawite layer became a triple corrosion-product layer, with mackinawite next to the steel surface, a layer of pyrrhotite next, and a layer of pyrite at the gas-corrosion product interface. (It should be noted that the effect of the NaCl solute in the humidifying medium is not at all clear, unless some mechanical transfer of brine from the solution to the specimens occurred. The possibility of this happening was not mentioned by the authors.) The tests of Meyer et al. had a duration of ~ 125 days.

Thomason (1978) studied the corrosion kinetics of a mild steel in a 3% NaCl solution saturated with H_2S at 1 atm pressure. Testing was done over the temperature range 30 to 90°C; the corrosion tests typically lasted for 6 days. Thomason found that the corrosion rates were highest at the lowest temperatures (30 to 50°C). Only mackinawite was observed, however, on any of the specimens.

Tapping et al. (1983) described methods for producing relatively protective sulfide films on steels, using a combination of exposure times and temperatures. They reported formation of pyrite at 50°C during a 12.2-day exposure in a loop containing "H_2S-saturated water," whereas films primarily composed of troilite and pyrrhotite (considered almost as protective as pyrite) formed at 150°C at a 7.1-day exposure. After 9 days at 150°C the film was primarily pyrrhotite.

Wikjord et al. (1980) exposed specimens of SAE 1010 mild steel to water solutions of H_2S at a total system pressure of 1.5 MPa (14.8 atm) at temperatures of 30°C, 100°C, and 160°C. The minimum test time was 30 days. The test specimen was a spinning disk, to simulate velocity effects of flowing process plant fluids. The disks, 51 mm (2.0 in.) in diameter, were typically rotated at 100 rpm.

At 30°C, mackinawite was found at test durations up to 3 h. At 72 h troilite was the principal reaction product. Troilite remained the principal product to the conclusion of the test (30 days). At 60°C, the principal corrosion product changed from troilite to the higher sulfide pyrrhotite over the 30-day test period. At 160°C, troilite converted quickly to the higher sulfide pyrrhotite (1 day), but pyrite did not evidence itself until near the end of the 35-day test. These tests show that higher sulfides are indeed favored by increased exposure time and increased temperature. However, the spinning-disk specimen makes it difficult to extrapolate the findings to a static system.

Tewari et al. (1979) provided qualitative insights into the effect of fluid velocity on the sulfide corrosion products formed on mild steel. They essentially duplicated the work of Wikjord et al. (1980), except that they varied the rotational speed of the disk from 0 to 1440 rpm while maintaining the temperature at 120°C. The total system pressure was 1.6 MPa (15.8 atm). They found that at high rotational speeds the predominant sulfide corrosion product on the disk was mackinawite, which continually dissolved in a steady-state fashion, whereas at low speeds (or static-solution conditions) pyrrhotite or pyrite would form. Presence of bubbles in contact with the disk also promoted the formation of the pyrrhotite/pyrite phases, as mass transport of the mackinawite constituents into the liquid phase was hampered by the bubbles. The high resultant concentration of Fe^{2+} ions induced a series of reactions leading to the formation of pyrrhotite and pyrite. Tewari et al. concluded that "the transformation of mackinawite to higher phases of iron sulphide will, therefore, be favored on corroding carbon steel exposed to aqueous H_2S solutions in a stagnant solution."

Tewari et al. (1979) also showed that a disk pre-filmed with pyrite would undergo no further observable corrosion when exposed to the aqueous H_2S environment.

Based on the investigations reported in the literature, it would be difficult to predict exactly which sulfide corrosion products would be produced on a low-carbon steel surface in static WIPP-relevant brine as a function of H_2S partial pressure and exposure time. It appears certain that long exposure times and high H_2S fugacities favor the protective high-sulfide corrosion products. The effect of the WIPP-site brine constituents on the reaction products, or the overall rate of reaction, cannot be predicted from the literature data.

4.3.2 Thermodynamic Considerations

The reaction of Fe with H_2S to form either FeS [Equation (14)] or FeS_2 [Equation (15)] and H_2 is strongly favored thermodynamically. Assigning $\Delta G°$ values at 27°C for H_2S and troilite, FeS (Chase et al., 1985) results in the expression

$$\frac{f_{H_2}}{f_{H_2S}} = 7 \times 10^{11} \tag{17}$$

The equivalent expression, also at 27°C, with pyrite, FeS_2 (Chase et al., 1985), as the product instead of troilite, is

$$\frac{f_{H_2}}{f_{H_2S}} = 1 \times 10^8 \tag{18}$$

The hydrogen fugacity potentially resulting from a reaction between steel and H_2S could, on an equilibrium thermodynamics basis, become extremely high, even at low H_2S fugacities. The same considerations hold true for H_2S as previously stated for CO_2 [Equation (8)], except that the theoretical pressurization potential associated with H_2S is even higher than that of CO_2 at equivalent fugacities. These considerations provide the incentive for the present PNL study of the kinetics of the reaction between steel and aqueous H_2S solutions.

4.3.3 Corrosion Kinetics, Experimental Studies

A wide range of corrosion kinetics of iron and low-carbon steel in aqueous H_2S environments have been reported. It has been shown that the specific sulfide corrosion product largely dictates the corrosion response, and the film formed depends on exposure time, H_2S activity, temperature, and other environmental factors such as fluid velocity, presence of CO_2, and (possibly) brine constituents.

The Fe-aqueous H_2S corrosion data available in the literature possibly having relevance to WIPP site conditions are presented in Table 4-1. The tests are of short duration (very short relative to expected WIPP conditions), and protective layers of higher sulfides would not, in general, be expected to have formed on the specimens. An exception would be the data of Meyer et al. (1958), in the "vapor over H_2O" environment, in which a layer of pyrite was shown to have eventually formed over layers of troilite and mackinawite, contributing some undefined degree of protection.

Table 4-1. Summary of Corrosion Rate Data, Aqueous H_2S Systems

Investigator	Specimen Material	H_2S Pressure, atm	Aqueous Medium	Temp. °C	Test Exposure, Days	Corrosion Rate mm/yr (mpy)	Comments
Sardisco and Pitts, 1965	unalloyed Fe	6.5×10^{-4} to 0.22 in CO_2 (1 atm total)	H_2O	24	~3	0.46(18)	rate at 0.22 atm H_2S
Greco and Wright, 1962	low-C steel	4×10^{-6} to 0.45 in CO_2 (1 atm total)	400 ppm NaCl brine	30	2	0.46(18)	rate at 0.45 atm H_2S
Meyer et al., 1958	low-C steel	~1	• vapor over H_2O	room	to 125	0.63(25) to 0.25(10)	rates after ~10 days
		~1	• vapor over 5% NaCl solution	room	to 125	0.63(25) to 1.7(68)	
		~0.5 + 0.5 atm CO_2	• vapor over 5% NaCl solution	room	to 125	~0.63(25)	
Thomason, 1978	low-C steel	~1	3% NaCl solution	30-90	~6	0.45(18) 1.8(71) 0.45(18) 0.12(4.7)	- 30°C - 40°C - 50°C - 60°C
Bruckhoff et al., 1985	low-C steel	~16	triethyleneglycol + 10% H_2O, 0-2% NaCl	25	42	0.2(7.9) to 0.5(20)	rates at 2% NaCl (maximum)
Hudgins and McGlasson, 1981	N-80 steel (0.45 C, 1.52 Mn)	1, 2	5% NaCl	25 to 204	30	0.4(16) <0.03(0.1) 0.2(8)	- 25°C - 50°C - 204°C
Tewari et al., 1979	low-C steel	~23	H_2O	120	3-10	nil	rotating disk with preformed pyrite
Seki et al., 1982	low-C steel	0-10	synthetic sea water	25	4	~0.1(4) ~0.6(24)	- 1 atm H_2S - 10 atm H_2S
Dougherty, 1988	low-C steel	4, with 51 atm CO_2 and 23 atm CH_4	0.6% NaCl brine	27	2, 14	3.9(154) 0.5(20)	- 2-day exposure - 14-day exposure

4-17

The data in Table 4-1 show some degree of consistency in a variety of liquid media over a wide range of H_2S pressures at temperatures of about 30°C. Under these conditions, the observed corrosion rate of steel is ~0.4 mm/yr (~16 mpy). This rate would be expected to diminish with increasing exposure times, based on 1) the expectation that thicker films of any corrosion product, even mackinawite, will eventually slow the kinetics of the sulfidation reaction; and 2) existing data correlating increased protectiveness with higher sulfide corrosion products.

4.4 Fe-CO$_2$-H$_2$S

The corrosive effect of mixtures of CO_2 and H_2S on low-carbon and alloy steels is of great interest to oil producers, because the two species frequently occur together in deep hot wells. The presence of both CO_2 and H_2S is relevant to WIPP waste isolation because of the potential occurrence of various microbial processes on both the waste and sulfate-bearing minerals, e.g., anhydrite. The simultaneous presence of the two gases complicates the already complex and aggressive corrosion situation caused by the presence of either one alone. The existing data are extremely limited and not obviously directly applicable to the WIPP site, but they will be presented here for the insights they might provide.

Sardisco and Pitts (1965) attributed no influence on rate or sulfide reaction product formed to the presence of CO_2 at ~1 atm pressure in their tests of iron corrosion at 24°C (see item 1, Table 4-1). This may be justified; on the other hand, CO_2 may be a causative factor in their observations of highest sulfides (e.g., pyrite) being formed at low H_2S pressures and the lowest sulfide (mackinawite) at the highest H_2S pressures used in their experiments. These results, which are contrary to Fe/H_2S kinetic expectations, have been noted in the previous section of this report. Greco and Wright (1962) also performed tests at ~1 atm total pressure with H_2S admixed in a CO_2 carrier gas. The H_2S ranged in partial pressure from 4×10^{-6} atm to 0.45 atm. The tests were performed using low-carbon steel specimens immersed in a dilute (400 ppm NaCl) static brine solution at a temperature of 30°C (item 2, Table 4-1). The tests were very short term (2 days). Greco and Wright found that the corrosion rates in pure CO_2 (~0.4 mm/yr, or 16 mpy) sharply decreased with the addition of small amounts of H_2S. At a partial pressure of 1.6×10^{-5} atm H_2S, the rate had decreased to ~1/5 of the pure-CO_2 rate. The corrosion rate stayed constant with H_2S partial pressure

4-18

until the H_2S partial pressure was greater than ~0.03 atm, at which time the corrosion rate began to increase. At a pressure of 0.45 atm H_2S (~0.5 atm CO_2) the corrosion rate was slightly higher (0.46 mm/yr, or 18 mpy) than the pure-CO_2 corrosion rate. Greco and Wright did not attempt to correlate the corrosion rates observed with the sulfide corrosion product, as the corrosion products were apparently not analyzed.

The rapid reduction of corrosion rate with H_2S additions to CO_2 was also reported by Seki et al. (1982), who tested mild steels in synthetic seawater solutions at 25°C. They employed H_2S-CO_2 gas mixtures at a maximum total pressure of ~15 atm. At a given CO_2 pressure, the corrosion rate decreased sharply with H_2S partial pressure, remained constant over a range of H_2S pressure, then increased to a rate similar to the CO_2-pressure rate. Seki et al. did not correlate corrosion rates with corrosion product compositions.

Meyer et al. (1958) determined the corrosion rates of steel samples in water vapor at room temperature with H_2S and CO_2, each present at ~0.5 atm partial pressure (see item 3, Table 4-1). Presence of the CO_2 diluent produced corrosion rates lower than those in pure H_2S. Meyer et al. reported that the corrosion product film formed in the presence of CO_2 was predominantly kansite and speculated that CO_2 might inhibit the formation of pyrrhotite and pyrite.

Dougherty (1988) immersed specimens of mild steel in a 0.6% NaCl brine, equilibrated with a mixture of H_2S (5%), CO_2 (65%), and CH_4 (30%) at 78 atm total pressure. The test temperature was 27°C and test durations were 2 days and 14 days (see item 9, Table 4-1). The corrosion rate started relatively high (2-day test), but decreased to a fairly typical value after 14 days. Dougherty apparently did not identify the corrosion product on his test specimens, so a correlation of rate with corrosion product is not possible.

The work described by the foregoing investigations apparently all involved specimens that became coated with sulfide corrosion products early in the course of the specimen exposures to the H_2S-containing environment, in spite of the presence of CO_2 at relatively high pressures. This is not surprising, as an examination of Equations (8), (17), and (18) clearly shows the thermodynamic stability of the FeS and FeS_2 corrosion products relative to the $FeCO_3$ corrosion product. If the previously used $\Delta G°$ values are assigned to the constituents of the equation

$$FeCO_3 + H_2S = FeS + H_2O + CO_2 \tag{19}$$

the equilibrium constant at 30°C is found to be

$$\frac{f_{CO_2} \times f_{H_2O}}{f_{H_2S}} = 3 \times 10^4 \tag{20}$$

At the low fugacity of H_2O expected (Brush et al., 1991b) in equilibrium with Brine A at 30°C (~ 0.03 atm)

$$\frac{f_{CO_2}}{f_{H_2S}} = 1 \times 10^6 \tag{21}$$

Equation (21) states that FeS will form rather than $FeCO_3$, if the fugacity of H_2S is $> 1 \times 10^{-6}$ x f_{CO_2}. Higher fugacities of H_2O, of course, would decrease the value of the ratio of Equation (21), in effect stabilizing $FeCO_3$ relative to FeS. The ratio of Equation (21) is consistent with the results of investigators who found sulfide corrosion products on steel specimens exposed to very low H_2S partial pressures in a CO_2 environment.

In their experimental corrosion studies, Ikeda et al. (1984) used an H_2S partial pressure in CO_2 insufficient to maintain a sulfide film on specimens of "pure iron" exposed to a flowing 5% NaCl solution. They used a temperature range of 25 to 250°C, a total gas pressure of 30 atm, and a H_2S addition of 3.3, 33, and 330 ppm (by volume). The H_2S was not replenished during the 4-day tests. At 25°C, the H_2S additions of 3.3 ppm and 33 ppm caused an acceleration of the corrosion reaction relative to "no H_2S addition" by the activation of the cathodic reaction. At 33 ppm H_2S the corrosion reaction was slowed relative to the 3.3 ppm H_2S test by the temporary deposition of FeS. Ikeda et al. postulated that, because the H_2S was not replenished, the deposited FeS redissolved and was eventually replaced by a $FeCO_3$ film.

The work of Ikeda et al. is relatively complex, in that 1) the flowing system was capable of affecting the formation kinetics of an $FeCO_3$ film, and 2) the H_2S was not replenished, so the available reactant disappeared with time, allowing $FeCO_3$ films to form.

4.5 Cu-Anoxic Brine

The gas-generation potential of unalloyed Cu and Cu-Ni alloys in WIPP-relevant brines is expected to be extremely low, as these metals are noble with respect to hydrogen. The thermodynamic driving force for the reaction

$$2Cu + H_2O = Cu_2O + H_2 \qquad (22)$$
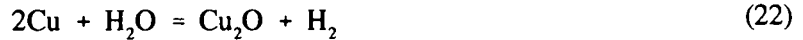
[using $\Delta G°$ values obtained from Rossini et al. (1952) for H_2O and Cu_2O] is positive, and leads to an equilibrium relationship at 25°C of

$$\frac{f_{H_2}}{f_{H_2O}} = 2 \times 10^{-16} \qquad (23)$$

If f_{H_2O} is assigned the expected value at 30°C of ~0.03 atm (Brush et al., 1991b), then

$$f_{H_2} = 6 \times 10^{-18} \qquad (24)$$

The f_{H_2}/f_{H_2O} ratio of Equation (23) is so small that one could well suspect that Cu would not react at all with deaerated water. This has been shown to be the case. Simpson and Schenk (1987) found that no H_2 evolution could be detected from the corrosion of Cu in dilute chloride solutions at 50 and 80°C, "supporting the thermodynamic evidence that water cannot be an oxidant for copper in pure water or dilute chloride media." They concluded that the small weight changes that the Cu specimens exhibited were due to a Cu chloride complex solubility and possible reaction with residual O_2 in the system.

Findings of Westerman (1988) are consistent with the same thermodynamic argument. Specimens of unalloyed Cu, 90-10 Cu-Ni, and 70-30 Cu-Ni were exposed to saturated Na-Ca-Mg-K chloride brine under anoxic test conditions at 90°C and 150°C for 3 months. At the conclusion of the test the specimens were found to be bright, with no apparent oxide or corrosion product layer. The linearized corrosion rates of the specimens at 90°C from weight loss determination were all

<0.2 μm/yr (<0.008 mpy). Thus, if the reaction of Cu with a given brine results in the formation of a corrosion product of no greater thermodynamic stability than Cu_2O, the fugacity of H_2 resulting from the reaction is expected to be negligible.

4.6 Cu-CO$_2$

The reaction between Cu and Cu-Ni alloys to produce H_2 from aqueous CO_2 solutions would be expected to take the form

$$Cu + CO_2 + H_2O = CuCO_3 + H_2 \tag{25}$$
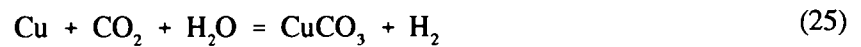
If $\Delta G°$ values at 25°C are assigned to CO_2 and H_2O (Rossini et al., 1952) and $CuCO_3$ (Silman, 1958), an expression relating H_2 fugacity to the fugacities of CO_2 and H_2O results:

$$\frac{f_{H_2}}{f_{CO_2} \times f_{H_2O}} = 4 \times 10^{-23} \tag{26}$$

Again setting f_{H_2O} = 0.03 atm, the expected fugacity of H_2O in equilibrium with a repository-relevant brine at 30°C, we have the expression

$$\frac{f_{H_2}}{f_{CO_2}} = 1 \times 10^{-24} \tag{27}$$

The expected fugacity of H_2, according to Equations (26) and (27), would be expected to be minimal if a corrosion product no more thermodynamically stable than $CuCO_3$ formed in the aqueous CO_2 solution. For lack of other insights as to what such a product might be, it would be reasonable to assume that no significant gas generation would take place due to the reaction of Cu or Cu-Ni alloys with a repository brine in equilibrium with even very high pressures of CO_2.

4.7 Cu-H₂S

Unlike anoxic aqueous solutions, or aqueous CO_2 solutions, aqueous sulfide solutions are known to readily attack Cu and Cu-base alloys (ASM, 1987). Because of the need to use natural waters, such as polluted seawater, as a coolant in heat exchangers tubed with Cu-base alloys, a great deal of research has been done in an attempt to understand and control the corrosion of Cu and Cu-base alloys by sulfides. Most of the corrosion research has therefore been done using oxygenated solutions that simulate natural waters (Vreeland, 1976; Macdonald et al., 1979; Gudas and Hack, 1979; Popplewell, 1980; Eiselstein et al., 1983; Gehring et al., 1983). Such studies have shown that the co-presence of sulfide and O_2 in seawater results in very high corrosion rates (tens of mm/yr metal penetration) of Cu-Ni alloys, far higher than if sulfide ion alone were present. The accelerated corrosion appears to be the result of the sulfide preventing the formation of a protective oxide corrosion product layer, supported by a cathodic reduction of O_2 (Eiselstein et al., 1983). Kato et al., 1984 have postulated that the sulfide layer's dominant role is that of a catalyst for O_2 reduction. Gudas and Hack (1979) demonstrated that sulfide concentrations as low as 0.01 g/m^3 (10 ppb by weight) can cause high corrosion rates of Cu-Ni alloys in aerated seawater.

4.7.1 Thermodynamic Considerations

In the absence of O_2, the reaction between H_2S and Cu can be written

$$Cu + H_2S = Cu_2S + H_2 \qquad (28)$$

Chalcocite, Cu_2S, is the corrosion product generally observed. The cathodic reduction of H^+ has been shown to take the place of O_2 reduction in anoxic systems (Macdonald et al., 1979). A thermodynamic analysis of Equation (28) shows a strong potential for H_2 generation. Assigning $_\Delta G°$ values to Cu_2S (Rossini et al., 1952) and H_2S (Chase et al., 1985) results in the expression

$$\frac{f_{H_2}}{f_{H_2S}} = 1 \times 10^9 \qquad (29)$$

for temperatures in the vicinity of 25°C. It is apparent that the fugacity of corrosion-product H_2 is very much higher than the fugacity of H_2S. The relationship shown in Equation (29) obviously gives incentive to determining 1) the availability of H_2S and 2) the rate of the Cu-H_2S reaction, should the use of a Cu-base alloy be considered as an alternative waste container material.

4.7.2 Kinetics of the Cu-H₂S Reaction

As previously noted, the literature on the kinetics of Cu-H_2S reactions in anoxic systems is sparse. Syrett (1977) studied the reaction kinetics of Cu with dilute H_2S solutions at 30°C with and without dissolved O_2. In his tests, a cylindrical copper specimen was rotated to produce turbulent flow conditions in an aqueous environment. Total system pressure was 1 atm. H_2S gas was bubbled through the solution at an unspecified partial pressure to produce a concentration in the solution of 1.94 ppm sulfide ion. Syrett calculated a Cu corrosion rate of ~0.01 mm/yr (0.4 mpy) at the end of the 2-day test. Addition of ~0.9 ppm O_2 to the solution accelerated the rate of attack by a factor of 30.

Booker et al. (1984) determined the corrosion behavior of a Cu-1.8% Be alloy in simulated oil field environments consisting of simulated sea water in equilibrium with various mixtures of H_2S, CO_2, and N_2. The total system pressure was 68 atm. Booker et al. used three test temperatures—66°, 121°, and 149°C—and test durations up to 30 days. They found average corrosion rates of 0.0078 mm/yr (0.31 mpy) at 66°C in a gas mixture of 1% H_2S and 20% CO_2, and an average corrosion rate of 0.019 mm/yr (0.75 mpy) at 66°C in a gas mixture of 10% H_2S and 20% CO_2. The corrosion rates over a 30-day test duration showed no tendency for corrosion rate reduction with time. The 30-day corrosion rates increased by a factor of ~4 between 66°C and 121°C in the 1% H_2S environment, and by a factor of ~10 in the 10% H_2S environment.

4.8 Ti-Anoxic Brine

Ti is an active metal that relies on its stable oxide film for its oxidation resistance. The thermodynamic driving force for the reaction

$$Ti + 2H_2O = TiO_2 + 2H_2 \qquad (30)$$

is extremely high. Assigning $\Delta G°$ values at $25°C$ for H_2O (Rossini et al., 1952) and TiO_2 (Turkdogan, 1980) yields the expression

$$\frac{f_{H_2}}{f_{H_2O}} = 4 \times 10^{35} \qquad (31)$$

If the repository is at $30°C$ and the water vapor is in equilibrium with a halite-saturated brine, then

$$f_{H_2} = \sim 1 \times 10^{34} \text{ atm} \qquad (32)$$

A container made of a Ti-base alloy reacting in an active manner with a brine solution would obviously be capable of compromising the integrity of the WIPP. An active reaction with brine at the expected temperature of $30°C$ is not expected, however, and there is a great deal of corrosion data to support that conclusion.

In an excellent summary of the corrosion behavior of Ti and Ti alloys relevant to nuclear repository conditions, Soo (1983) shows, from the data of several investigators, that the uniform corrosion rates of both commercial-purity Ti and Ti Grade 12 [a Ti-Ni-Mo alloy that exhibits a high degree of crevice (and uniform) corrosion resistance] are <0.1 μm/yr (<0.004 mpy) in deoxygenated WIPP Brine A at $30°C$.

Braithwaite and Molecke (1980) and Molecke et al. (1983) investigated the corrosion behavior of Ti-base alloys in nuclear waste disposal applications and concluded that Ti-base alloys offered an excellent degree of corrosion resistance for this service.

In a saturated NaCl brine, over a pH range of 0 to 14, both commercial-purity Ti and Ti Grade 12 are expected to be essentially completely resistant to both uniform corrosion and crevice corrosion at temperatures $<70°C$. In saturated NaCl brine at pH of 8, the "nil corrosion" temperature is $\sim150°C$ for commercial-purity Ti and $\sim270°C$ for Ti Grade 12 (ASM, 1980). Similar findings were recently published by Japanese investigators, who used an electrochemical repassivation method to establish permissible operating conditions for commercial-purity Ti as a function of Cl^- concentration and system temperature. They concluded that, in saturated NaCl brine, an exposure temperature below $\sim55°C$ would preclude crevice corrosion (Asano et al., 1992).

Conditions anticipated in the WIPP would appear to be totally compatible with the use of a Ti or a Ti Grade 12 container as long as the repository temperature lies in the vicinity of 30°C. The amount of gas generated by corrosion reactions under these circumstances would be expected to be extremely small.

4.9 Ti-CO$_2$ and Ti-H$_2$S

The passive film formed on the surface of Ti makes the metal resistant to attack by a broad range of chemical environments, including aqueous H_2CO_3 and H_2S solutions (Jones, 1992; Schutz, 1986). Titanium is considered to be "excellent" in carbonic acid service, at temperatures to 100°C (Schweitzer, 1986). It is expected to exhibit corrosion rates <0.05 mm/yr (<2 mpy) under these conditions. Schutz (1986) stated that Ti can be used to temperatures "in excess of 200°C" in wet or dry CO_2 and H_2S. Aqueous solutions of H_2S, in equilibrium with H_2S pressures as high as 15 atm are routinely contained in titanium autoclaves (Tewari et al., 1979; Wikjord et al., 1980).

It appears from the foregoing accounts of Ti applications in aqueous H_2CO_3 and H_2S solutions that no significant reaction would be expected between Ti containers and aqueous CO_2 or H_2S solutions in the WIPP.

5.0 APPROACH

All of the H_2-generation studies are being performed using laboratory test equipment and laboratory facilities. Each test follows one of two basic testing methods, according to the type of reaction vessel employed. The test methods, the metallic test materials, and the brine used in the testing program are described in this section of the report.

5.1 Testing Methods

Two test methods are being used in the program: the seal-welded-container test method and the autoclave test method.

5.1.1 Seal-Welded-Container Test Method

Tests performed in the presence of brine and low-to-intermediate gas pressures (e.g., 0 to 20 atm) make use of seal-welded containers made of Hastelloy C-22,® a corrosion-resistant Ni-Cr-Mo alloy (Figures 5-1 and 5-2). The specimen rack shown in Figure 5-1 is used for low-carbon-steel tests, and is discussed in more detail in Section 6.1.1 of this report. The alternative packaging material tests used a somewhat different arrangement, described in Section 6.2. In both cases, the same specimen support rack geometry is used. The rack shown in Figure 5-1 is in the position used for immersed-specimen testing. For vapor-phase testing the rack would be inverted.

Because the course of the reaction is monitored by the pressure of H_2 retained within the container by means of the pressure gauge, and because atmospheric gases must be rigorously excluded from the test environment, it is imperative that the containers be leak-free. To that end, the containers are of all-welded construction (with the exception of the gauge's pipe-thread joint with the

---

® Hastelloy C-22 is a registered trademark of Haynes International, Kokomo, IN.
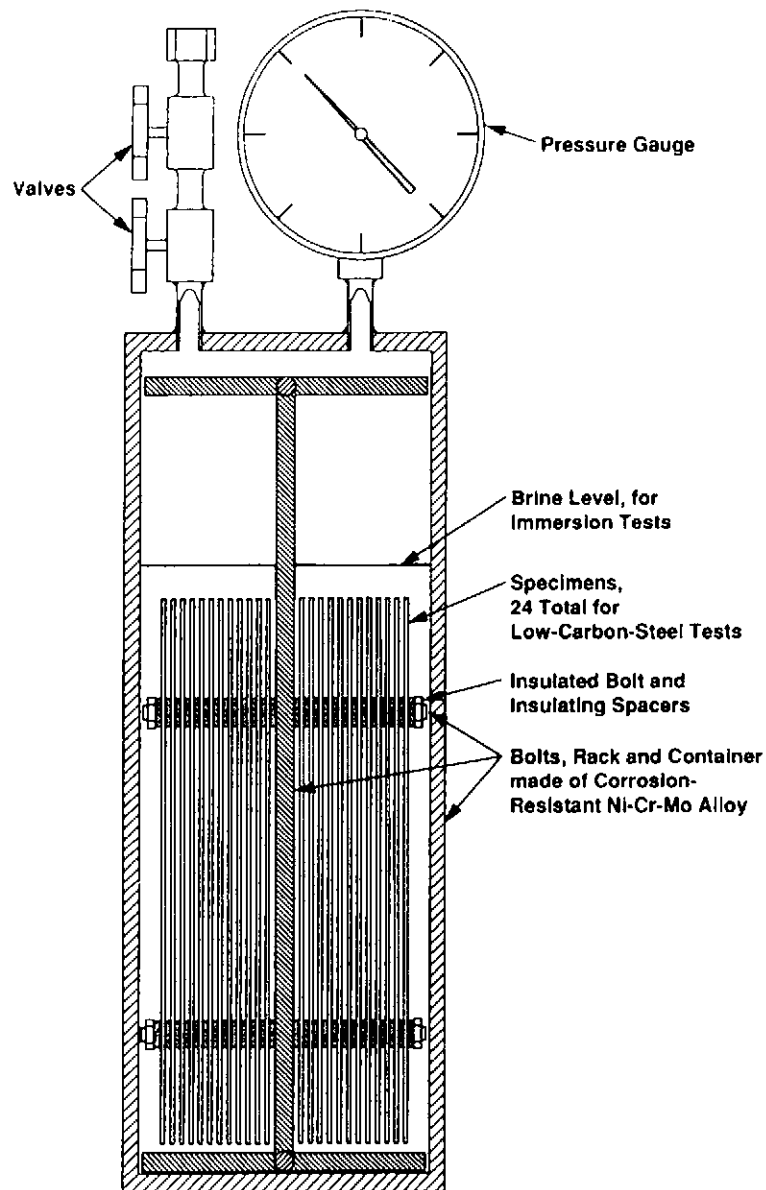
Figure 5-1. Seal-welded test container with specimen rack in place. Inside dimensions (typical): 28.9 cm (11.4 in.) high, 10.2 cm (4.0 in.) diameter.
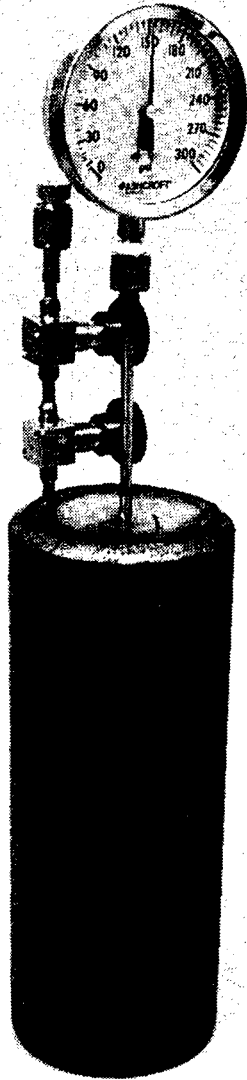
Figure 5-2. Seal-welded test container, fully charged, ready for placement in oven.

body of the container, which is made up very tightly, with Teflon® tape applied to the threads). The pre-weighed test specimens (of large area, to expedite rapid quantification of gas generation) and the brine are placed in the container before welding the top on the container. The sealed containers are then pressurized with He gas (at 4.4 atm, or 50 psig). Two He fills with intermediate evacuations are made to ensure minimization of contamination with residual air. The containers are then given a standard He leak-check test capable of sensing a He leak rate of 1.2×10^{-10} atm-cc/s. A container that does not pass the leak test is not used. If the leak test is successfully passed, the He is evacuated from the container and the appropriate overpressure gas is added. The containers are then placed in forced-convection (incubator) ovens maintained at 30 ± 5°C, and the course of the gas-generating reaction is monitored by observing the pressure changes on the pressure gauges. Gas samples can be obtained from the containers at any time for gas analysis, though taking such a sample greatly perturbs the container gas inventory and gas pressure. For this reason, gas sampling is generally performed at the conclusion of a test, after the final pressure readings have been obtained.

In the seal-welded-container tests, two methods are used to determine the rates of the corrosion and gas-generation reactions: 1) determination of the container gas pressure as a function of time and 2) determination of the amount of metal lost from each specimen at the conclusion of a test by gravimetric methods. The former method has the advantage of yielding real-time information on the course of the gas-generating reaction. Confidence in the results obtained in any given test environment is dependent on accurate pressure gauge information and accurate estimations of specimen area and the plenum volume (vapor space) of the test container. The result obtained represents the gross integrated reaction of the specimen assembly, without quantifying the contribution of each specimen, hence each lot of material, to the H_2 being generated. The latter method has the advantage of being capable of specifying the contribution of each specimen to the H_2 generated during the test. Confidence in the results obtained using any given set of test conditions is dependent on accurate pre- and post-test specimen weights, accurate determination of specimen areas, and carefully controlled specimen surface preparation and corrosion-product-stripping procedures.

Because pressure gauge accuracy is an important factor in the quantitative determination of gas produced by the pressure-volume method, the inherent accuracy of the pressure gauges used in the tests was investigated by analyzing the pressure readings of new gauges in comparison with a

calibration standard.[a] Two gauge ranges were used in the tests; 200-psig full-scale and 300-psig full-scale. All were supplied by the same manufacturer, and all were basically the same type of simple bourdon-tube gauge. All gauges were tested against a calibration standard before use to ensure that the accuracy of the gauge met the manufacturer's specifications ($\pm 3\%$ of full-scale reading). Each 200-psig gauge was tested at five pressure levels; each 300-psig gauge was tested at six pressure levels. The full statistical experiment consisted of calibration data from sixteen new 200-psig gauges and eight new 300-psig gauges. A one-way random-effects analysis of variance was used to characterize the bias in the gauges and the gauge-to-gauge and experimental variabilities. These estimates of bias and variability were then used to construct a confidence on a true pressure value.

If M is a single reading obtained from a 200-psig gauge, the confidence limits associated with this single reading have been determined to be

90% confidence: M -2.9/+1.9 psi

95% confidence: M -3.4/+2.4 psi

99% confidence: M -4.3/+3.3 psi.

For a single reading obtained from a 300-psig gauge, the confidence limits have been determined to be

90% confidence: M -7.9/+5.8 psi

95% confidence: M -9.2/+7.1 psi

99% confidence: M -11.8/+9.7 psi.

Repeated readings of the same gauge or use of more than one gauge to report a given pressure would increase the level of confidence in the reading obtained.

The 200-psig gauges are clearly more accurate than the 300-psig gauges. At the 95% confidence level, the 200-psig gauges can be approximately characterized as being within $\pm 1.5\%$ of the

---

[a] All gauges used in the present test series were tested against calibration standards by the Westinghouse Hanford Company Standards Laboratory. The pressure standards (250 psig full-scale for the 200-psig gauges; 500 psig full-scale for the 300-psig gauges) have a reported accuracy of 0.1% of the full-scale reading. In the statistical analysis described here the calibration standard was assumed to be absolutely accurate.

full-scale reading; the 300-psig can be approximately characterized as being within ±3% of the full-scale reading. The volume of the plenum of the test containers can be known with a high degree of confidence to ±3%. The error in determining the area of the sample array is much less than that associated with the gauge pressure and the plenum volume (< ±1%). If a simple propagation-of-error approach is used, it can be seen that, at pressures near the full-scale range, the amount of gas in moles (proportional to pressure x volume) present in the test container equipped with a 300-psig gauge is given to ±6% by the pressure gauge/plenum volume method. If the pressure gauge is not near its limit, the error, by the same reasoning, can increase. For example, in the case of a 300-psig gauge reading 150 ±9 psig (95% confidence level), the contribution of gauge error in estimating the moles of gas present in the test container is ±6%, with a total error of ±9%.

The tables summarizing the test conditions for all of the seal-welded-container test, Tables 3-1 and 3-2, call out the tests that were equipped with 300-psig gauges. All other tests were equipped with 200-psig gauges.

The sources of variability in the gravimetric data include

- container-to-container variability, reflecting differences in the handling of the containers and the conditions within the containers throughout the experiment;

- alloy-to-alloy variability, reflecting differences between alloys (or heats of the same alloy) that affect the corrosion rate;

- sample-to-sample variability, which includes variability in alloy composition from location to location within the parent sheet stock; differences in surface preparation; errors associated with weighing and surface area determination; and differences in the local environment within the sample container.

At the conclusion of a test, the container is opened by means of a milling operation that removes the top closure weld. The specimens are quickly lifted from the container, removed from the specimen rack, rinsed, and placed in desiccators. X-ray diffraction (XRD) analyses of the corrosion products are typically performed on selected specimens, usually within 24 h if there is judged to be a possibility of oxidation of the corrosion product by contact with air. The brine from the test container is retained for chemical analysis. The corrosion product is stripped from the specimens by means of an inhibited acid solution, and the amount of metal lost from each specimen is determined. The gravimetric analysis permits an estimate to be made of the metal loss from (or penetration of)

each specimen. These metal-loss data are compared with the quantity of H_2 generated and the corrosion product formed, for determination and corroboration of the overall corrosion/gas generation processes.

5.1.2 Autoclave Test Method

Tests performed at high gas overpressures, e.g., pressures greater than ~20 atm, utilize heavy-wall autoclave systems. The autoclaves are typically of 3.8-L capacity. Because autoclaves have high-pressure gasket seals, they cannot be expected to be as gas tight as the seal-welded containers. However, pressure-time data can be obtained from an autoclave pressure gauge when the autoclave is extremely well sealed. Otherwise, the data from an autoclave system consist of the gravimetric results and the analysis of the corrosion product film by XRD or other methods.

While autoclave systems are often employed for high-pressure studies, they have additional uses associated with their relatively large volume. For example, if it is considered necessary to keep major components of a test separate, as in the case of a mass of salt containing test specimens suspended in the vapor phase over a pool of brine, the autoclave can provide the flexibility and volume required.

5.2 Materials

The H_2-generation study has focused on two major material classes: low-carbon steel, intended to closely represent the drum steel and the waste-box steel materials while approximately representing the steel wastes within the containers; and alternative packaging materials, consisting of unalloyed Cu and Ti and selected alloys of these two materials.

5.2.1 Low-Carbon Steels[a]

The drums and waste boxes containing the TRU waste will make by far the greatest contribution of metallic Fe to the WIPP repository (Brush, 1990). This Fe will be in the form of low-carbon steel, ranging in composition from the low-C, low-Mn material used in the fabrication of the Department of Transportation (DOT) 17-C drums (0.04 to 0.1% C, 0.25 to 0.5% Mn) to the somewhat more highly alloyed material used in the waste boxes (for example, ASTM Grade A36 steel, with 0.25% C maximum and 0.8 to 1.2% Mn; and ASTM Grade A569 steel, with 0.15% C and 0.60% Mn maximum). The steel waste contained within the waste boxes can be expected to range widely in composition, from low-carbon steel (for example, nails, wire, structured steel) to highly alloyed material (for example, tools, high-strength fasteners, machine components).

Ideally, a corrosion or a gas-generation study would utilize test specimens and a test environment that exactly duplicate the field conditions. In the present case, this is of course not possible, as a very wide range of steel compositions will exist in the repository, and the compositions cannot ever be known with a high degree of certainty. It is therefore necessary to simulate the WIPP site conditions by using a range of steel compositions approximating the range of material compositions expected in the WIPP site. To this end, four lots (heats) of steel were obtained for test specimens, two lots each of ASTM Grade A366 (standard specification for cold-rolled sheet), representative of steel waste drums, and ASTM Grade A570 (standard specification for hot-rolled carbon steel sheet and strip), representative of steel waste boxes and other steel waste materials. The two lots of ASTM Grade A366 steel are designated "J" and "K," and the two lots of ASTM Grade A570 steel are designated "L" and "M." The thickness of the as-received material is given below:

---

[a] The term "low-carbon steels" is a broad material classification, generally considered to include steels having less than 0.25% C, 1.65% Mn, and 0.60% Cu, along with small amounts of other elements (ASM, 1978). According to this definition, the drum materials and the waste box materials are "low-carbon steels."

Lot	Thickness, mm (in.)
J	0.70 (0.028)
K	0.86 (0.034)
L	1.5 (0.059)
M	1.6 (0.063)

The compositions of the four lots of steel are presented in Table 5-1. Two values are presented for the C content of each lot of steel, representing analyses provided by 1) the steel vendor and 2) an independent testing laboratory.[a] The discrepancies in C concentration noted for the J and K lots between the two analyses are not considered important to the results of the study.

Table 5-1. Compositions of Low-Carbon Steels

| Specie | ASTM A366 | | ASTM A570 | |
	Lot J	Lot K	Lot L	Lot M
C	0.06/0.10	0.05/0.09	0.13/0.14	0.13/0.13
Mn	0.30	0.30	0.77	0.75
Si	0.08	0.07	0.11	0.10
P	0.015	0.015	0.017	0.020
S	0.012	0.009	0.015	0.015
Cu	0.015	0.020	0.015	0.040
Fe	bal	bal	bal	bal

In all of the calculations conducted in the present work equating molar equivalencies of corrosion reactants and corrosion products, and in all calculations equating corrosion (penetration) rates with metal lost, the steels are treated as though they are pure Fe, with a molecular weight of 55.85 and a density of 7.86.

---

[a] Koon-Hall Testing Corporation, 5687 S.E. International Way #A, Portland, OR 97222.

The microstructures of the steel are shown in Figures 5-3 and 5-4. The microstructures appear quite similar, from lot to lot, except for 1) the carbon-content-related effects, e.g., the amount of carbide-rich phases (notably pearlite) present; and 2) the fact that the as-received hot-rolled materials (lots L and M) have a layer of mill scale (iron oxide) 5 to 13 μm (0.2 to 0.5 mil) thick on their surfaces. This oxide was abraded off before the gas-generation tests. All of the microstructures appear to be in the annealed condition, and all of the grain sizes are similar (60 to 90 grains/cm^2 at 100x). The "cold-rolled" material exhibits little, if any, evidence of cold work.

Lot J   Lot K
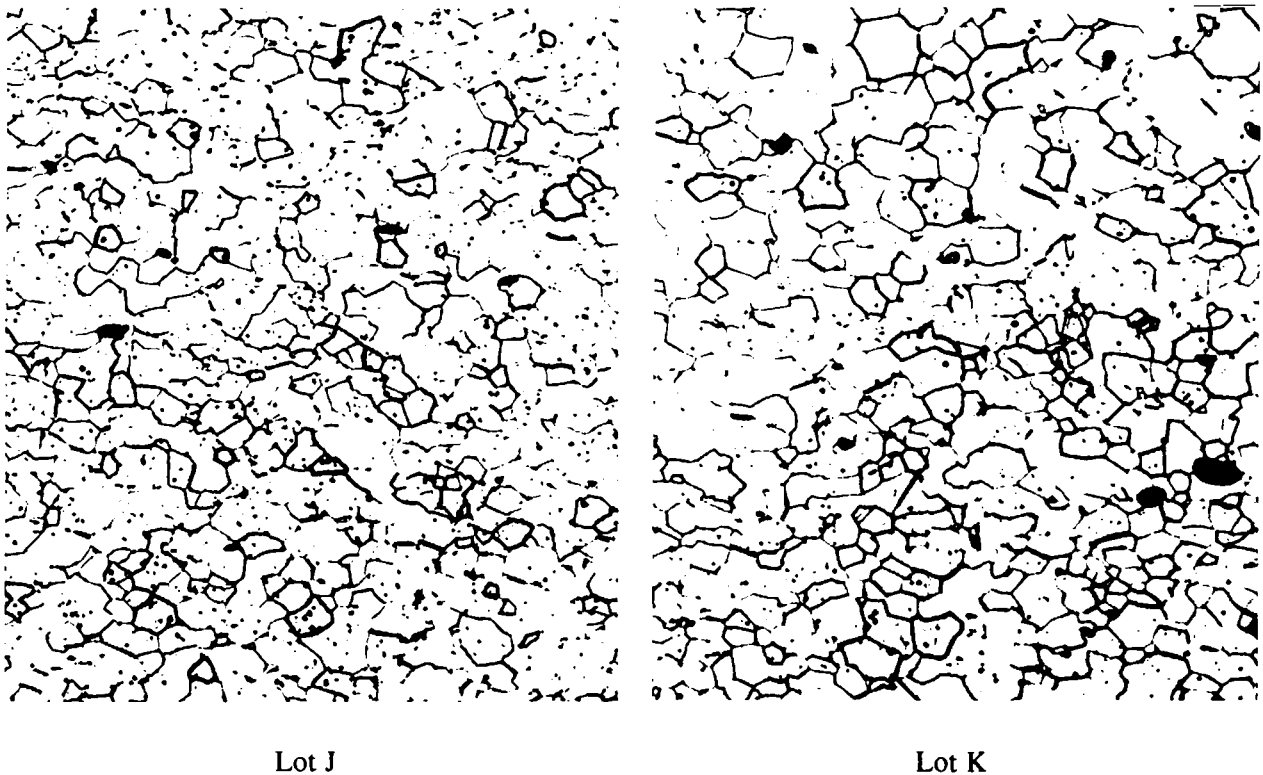
Figure 5-3. Microstructure of steel, lots J and K. 350X.

It is expected that the corrosion and gas-generation characteristics of steel lots procured for test would closely simulate the characteristics not only of the drums and waste boxes, but of the low-alloy steels contained within the wastes as well. The reason for this is that many studies have shown that the alloying elements present within carbon and low-alloy steels do not have a very strong effect on
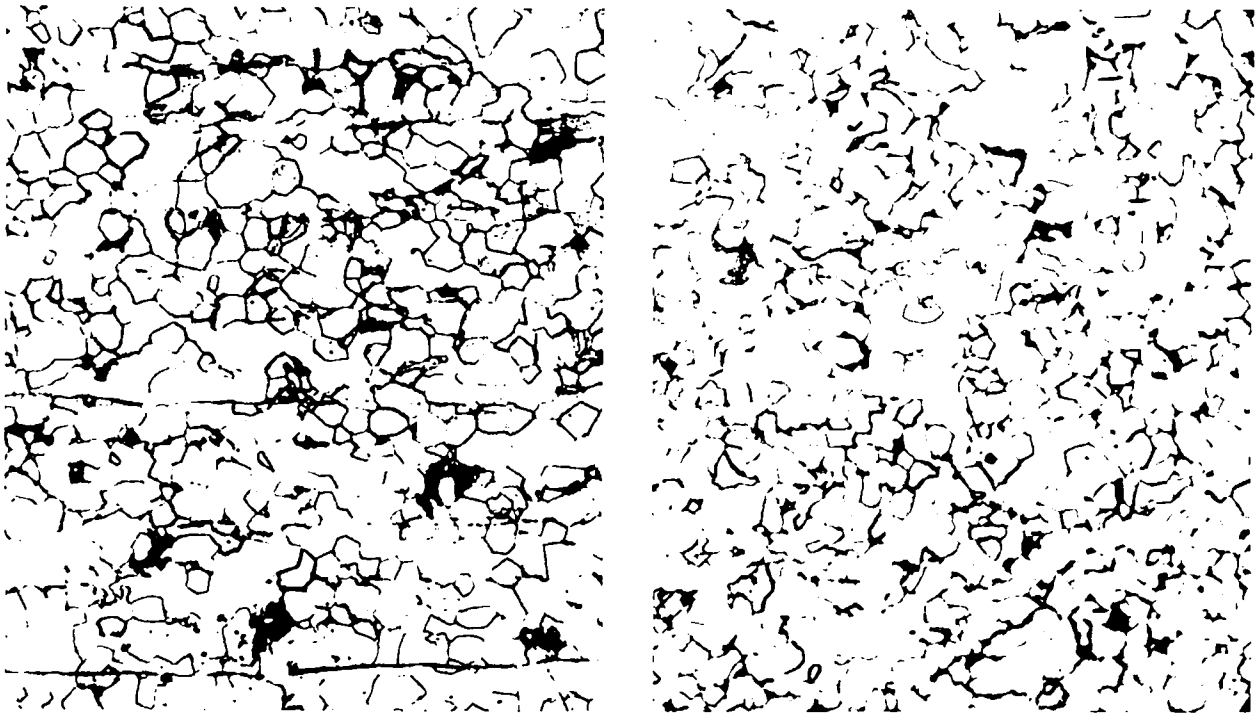
Lot L   Lot M

Figure 5-4. Microstructure of steel, lots L and M. 350X.

their corrosion behavior in aqueous brine environments. As an example of such a study, Reinhart and Jenkins (1972) reported corrosion results obtained from exposure of a large number of low-carbon and low-alloy steels to seawater at various depths (to 1,830 m or 6,000 ft), hence different O_2 activities and temperatures, for time periods up to 18 months. Low-carbon steels, hardenable low-alloy steels (e.g., AISI types 4140 and 4340), Fe-Ni alloys containing up to 9% Ni, and many other wrought and cast alloys were included in the study. Little effect of steel composition on corrosion rates was found at the conclusion of these studies. General corrosion behavior was dominated by duration of exposure, depth in the ocean, and O_2 availability. Southwell and Alexander (1969) reported corrosion results obtained from 10 low-alloy steels exposed for 16 yr at a depth of 14 ft in the ocean near the Panama Canal. The corrosion rates of the alloys within the group, which included a low-carbon steel and steels containing up to 5% Cr, up to 0.9% Cu, and up to 5.5% Ni, were all 97 ±30 μm/yr (3.8 ± 1.2 mpy) after 16 yr. Again, little effect of alloy composition was observed in the brine environment. Given findings such as these, it appears reasonable to deduce the approximate

behavior of low-carbon steel packaging materials and low-alloy-steel wastes contained within the packages from the four lots of steel procured for laboratory testing in the present project, where "approximate behavior" would mean to within a factor of ~2.

5.2.2 Alternative Packaging Materials

The potential for gas pressurization of the WIPP underground facility due to corrosion of packaging materials and metal waste has necessitated consideration of several different options for waste form modification. One possible option involves repackaging the waste in containers that do not have the gas-generation characteristics of mild steel. To identify suitable alternative materials for waste packaging, an expert panel referred to as the Waste Container Materials Panel (WCMP) was convened August 20 and 21, 1990, by the DOE WIPP Project Office, as a part of the Engineered Alternatives Task Force (EATF) activities. The panel evaluated a wide range of metallic, ceramic, cementitious, polymeric, and coating materials for their applicability to WIPP containers (EATF, 1991).

An important criterion for the selection of suitable metallic materials was absence or significant minimization of gas-generation tendency. Additional criteria were fabricability, availability, fabrication capacity (industrial production capacity), status of technology development, cost, and mechanical properties.

The metal categories selected by the panel for in-depth consideration were

• Cu and Cu alloys

• Ti and Ti alloys

• high-Ni alloys

• Zr and Zr alloys

• stainless steels.

The panel then determined the degree to which each metal class met the previously set container material requirements. The overall ranking of materials indicated that the Cu-base and Ti-base

material classes offered the best combination of material properties and overall economic incentive for replacing carbon steel as a metallic container material at the WIPP site. Cu-base materials, though obviously susceptible to attack by and reaction with certain chemical species such as nitrates and sulf-des, offer a high degree of thermodynamic stability in near-neutral aqueous solutions. Ti-base materials are extremely corrosion resistant in a wide variety of low- and intermediate-temperature brines because of the protection afforded by their oxide film (see Sections 4.8 and 4.9 of this report). Unalloyed Cu (oxygen-free, electronic) and unalloyed Ti (Ti Grade 2) were accordingly selected from the candidate material list for an investigation of their corrosion/gas-generation characteristics in simulated WIPP environments. In addition, cupronickel 90-10 was chosen for study, as its mechanical properties are far superior to unalloyed Cu due to the presence of 10% Ni, Ti Grade 12, a Ti-Ni-Mo alloy, was also selected because of its well known resistance to crevice corrosion. The chemical compositions of the specific materials procured for study are presented in Table 5-2.

Table 5-2. Compositions of Alternative Materials Used in Corrosion/Gas-Generation Study

Material[a]	Weight Percent, or (ppm)										
	Cu	Ti	Ni	Zn	Mn	Mo	Fe	Pb	O	S	C
Unalloyed Cu (C10100)	99.99	--	--	--	--	--	--	(3)	(2)	(10)	--
Cupronickel 90-10 (C70600)	87.58	--	10.4	0.2	0.5	--	1.3	0.01	--	0.005	0.01
Ti Grade 2 (R50400)	--	Bal	--	--	--	--	0.16	--	0.13	--	0.01
Ti Grade 12 (R53400)	--	Bal	0.80	--	--	0.30	0.14	--	0.12	--	0.01

a   Unified Numbering System (UNS) designations are in parentheses.

5.2.3 Brine

The brine used in the present study is based on the WIPP Brine A composition described by Molecke (1983). It is a high Mg, K, and Na chloride-sulfate brine and is used as a simulant for intergranular Salado Formation brine that might intrude into the WIPP repository horizon. The composition of Brine A, as well as the average value and range of compositions of the three lots of brine made up to date for usage at PNL in the present study, are given in Table 5-3.

Table 5-3. Composition of Brines Used in Tests

Chemical Specie	Concentration, mg/L	
	Brine A (target)	PNL Brines
Na	42,000	$39,400^{+1200}_{-1100}$
Mg	30,000	$34,700^{+1000}_{-1500}$
K	35,000	$29,900^{+600}_{-400}$
Ca	600	560^{+40}_{-60}
B	220	220^{+1}_{-4}
Cl	190,000	$188,300^{+2700}_{-4300}$
SO$_4$	3,500	$4,130^{+50}_{-60}$
HCO$_3$	700	680^{+30}_{-60}
pH	6.5	$7.4^{+0.5}_{-0.7}$

Only the major constituents of the brine as described by Molecke (1983) were used to make up the PNL brines. Omitted minor constituents, deemed to have little or no effect on the corrosiveness of the brine, were Fe, Cs, Rb, Li, Sr, and I. These minor elements totaled only 58 mg/L in the composition described by Molecke.

5.2.4 Salt (Halite)

Two corrosion and gas-generation tests (tests AUT-5 and AUT-6) were conducted in which the specimens were packed in particulate salt (halite). The salt used in the tests was shipped to PNL from SNL in two 1-gallon containers, identified as "WIPP Salt E 140-N635." The salt was originally gathered from the floor of "E 140 drift, 194 m (635 ft) north of the salt shaft." It was assumed to be essentially pure (>95%) NaCl, and was not analyzed.

6.0 RESULTS

Two major efforts were undertaken in the present corrosion and gas-generation laboratory study: experiments directed toward determining the behavior of current packaging materials (low-carbon steels in simulated WIPP environments); and experiments directed toward determining the behavior of alternative packaging (Cu- and Ti-base) materials in simulated WIPP environments. The experimental results associated with each major materials group will be discussed separately in this section of the report. (This basic division in the experimental work is reflected in the summary test matrices for the project, presented in Tables 3-1 and 3-2. Reference may be made to these tables for information on the individual tests described in this section of the report.)

In general, each test was designed to provide 1) time-dependent container pressure, from which H_2 pressure data could be determined; 2) gas composition data, for quantification of corrosion-product gas generation rates in conjunction with item 1; 3) corrosion rate (metal penetration) data, obtained gravimetrically after corrosion-product film stripping; and 4) corrosion product identification. Post-test brine analyses were also obtained. Items 1 and 2 have the most value and are most defensible when obtained from a demonstrably leak-tight container, such as the seal-welded containers used in the present tests. Information from items 1, 2, and 3 permit a comparison of the moles of H_2 formed versus moles of metal reacted, to verify the legitimacy of the conclusions drawn. Item 4 provides insights into the potential protectiveness of the corrosion product film and also ensures that the appropriate reaction is being considered when the molar equivalency of metal and H_2 are being compared.

The raw data describing container pressure as a function of time for the anoxic brine (brine/N_2) and the brine/CO_2 seal-welded container tests are contained in Appendix A to this report. All of the individual specimen data from all concluded corrosion tests are contained in Appendix B. These data are presented to permit additional, independent evaluation and corroboration of the results presented and conclusions drawn in the present report and to facilitate statistical treatment of the data according to the specific future needs of the WIPP Project modelers. Such treatments were not attempted in the present report because of the many different approaches to the data that could be taken in such statistical analyses.

6.1 Low-Carbon Steel Tests

The corrosion and gas-generation behavior of low-carbon steels was evaluated in three environments: anoxic brine (brine/N_2)[a], brine/CO_2, and brine/H_2S. In each environment specimens were exposed either fully immersed in the brine (Brine A) or in the vapor phase over the brine. All tests were performed at 30 $\pm 5°C$. The test conditions are summarized in Table 3-1.

All steel specimens were surface ground using 60-grit emery cloth to remove mill scale or other surface deposits. After grinding, they were dimensionally measured, degreased (using trisodium phosphate followed by a water rinse, and an absolute alcohol rinse), and weighed. The specimen dimensions were obtained to a minimum accuracy of ± 0.025 mm (± 0.001 in.); the specimen weights (pre- and post-test) were obtained to ± 0.0001 g. After the final degreasing and weighing operations, the specimens were stored in a desiccator until needed. At this time, the steel specimens exhibited a bright, clean, as-ground appearance.

Upon conclusion of a test, the specimens were removed from the test container, rinsed in deionized water and alcohol, and placed in a desiccator to minimize the possibility of further reactions. Selected specimens were held in reserve for analysis of corrosion products, usually accomplished by x-ray diffraction (XRD). The corrosion product layer was removed from the remainder of the specimens by immersing the specimens in an inhibited HCl corrosion-product stripping solution per National Association of Corrosion Engineers (NACE) standard TM-01-69, 1976 revision. The stripping solution is made by adding 12 ml formaldehyde to 1 L of 50% HCl solution. A final weighing was then performed so that the mass of metal lost from each specimen by corrosion could be calculated.

---

[a] Strictly speaking, each of the environments investigated consists of anoxic brine, as O_2 has been excluded from the test containers. The term "anoxic brine" as used here to describe the environment having no reactive gas (CO_2, H_2S) overpressure signifies that the reactant is anoxic brine alone, without an added reactive constituent.

6.1.1 Seal-Welded-Container Tests

Each seal-welded container test described in this section of the report contained a rack of 24 test specimens, comprising six replicate test specimens of each of the four lots of low-carbon steel previously described in Section 5.2. The six test specimens of each lot of steel consisted of three wide specimens, 86 mm (3.4 in.) x 190 mm (7.5 in.), and three narrow specimens, 51 mm (2.0 in.) x 190 mm (7.5 in.). Each specimen had two holes, 8 mm (0.31 in.) in diameter, to accommodate the insulated rack supports. The narrow specimens were placed on the outer part of the rack to optimize material loading in the container. The total specimen area in each container lay in the range 0.60 to 0.64 m². In the immersed-specimen tests, sufficient Brine A (1.34 to 1.39 L) was added to the container to cover the tops of the specimens to a depth of ~6.4 mm (~0.25 in.). In the vapor-phase exposure tests, 0.25 L of brine was placed in the bottom of the test container. The level of the brine was below the racked specimens, though the brine unintentionally splashed on the bottoms of the specimens during container handling. The immersed-specimen containers had a calculated vapor-space plenum volume of 0.634 L. The plenum volume in the vapor-phase exposure tests was 1.74 L. The specimen area-to-plenum volume ratio was made large to promote a rapid response on the test container pressure gauge to the H_2 generated by corrosion reactions.

6.1.1.1 ANOXIC BRINE (BRINE/N_2)

The anoxic brine tests were intended to provide basic information on the corrosion/gas-generation proclivity of low-carbon steel in the absence of reactants other than low-carbon steel and Brine A. The anoxic brine immersed-specimen testing regimen includes test containers 1, 2; 9, 10; 17, 18; and 25, 26; the vapor-phase-specimen testing regimen includes test containers 5, 6; 13, 14; 21, 22; and 29, 30. Proximate identification numbers (e.g., 1, 2) signify duplicate tests. These test container identification data are also contained in Table 3-1.

All of the pressure-time plots from the brine/N_2 test series are presented in Figure 6-1. The corresponding raw data are presented in Appendix A. In each case, the initial starting pressure of N_2 gas (99.99% N_2 by analysis) was approximately 10 atm absolute (~9 atm gauge). At 30°C the partial pressure of water vapor in equilibrium with Brine A is ~0.03 atm, so the pressure gauge reading
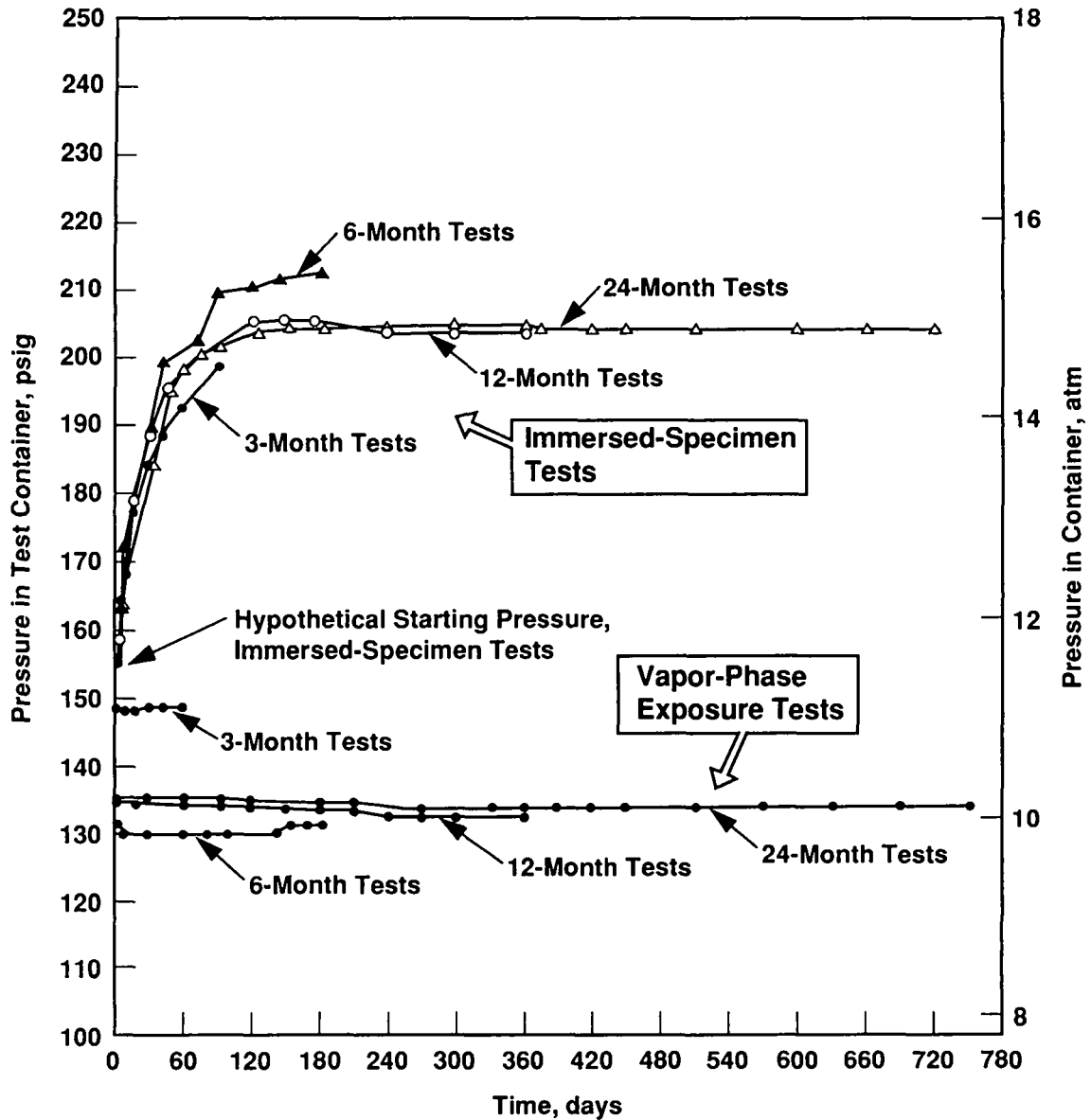
Figure 6-1. Pressure-time curves, low-carbon steel anoxic brine tests. Each curve represents two (duplicate) tests.

essentially represents the starting N_2 pressure plus the pressure of corrosion-product H_2. Because of the very close agreement in pressure between duplicate containers (typically within 2 to 3 psi), the pressure readings of duplicate containers were averaged in all cases to develop the curves shown in

Figure 6-1. The eight curves shown, therefore, represent the results of all 16 tests. Pressures were recorded at a minimum frequency of weekly; the test temperature was continually plotted to ensure conformity with the specified 30 ±5°C temperature range.

The test containers used for the 24-month tests had been equipped with pressure gauges limited to a maximum pressure of slightly over 200 psig. For this reason, the 24-month test containers were vented approximately halfway through the test, as it could be seen that the pressure limit of the gauges would be exceeded by the end of the test if some of the corrosion-product H_2 were not released.

The curves of Figure 6-1 show 1) that a good test-to-test agreement in the pressure-generation-rate results between the various tests had been attained; 2) that the immersed-specimen tests can be characterized by a steady, approximately linear H_2 generation rate; and 3) that the vapor-phase exposure of the mild steel did not produce measurable H_2 after an initial short period of pressure increase. The pressure increase at the beginning of these latter tests is ascribed to corrosion taking place on the bottom of the specimens, because the brine in the bottom of the vapor-phase-exposure containers contacts the bottom of the specimens by unintentional splashing when the containers are handled after brine-charging and container closure. Approximately 10% of the surface area of the test specimens in these tests is typically affected in this manner.

An analysis of the gas samples taken from the containers just before they were opened is presented in Table 6-1. The analyses confirm that the pressure increase observed in the containers was due to corrosion-product H_2. The consistency in the gas generation between duplicate test containers is evident from the table. Significant differences are evident between the H_2 contents of the vapor-exposure containers. This is attributed to the varying test specimen surface area splashed by brine from one container to another.

The post-test appearance of the steel specimens is shown in Figure 6-2 (immersed specimens, 6 and 24 months exposure) and Figure 6-3 (vapor-phase-exposure specimens, 24 months exposure).

The appearance of the specimens (Figure 6-2) changed somewhat between 6 and 24 months exposure, with the specimens maintaining a general metallic appearance, but darkening with increasing exposure time. The 3- and 12-month test specimens resembled the 6-month-exposure specimens more than the 24-month-exposure specimens. The bulk of the greenish-gray, flocculent corrosion

6-5

Table 6-1. Composition of Gas at Conclusion of Test, Anoxic Brine (Brine/N$_2$) Tests. Each
tabulated value is average of two analyses. Results are given in vol% (mol%).

	Immersed-Specimen Tests				Vapor-Phase-Exposure Tests			
	Test Numbers				Test Numbers			
	3-mo	6-mo	12-mo	24-mo	3-mo	6-mo	12-mo	24-mo
Specie	1/2[a]	9/10	17/18	25/26	5/6	13/14	21/22	29/30
N$_2$	89.5	80.2	74.5	60.1	99.6	99.5	99.7	99.2
	89.8	81.1	73.1	61.5	99.8	99.4	99.5	99.2
H$_2$	10.5	19.5	25.5	39.7	0.42	0.20	0.20	0.66
	10.1	18.7	26.8	38.5	0.15	0.32	0.35	0.56
He	<0.01	0.34	0.08	0.06	0.02	0.26	0.10	0.19
	0.08	0.30	0.09	0.06	0.02	0.24	0.13	0.28
O$_2$	<0.1, all tests							

[a] 1/2, 9/10, etc. indicates that tests numbered 1 and 2 are duplicate tests, 9 and 10 are duplicate tests, etc. In the
table, the average of two separate gas analyses for test 1 is over the average analyses for 2, the average of two
separate gas analyses for test 9 is over the average of two separate gas analyses for 10, etc. In all cases the two
separate analyses made on gas samples from one container showed excellent agreement.

product that typically forms in these tests does not adhere to the surface of the specimens, but instead
settles to the bottom of the test container. The darkening with exposure time suggests a change in the
nature of the surface and the film associated with the specimen surface.

The appearance of the specimens in Figure 6-3 is also typical of the appearance of the speci-
mens from the 3-, 6-, and 12-month anoxic-brine-vapor exposures. The specimens removed from the
vapor-phase (humid) tests typically appeared to be shiny and unreacted except for the bottom ~10%
of the specimens that had been splashed by brine placed in the bottom of the test containers (see Fig-
ure 6-3). This description implies that corrosion products did not form on the specimen surfaces con-
tacted by vapor only. An effort was undertaken to quantify the limits of oxidation/metal consumption
that can take place on the surfaces of such specimens while the corrosion product film remains
undetectable by the human eye.
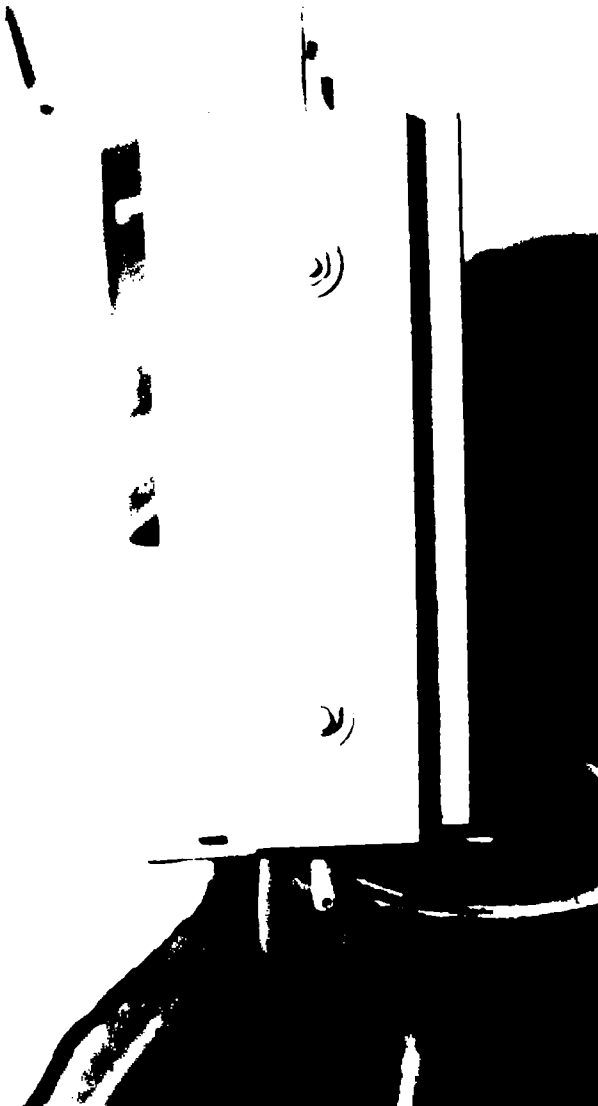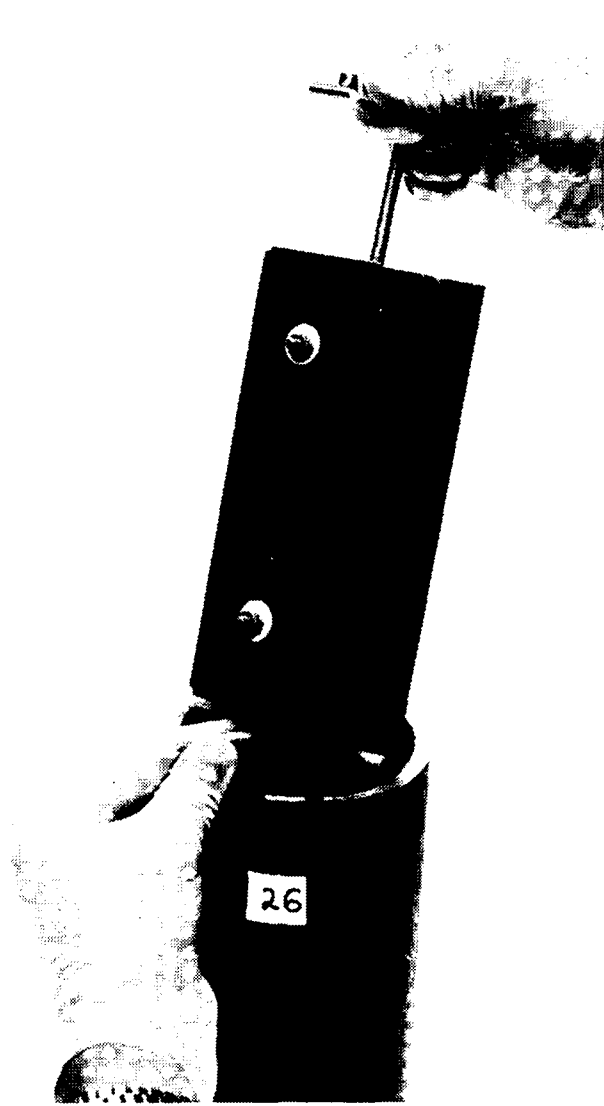
6-Month Exposure   24-Month Exposure

Figure 6-2.   Post-test appearance of steel specimens, immersed, 6- and 24-month anoxic brine tests.
              The 24-month specimens appear dark, though essentially none of the corrosion product
              is found on the specimen surfaces.

Preliminary scoping tests confirmed that visible films could be readily produced on surface-ground low-carbon steel specimens by heating them in air for ~10 min at temperatures of 250°C (straw color) and 300°C (dark blue color). Accordingly, two specimens of Lot J steel, each 51 mm (2.0 in.) x 190 mm (7.5 in.) x 0.70 mm (0.028 in.), were carefully cleaned, then weighed five times

6-7
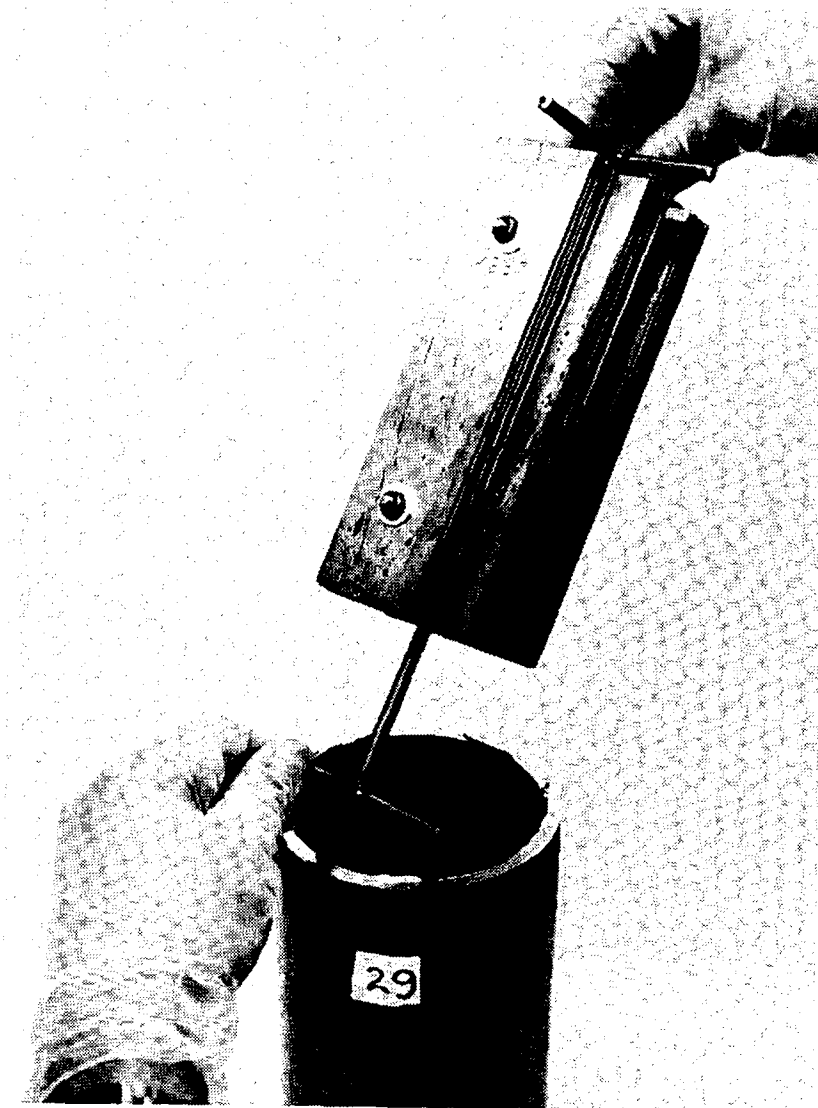
Figure 6-3. Post-test appearance of steel specimens, vapor-phase exposure, 24-month anoxic brine tests. No reaction is evident except where brine has contacted the bottoms of the specimens.

each (once on each of five successive days), using the same 4-place (0.0001 g) balance. The average weight of the five weighings was taken as the starting weight. The specimens were then heated for 18 min each at either 250°C or 300°C, to produce the straw-colored and dark-blue-colored oxide films. The post-treatment weights of the specimens were then obtained in the same manner as the

pre-treatment weights, and the average of the five weights was taken as the final weight of each specimen. It was ascertained that the specimen heated at 250°C showed a net weight change of -0.0001 g; the specimen heated at 300°C showed a net weight change of +0.0009 g. The effective zero net weight change exhibited by the straw-colored specimen justifies the conclusion of zero corrosion on a "clean and shiny" specimen, as the clean, shiny specimen has obviously formed less surface corrosion product than the straw-colored specimen. Even the maximum weight change found in the investigation, +0.0009 g on the dark-blue specimen, represents a metal loss (assuming FeO formation) of only ~ 1 % of that taking place on an immersed specimen of Lot J steel in anoxic 30°C Brine A with a N_2 overpressure during a 1-year exposure. Thus, assumption of essentially zero corrosion on a specimen that emerges "clean and shiny" from a vapor-phase corrosion test is justified by the test described. Such a conclusion is also consistent with the lack of pressure increase in the test container after the first few days of exposure, signifying essentially a complete lack of water vapor reaction between the steel and the test environment.

All of the specimen weight-change data from the 3-, 6-, 12-, and 24-month immersed-specimen tests are presented in Appendix B-1; data from the vapor-phase-exposure tests are presented in Appendix B-2. The data from the immersed-specimen tests are summarized in Table 6-2 in terms of metal penetration (uniform corrosion) rate.

Later in this report section the equivalence between metal lost to corrosion and container pressure increase will be demonstrated, and the corrosion and gas generation rate followed during the last 12 months of the 24-month test will be the rate recommended for WIPP repository modeling purposes. This rate is lower than the lowest rate shown in Table 6-2.

The four lots of steel exhibited similar corrosion characteristics in the anoxic brine environment. The rates are obviously decreasing with time; this is also evident from the pressure-time curves of Figure 6-1.

The post-test compositions of the brines obtained from the test containers after the 6-, 12-, and 24-month tests are compared with the starting brine composition in Table 6-3. It is evident from the table that 1) there are no significant differences in brine composition between the immersed-specimen tests and the vapor-phase-specimen tests, at the same test duration; and 2) there is no significant

Table 6-2. Summary of Corrosion-Rate Data, Immersed Specimens, Anoxic Brine (Brine/N_2) Tests. Penetration rate means and standard deviations are presented. Each penetration rate value in the columns J, K, L, and M represents an average of five specimens; the sixth specimen of each lot was reserved for XRD and archive. Penetration rate is expressed in μm/yr.

Test Duration, Months	Test Containers	Steel Lot and Penetration Rate[a]				
		J	K	L	M	All Lots
3	1, 2	1.94±0.16	2.03±0.26	2.10±0.19	1.79±0.16	1.96±0.22
6	9, 10	1.61±0.07	1.65±0.37	1.91±0.04	1.71±0.08	1.72±0.13
12	17, 18	1.05±0.05	1.26±0.04	1.31±0.04	1.29±0.03	1.23±0.11
24	25, 26	0.95±0.05	1.14±0.08	0.91±0.04	0.95±0.04	0.99±0.11

[a] To convert from a penetration rate expressed in μm/yr to moles Fe reacted/m^2 - yr, multiply the penetration rate by 0.141 mol/μm - m^2.

Table 6-3. Results of Brine Analyses, Anoxic-Brine Seal-Welded Container Tests. Comparison of brine compositions after 6-, 12-, and 24-month tests with original brine composition. Concentrations given in mg/L.

Specie	Brine A	Test Duration and Specie Concentration					
		6 month		12 month		24 month	
		Imm[a]	Vapor[b]	Imm[c]	Vapor[d]	Imm[e]	Vapor[f]
Na	38,300	43,000	42,000	40,900	39,800	40,200	41,000
Mg	35,700	35,800	35,400	35,100	34,700	32,900	34,000
K	29,500	29,900	29,700	30,500	30,700	31,000	31,000
Ca	560	600	610	630	590	581	572
B	230	230	230	240	230	230	228
Fe[g]	<10	<10	<10	<10	<10	<10	<10
Cl	190,000	196,000	196,000	190,000	187,000	192,000	192,000
SO_4	4070	4240	4190	3600	3800	4660	4620
pH	6.7	8.3	8.0	8.3	8.0	8.4	8.4

[a] Test container 10; [b] 14; [c] 17; [d] 21; [e] 25; [f] 29.
[g] Fe not detectable in these solutions. Solutions were exposed to air prior to analysis, permitting Fe oxidation and precipitation from solution.

difference between <u>any</u> brine composition and the starting brine composition. These observations suggest that the diminution in corrosion rate observed with increasing test time is not due to a decrease in concentration of a potential reactant (e.g., Mg^{2+}) supplied by the brine, but a steadily increasing inhibition of corrosion by a corrosion product adhering to the surface of the steel.

XRD analyses of the corrosion product collected from the bottoms of the test containers used in the immersed-specimen tests were unsuccessful in defining the corrosion product.[a] The XRD results showed that similar corrosion products formed after all exposure durations. As an example, the diffraction results obtained from the 12- and 24-month corrosion products are presented graphically in Figure 6-4.

The XRD analysis was completed within a few hours of collecting the corrosion product from the test container to minimize oxidation of the corrosion product through contact with air. A color change, from gray-green to orange-red, over a period of several days of exposure to air confirmed the air-oxidizability of the corrosion product and is consistent with a 2+ valence state of the iron in the corrosion product as it existed in the anoxic test container environment.

The corrosion product adhering to the bottoms of the specimens removed from the vapor-phase-exposure tests was $\beta Fe_2(OH_3)Cl$, beta iron chloride hydroxide, in all cases. This tan-to-dark brown corrosion product bore no visual resemblance to the corrosion product formed in the immersed-specimen tests.

The corrosion product in all cases is expected to contain iron in the reduced (Fe^{2+}) valence state, which would require that the Fe reactant and the H_2 reaction product be equivalent on a molar basis:

$$Fe + 2H^+ = Fe^{2+} + H_2 \tag{33}$$

<hr>

[a] The principal XRD reference database used in the XRD corrosion product analyses is that of the International Center for Diffraction Data (ICDD) Powder Diffraction File on CD-ROM (PDF-2), including all entries through Sec 41 (1991). The database comparison was effected by means of the search/match code <u>Micro-ID Plus</u>, available from MDI, Inc., Livermore, CA.

IO: 1013928 Container #25 Corrosion Product (wet)

File: 1013928.MDI   Scan: 5-75/.02/1/#3501,   Anode: CU   Zero=0.0

2-Theta
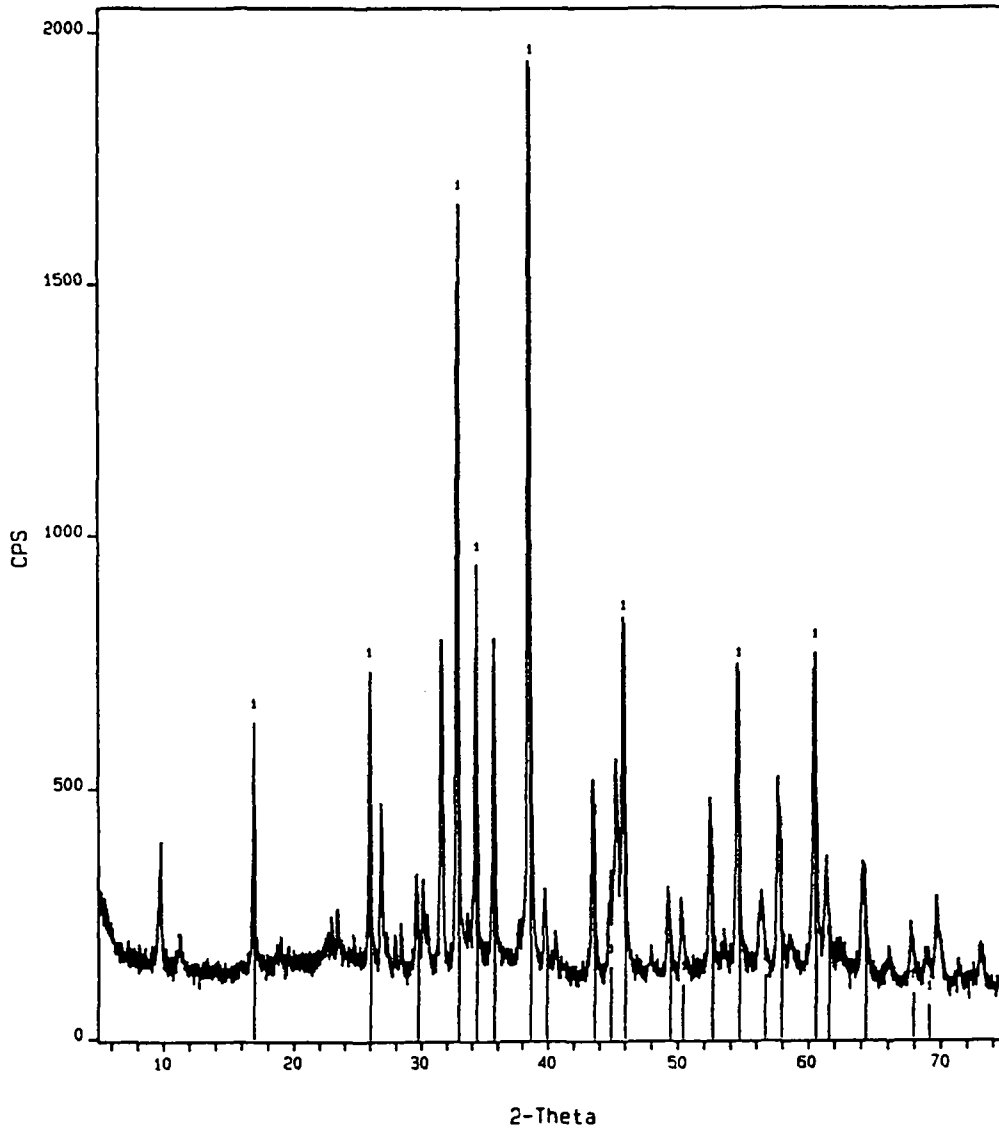
Figure 6-4. XRD results obtained from the unidentifiable 12- and 24-month-test corrosion products, anoxic brine tests. The vertical lines (labeled "1") correspond to the principal 12-month corrosion-product diffraction peaks; they are superimposed on the raw data obtained from the 24-month corrosion product. More than one compound may be present in each lot of corrosion product.

Knowledge of the plenum volume in the test containers, the test temperature, the container pressure at the end of a test, and the final gas composition permits a calculation to be made of the moles of H_2 present in a test container at the conclusion of a test. This can be compared with the amount of steel reacted, determined by a gravimetric analysis of the specimens exposed to the test medium. The results of this analysis for the anoxic brine seal-welded container tests are shown in Table 6-4.[a] The results from the two duplicate test containers are averaged in the table. H_2 was considered to be insoluble in the brine for the purpose of these calculations.

Table 6-4. Comparison of Moles of H_2 Formed (by pressure increase) with Moles of Fe Reacted (by specimen weight change), Anoxic Brine Tests

Test Duration, Months	Average Moles Fe Reacted, mol/m^2 - yr	Average Moles H$_2$ Formed, mol/m^2 - yr	Moles H$_2$/ Moles Fe
3	0.276	0.190	0.69
6	0.243	0.209	0.86
12	0.173	0.156	0.90
24	0.140	0.141	1.0

The tabulated data show that for tests of >6 months duration the agreement between container pressure increase and gravimetric data are very good. This finding validates the use of pressure-time data as a means of describing the rate at which hydrogen is produced per unit area of steel exposed to the simulated WIPP environment, as it ties observed pressure to actual metal reacted. This finding supports the use of pressure-time curve slopes (tangents) to estimate the rate at which H_2 is being generated as a f(t), as long as the slopes are not determined at short (<6 month) test times where they will under-represent the rate of Fe reaction.

The improvement in agreement in molar equivalence between H_2 formed and Fe reacted with increasing test time can be explained by a *relatively* greater loss of corrosion-product H_2 in the short-term tests, due to

[a] The calculations involved in arriving at the values presented in Table 6-4 are shown in Appendix C.

- H_2 reactions with iron oxides on the specimen surfaces

- H_2 reactions with other oxides or residual O_2, present in the system

- H_2 absorption by the steel and the container walls

- some H_2 solution in the brine phase.

Pressure-time data[a] from the long-term tests and from the longest-term portions of the long-term tests are believed to have the most credibility in repository-behavior modeling because long-term tests would be more relevant to the time scales used in repository performance assessment. Thus, from Figure 6-1, the relatively low rate of H_2 evolution over the last 12 months of the 24-month test, amounting to 0.71 μm/yr metal penetration or 0.10 mol H_2/m^2 steel-yr,[b] would be considered the best basis for estimating H_2 generation by steel in the WIPP repository of the data bases available, *assuming* that the steel in the repository is totally immersed in brine. Over long periods of time, this rate would be expected to continually decrease if the environment were maintained static and unrefreshed. The rate of 0.71 μm/yr is one-fourth to one-half the H_2-generation rates determined by Simpson and Schenk (1989) in relatively dilute (800 to 8000 ppm Cl⁻) NaCl brines at 50°C. This is considered to be good agreement, considering the relatively long duration of the PNL tests and the difference in test temperatures between the two investigations.

6.1.1.2 BRINE/CO₂

The brine/CO_2 tests were intended to provide information on the corrosion and gas-generation proclivity of low-carbon steel in the presence of Brine A and CO_2. The presence of CO_2 in the WIPP at significant fugacities is considered to be a distinct possibility because it is an expected byproduct of the microbially mediated degradation of cellulosic materials and other organic materials that will presumably be disposed of in the WIPP in large quantities.

---

[a] This statement is not meant to imply that gas-generation estimates based on container pressure are superior to those based on gravimetric data, as the equivalence of the two methods has been demonstrated (Table 6-4). The pressure-time curves, however, provide a means of estimating gas-generation (or corrosion) rates as a f(t) over the course of a test, something the gravimetric data do not permit.

[b] Obtained from the final slope of the 24-month curve, Figure 6-1.

Two types of brine/CO_2 experiments were performed: experiments in which CO_2 was present in the test containers in quantities so large that its complete consumption was not possible (the "excess-CO_2" tests); and tests in which the quantities of CO_2 added to the test containers were controlled so as to permit the essentially complete consumption of the CO_2 in some of the tests, but not in others (the "controlled-CO_2-addition" tests). These tests will be discussed separately in the following subsections.

Excess-CO_2 Tests

The excess-CO_2 tests were intended to provide information on the corrosion and gas-generation characteristics of low-carbon steel in the presence of Brine A and excess CO_2. The brine/CO_2 immersed-specimen testing regimen includes test containers 3, 4; 11, 12; 19, 20; and 27, 28. The brine/CO_2 vapor-phase-specimen testing regimen includes containers 7, 8; 15, 16; 23, 24; and 31, 32. Proximate identification numbers (e.g., 3, 4) signify duplicate tests.

In the immersed-specimen tests the CO_2 was added to the test containers at an initial hypothetical starting pressure of ~155 psig (~170 psia, or ~12 atm). This starting pressure is termed "hypothetical" because, in general, equilibration between the CO_2 present in the plenum of the test container and CO_2 present in the brine was not achieved for several days after test initiation, in spite of the fact that each container was agitated (by hand-shaking) for a period of 10 to 15 min after addition of the final CO_2 charge. (The containers with specimens exposed only to CO_2/H_2O vapor were not purposefully shaken to effect CO_2 dissolution in the brine. Any agitation that these containers received was inadvertent.) Though this agitation effected a fairly good dissolution of the CO_2 in the brine phase, for the first few days of each test the pressure tended to decrease as gaseous CO_2 continued to dissolve in the brine. The amount of CO_2 added to these test containers was determined both by knowledge of the gas added to the plenum of each container and by weighing each test container after the gas addition on a balance sensitive to ±1 g. The two months showed good agreement. The average quantity of CO_2 added to each of the immersed-specimen test containers was 19.3 g, or 0.44 mol. As the average steel area in each test container in this series of tests was 0.604 m², the initial CO_2 charge in each test container was equivalent to 0.73 mol per square meter of steel in an $FeCO_3$-forming reaction.

The Henry's Law coefficient, S, for CO_2 in equilibrium with Brine A

$$S = \frac{\text{moles } CO_2 \text{ in solution}}{\text{pressure } CO_2, \text{ atm}} \tag{34}$$

was experimentally determined to be equal to 0.012 at 20°C, and 0.010 at 30°C. During a 30°C test, assuming equilibrium conditions, the major portion of the CO_2 ($\sim 65\%$) would be expected to be present in the gas phase with the remainder ($\sim 35\%$) dissolved in the brine. The H_2 generated by the corrosion reaction, on the other hand, would collect in the plenum region of the test container only, as it is essentially insoluble in the brine phase. As the CO_2 is consumed by the corrosion reaction [Equation (7)], the pressure will tend to decrease in the plenum, but not to the extent that the pressure increases due to H_2 formation because the brine phase will continually supply a fraction of the CO_2 involved in the corrosion reaction. Thus, a pressure buildup in the plenum will be observed on the pressure gauge as the reaction proceeds, even though Equation (7) states that a mole of CO_2 will be consumed for each mole of H_2 formed.

The pressure-time curves for the excess-CO_2 tests are presented in Figure 6-5. The corresponding raw data are presented in Appendix A. The starting pressure of the immersed-specimen tests is given as 155 psig in the figure; the pressure variations that occurred during the first few days of the tests are not shown for clarity. The actual starting pressures of the vapor-phase-exposure tests are those given in the figure.

All of the container pressures of the duplicate tests have been averaged, so that the curves of Figure 6-5 actually represent data obtained from 16 test containers. The close agreement in pressure between duplicate containers, typically within 2 to 3 psi, justifies this averaging. An exception to this close agreement was the pressure data from the 6-month immersed-specimen tests, where the pressure disparity between the two tests (containers 11 and 12) attained a value of 8 psi during the fourth month of the test and 10 psi during the last two months (the highest system pressure was associated with container 11). In spite of this relatively large disparity between the two test containers, the data were averaged to produce the single curve shown for simplicity of presentation.
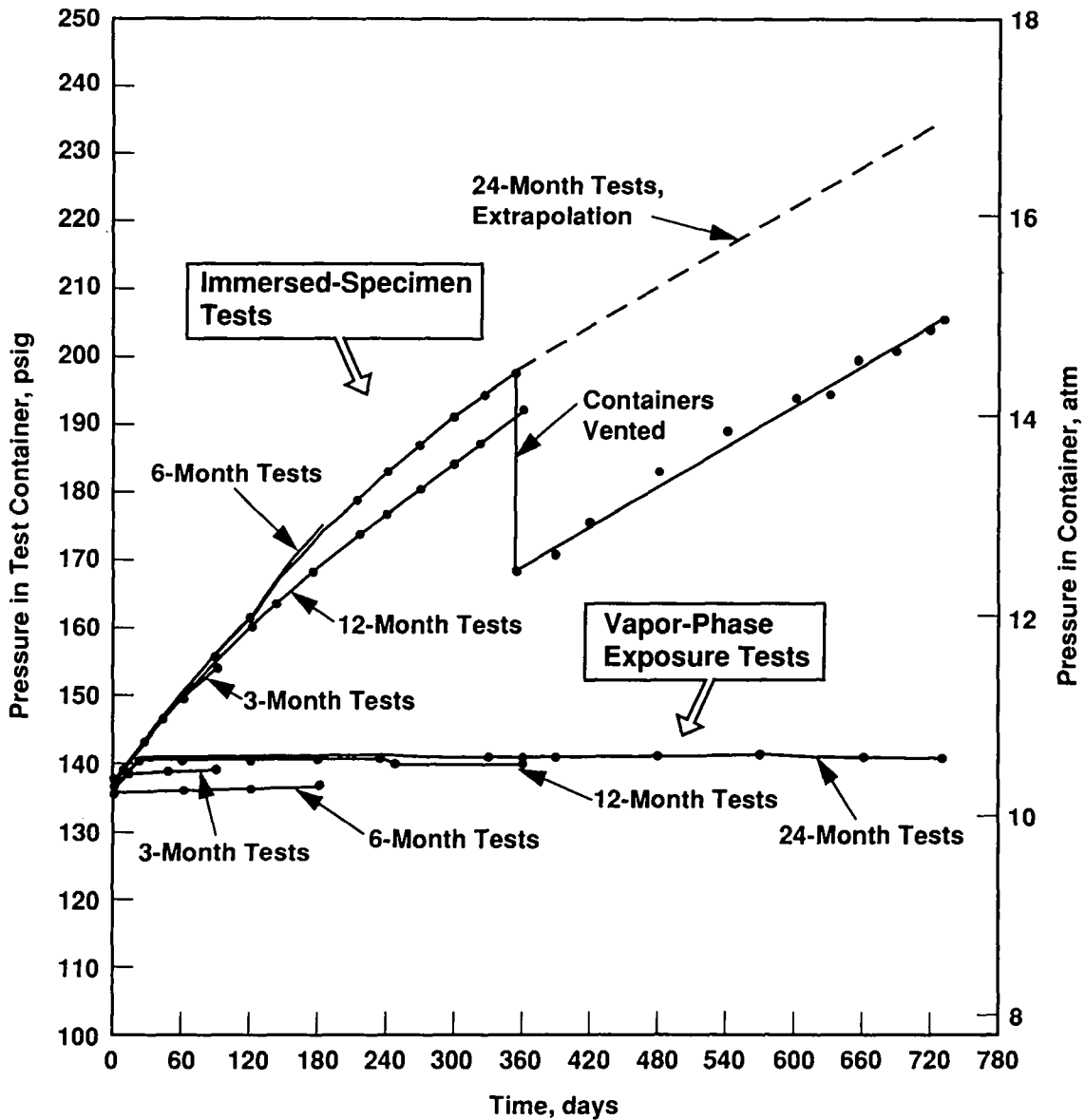
Figure 6-5. Pressure-time curves, low-carbon steel/brine-CO_2 tests. Each curve represents two (duplicate) tests.

The curves of Figure 6-5 show generally good agreement. The immersed-specimen tests are characterized by a rapid increase in pressure for a period of about 100 days, followed by a period in which the specimens appear to have become totally non-reacting (passivated).

An analysis of the gas samples taken from the containers just before they were opened is presented in Table 6-5. The analyses confirm that the pressure increase observed in the containers was due to corrosion-product H_2. Though not as good as that evidenced in the anoxic-brine tests, the consistency in the composition of gas generated between the duplicate immersed-specimen test containers is observable in the tabulated data. A significant unexplained disparity exists between the two 6-month test containers; container 11 shows a significantly higher H_2 generation rate than container 12. The difference in the pressure-time curves in the 6-month tests (as much as 10 psi) has already been alluded to. Significant differences are also evident between the H_2 contents of the vapor-exposure containers. As in the case of the anoxic brine (brine/N_2) tests, this is attributed to the varying test specimen surface area splashed by brine from one test container to another.

Table 6-5. Composition of Gas at Conclusion of Test, Brine/CO_2 Tests. Each tabulated value is average of two analyses. Results are given in vol% (mol%).

Specie	Immersed-Specimen Tests				Vapor-Phase-Exposure Tests			
	Test Numbers				Test Numbers			
	3-month	6-month	12-month	24-month	3-month	6-month	12-month	24-month
	3/4[a]	11/12	19/20	27/28	7/8	15/16	23/24	31/32
CO_2	51.1	28.0	40.0	41.3	98.8	97.4	98.6	98.5
	50.8	35.6	43.7	38.4	98.9	97.5	98.4	97.7
H_2	47.7	71.1	59.0	58.0	0.12	1.65	0.25	0.48
	47.9	63.4	64.4	61.0	0.12	1.62	0.48	1.25
He	0.13	0.11	0.05	0.09	0.02	0.25	0.22	0.24
	0.27	0.27	0.05	0.07	0.02	0.30	0.24	0.27
N_2	1.08	0.79	0.90	0.63	1.08	0.72	0.92	0.76
	1.01	0.83	0.85	0.57	0.98	0.63	0.91	0.81
O_2	<0.1, in all tests							

[a] 3/4, 11/12, etc. indicates that tests numbered 3 and 4 are duplicate tests, 11 and 12 are duplicate tests, etc. In the table, the average of two separate gas analyses for test 3 is over the average of two separate gas analyses for 4, the average of two separate gas analyses for test 11 is over the average of two separate gas analyses for 12, etc. In all cases the two separate analyses made on gas samples from one container showed excellent agreement.

The brine/CO_2 corrosion rate data are summarized in Table 6-6. The corrosion rates of Table 6-6 are far lower than the corrosion rates found by other investigators who used only short-term tests (see Section 4.2.3.2 of this report). All of the individual-specimen data from the immersed-specimen tests with CO_2 overpressure are shown in Appendix B-3; data from the vapor-phase-exposure tests are shown in Appendix B-4.

Table 6-6. Summary of Corrosion-Rate Data, Immersed Specimens, Brine/CO_2 Tests. Penetration rate means and standard deviations are presented. Each penetration rate value in the columns labeled J, K, L, and M represents an average of five specimens; the sixth specimen of each lot was reserved for surface analysis/archive. Penetration rate is expressed in μm/yr.

Test Duration, Months	Test Containers	Steel Lot and Penetration Rate,[a] μm/yr				
		J	K	L	M	All Lots
3	3, 4	12.7±3.1	9.59±1.02	5.29±0.85	7.41±2.43	8.76±3.44
6	11, 12	8.47±1.91	7.91±2.50	3.82±0.74	5.00±0.90	6.31±2.54
12	19, 20	3.68±0.70	3.58±0.78	1.72±0.20	2.69±2.61	2.91±1.00
24	27, 28	1.63±0.34	1.85±0.43	1.12±0.49	1.26±0.20	1.46±0.47

[a] To convert from a penetration rate expressed in μm/yr to moles Fe reacted /m^2 - yr, multiply the penetration rate by 0.141 mol/μm - m^2.

Unlike the corrosion results obtained from the anoxic brine tests (summarized in Table 6-2), the four lots of steel immersed in the brine/CO_2 environment showed a significant difference in corrosion rate from lot to lot of steel. The corrosion rates of the higher-carbon lots of steel (lots L and M) average ~60% of the corrosion rates exhibited by the low-carbon lots (lots J and K).[a] Also, in comparison with the anoxic brine data, the specimen-to-specimen variability of the brine/CO_2 test is much greater. This is believed to be at least partly caused by the much greater difficulty encountered in stripping the $FeCO_3$ corrosion product films from the brine/CO_2 test specimens. For example, the immersion time for stripping a specimen in the inhibited HCl stripping solution varied from ~ 1 min

[a] This behavior reverses at high CO_2 overpressures. Possible reasons for the corrosion dependence exhibited is discussed in Section 6.1.2.3.

for the anoxic brine test to 6 to 7 min for the brine/CO_2) tests. Accordingly, there was a possibility of 1) over-etching the steel substrate while attempting to remove the last traces of corrosion product, or 2) leaving small quantities of corrosion product unremoved, even after long exposure times.

Knowledge of the plenum volume in the test containers, the test temperature, the container pressure at the end of a test, and the final gas composition permits a calculation to be made of the moles of H_2 present in a test container at the conclusion of a test. This can be compared with the amount of steel reacted, determined by a gravimetric analysis of the specimens exposed to the test medium. The results of this analysis for the brine/CO_2 seal-welded container tests are shown in Table 6-7. (The calculations are presented in Appendix C.)

Table 6-7. Comparison of Moles of H_2 Formed (gas analysis) with Moles of Fe Reacted (by specimen weight change), Brine/CO_2 Tests

Test Duration, Months	Average Moles Fe Reacted, $mol/m^2 - yr$	Average Moles H_2 Formed, $mol/m^2 - yr$	$\dfrac{\text{Moles } H_2}{\text{Moles Fe}}$
3	1.24	1.11	0.89
6	0.890	0.877	0.99
12	0.410	0.386	0.94
24	0.206	0.186	0.90

The agreement between moles H_2 formed and moles Fe reacted is good throughout the test, validating the proposed reaction given by Equation (7). Even in the case of the long-term tests, however, the moles of H_2 formed are not quite equivalent to the moles Fe lost from the test specimens, as was the case in the anoxic brine tests (Table 6-4). A possible reason for this is the difficulty of stripping the Fe CO_3 from the steel specimens prior to final weighing, which can lead to some over-etching of the steel and an exaggeration of the metal apparently lost to the corrosion reaction.

The corrosion rates are obviously decreasing strongly with time, in accordance with the specimen-passivation information provided by the pressure-time curves (Figure 6-5). A comparison of the 12- and 24-month corrosion rates in Table 6-6 shows that no corrosion occurred in the last 12 months of the 24-month test, suggesting eventual complete passivation of the steel in the test

environment. XRD analyses of the corrosion-product films formed on these specimens showed them to be composed of siderite, $FeCO_3$, as expected. No $CaCO_3$ was observed by XRD. The ability of siderite to passivate a steel substrate, especially in stagnant solutions in the presence of high fugacities of CO_2, has been reported by a number of investigators, though the passivating ability generally has been reported to be most effective at temperatures $>60\,^{\circ}C$ (see Section 4.2 of this report).

The amount of CO_2 required to passivate the steel under the test conditions employed can be estimated from the data of Table 6-6 and the information provided in Figure 6-5. From the figure, the steel has apparently passivated at a time period <6 months. If it is assumed that no reaction has taken place on any specimen after 6 months, and that the corrosion reaction can be expressed by Equation (7), then the amount of Fe lost to corrosion during the 6-, 12- and 24-month tests can be averaged to determine the amount of CO_2 (and Fe) contributing to the corrosion reaction and the attainment of the passivated state. From Table 6-6 the average Fe loss to corrosion during the 6-month test was 6.31 μm/yr x 1/2 yr, or 3.16 μm; during the 12-month test it was 2.91 μm; and during the 24-month test it was 1.46 μm/yr x 2 yr, or 2.92 μm. The average penetration over these three tests was therefore 3.00 μm prior to passivation. A penetration of 1 μm over 1 m^2 is equivalent to 1 cm^3 (7.86 g) Fe/μm - m^2, or 0.141 mol/μm - m^2. The 3.00 μm penetration observed is therefore equivalent to 3.00 μm x 0.141 mol/μm - m^2, or 0.42 mol CO_2 (or Fe)/m^2 of steel required for passivation.

The post-test appearance of the steel specimens is shown in Figure 6-6 (immersed specimens, 24 months exposure) and Figure 6-7 (vapor-phase exposure specimens, 24 months exposure). The dark gray, adherent corrosion product observed on the specimens is $FeCO_3$.

The post-test compositions of the brines obtained from the test containers after the 6-, 12- and 24-month tests are compared with the starting brine composition in Table 6-8. The brines from the immersed-specimen tests differ significantly from the starting brine composition, in that the pH is considerably lower and the Fe composition has attained a significant value. In addition, the Ca concentration of the brine has been reduced significantly, though no evidence of Ca compounds was found in the XRD investigations of the corrosion product layer. [The reduction of Ca concentration in the brine is consistent with the observations of Murata et al. (1983), who found $CaCO_3$ in the $FeCO_3$ layers formed on steels corroding in CO_2-saturated brines containing Ca.]
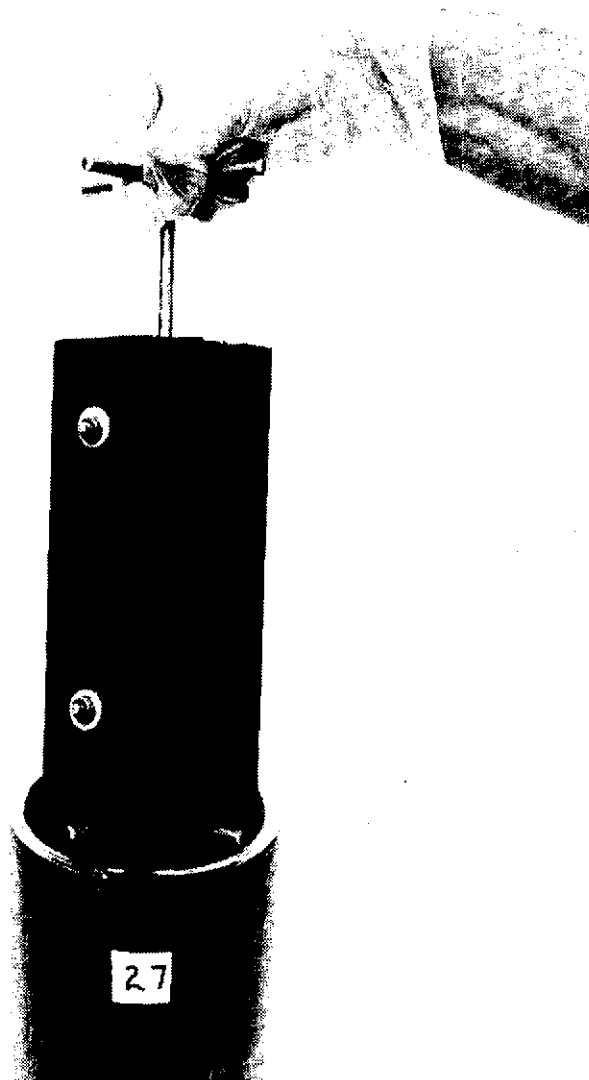
Figure 6-6.   Post-test appearance of steel specimens, immersed, 24-month brine/CO₂ tests.
Specimens are coated with an adherent black FeCO₃ corrosion product.

The pH and Fe concentration in the brine shown in Table 6-8 cannot be taken as representative of the conditions existing within the test container during an actual test, as CO_2 escapes from the system as soon as the container is opened, and Fe^{2+} oxidizes rapidly and precipitates from solution as the
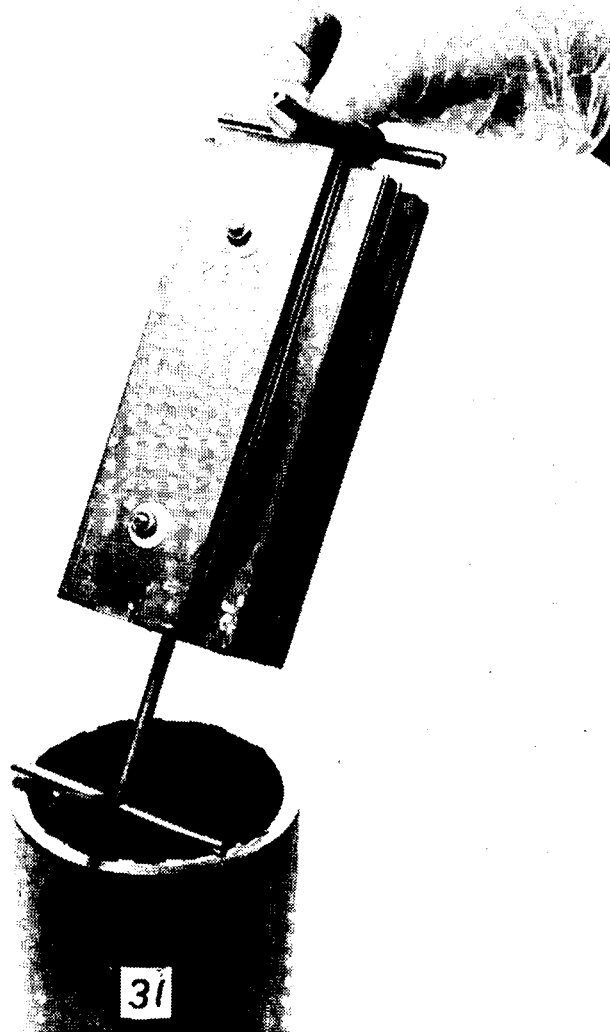
Figure 6-7. Post-test appearance of steel specimens, vapor-phase exposure, 24-month brine/CO_2 tests. No significant corrosion reaction is evident except where brine has contacted the bottoms of the specimens.

solution comes in contact with air. Also, the concentration of Fe^{2+} reported as being in solution in the CO_2/brine tests may actually be high, as a fine particulate suspension may be contributing to the concentration values reported.

Table 6-8. Results of Brine Analyses, Brine/CO$_2$ Seal-Welded-Container Tests. Comparison of brine compositions after 6-, 12- and 24-month tests is made with original brine composition. Concentration given in mg/L.

Specie	Brine A	Test Duration					
		6 months		12 months		24 months	
		Imm.[a]	Vapor[b]	Imm.[c]	Vapor[d]	Imm.[e]	Vapor[f]
Na	38,300	42,600	41,000	40,300	40,500	40,500	40,300
Mg	35,700	35,500	34,900	34,500	35,000	33,200	33,500
K	29,500	30,600	29,900	29,800	30,200	30,000	30,000
Ca	560	240	590	270	600	230	567
B	230	220	230	230	240	220	226
Fe	<10	1,480	5	1,230	<10	1,320	<10
Cl	190,000	196,000	196,000	191,000	189,000	194,000	188,000
SO$_4$	4,070	4,230	4,240	3,900	4,200	4,540	3,920
pH	6.7	5.1	7.1	3.4	7:3	5.9	6.9

[a] Test container 12; [b] 16; [c] 19; [d] 23; [e] 27; [f] 31.

Controlled-CO$_2$-Addition Tests

When the activity of CO$_2$ dissolved in Brine A is increased, two opposing effects are manifested: the brine becomes a more aggressive corrodant toward steel due to effects already discussed [Equations (1) through (7)]; and the presence of CO$_2$ tends to stop the reaction through the formation of a stable FeCO$_3$ layer. The controlled-CO$_2$-addition tests were intended to provide information on the amount of CO$_2$ required/unit area of steel to attain a passivated state, such as was attained in the excess-CO$_2$ tests after CO$_2$ had reacted with the steel to the extent of ~0.42 mol CO$_2$/m^2 steel.

The controlled-CO$_2$-addition tests comprised test containers 33 through 38. The test conditions are summarized in Table 6-9. A N$_2$ addition was made to test containers 36 through 38 so that the pressure gauges would provide a positive reading.

Table 6-9. Summary of Test Conditions, Controlled-CO_2-Addition Tests

Test Container	Initial CO_2 Charge Pressure, atm (psia)[a]		N_2 Pressure, atm (psia)	Mol CO_2/m^2 Steel[b]
33	7.8	(115)	no N_2	0.32
34	3.8	(56)	no N_2	0.16
35	1.5	(22)	no N_2	0.063
36	0.75	(11)	2.0 (30)	0.032
37	0.39	(5.7)	2.0 (30)	0.016
38	0	(0)	3.1 (45)	0.0

[a] Assumes plenum = 0.634 L, T = 30°C, no CO_2 dissolution in brine at the time of CO_2 charging.

[b] Total area of steel specimens in each test container = 0.629 m^2.

The highest ratio of mol CO_2/m^2 steel (0.32) employed in the test series was intended to approximate the 0.42 mol/m^2 value causing passivation in the excess-CO_2 tests (Table 6-6). Lesser quantities of CO_2 were also used to determine if passivation, or temporary passivation, would develop under conditions of relatively low concentrations of CO_2.

The pressure-time curves for the controlled-CO_2-addition tests are shown in Figure 6-8. It is apparent that at least some degree of passivity has been attained in the test containers with the maximum amount of CO_2 added (containers 33 and 34). Though the pressure-time curves for these two containers appear to attain a near-zero slope after a time period of ~ 150 days, the curves indicate some degree of reaction even to the maximum test duration shown in the figure. This test will be allowed to continue so that the ability of the steel to passivate completely under the test conditions can be more fully evaluated. A continual pressure increase was not observed in the excess-CO_2 tests after passivation of the specimens was achieved (see Figure 6-5 and Table 6-6).

The raw pressure-time data for the test containers 33 through 38 corresponding to the curves of Figure 6.8 are presented in Appendix A. The gravimetric data for the individual specimens will not be available until the study is concluded.

Symbol	Container	Mol CO_2/m^2 Steel
●	33	0.32
■	34	0.16
□	35	0.063
△	36	$0.032 + N_2$
▽	37	$0.016 + N_2$
○	38	$0.00\ (N_2\ only)$
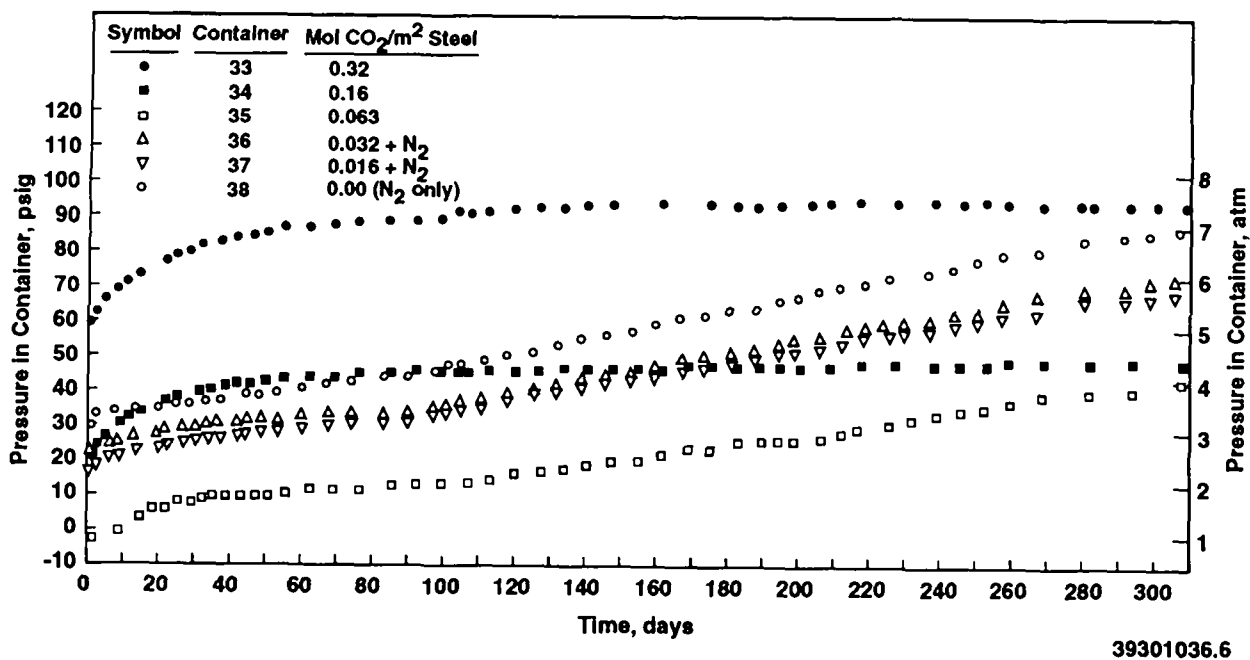
Figure 6-8. Pressure-time curves, controlled-CO_2-addition tests.

39301036.6

Assuming that all of the H_2 resulting from the corrosion reaction collects in the plenum of the test container, that all of the H_2 resulting from the corrosion reaction is accounted for, that passivation of the steel does not stop the corrosion reaction, and that the reaction

$$Fe + CO_2 + H_2O = FeCO_3 + H_2 \tag{35}$$
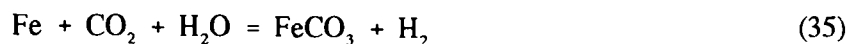
is the only H_2-producing reaction, then the reaction will stop when the H_2 pressure in the plenum equals the original starting CO_2 charge pressure (i.e., the CO_2 pressure in the container plenum before its dissolution in the brine).[a] The initial charge pressures are given in Table 6-9. From these data

---

[a] Strictly speaking, there will always be some CO_2 remaining unreacted, as equilibrium conditions [as given by the equilibrium constant of Equation (8)] require a residual CO_2 fugacity equal to $\sim 2 \times 10^{-4}\ f_{H2}$. In the practical terms of the present test, this CO_2 fugacity will not be sensed by the pressure gauges employed, nor will it affect the conclusions drawn in the subsequent discussion.

and associated assumptions it can be calculated that the reaction in container 33 has consumed 95% of the original CO_2 charge at 250 days, that the reaction in container 34 has consumed the equivalent of 110% of the original CO_2 charge at 250 days, and that the reaction in container 35 has consumed the equivalent of 220% of the original CO_2 charge at 250 days. Obviously, an $Fe-H_2O$ reaction is proceeding and producing H_2 in the latter two cases cited. The containers with less CO_2 than container 35 essentially behaved as though no CO_2 had been added at all, as their pressure-time curves closely simulate that of the CO_2-free control, container 38.

The pressure-time curve of container 35 appeared to temporarily passivate in the time period 30-50 days. If it is assumed as before that H_2 generated is equivalent to CO_2 consumed, at 50 days the initial CO_2 charge has been 110% consumed. This good agreement between apparent passivation and CO_2 consumption suggests that a state of imperfect passivation was produced by the available CO_2, perhaps produced by a siderite layer containing defects that could not remain "healed" due to the absence of a continuing supply of CO_2. The defective film then eventually lost its protectiveness entirely, and permitted the competing $Fe-H_2O$ reaction to proceed at a normal rate, as in the case of the Fe-anoxic brine (brine/N_2) tests or the case of container 38.

The controlled-CO_2-addition tests are still in progress, so the final assessment of the results of the test cannot yet be made. The test results obtained to date suggest, however, that the best passivation obtained under the conditions used in the controlled-CO_2-addition study is still questionable and does not yet evoke confidence as a true, stable state of corrosion prohibition.

6.1.1.3 BRINE/H_2S

The brine/H_2S tests were intended to provide information on the corrosion and gas generation proclivity of low-carbon steel in the presence of Brine A and H_2S. Like CO_2, H_2S is a potential byproduct of microbial activity through sulfate reduction in the WIPP, so its presence in the site environment is considered to be a credible possibility. As has been shown [Equations (17) and (18)], the thermodynamic tendency for reaction of Fe with H_2S is strong. There is a possibility, however, of passivating steel in the presence of H_2S at sufficient activity to form the high sulfides, such as pyrite (see Section 4.3 of this report).

The brine/H$_2$S tests of low-carbon steel were performed in test containers 40, 41, 42, and 43. In replicate test containers 40 and 41, the specimens were exposed under immersed conditions; in test containers 42 and 43 the specimens were suspended in the vapor phase over Brine A. The method of racking the specimens in test containers was similar to that used in the anoxic brine (brine/N$_2$) and the CO$_2$-brine tests previously described, and the amount of brine used in each test container was essentially the same as that used in the previous tests: 1.4 L in the immersed-specimen tests, 250 mL in the vapor-phase tests. The area of steel specimens present in each test container was 0.497 m^2.

The partial pressure of H$_2$S in these initial Fe/H$_2$S tests was purposefully chosen to be a high value relative to H$_2$S concentrations expected in the WIPP. An arbitrary (equilibrium) partial pressure of 5 atm was selected for these tests. For H$_2$S, the gas-charging method employed was similar to that used for N$_2$ and CO$_2$ in tests previously described, in that the H$_2$S gas was charged into the plenum of a previously evacuated test container with both steel specimens and Brine A already in place.

The H$_2$S gas dissolved much more rapidly into the brine than did the CO$_2$. The Henry's Law coefficient, S, for H$_2$S was determined to be

$$S = 0.050 \text{ mol/atm-L} \tag{36}$$

at the gas-charging temperature of ~25°C. As a consequence of the high solubility of the H$_2$S in Brine A, the major amount of the H$_2$S charged into the immersed-specimen test containers is dissolved in the brine phase.[a]

The pressure-time curves for tests 40 through 43 are shown in Figure 6-9. After an initial period of activity lasting about 6 days, the specimens appear to be essentially nonreactive in the brine/H$_2$S environment. During the initial period of activity the immersed specimens appeared to generate corrosion-product H$_2$. The vapor-phase tests appeared to simply show the effect of continued H$_2$S dissolution in the brine phase present (the vapor-phase test containers were not shaken after gas addition to expedite equilibration of gas between vapor space and brine).

---

[a] Because H$_2$S shows significant non-ideal behavior, even at pressures as low as 5 atm, a van der Waals relationship was used to determine the relationship between moles H$_2$S and pressure of H$_2$S throughout all of the H$_2$S investigations (Lange's Handbook, 1985).
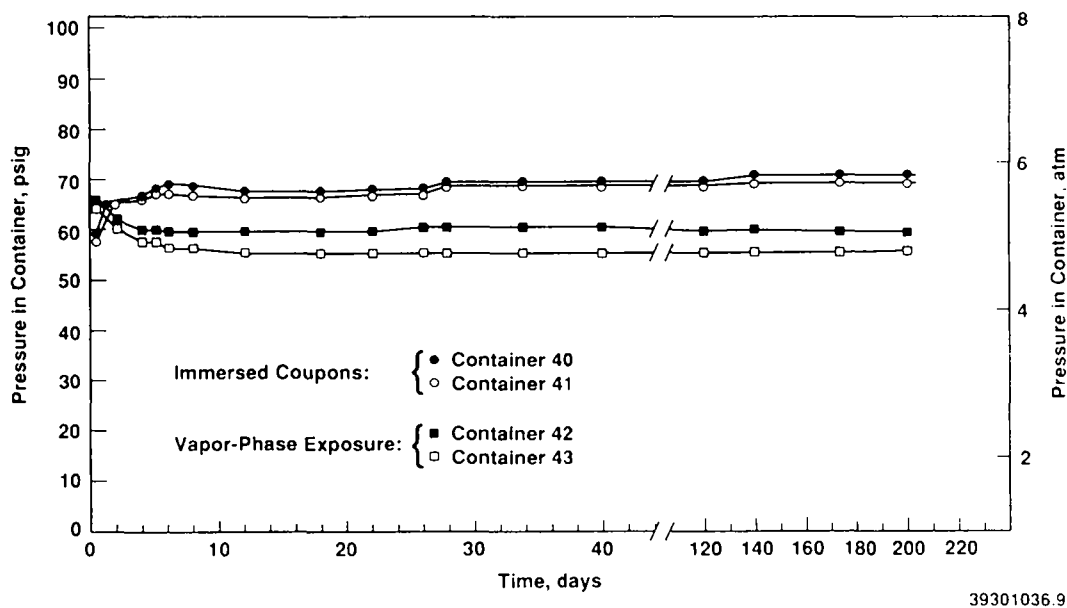
Figure 6-9. Pressure-time curves, Fe-H₂S tests, test containers 40-43.

The lack of continued reaction after a time period of about 6 days in the immersed-specimen test condition suggests that pyrite or other high sulfide had rapidly formed on the specimen surfaces and stopped further reaction from taking place. This could be considered at least partially consistent with the observations of other investigators (see Section 4.3 of this report), in that higher sulfides are highly passivating, and high pressures of H_2S are consistent with formation of higher sulfides. However, other investigators (such as Meyer et al., 1958) have found that 1 atm H_2S is not readily passivating, in that nonprotective lower sulfides form under these conditions. The preliminary results of the present tests suggest that 5 atm partial pressure is passivating even though 1 atm partial pressure H_2S may not be.

6.1.2 High-Pressure Autoclave Tests

The seal-welded container tests were charged with overpressure gas to equilibrium pressures in the range of 5 to 12 atm. These pressures are, of course, low by comparison with total pressure expected when the WIPP approaches lithostatic pressure. High-pressure autoclave tests were conducted to gain insights into the effect of high CO_2, H_2 and N_2 pressures on the reaction kinetics, with

equilibrium pressures in the range 36 to 73 atm. The high-pressure testing regimen comprised tests AUT-1, -2, -3, -4, -7, and -8 (Table 3-1). In general, the steel specimens were prepared pre-test and examined post-test in the same manner as that used for the seal-welded-container tests. The specimen area per test was much smaller in the autoclave tests because emphasis was placed on gravimetric analysis of the specimens rather than following the pressure as a function of time. This basic difference in test approach is based on the fact that an autoclave system cannot be relied upon to be (essentially) leak free for very long periods of time, even though this is sometimes observed to be the case in practice.

6.1.2.1 HIGH H_2 PRESSURE TESTS

Tests AUT-1, AUT-3, and AUT-4 were initiated to determine to what extent, if any, high H_2 pressures inhibit the progress of the Fe-H_2O (Brine A) reaction. The steel test specimens, five specimens of lot J and five of lot K, were completely immersed in Brine A in this test series. A summary of these tests, extending the data of Table 3-1, is presented in Table 6-10. The individual specimen-corrosion data for tests AUT-1, AUT-3, and AUT-4 are tabulated in Appendices B-5, B-6, and B-7, respectively.

At the conclusion of the high H_2 pressure tests, the specimens were clean and shiny in appearance. A small amount of corrosion product was present in the autoclave at the conclusion of each test. XRD analysis of the dark gray particulate corrosion-product residues left after the 6-month test (AUT-1) showed evidence of reevesite, $(Ni,Fe)_6Fe_2(CO_3)(OH)_{16} \cdot 4H_2O$, nickel iron carbonate hydroxide hydrate, with perhaps as many as two additional unidentifiable phases. Because of the small amount of corrosion product recovered and because of the nickel content exhibited by the identifiable phase (suggesting a possible autoclave-wall contribution),[a] little significance was attached to the XRD results obtained. Chemical analysis of the corrosion product revealed a significant Mg presence

---

[a] The autoclaves used in these studies were made of Ni-Cr-Mo alloys.

Table 6-10. Summary of Test Conditions, H_2-Overpressure Tests AUT-1, AUT-3, and AUT-4. Number of specimens of each material lot: 5. Test temperature: 30°C.

Test	Initial Mean H_2 Overpressure	Brine Volume, L	Total Specimen Area, m^2	Test Duration, Months
AUT-1	1030 psia (70 atm)	2.79	0.199	6
AUT-3	515 psia (35 atm)	2.79	0.199	12
AUT-4	1010 psia (69 atm)	2.78	0.198	12

(15%) and a Ni concentration of 4%. The high Mg concentration suggests that the portion of the corrosion product unidentifiable by XRD could be of the form $Fe,Mg(OH)_2$, a corrosion product found in another study where steel was allowed to react with a high-Mg brine at elevated temperatures (Westerman et al., 1987).

The gravimetrically determined corrosion rates obtained from the high H_2 pressure tests are presented in Table 6-11. The corrosion rates are compared in the table with results obtained from seal-welded corrosion tests of 6- and 12-month test durations having a N_2 overpressure, to aid in evaluating the effect of the H_2 overpressure on the reaction kinetics.

The data of Table 6-11 show that presence of a high H_2 pressure can significantly inhibit the corrosion rate of low-carbon steels in Brine A, relative to tests having an N_2 overpressure only. A H_2-induced factor of five reduction in corrosion rate, at the same test times, is evident from the table when the autoclave and the N_2/immersed seal-welded-container tests are compared. (Reduction in steel corrosion rate in a high-Mg-brine environment by a H_2 overpressure at 150°C has been reported previously by Westerman et al., 1987.)

Doubling the H_2 pressure from 35 to 69 atm (Tests AUT-3 and AUT-4) did not exert an inhibiting effect on the corrosion rate beyond that observed at the lower pressure. It is believed that this is due to the rate-decreasing effect of the additional H_2 pressure being effectively counterbalanced by the rate-increasing effect of the additional system pressure. This pressure-induced increase in

Table 6-11. Corrosion Rates of Steel Specimens in High H_2 Pressure Tests Compared with Corrosion Rates in Brine/N_2 Seal-Welded Container Tests

Test	Corrosion Rate, μm/yr[a]	
	Steel Lot J	Steel Lot K
AUT-1 70 atm H_2, 6 months	0.32±0.01	0.40±0.04
AUT-3 35 atm H_2, 12 months	0.20±0.01	0.25±0.02
AUT-4 69 atm H_2, 12 months	0.20±0.01	0.27±0.03
Seal-Welded Container N_2/Immersed Tests, 10 atm N_2		
6-month test	1.61±0.07	1.65±0.37
12-month test	1.05±0.05	1.26±0.04

[a] Average linearized corrosion rate of all specimens of each material lot in each test, with standard deviation.

corrosion rate has been observed in other studies in which steel-brine systems were subjected to an overpressure of inert gas (Westerman et al., 1987), and will be discussed further in the next section of this report.

It is interesting to note that steel lot J corroded at a consistently lower rate than lot K in the H_2-overpressure studies, as it did in all of the N_2/immersed seal-welded container tests. Because the two steels are alike in composition and microstructure, no explanation can be offered for the observed corrosion differences on the basis of the available information.

6.1.2.2 HIGH N_2 PRESSURE TEST

The effect of high N_2 pressure on the reaction rate of steel in Brine A was investigated by determining the corrosion rate of low-carbon steel under a relatively high N_2 pressure. The test, designated AUT-2, was performed in a manner similar to that described for the high-pressure H_2 tests in the preceding section of this report. The initial N_2 pressure was 1070 psia (73 atm); the volume of the brine in the 4 L autoclave was 2.79 L; the total area of the steel specimens was 0.199 m^2. Five

specimens of steel lot J and five of lot K were exposed to the brine in the completely immersed condition. The test duration was 6 months. The individual-specimen data from test AUT-2 are presented in Appendix B-8.

The test specimens appeared clean and shiny when removed from the autoclave and were free of adherent corrosion products. The corrosion product, present in copious quantities compared to the H_2-overpressure tests, was found adhering to the specimen rack and the autoclave walls. It was of a cream-beige color when removed from the autoclave (with a spatula); upon exposure to the air it gradually turned a dark yellow-brown color. In texture and distribution it resembled the corrosion product associated with the N_2/immersed seal-welded-container tests.

A specimen of the corrosion product was analyzed by XRD within an hour of its being removed from the test autoclave. It proved to be unidentifiable. The diffraction pattern had the same characteristics as the unidentifiable patterns obtained from the N_2/immersed seal-welded container tests (see Section 6.1.1.1 of this report).

The chemical composition of the corrosion product was determined in an attempt to gain some insights into its nature. The analysis showed the cationic constituents of the corrosion product to be essentially Fe, with $\sim 12\%$ Mg. As in the case of the high H_2 pressure tests, this suggests a corrosion product of the form $Fe,Mg(OH)_2$. The averaged corrosion rates, determined gravimetrically using all of the 10 specimens included in the test, are shown in Table 6-12.

The N_2 overpressure substantially increased the corrosion rate over that observed in the seal-welded container test. This same phenomenon was observed in studies by Westerman et al. (1987), in steel-brine systems pressurized with Ar.

Apparently, that portion of the overall cathodic reaction

$$HOH + 1e = \frac{1}{2}H_2 + (OH)^-$$
(37)
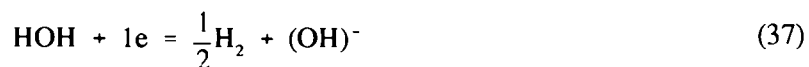
responsible for the actual rate control has associated with it an activated complex with a smaller net volume than the reactants it comprises. Increasing the total system pressure would cause this decrease in volume to decrease the activation energy required for its production and thereby cause an increase

Table 6-12. Corrosion Rates of Steel Specimens in High N_2 Pressure Tests Compared with Corrosion Rates in Brine/N_2 Seal-Welded Container Tests

Test	Corrosion Rate, $\mu m/yr^a$	
	Steel Lot J	Steel Lot K
AUT-2: 73 atm N_2, 6 months	2.76 ± 0.24	3.17 ± 0.04
Seal-Welded-Container, N_2/Immersed Test, 10 atm N_2, 6 months	1.61 ± 0.07	1.65 ± 0.37

a   Average linearized corrosion rate of all specimens included in category, with standard deviation.

in the cathodic reaction rate. Because either N_2 or H_2 could cause such an activation energy decrease, increasing a H_2 overpressure could decrease the reaction rate (back reaction tendency) while increasing the reaction rate by the mechanism just described, whereas under the same circumstances increasing the N_2 overpressure would be expected to increase only the reaction rate.

The foregoing explanation of the effects of system pressure on corrosion reaction rate is obviously highly qualitative and not capable of explaining the quantitative relationships between reaction inhibition by back-reaction and reaction promotion by system pressure. The reaction mechanisms involved, and the pressure dependence of the mechanisms, are not specifically known.

6.1.2.3 HIGH CO_2 PRESSURE TESTS

The dichotomy in CO_2 behavior toward steel, in which increasing the pressure of CO_2 increases the reactivity of the system while enhancing the ability of steel to passivate itself through formation of a relatively stable and impervious layer of $FeCO_3$, has already been described. The tendency of the $FeCO_3$ reaction product to dissolve in the test solution, and the fairly high Fe^{2+} concentrations associated with the terminal solubility of $FeCO_3$ in solutions having high CO_2 concentrations, complicates the prediction of corrosion rates and ultimate disposition of reaction products. The high CO_2 pressure

tests AUT-7 and AUT-8 were intended to further the understanding of the CO_2-steel system by providing steel corrosion data obtained at the relatively high CO_2 pressure of 36 atm.

Tests AUT-7 and AUT-8 utilized two 4L autoclaves. Each autoclave contained four specimens of each of the following steel lots: J, K, L, and M. The total area of the steel specimens was 0.095 m^2 in AUT-7, and 0.094 m^2 in AUT-8. Each autoclave was charged with 3.1 L of Brine A at the beginning of the test. The specimens were completely immersed in the brine phase throughout the tests. Test AUT-7 was terminated after 6 months; test AUT-8 has a projected test duration of 12 months. At the present time, only data from test AUT-7 are available. Individual-specimen data for test AUT-7 are presented in Appendix B-9 of this report.

Before opening the AUT-7 test autoclave for specimen examination, a complete analysis was made of the gas in the autoclave plenum. The gas was composed almost entirely of CO_2 (87.4%) and H_2 (12.3%). The pressure in the autoclave increased from 535 psia to 590 psia during the test as corrosion-product H_2 was generated.

The steel specimens were covered with a brownish-black, adherent corrosion product when they were removed from the autoclave. XRD analysis of the corrosion product showed that the corrosion product was closely approximated by $(Fe,Mn,Zn)CO_3$, "oligonite." The crystal structure of oligonite differs somewhat from the $FeCO_3$ (siderite) diffraction patterns obtained from specimens exposed in the past to CO_2-brine environments. To clarify the compositional question, especially the implication of the presence of Zn, a small amount of corrosion product was scraped from the surface of a specimen and its composition was determined by x-ray fluorescence analysis (XRFA). The composition of the corrosion product so determined is given below, in weight percent:

Fe	92.2
Ca	6.1
Mn	0.76
Ni	0.31
Zn	0.18
Cu	0.17

Other than Fe, the major constituent of the corrosion product is obviously Ca derived from the brine. The coprecipitation of Ca in the carbonate film has been mentioned previously (Section 6.1.1.2 of this report); its presence in the corrosion product film is therefore not surprising. The small amount of

Zn present belies the crystal structure nomenclature derived from the XRD database. It is most likely not a major crystal-structure-defining constituent in the corrosion product at the level of concentration observed. The source of Zn is not known; it may have been derived from the chemicals used to make up the brine. The relatively high level of Mn could have as its source the steel itself, as the steels exposed to the brine contain 0.3 to 0.8 wt% Mn.

Both the AUT-7 and the seal-welded container test environments (36 atm and 12 atm overpressure CO_2, respectively) are potentially highly reactive with unprotected steel. The pH values associated with these CO_2 pressures, in a 0.5 M NaCl medium, have been estimated to be 3.1 and 3.3, respectively (Crolet and Bonis, 1984).

The linearized corrosion rates over the 6-month test period of the specimens from test AUT-7 are presented in Table 6-13.

It is interesting to note that in test AUT-7 the lots of steel having a relatively low C content, J and K, corroded at significantly lower rates than steel lots L and M. This is contrary to the findings from the 3-, 6-, and 12-month seal-welded container tests with immersed specimens and an initial overpressure of 12 atm CO_2 (Section 6.1.1.2).

The corrosion rates of the specimens from test AUT-7 are considerably higher (by a factor of 4.7) than those determined in seal-welded container tests of 6-month duration originally charged with 12 atm CO_2, as listed in Table 6-6. However, the specimens in the seal-welded container tests passivated well before the end of the 6-month test exposure, with the corrosion process coming essentially to a complete stop at that time.

The complexities associated with the explanation and prediction of corrosion rates of specimens of nearly identical commercial steels has been long recognized. Cleary and Greene (1967) attempted to isolate the factors contributing to the corrosion of carbon steels by subjecting a large number of steel specimens having widely varying compositions and microstructures to an anoxic environment of dilute sulfuric acid at 30°C. By means of a multiple correlation analysis they were able to deduce the compositional and microstructural factors important to the corrosion of the steels. They found that C and P were particularly detrimental to corrosion resistance. Mn was beneficial to ~0.6 wt%; beyond 1.0 wt% it was detrimental. Si is also detrimental, whereas Cu is beneficial. If the environment

Table 6-13. Corrosion Rates of Steel Specimens, Test AUT-7

Sample Identification	Corrosion Rate, μm/yr	Average Corrosion Rate, μm/yr with Standard Deviation
J71	23.7	22.1 ± 1.8
J72	NA	
J73	20.1	
J74	22.5	
K71	23.6	24.9 ± 1.0
K72	25.2	
K73	25.0	
K74	25.8	
L71	34.4	36.0 ± 1.3
L72	37.6	
L73	35.9	
L74	36.3	
M71	37.8	35.8 ± 1.7
M72	35.8	
M73	35.8	
M74	33.7	

employed by Cleary and Greene can be considered analagous to the anoxic, CO_2-overpressured brine environments used in present study, the composition of the steels used (Table 5-11) gives possible insights into the pre-passivation corrosion behavior observed. In the seal-welded container tests, lots L and M showed the highest corrosion resistance. These alloys have a higher Mn content than lots J and K, and this factor could be responsible for the corrosion rate differential observed. At the higher CO_2 overpressures (higher H^+ activities) it is reasonable to expect the C content to have a more profound effect, because of its direct involvement in the cathodic H^+-reduction process, usually rate-limiting. One might therefore postulate that the Mn content of lots L and M could contribute to their corrosion resistance at low CO_2 overpressures, while their high C-content could be responsible for

their higher corrosion rates at higher CO_2 overpressures. These considerations apply only to the corrosion occurring prior to the formation of the passivating film. The processes associated with the film formation and the transport-inhibiting properties of the resulting film, ignored in the foregoing speculative analysis, could be more important than the considerations presented.

In order to gain some insight into the kinetics of the corrosion process taking place in test AUT-7 over the 6-month test period, an analysis was made of the pressure data from the autoclave pressure gauge. This is a necessarily limited analysis, because of the characteristics of the autoclave gauge (2000-psig range; smallest division 20 psi; reading accuracy approximately ± 5 psi); the fact that all autoclave systems can be expected to leak gas to some extent, especially low-molecular-weight gases such as H_2; and the fact that CO_2 is consumed as H_2 is generated, complicating the pressure-time analysis. Also, the non-ideal nature of CO_2 precludes use of the ideal gas law under all high-pressure conditions, if a reasonable degree of accuracy is expected, and the high solubility of CO_2 in the brine phase has to be considered in all gas-accounting analyses. In all of the computations it was assumed that the H_2 produced was insoluble in the brine phase, and that the Henry's Law constant governing the solubility of CO_2 in the brine phase had a value of 0.0102 mol/atm under all pressure conditions. The van der Waals equation was used to define the CO_2 pressure/volume/mole relationships. The pressure-time curves for tests AUT-7 and AUT-8 are presented in Figure 6-10.

The experimentally determined increase in total system pressure for test AUT-7 over the 6-month test duration was 55 psi. This value was in reasonably good agreement with the pressure increase expected if all of the Fe lost from the specimens (0.199 mole) was converted on an equimolar basis to H_2 (102 psia in the autoclave plenum region), and if the corresponding CO_2 pressure drop in the autoclave (44 psi) was subtracted from this H_2 pressure (102 psi - 44 psi = 58 psi). This agreement gives assurance that the autoclave was extremely well sealed and that the pressure-time data of Figure 6-10 have a strong measure of credibility. Not surprisingly, in spite of this good pressure agreement, some of the theoretical H_2 is not accounted for, as evidenced by comparing the CO_2/H_2 ratio from the gas analysis results (~ 7.1) with the calculated CO_2/H_2 ratio assuming complete H_2 accountability in the plenum of the autoclave (~ 5.9). This lack of complete H_2 accountability was encountered in the short-term seal-welded-container tests as well. It can be ascribed to a) reaction of H_2 with metal oxides present in the system; b) solution of H_2 in both brine and metal; and/or c) some H_2 leakage from the system. The loss of H_2 from the system does not appear severe enough to call
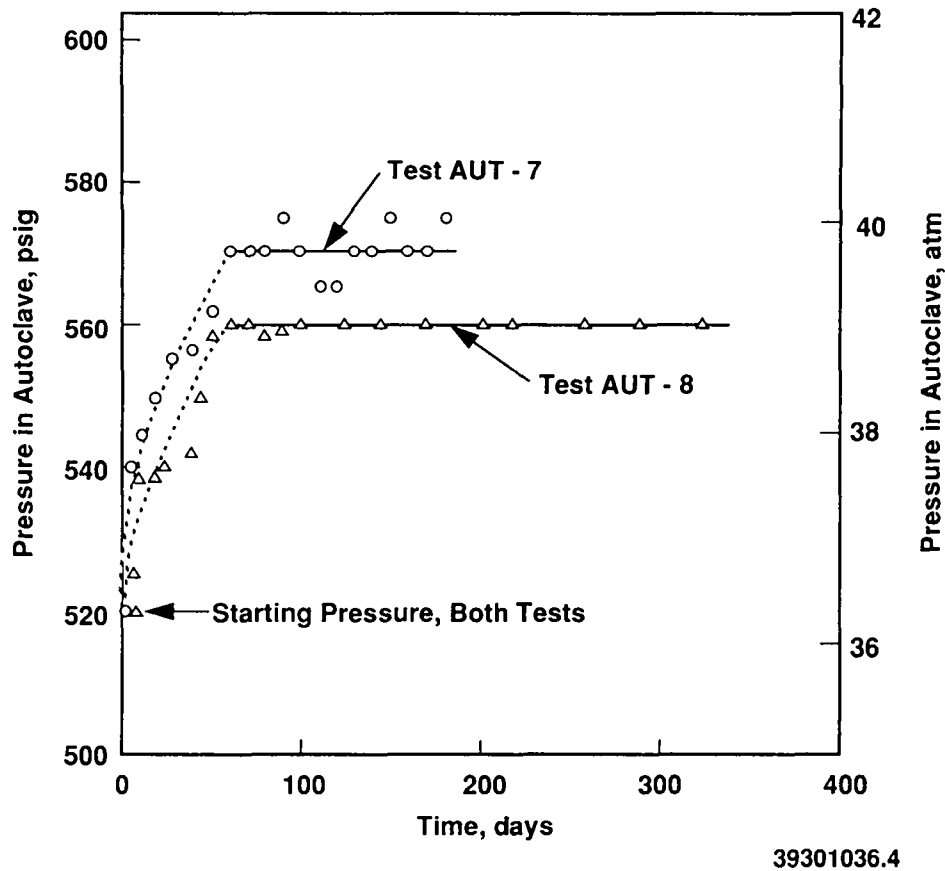
Figure 6-10. Pressure-time curves, tests AUT-7 and AUT-8.

the AUT-7 pressure-time curve of Figure 6-10 into question. The value of the AUT-8 pressure-time curve in predicting corrosion kinetics will not be known until the test is concluded and the amount of steel lost in the course of that test is determined. These results will be reported in the future.

The curves of Figure 6-10 suggest that the steel specimens first underwent a significant attack, due to the high CO_2 activity present in the system, but that either passivation of the specimens or saturation of the brine with Fe^{2+} occurred after a time period of ~2 months. The saturation of the brine phase with Fe^{2+} is currently not considered a totally satisfactory explanation for the complete stopping of the corrosion process, either in the AUT-7 test or in the seal-welded container tests. The amount of corrosion taking place in the AUT-7 test amounted to 4.0 g Fe/L of brine; in the case of the seal-welded-container tests, the corrosion amounted to 11.0 g Fe/L of brine. The fact that the higher-pressure test showed a lower Fe loss per liter of solution than the lower-pressure test is not

6-39

consistent with the expectations of siderite solubility as a function of CO_2 pressure. Also, both tests lost far more Fe/L than can be accounted for by estimating the solubility of Fe^{2+} in the brine phase. (Ikeda et al., 1983 attempted to calculate the concentration of Fe^{2+} in a brine solution in equilibrium intruding with $FeCO_3$, but an error in their reasoning produced results that were as much as three orders of magnitude too high at 30°C.) The concentration of Fe^{2+} in equilibrium with $FeCO_3$ in Brine A at 30°C is currently not known. The gravimetric data from the 12-month test (test AUT-8) will be required in order to make a definitive judgment on whether or not the surface passivation suggested by the pressure-time curves of Figure 6-10 in fact took place.

6.1.3 Salt-Phase Autoclave Tests

A probable scenario in the corrosion of steel in the WIPP involves the contact of steel by a moist mass of salt rather than brine. The moisture could be derived from intruding brine from a distant source "wicked" to the surface of the steel by capillary action or water vapor from a distant source equilibrating with the salt contacting the steel.

Two autoclave scoping tests, designated AUT-5 and AUT-6, were conducted to determine the approximate corrosion kinetics associated with the two scenarios described. The test arrangements are shown schematically in Figure 6-11. Test AUT-5 was designed to investigate the effect of wicking. The bottom of the salt mass was below the level of the brine, but the bottom of the specimens was above the brine liquid level. Test AUT-6 was designed to investigate the effect of vapor transport, so the bottom of the salt mass was above the liquid level of the brine. In each test 12 specimens of lot J steel were embedded in particulate salt (natural halite from the WIPP site) contained in a stainless steel mesh basket suspended from the top of the autoclave. The specimens were 51 mm x 25 mm (2 in. x 1 in.). Care was taken to prevent the specimens from contacting the basket or each other. A coarse fraction of the salt supplied was used (particles approximately 2 to 6 mm in major dimension) to permit at least initial vapor transport through the salt mass. Approximately 2 kg of salt was placed in each basket. The volume of Brine A placed in the bottom of the autoclave in test AUT-5 was 890 mL; in test AUT-6 the brine volume added was 350 mL. The initial N_2 overpressure in each test was 10 atm; the test duration was three months.
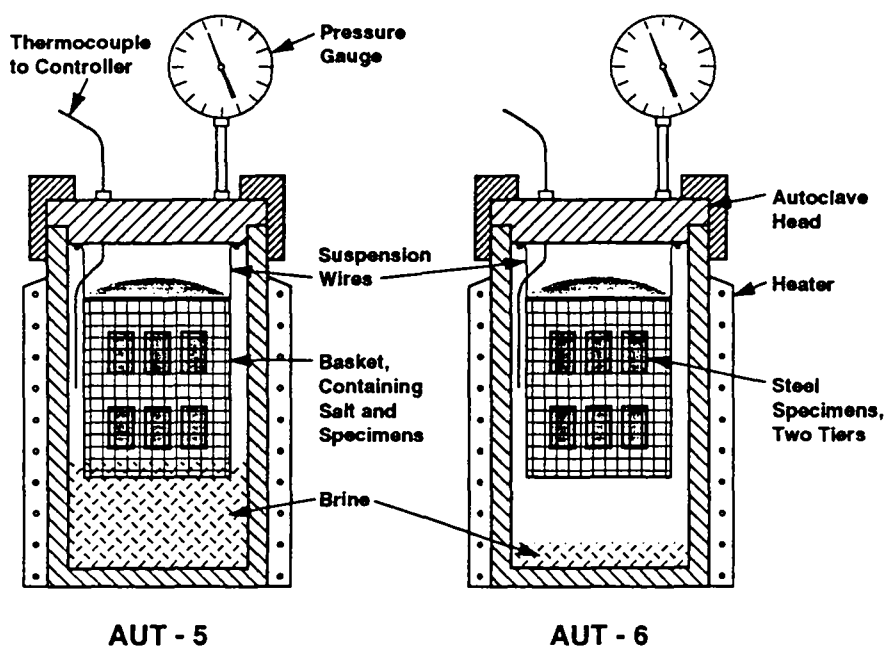
Figure 6-11. Test arrangements, tests AUT-5 and AUT-6.

6.1.3.1 POST-TEST OBSERVATIONS, TEST AUT-5

This wicking test functioned as intended. At the conclusion of the test the salt was still mounded in the basket, and the specimens were all entirely covered with salt. Salt crystals were adhering to both the basket and the autoclave wall above the liquid level. A mass of crystalline salt was present in the bottom of the autoclave in the brine. The salt in the basket was hard, and the samples were chipped out with difficulty. No red oxides (traces of ferric ion) were present in the test assembly. The samples were mottled due to a discontinuous tarnish film, but had an essentially metallic appearance when removed from the salt. Predictably, the mottled regions rapidly darkened and assumed a reddish hue when the specimens were exposed to air. The specimens were washed sequentially in deionized water and ethanol and stored in a desiccator.

The brine was "water-white" when removed from the autoclave, but developed a light yellow hue upon standing for a few hours, indicating the presence of Fe^{2+} ions in the brine removed from the autoclave.

6-41

6.1.3.2 POST-TEST OBSERVATIONS, TEST AUT-6

In this test the bottom of the salt mass was above the level of the brine. The intent of the test arrangement was to make the vapor-phase transport of water the only method of water transport. Because of the reduced activity of water in the Brine A water source and the expectation that at the low test temperature employed a large temperature gradient between the underside of the autoclave head and the contents of the autoclave would not exist, it was assumed that no water would condense on the bottom of the autoclave head and drip onto the salt. Such was not the case. For some period of time water apparently dripped from the underside of the autoclave head onto the salt, as the top of the salt was partially eroded in a non-uniform manner, and the top of one top-tier specimen was slightly exposed. Also, as the autoclave head was lifted from the autoclave, some water droplets were noted clinging to the tubing.

At 30°C, the partial pressure of H_2O over saturated Brine A is 0.03 atm or 23 mm Hg (Brush, 1990). At this pressure, pure H_2O will condense at a temperature equal to or less than 25°C. This means that a temperature gradient of at least 5°C existed in the autoclave, permitting H_2O to condense on the head of the autoclave. Though this magnitude of temperature gradient was not expected, it apparently occurred for at least some portion of the 3-month operating period of the autoclave test. The test employing the partially submerged salt (AUT-5) did not show any evidence of water transport by dripping, as the salt dome was smooth with no signs of dripping-induced erosion. The dripping transport obviously precludes characterizing the test as a vapor-phase-transport test. Instead, it can best be characterized as a vapor-phase-transport, dripping-transport test, with the time period of dripping and the amount of water transported by dripping unknown.

As in test AUT-5, salt crystals were found clinging to the outside of the basket and to the inside wall of the autoclave above the brine level, and a mass of salt crystals was in the bottom of the autoclave in the brine. The brine was "water-white" when removed from the autoclave, but developed a light yellow hue upon standing for a few hours, indicating some iron specie(s) in solution. As in the case of test AUT-5, the steel specimens were removed from test AUT-6 with some difficulty, as the salt particles in the salt adhered strongly to one another. The steel specimens removed from test AUT-6 were shinier and more metallic in appearance than those removed from AUT-5; i.e., the extent of corrosion tarnish was somewhat less, though the mottled appearance was similar. No red corrosion product was observed anywhere in the system.

The corrosion rates of the steel specimens from tests AUT-5 and AUT-6 were determined by the conventional gravimetric method. These results are presented in Table 6-14, compared to 3- and 6-month corrosion data from N_2/immersed seal-welded container tests. Individual-specimen data for tests AUT-5 and AUT-6 are tabulated in Appendices B-10 and B-11, respectively.

The corrosion rates obtained from specimens lying in the bottom tier of the wicking test AUT-5 are the only ones that approach the corrosion rates of specimens actually immersed in Brine A with a N_2 overpressure, as reflected by the seal-welded-container test results. The reason for the relatively low corrosion rates observed in the top tier of test AUT-5, or the generally low rates observed in test AUT-6, could be due to either 1) a reduced H_2O availability or 2) a reduced Mg availability, as the corrosiveness of brines toward steel are markedly dependent on their Mg concentration (Westerman et al., 1987).

Table 6-14. Corrosion Rates of Steel Specimens in Solid-Salt Tests, Compared with Corrosion Rates in Brine/N_2 Seal-Welded Container Tests

Test	Tier	Corrosion Rate, μm/yr[a]
AUT-5 3 months	Top	1.15±0.22
	Bottom	1.92±0.45
AUT-6 3 months	Top	0.79±0.04
	Bottom	0.64±0.09
N_2/Immersed, Seal-Welded Container Tests, Steel Lot J		
3-month test		1.94±0.16
6-month test		1.61±0.37

[a] Average linearized corrosion rate of all specimens included in category, with standard deviation.

As previously mentioned, the corrosion rates that would be obtained under a strictly controlled vapor-transport test cannot be estimated from the results of the tests described above. If a vapor-transport test were to be repeated, an insulating cover on the autoclave head and a drip shield over the salt basket would be reasonable precautions. Further wicking and vapor-phase tests, with steel specimens embedded in simulated backfill material, will be conducted in the future. The results of those tests will be compared with the results of the tests described here.

6.2 Alternative Material Tests

The corrosion and gas-generation behavior of the four candidate alternative packaging materials [high-purity Cu; cupronickel 90-10; commercial-purity Ti (Ti Grade 2) and Ti Grade 12] was investigated in three environments—anoxic brine (Brine A with N_2); Brine A with CO_2; and Brine A with H_2S. Only the seal-welded-container method of testing was used, as reliance was placed on gas-pressure measurements as well as gravimetric analyses of the test specimens to establish the behavior of the materials in the test environments. The test matrix summarizing these tests is shown in Table 3-2.

The manner of racking the specimens in the alternative material tests was different from the method of racking used in the low-carbon steel tests. In the latter tests, the specimens were held on a specimen rack with no effort made to produce well defined crevices between the test specimens. In the alternative material tests, two specimen geometries were used: rectangular specimens 19.1 cm x 6.35 cm (7.5 in. x 2.5 in.), and circular specimens 3.81 cm (1.50 in.) in diameter. The rectangular specimens were provided with two holes, each 0.79 cm (0.31 in.) in diameter for rack mounting; the circular specimens had one centrally located hole of the same size. The manner of racking the specimens is shown in Figure 6-12.

Each test involved 16 rectangular specimens and 16 circular specimens. The 16 circular specimens were tightly compressed between adjacent rectangular specimens, as shown in Figure 6-12, to provide regions for crevice corrosion if the tendency for that degradation mode existed in a given test system.
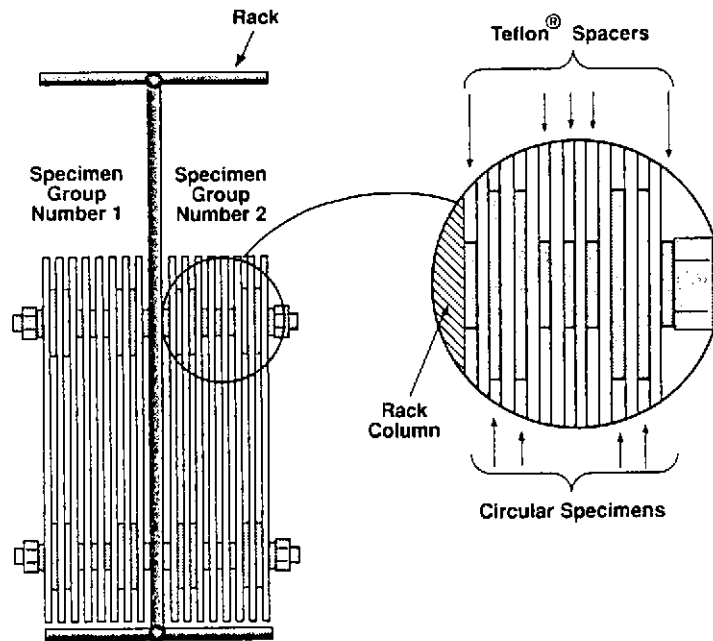
Figure 6-12. Method of mounting specimens on specimen rack for alternative packaging materials tests.

During alternative material testing, Cu-base and Ti-base materials were always tested in separate containers. In tests of Cu-base materials, all of the high-purity-Cu specimens (8 rectangular, 8 circular) were placed on one side of a specimen rack, and 16 equivalent specimens of cupronickel were situated on the other side of the rack. In a similar manner, in a test of Ti-base materials, specimens of Ti Grade 2 were placed on one side of a rack, and specimens of Ti Grade 12 on the other. The specimens were always completely immersed in Brine A during a test. All tests were conducted at 30 ±5°C.

The alternative packaging materials investigation comprised tests 1A through 19A. Details of the tests, expanding on the information presented in Table 3-2, are presented in Table 6-15. Individual-specimen data for completed tests are presented in Appendices B-12 through B-17.

6.2.1 Cu in Brine A with N₂

Cu and cupronickel 90-10 specimens exposed to anoxic Brine A showed no significant reaction, as indicated by either pressure increase within the test container or by consumption of metal by a corrosion reaction. This is consistent with thermodynamic expectations [Equation (24)].

Specimens removed from test containers 1A and 7A after test periods of 10 and 15 months, respectively, exhibited freshly ground, as-received surface conditions reminiscent of the pre-test specimen conditions. A gravimetric analysis of specimens from test 7A (see Appendix B-12 for individual

Table 6-15. Initial Conditions, Tests 1A through 19A

Test Identification	Material Base	Initial Overpressure Gas/atm[a]	Total Specimen Area, m²	Brine Volume, L	Actual Test Duration, Months
1A	Cu	N₂/10.6	0.43	1.415	10
2A	Cu	CO₂/11.5	0.43	1.375	10
3A	Cu	H₂S/4.9	0.43	1.390	9
4A	Ti	N₂/10.7	0.44	1.435	10
5A	Ti	CO₂/11.6	0.44	1.360	10
6A	Ti	H₂S/4.7	0.44	1.415	9
7A	Cu	N₂/10.4	0.43	1.420	15
8A	Cu	CO₂/11.0	0.43	1.405	15
9A	Cu	H₂S/5.1	0.43	1.405	15
10A	Ti	N₂/10.5	0.44	1.420	15
11A	Ti	CO₂/10.9	0.44	1.400	15
12A	Ti	H₂S/5.1	0.44	1.360	15
13A	Cu	N₂/10.2	0.43	1.380	open
14A	Cu	CO₂/10.9	0.43	1.410	open
15A	Cu	H₂S/4.9	0.43	1.420	open
16A	Ti	N₂/10.2	0.44	1.365	open
17A	Ti	CO₂/10.8	0.44	1.360	open
18A	Ti	H₂S/5.1	0.44	1.360	open
19A	Control	H₂S/4.5	--	1.740	open

[a] At attainment of 30°C test temperature.

specimen weight-change data) showed that the weight changes undergone by the circular specimens were within the accuracy limits of the four-place balance used for the analysis. The rectangular specimens showed weight gains up to 0.0117 g. The pressure changes in the two test containers over the entire period of the tests were within ±1 psi. Thus, it can be concluded on the basis of the evidence currently available that Cu and cupronickel 90-10 will not react with Brine A to form significant H_2 under the anoxic test conditions employed. The container pressure of the continuing test (test 13A) is consistent with this observation; the pressure has not increased over a 16-month test period.

6.2.2 Cu in Brine A with CO_2

Cu and cupronickel 90-10 specimens exposed to Brine A with CO_2 showed no significant reaction, as indicated by either pressure increase within the test container or by consumption of metal by a corrosion reaction. This is consistent with thermodynamic expectations [Equation (27)].

Specimens removed from test containers 2A and 8A after test durations of 10 and 15 months, respectively, appeared clean and uncorroded. The pressure in both these containers dropped during the test periods by approximately 2 psi. The test specimens from test 8A lost a small amount of weight during the test, possibly due to Cu dissolution or Cu-complex dissolution effects. (See Appendix B-13 for individual specimen weight-change data.) It can be concluded, on the basis of the available evidence, that Cu and cupronickel 90-10 will not react with Brine A to form significant H_2 under the test conditions used. The container pressure of the continuing test (test 14A) is following a course consistent with these observations, in that the pressure has not increased after 16 months.

6.2.3 Cu in Brine A with H_2S

Cu and cupronickel 90-10 specimens exposed to Brine A with H_2S show a rapid H_2-generating reaction. These observations can be said to be consistent with thermodynamic predictions [Equation (29)], though the upper limits of H_2 pressure suggested by those limits have not been nearly approached in the present tests.

The pressure histories of the three tests 3A, 9A, and 15A, originally charged with Cu-base materials, Brine A, and H_2S gas, are summarized in Figure 6-13. Test 3A was opened for specimen examination after a 3-month test exposure. Test 15A is an ongoing test. Containers 9A and 15A
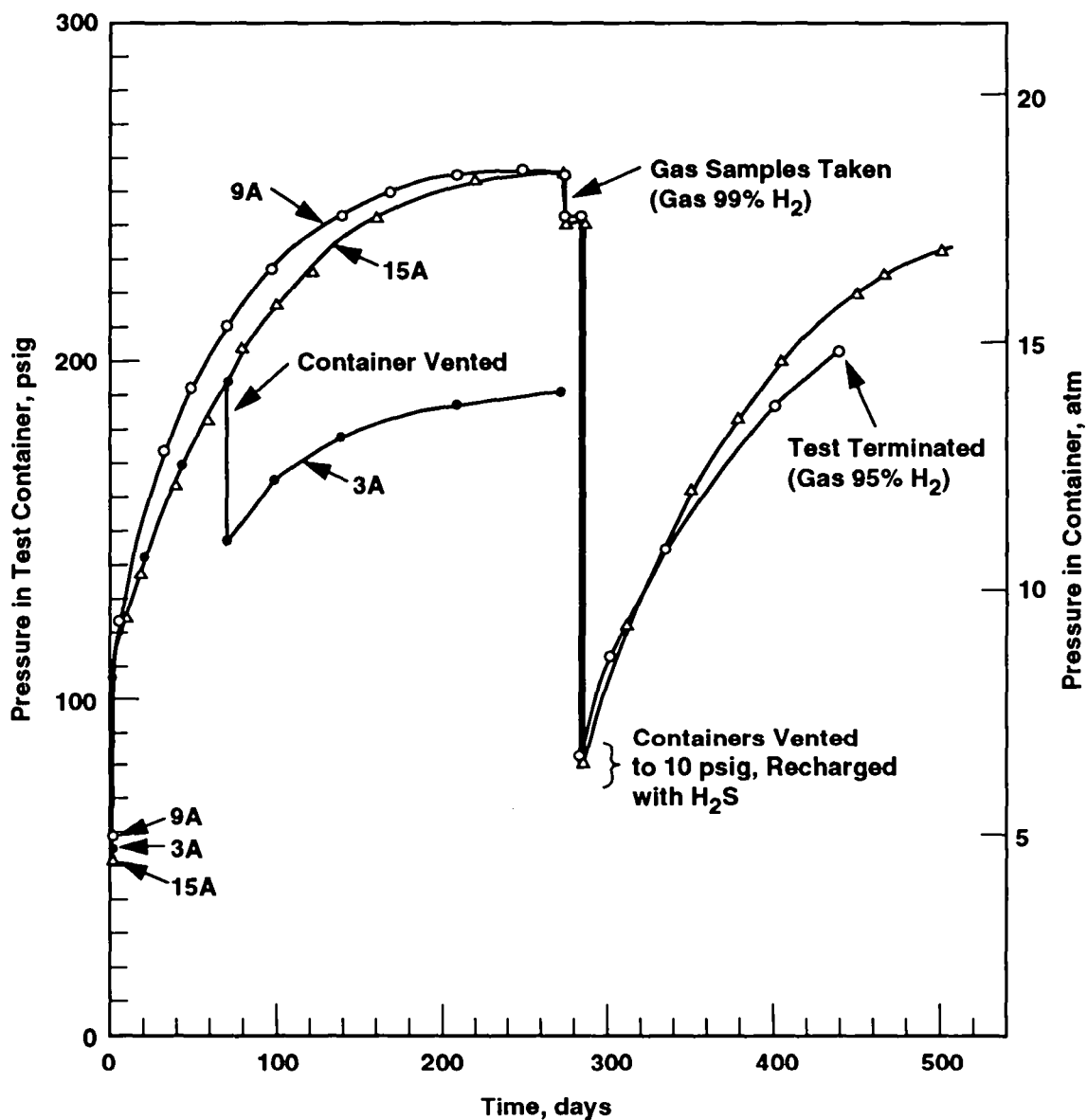
Figure 6-13. Pressure-time curves, tests 3A, 9A, and 15A.

were vented and repressurized with H_2S gas after 9 months exposure. (The intent of the venting and repressurization was to reveal whether the specimens had originally stopped reacting due to formation of a protective sulfide film, or whether the decrease in reaction rate with time was simply a result of H_2S consumption.) The vented gas was essentially pure H_2 in both cases. The pressure buildup as a function of time in the vented-and-repressurized test containers has approximately duplicated the initial pressure buildup in the containers.

These observations demonstrate that the reduction of apparent reaction rate observed was due to consumption of the H_2S reactant, not formation of a passive film. Further supporting this conclusion are two additional observations: 1) the buildup in pressure before venting and refilling the containers at nine months was caused by an amount of H_2 calculated to be equivalent, on a molar basis, to the H_2S originally charged into the containers; and 2) a gravimetric determination of the amount of Cu lost from a sampling of the test specimens in the two containers in which the specimens were examined (3A and 9A) showed a close agreement in molar equivalency between the metal lost to the corrosion reaction and the H_2 generated, assuming the reaction of 2 moles of Cu with 1 mole of H_2S to form 1 mole of Cu_2S and 1 mole of H_2. Cu_2S, chalcocite, is the only reaction product found on the surface of the specimens. Individual specimen weight-change data for tests 3A and 9A are presented in Appendix B-14.

At this time it can be concluded that Cu and cupronickel 90-10 react rapidly and essentially completely with H_2S under the test conditions imposed to form Cu_2S and H_2 in the expected quantities, with little if any inhibition of reaction rate ascribable to the corrosion product film forming on the specimen surface. Because the reaction proceeds at a rapid rate (on a WIPP-relevant time scale) to very low activities of H_2S, it is difficult to conceive of a useful Cu-alloy container if H_2S has a significant probability of being present in the environment.

6.2.4 Ti in Brine A with N_2, CO_2, and H_2S

All alternative-material tests of Ti Grade 2 and Ti Grade 12 have shown essentially complete stability of the Ti-base materials in the test environments. The pressure changes observed in the Ti with N_2 and Ti with CO_2 tests have been within 4 psi of the starting pressure over the entire period of the tests; the pressure changes observed were pressure drops. The Ti with H_2S tests, on the other

hand, all showed a pressure increase of 9 to 10 psi within the first 30 h of gas addition, after which time the pressure stabilized, within ± 2 psi, for the remainder of the test period. Gas taken from the 15-month-exposure test (test 12A) before test termination showed a trace of H_2 (0.5%), consistent with a limited corrosion reaction at the beginning of the test.

All of the Ti-base specimens appeared clean, shiny, and unreacted upon removal from the containers of terminated tests. A gravimetric analysis of a random sample of specimens from the 15-month tests (tests 10A, 11A, and 12A)[a] showed that the majority of specimens from the N_2/brine tests gained weight, up to 0.0018 g; whereas all of the specimens from the other two environments (brine/CO_2 and brine/H_2S) lost weight, as much as 0.0014 g. As in the case of the Cu-base alloys, weight changes to the extent observed in the present tests have little significance in an assessment of gas-generation potential.

It appears, on the basis of the information obtained to date, that Ti Grade 2 and Ti Grade 12 could be used as alternative packaging materials in the WIPP without concern about gas generation.

---

[a] Individual-specimen data from test 10A, an anoxic brine (brine/N_2) test, are presented in Appendix B-15; specimen data from test 11A, a brine/CO_2 test, are presented in Appendix B-16; and specimen data from test 12A, a brine/H_2S test, are presented in Appendix B-17.

7.0 CONCLUSIONS

The present report describes progress made through December 1992 toward achieving the objectives of the Sandia National Laboratories support project at PNL. Because several of the corrosion and gas-generation tests are still in progress, not all of the areas of investigation initiated can be completely assessed and summarized. The current conclusions that can be made are presented in this section of the report.

- The corrosion rate of low-carbon steel immersed in anoxic Brine A at 30°C for test durations of 24 months decreased slowly with time. The corrosion rate of the steel during the final 12-month period of the 24-month test was 0.71 μm/yr, equivalent to the generation of 0.10 mol H_2/m^2-Fe-yr.

- The corrosion rate of low-carbon steel in anoxic Brine A (Brine A with N_2) increased with increasing N_2 pressure and decreased with imposition of a 36-atm H_2 overpressure. A 70-atm H_2 overpressure caused no further reduction in rate, possibly because of a balance between the rate-reduction effect of the reactant back-pressure and the rate enhancement caused by pressure per se.

- In the long-term tests (12 and 24 months) of steel immersed in anoxic brine there was excellent agreement between moles of Fe reacted and moles of H_2 produced, assuming the Fe in the corrosion product is only in the divalent state. The non-adherent, greenish-gray corrosion product could not be identified by XRD.

- Steel specimens exposed only to the vapor phase of Brine A under anoxic conditions showed no discernible corrosion reaction. The corrosion product adhering to the bottoms of these specimens where they were contacted by the brine during handling of the containers was $\beta Fe_2(OH)_3Cl$ in all cases investigated.

- CO_2 in Brine A causes an initial increase in the reaction rate of steel, relative to anoxic conditions. The initial reaction rate increases with the CO_2 pressure imposed. Additions of CO_2 beyond a certain threshold amount cause the reaction to essentially stop, however, typically in ~ 100 days, due to the formation of an adherent carbonate reaction product [$FeCO_3$, siderite, or $Fe,Mn,Zn(CO_3)$, oligonite]. The "threshold" CO_2 required is the subject of a continuing investigation.

- The immersed-specimen tests in Brine A with CO_2 showed fairly good agreement between moles of Fe reacted and moles of H_2 produced, assuming that Fe is only in the divalent state in the corrosion product.

- Steel specimens exposed to a 10 atm CO_2 pressure and vapor of Brine A at 30°C showed insignificant corrosion. Corrosion product in the splash zone of the test specimens was siderite, $FeCO_3$.

- The brine in the test containers does not, in general, undergo an appreciable change in composition during the N_2/immersed or the CO_2/immersed tests. Exceptions are the relatively high Fe concentration and the relatively low Ca concentration and low pH of the brines at the conclusion of the CO_2/immersed tests.

- Steel specimens exposed in the immersed and vapor-phase test conditions to Brine A and a 5-atm pressure of H_2S have shown no significant ongoing reaction. It is assumed that a high sulfide, such as FeS_2, pyrite, rapidly formed on the specimen surfaces and prevented further reaction. These tests are continuing.

- Steel specimens embedded in a mass of particulate salt wicking brine from a pool of Brine A under anoxic test conditions corroded at a rate slower but not dissimilar to the rate observed under anoxic brine-immersed conditions. The test lasted only 3 months. Specimens in a similar test in which condensate dripped from the underside of the autoclave lid onto the salt produced significantly lower corrosion rates, presumably because of the lower Mg concentration in the specimen environment.

- The Cu-base alternative packaging materials showed insignificant reaction in N_2/immersed and CO_2/immersed test conditions. Reaction with H_2S was rapid and complete and produced H_2 equivalent to the H_2S added. Cu-base packaging materials are unsuitable if H_2S is considered to be a likely environmental constituent, such as from microbial degradation or sulfate reduction processes.

- The Ti-base alternative packaging materials showed insignificant reaction in all test environments; i.e., in N_2/immersed, CO_2/immersed, and H_2S/immersed environments. It appears at the present time that Ti-base packaging materials could be used in the WIPP site without concern for corrosion or gas generation.

8.0 FUTURE WORK

PNL and Sandia-WIPP Gas Generation Program personnel will continue to work cooperatively in interpreting the existing and forthcoming corrosion and gas generation data. Such data results, conclusions, predictions, etc., will be tailored to satisfy the informational needs of the WIPP Project gas generation modeling and performance assessment efforts. PNL and Sandia personnel will also continue to update or modify the current PNL corrosion program to help satisfy these informational needs as the WIPP Project evolves. Significant expansions to the laboratory program are being contemplated or proposed to evaluate gas generation impacts due to potential interactions of corrosion (and corrosion byproducts) with microbial degradation and/or brine-radiolysis reaction products.

The following ongoing or new laboratory efforts are planned for CY 1993:

- The seal-welded-container tests of low-carbon steel in CO_2 and H_2S will be continued. A decision will be made, perhaps at mid-year, as to the conclusion of, or possible alteration to, these tests. Further evaluations of the passivating nature of these gases, in WIPP-specific environments, are planned.

- The high-pressure autoclave test (AUT-8) of low-carbon steels in CO_2 will be terminated in January 1993 for specimen examination. Further high-pressure studies are being considered by the WIPP Gas Generation Program and may be initiated.

- The corrosion testing of two Al-base materials, high-purity Al and alloy 6061, will be initiated. These materials represent metallic Al in the waste. Test environments utilizing Brine A with N_2, CO_2, and H_2S are planned, with both immersed and vapor-phase exposure of test specimens. Tests as a f(pH) will also be conducted

- The long-term seal-welded container tests of Cu-base and Ti-base materials will be continued as a longer-term monitoring effort. A decision on their continuation will be made at mid-year.

- It is anticipated that one or more tests will be initiated that will involve the corrosion testing of low-carbon steel specimens in contact with a simulated backfill materials. The test parameters and overall matrix have not yet been finalized.

- Gravimetric data obtained in past studies will be statistically analyzed in order to provide confidence limits for the resulting metal consumption-time curves.

- WIPP-brine-specific, anoxic steel corrosion and gas generation studies as a f(pH) are being considered and may be initiated.

9.0 REFERENCES

Asano, H., H. Wakamatsu, and M. Akashi. 1992. "Corrosion Lifetime Assessment for Candidate Materials of Geological Disposal Overpack for High-Level Nuclear Waste Canisters: Perspective of R&D in Japan," *High Level Radioactive Waste Management Proceedings of the Third International Conference, Las Vegas, NV, April 12-16, 1992.* La Grange Park, IL: American Nuclear Society, Inc.; New York, NY: American Society of Civil Engineers. Vol. 2, 1658-1669.

ASM (American Society for Metals). 1978. *Metals Handbook, Volume 1 Properties and Selection: Irons and Steels.* 9th ed. Metals Park, OH: American Society of Metals. 161.

ASM (American Society for Metals). 1980. *Metals Handbook. Volume 3 Properties and Selection: Stainless Steels, Tool Materials, and Special-Purpose Materials.* 9th ed. Metals Park, OH: American Society for Metals. 381.

ASM International. 1987. *Metals Handbook. Volume 13 Corrosion.* 9th ed. Metals Park, OH: ASM International. 618-619, 632.

Booker, J., W.R. Cribb, J.C. Turn, Jr., and R.D. Kane. 1984. "Corrosion Behavior of Beryllium Copper and Other Nonmagnetic Alloys in Simulated Drilling Environments," *Corrosion '84, New Orleans, LA, April 2-6, 1984.* Paper No. 220. Houston, TX: National Association of Corrosion Engineers.

Braithwaite, J.W., and M.A. Molecke. 1980. "Nuclear Waste Canister Corrosion Studies Pertinent to Geologic Isolation," *Nuclear and Chemical Waste Management.* Vol. 1, 37-50.

Bruckhoff, W., O. Geier, K. Hofbauer, G. Schmitt, and D. Steinmetz. 1985. "Rupture of a Sour Gas Line Due to Stress Oriented Hydrogen Induced Cracking Failure Analyses, Experimental Results and Corrosion Prevention," *Corrosion/85, Boston, MA, March 25-29, 1985.* Paper No. 389. Houston, TX: National Association of Corrosion Engineers.

Brush, L.H. 1990. *Test Plan for Laboratory and Modeling Studies of Repository and Radionuclide Chemistry for the Waste Isolation Pilot Plant.* SAND90-0266. Albuquerque, NM: Sandia National Laboratories.

Brush, L.H., M.A. Molecke, A.R. Lappin, R.E. Westerman, X. Tong, J.N.P. Black, D. Grbic-Galic, R.E. Vreeland, and D.T. Reed. 1991a. "Laboratory and Bin-Scale Tests of Gas Generation for the Waste Isolation Pilot Plant," *Waste-Generated Gas at the Waste Isolation Pilot Plant: Papers Presented at the Nuclear Energy Agency Workshop on Gas Generation and Release from Radioactive Waste Repositories, Aix-en-Provence, France, September 23-26, 1991.* Eds. P.B. Davies, L.H. Brush, M.A. Molecke, F.T. Mendenhall, and S.W. Webb. SAND91-2378. Albuquerque, NM: Sandia National Laboratories. 2-1 through 2-13.

Brush, L.H., D. Grbic-Galic, D.T. Reed, X. Tong, R.H. Vreeland, and R.E. Westerman. 1991b. "Preliminary Results of Laboratory Studies of Repository Chemistry for the Waste Isolation Pilot Plant," *Scientific Basis for Nuclear Waste Management XIV, Materials Research Society Symposium Proceedings, Boston, MA, November 26-29, 1990.* Eds. T.A. Abrajano, Jr. and L.H. Johnson. SAND90-1031C. Pittsburgh, PA: Materials Research Society. Vol. 212, 893-900.

Burke, P.A. 1984. "Synopsis: Recent Progress in the Understanding of CO_2 Corrosion," *Advances in CO_2 Corrosion in the Oil and Gas Industry, Proceedings of the Corrosion/83 Symposium, Anaheim, CA, April 18-19, 1983.* Ed. R.H. Hausler. Houston, TX: National Association of Corrosion Engineers. Vol. 1, 3-9.

Butcher, B.M. 1990. *Preliminary Evaluation of Potential Engineered Modifications for the Waste Isolation Pilot Plant (WIPP).* SAND89-3095. Albuquerque, NM: Sandia National Laboratories.

Chase, M.W., Jr., C.A. Davies, J.R. Downey, Jr., D.J. Frurip, R.A. MacDonald, and A.N. Syverud. 1985. *JANAF Thermochemical Tables.* 3rd ed. [Washington, DC]: American Chemical Society; New York, NY: American Institute of Physics. Pts. I-II.

Cleary, H.J., and N.D. Greene. 1967. "Corrosion Properties of Iron and Steel," *Corrosion Science.* Vol. 7, no. 12, 821-831.

Crolet, J.L., and M.R. Bonis. 1984. "pH Measurements Under High Pressures of CO_2 and H_2S," *Corrosion '84, International Corrosion Forum Devoted Exclusively to the Protection and Performance of Materials, New Orleans, LA, April 2-6, 1984.* Paper no. 294. Houston, TX: National Association of Corrosion Engineers.

DeBerry, D.W., and W.S. Clark. 1984. "Corrosion Due to Use of Carbon Dioxide for Enhanced Oil Recovery," *CO_2 Corrosion in Oil and Gas Production—Selected Papers, Abstracts, and References.* Compiled and edited by NACE Task Group T-13. Houston, TX: National Association of Corrosion Engineers. 7-74.

de Waard, C., and D.E. Milliams. 1975a. "Prediction of Carbonic Acid Corrosion in Natural-Gas Pipelines," *Proceedings of the First International Conference on the Internal and External Protection of Pipes, University of Durham, Durham, England, September 1975.* Paper F1. Bedford, England: BHRA Fluid Engineering.

de Waard, C., and D.E. Milliams. 1975b. "Carbonic Acid Corrosion of Steel," *Corrosion.* Vol. 31, no. 5, 177-181.

Dougherty, J.A. 1988. "Factors Affecting H_2S and H_2S/CO_2 Attack on Carbon Steels Under Deep Hot Well Conditions," *Corrosion '88, St. Louis, MO, March 21-25, 1988.* Paper no. 190. Houston, TX: National Association of Corrosion Engineers.

Dunlop, A.K., H.L. Hassell, and P.R. Rhodes. 1983. "Fundamental Considerations in Sweet Gas Well Corrosion," *Corrosion '83, Anaheim, CA, April 18-22, 1983.* Paper no. 46. Houston, TX: National Association of Corrosion Engineers.

EATF (Engineered Alternatives Task Force). 1991. "Appendix H: Report of the Waste Container Materials Panel," *Evaluation of the Effectiveness and Feasibility of the Waste Isolation Pilot Plant Engineered Alternatives: Final Report of the Engineered Alternatives Task Force.* DOE/WIPP 91-007, Rev. 0. Carlsbad, NM: Waste Isolation Pilot Plant. Vol. II, H-i through H-39.

Eiselstein, L.E., B.C. Syrett, S.S. Wing, and R.D. Caligiuri. 1983. "The Accelerated Corrosion of Cu-Ni Alloys in Sulphide-Polluted Seawater: Mechanism No. 2," *Corrosion Science.* Vol. 23, no. 3, 223-239.

Gehring, G.A., Jr., R.L. Foster, and B.C. Syrett. 1983. "Effect of Sulfide on the Corrosion and Protection of Seawater-Cooled Condenser Alloys," *Corrosion '83, International Corrosion Forum, Anaheim, CA, April 18-22, 1983.* Paper no. 76. Houston, TX: National Association of Corrosion Engineers.

Grauer, R., B. Knecht, P. Kreis, and J.P. Simpson. 1991. "Hydrogen Evolution from Corrosion of Iron and Steel in Intermediate Level Waste Repositories," *Scientific Basis for Nuclear Waste Management XIV, Materials Research Society Symposium Proceedings, Boston, MA, November 26-29, 1990.* Eds. T.A. Abrajano, Jr. and L.H. Johnson. Pittsburgh, PA: Materials Research Society. Vol. 212, 295-302.

Greco, E.C., and W.B. Wright. 1962. "Corrosion of Iron in an $H_2S-CO_2-H_2O$ System," *Corrosion.* Vol. 18, no. 3, 119t-124t.

Gudas, J.P., and H.P. Hack. 1979. "Sulfide Induced Corrosion of Copper Nickel Alloys," *Corrosion.* Vol. 35, no. 2, 67-73.

Guzowski, R.V. 1990. *Preliminary Identification of Scenarios That May Affect the Escape and Transport of Radionuclides from the Waste Isolation Pilot Plant, Southeastern New Mexico.* SAND89-7149. Albuquerque, NM: Sandia National Laboratories.

Haberman, J.H., and D.J. Frydrych. 1988. "Corrosion Studies of A216 Grade WCA Steel in Hydrothermal Magnesium-Containing Brines," *Scientific Basis for Nuclear Waste Management XI, Materials Research Society Symposium Proceedings, Boston, MA, November 30-December 3, 1987.* Eds. M.J. Apted and R.E. Westerman. Pittsburgh, PA: Materials Research Society. Vol. 112, 761-772.

Hausler, R.H. 1983. "Laboratory Investigations of the CO_2 Corrosion Mechanism as Applied to Hot Deep Gas Wells," *Corrosion '83, International Corrosion Forum, Anaheim, CA, April 18-22, 1983.* Paper no. 47. Houston, TX: National Association of Corrosion Engineers.

Hausler, R.H., and D.W. Stegmann. 1988. "CO_2 Corrosion and Its Prevention by Chemical Inhibition in Oil and Gas Production," *Corrosion '88, National Association of Corrosion Engineers Meeting, St. Louis, MO, March 21-25, 1988*. Houston, TX: National Association of Corrosion Engineers.

Hudgins, C.M., Jr., and R.L. McGlasson. 1981. "The Effect of Temperature (75°F-400°F) on the Aqueous Sulfide Stress Cracking Behavior of an N-80 Type Steel," *H_2S Corrosion in Oil and Gas Production—A Compilation of Classic Papers*. Eds. R.N. Tuttle and R.D. Kane. Houston, TX: National Association of Corrosion Engineers. 90-94.

Ikeda, A., M. Ueda, and S. Mukai. 1983. "CO_2 Corrosion Behavior and Mechanism of Carbon Steel and Alloy Steel," *Corrosion '83, Anaheim, CA, April 18-22, 1983*. Paper no. 45. Houston, TX: National Association of Corrosion Engineers.

Ikeda, A., S. Mukai, and M. Ueda. 1984. "Prevention of CO_2 Corrosion of Line Pipe and Oil Country Tubular Goods," *Corrosion '84, New Orleans, LA, April 2-6, 1984*. Paper no. 289. Houston, TX: National Association of Corrosion Engineers.

Jones, D.A. 1992. *Principles and Prevention of Corrosion*. New York, NY: Macmillan Publishing Company. 523.

Kato, C., H.W. Pickering, and J.E. Castle. 1984. "Effect of Sulfide on the Corrosion of Cu-9.4Ni-1.7Fe Alloy in Aqueous NaCl Solution," *Journal of the Electrochemical Society*. Vol. 131, no. 6, 1225-1229.

Lange's Handbook. 1985. *Lange's Handbook of Chemistry*. 13th ed. Ed. J.A. Dean. New York, NY: McGraw-Hill. 11-21.

Lappin, A.R., R.L. Hunter, D.P. Garber, and P.B. Davies, eds. 1989. *Systems Analysis, Long-Term Radionuclide Transport, and Dose Assessments, Waste Isolation Pilot Plant (WIPP), Southeastern New Mexico; March 1989*. SAND89-0462. Albuquerque, NM: Sandia National Laboratories.

Macdonald, D.D., B.C. Syrett, and S.S. Wing. 1979. "The Corrosion of Cu-Ni Alloys 706 and 715 in Flowing Sea Water. II - Effect of Dissolved Sulfide," *Corrosion*. Vol. 35, no. 8, 367-378.

Masamura, K., S. Hashizume, K. Nunomura, J. Saki, and I. Matsushima. 1983. "Corrosion of Carbon and Alloy Steels in Aqueous CO_2 Environment," *Corrosion '83, Anaheim, CA, April 18-22, 1983*. Paper no. 19. Houston, TX: National Association of Corrosion Engineers.

Meyer, F.H., O.L. Riggs, R.L. McGlasson, and J.D. Sudbury. 1958. "Corrosion Products of Mild Steel in Hydrogen Sulfide Environments," *Corrosion*. Vol. 14, no. 2, 109t-115t.

Milton, C. 1966. "'Kansite' = Mackinawite, FeS (Technical Note)," *Corrosion*. Vol. 22, no. 7, 191-193.

Molecke, M.A. 1983. *A Comparison of Brines Relevant to Nuclear Waste Experimentation.* SAND83-0516. Albuquerque, NM: Sandia National Laboratories.

Molecke, M.A., J.A. Ruppen, and R.B. Diegle. 1983. "Materials for High-Level Waste Canister/ Overpacks in Salt Formations," *Nuclear Technology.* Vol. 63, no. 3, 476-510.

Murata, T., E. Sato, and R. Matsuhashi. 1983. "Factors Controlling Corrosion of Steels in CO_2— Saturated Environments," *Advances in CO_2 Corrosion in the Oil and Gas Industry, Proceedings of the Corrosion/83 Symposium, Anaheim, CA, April 18-19, 1983.* Ed. R.H. Hausler. Houston, TX: National Association of Corrosion Engineers. Vol. 1, 64-71.

National Association of Corrosion Engineers. 1976. *Laboratory Corrosion Testing of Metals for the Process Industries.* TM-01-69. Houston, TX: National Association of Corrosion Engineers.

Popplewell, J.M. 1980. "The Effect of Sulfides on the Corrosion Resistance of Copper Base Alloys in Salt Water," *Corrosion '80, International Corrosion Forum Devoted Exclusively to the Protection and Performance of Materials, Chicago, IL, March 3-7, 1980.* Paper No. 180. Houston, TX: National Association of Corrosion Engineers.

Reinhart, F.M., and J.F. Jenkins. 1972. *Corrosion of Materials in Surface Seawater After 12 and 18 Months of Exposure, Final Report.* NCEL-TN-1213. Port Hueneme, CA: US Naval Civil Engineering Laboratory.

Rhodes, F.H., and J.M. Clark, Jr. 1936. "Corrosion of Metals by Water and Carbon Dioxide Under Pressure," *Industrial Engineering Chemistry.* Vol. 28, 1078-1079.

Rossini, F.D., D.D. Wagman, W.H. Evans, S. Levine, and I. Jaffe. 1952. *Selected Values of Chemical Thermodynamic Properties.* National Bureau of Standards Circular 500. Washington, DC: US Government Printing Office.

Sardisco, J.B., and R.E. Pitts. 1965. "Corrosion of Iron in an H_2S-CO_2-H_2O System—Mechanism of Sulfide Film Formation and Kinetics of Corrosion Reaction," *Corrosion.* Vol. 21, no. 8, 245-253.

Sardisco, J.B., W.B. Wright, and E.C. Greco. 1963. "Corrosion of Iron in an H_2O-CO_2-H_2O System: Corrosion Film Properties on Pure Iron," *Corrosion.* Vol. 19, no. 10, 354t-359t.

Schmitt, G. 1983a. "Fundamental Aspects of CO_2 Corrosion," *Advances in CO_2 Corrosion in the Oil and Gas Industry, Proceedings of the Corrosion/83 Symposium, Anaheim, CA, April 18-19, 1983.* Ed. R.H. Hausler. Houston, TX: National Association of Corrosion Engineers. Vol. 1, 10-19.

Schmitt, G. 1983b. "CO_2 Corrosion of Steels—An Attempt to Range Parameters and Their Effects," *Advances in CO_2 Corrosion in the Oil and Gas Industry, Proceedings of the Corrosion/83 Symposium, Anaheim, CA, April 18-19, 1983.* Ed. R.H. Hausler. Houston, TX: National Association of Corrosion Engineers. Vol. 1, 1-2.

Schutz, R.W. 1986. "Titanium," *Process Industries Corrosion—The Theory and Practice, International Process Industries Corrosion Seminar, New Orleans, LA, 1986.* Eds. B.M. Moniz and W.I. Pollock. Houston, TX: National Association of Corrosion Engineers. 503-527.

Schweitzer, P.A. 1986. *Corrosion Resistance Tables.* New York, NY: Marcel Dekker, Inc. 256.

Seki, N., T. Kotera, T. Nakasawa, Y. Kobayashi, and T. Taira. 1982. "The Evaluation of Environmental Conditions and the Performance of Linepipe Steels Under Wet Sour Gas," *Corrosion '82, International Corrosion Forum, Houston, TX, March 22-26, 1982.* Paper no. 131. Houston, TX: National Association of Corrosion Engineers.

Silman, J.F.B. 1958. "The Stabilities of Some Oxidized Copper Minerals in Aqueous Solutions at 25°C and 1 Atmosphere Total Pressure." Ph.D. dissertation. Cambridge, MA: Harvard University.

Simpson, J.P., and R. Schenk. 1987. "Hydrogen Evolution from Corrosion of Pure Copper," *Corrosion Science.* Vol. 27, no. 12, 1365-1370.

Simpson, J.P., and R. Schenk. 1989. "Corrosion Induced Hydrogen Evolution on High Level Waste Overpack Materials in Synthetic Groundwaters and Chloride Solutions," *Scientific Basis for Nuclear Waste Management XII, Materials Research Society Symposium Proceedings, Berlin, Germany, October 10-13, 1988.* Eds. W. Lutze and R.C. Ewing. Pittsburgh, PA: Materials Research Society. Vol. 127, 389-396.

Soo, P., ed. 1983. *Review of DOE Waste Package Program—Subtask 1.1, National Waste Package Program, April-September 1982.* NUREG/CR-2482, BNL-NUREG-51494. Upton, NY: Department of Nuclear Energy, Brookhaven National Laboratory. Vol. 3, 89.

Southwell, C.R., and A.L. Alexander. 1969. "Corrosion of Structural Ferrous Metals in Tropical Environments—Sixteen Years' Exposure to Sea and Fresh Water," *Proceedings of the 24th Conference, National Association of Corrosion Engineers, Cleveland, OH, March 18-22, 1968.* Houston, TX: National Association of Corrosion Engineers. 685-695.

Syrett, B.C. 1977. "Accelerated Corrosion of Copper in Flowing Pure Water Contaminated with Oxygen and Sulfide," *Corrosion.* Vol. 33, no. 7, 257-262.

Tapping, R.L., P.A. Lavoie, and R.D. Davidson. 1983. "Effect of H_2S Neutralization Methods on Sulfide Films in Heavy Water Plants," *Corrosion '83, Anaheim, CA, April 18-22, 1983.* Paper no. 11. Houston, TX: National Association of Corrosion Engineers.

Tewari, P.H., M.G. Bailey, and A.B. Campbell. 1979. "The Erosion-Corrosion of Carbon Steel in Aqueous H_2S Solutions Up to 120°C and 1.6 MPa Pressure," *Corrosion Science.* Vol. 19, no. 8, 573-585.

Thomason, W.H. 1978. "Formation Rates of Protective Iron Sulfide Films on Mild Steel in H_2S-Saturated Brine as a Function of Temperature," *Corrosion '78, Houston, TX, March 6-10, 1978.* Paper no. 41. Houston, TX: National Association of Corrosion Engineers.

Turkdogan, E.T. 1980. *Physical Chemistry of High Temperature Technology.* New York, NY: Academic Press.

Videm, K., and A. Dugstad. 1987. "Effect of Flow Rate, PH, Fe^{2+} Concentration and Steel Quality on the CO_2 Corrosion of Carbon Steels," *Corrosion '87, Corrosion Control and Monitoring in Gas Pipelines and Well Systems, Calgary, Alberta, Canada, March 9-10, 1987.* Houston, TX: National Association of Corrosion Engineers. 53-64.

Vreeland, D.C. 1976. "Review of Corrosion Experience with Copper-Nickel Alloys in Sea Water Piping Systems," *Materials Performance.* Vol. 15, no. 10, 38-41.

Westerman, R.E. 1988. "Evaluation of the Corrosion Behavior of Nickel- and Copper-Base Alloys in High-Magnesium Brine," *Joint U.S. DOE/FRG Workshop on Nuclear Package Materials, Albuquerque, NM, March 9, 1988.* PNL/SRP-SA-15685. Richland, WA: Pacific Northwest Laboratory.

Westerman, R.E., J.H. Haberman, S.G. Pitman, K.H. Pool, K.C. Rhoads, and M.R. Telander. 1987. *Corrosion Behavior of A216 Grade WCA Mild Steel and Ti Grade 12 Alloy in Hydrothermal Brines, Salt Repository Project: Annual Report, FY 1986.* PNL-SRP-6221. Richland, WA: Pacific Northwest Laboratory.

Wikjord, A.G., T.E. Rummery, F.E. Doern, and D.G. Owen. 1980. "Corrosion and Deposition During the Exposure of Carbon Steel to Hydrogen Sulfide-Water Solutions," *Corrosion Science.* Vol. 20, 651-671.

APPENDIX A: PRESSURE HISTORIES, ANOXIC BRINE (BRINE /N_2) AND BRINE/CO_2 SEAL-WELDED CONTAINER TESTS

A-1

Summary of Container Environments:

Containers 1 and 2: Immersed Specimens, N2 Overpressure
Containers 3 and 4: Immersed Specimens, CO2 Overpressure
Containers 5 and 6: Vapor-Phase Exposure, N2 Overpressure
Containers 7 and 8: Vapor-Phase Exposure, CO2 Overpressure

Pressure in Container, psig

Time, days	Cont. 1	Cont. 2	Cont. 3	Cont. 4	Cont. 5	Cont. 6	Cont. 7	Cont. 8
0	138	137	157	175	138	138	149	148
1	138	138	164	170	138	139	149	147
5	139	139	167	165	138	138	148	147
6	139	139	168	166	138	139	148	147
7	139	140	171	167	138	139	148	147
8	139	139	171	167	138	138	148	147
12	140	140	175	173	138	139	148	147
20	141	142	180	178	138	139	148	147
27	142	142	183	182	138	138	148	147
40	145	146	186	186	139	139	149	147
48	147	148	189	188	140	139	148	148
55	147	147	191	190	140	139	148	148
62	149	150	192	192	140	139	148	148
69	150	150	193	192	140	139	148	148
83	153	153	198	198	140	140	149	149
90	155	154	198	198	140	139	148	148

Summary of Container Environments:

Containers 9 and 10: Immersed Specimens, N2 Overpressure
Containers 11 and 12: Immersed Specimens, CO2 Overpressure
Containers 13 and 14: Vapor-Phase Exposure, N2 Overpressure
Containers 15 and 15: Vapor-Phase Exposure, CO2 Overpressure

Pressure in Container, psig

Time, days	Cont. 9	Cont. 10	Cont. 11	Cont. 12	Cont. 13	Cont. 14	Cont. 15	Cont. 16
0	138	138	183	179	136	135	131	131
1	139	139	192	170	---	---	---	---
4	139	139	160	164	137	137	130	130
5	140	140	160	165	137	137	130	130
6	140	140	162	167	136	136	130	130
7	140	140	165	168	136	136	130	130
8	140	140	167	169	136	136	130	130
11	140	141	171	173	137	136	130	130
18	142	141	179	178	137	136	130	130
25	143	143	185	183	137	136	130	130
32	144	144	190	187	137	136	130	130
39	145	145	194	192	137	135	130	130
46	147	146	199	197	137	136	131	131
53	148	147	201	200	137	136	131	132
60	149	149	204	200	137	136	131	132
67	150	149	206	201	137	136	131	131
74	152	151	206	201	137	136	131	131
81	153	152	210	204	137	136	131	132
88	155	154	212	204	137	136	131	132
95	157	156	212	204	138	136	131	132
102	158	157	214	204	137	136	131	132
109	160	159	215	206	137	136	131	132
116	161	160	215	206	137	136	131	132
123	163	162	215	206	137	136	131	132
130	165	164	216	206	137	136	131	132
137	167	166	216	206	137	136	131	132
144	168	167	216	206	137	136	131	132
151	170	168	216	206	138	136	131	132
158	171	169	216	206	138	136	131	132
168	173	172	216	206	138	136	131	132
172	174	173	217	207	138	136	131	132
179	176	174	217	207	138	135	131	132
183	176	174	217	207	---	---	---	---

APPENDIX A, TABLE A-3
Pressure History, 12-Month Seal-Welded Container Tests

Summary of Container Environments:
Containers 17 and 18: Immersed Specimens, N2 Overpressure
Containers 19 and 20: Immersed Specimens, CO2 Overpressure
Containers 21 and 22: Vapor-Phase Exposure, N2 Overpressure
Containers 23 and 24: Vapor-Phase Exposure, CO2 Overpressure

Time, days	Pressure in Container, psig				Time, days	Pressure in Container, psig			
	Cont. 17	Cont. 18	Cont. 19	Cont. 20		Cont. 21	Cont. 22	Cont. 23	Cont. 24
0	134	134	191	187	0	137	137	135	135
3	139	138	158	158	7	141	141	134	135
5	141	140	163	164	13	141	141	134	135
10	141	141	172	173	20	141	141	134	135
18	142	142	178	181	27	141	141	134	135
24	143	143	182	186	34	141	141	134	135
31	144	144	187	190	41	141	141	134	135
38	145	145	190	194	46	141	141	134	135
45	146	146	193	197	53	141	141	133	134
52	147	147	194	198	60	141	141	133	134
57	148	148	196	200	67	141	141	133	134
64	149	149	197	200	74	141	141	133	134
71	150	150	198	200	81	141	141	133	134
78	151	151	198	200	88	141	141	133	134
85	153	153	198	200	95	141	141	133	134
92	154	154	200	205	102	141	141	133	134
99	156	156	200	207	109	141	141	133	134
106	157	157	200	207	119	141	141	133	134
113	158	158	200	208	123	141	141	133	134
120	160	160	201	209	130	141	141	133	134
130	162	162	201	209	137	141	141	133	133
134	162	163	201	209	144	141	141	133	133
141	163	164	201	209	151	141	141	133	133
148	164	164	201	209	159	141	141	133	133
165	165		201	209	165	141	141	133	133
162	167	167	201	209	173	141	141	132	133
170	167	168	200	207	179	141	141	132	133
176	168	169	200	206	186	141	141	132	133
184	170	170	200	206	200	141	141	132	133
190	170	171	200	206	207	141	141	132	133
197	172	173	200	206	214	141	141	132	133
211	173	174	200	206	221	141	141	132	133
218	174	175	200	206	228	141	141	132	133
225	175	176	200	206	235	141	141	132	133
232	175	176	200	206	242	141	141	132	133

	Pressure in Container, psig					Pressure in Container, psig			
Time, days	Cont. 17	Cont. 18	Cont. 19	Cont. 20	Time, days	Cont. 21	Cont. 22	Cont. 23	Cont. 24
239	176	177	200	206	249	140	140	132	133
246	177	178	200	206	256	140	140	132	133
253	178	179	200	206	263	140	140	132	133
260	179	180	200	206	270	140	140	132	133
267	180	181	200	206	277	140	140	132	133
274	181	182	200	206	284	140	140	132	133
282	182	183	200	206	291	140	140	132	133
288	183	184	200	206	298	140	140	132	133
295	183	184	200	206	305	140	140	132	133
302	184	185	200	206	312	140	140	132	133
309	185	186	200	206	319	140	140	132	133
316	186	187	200	206	326	140	140	132	133
323	187	188	200	206	333	140	141	132	133
330	187	189	200	206	340	140	141	132	133
337	188	190	200	206	347	140	140	132	133
344	189	191	200	206	354	140	140	132	133
351	190	192	200	206					
358	191	192	200	206					
365	192	193	200	206					

Summary of Container Environments:

Containers 25 and 26 Immersed Specimens, N2 Overpressure
Containers 27 and 28: Immersed Specimens, CO2 Overpressure
Containers 29 and 30: Vapor-Phase Exposure, N2 Overpressure
Containers 31 and 32: Vapor-Phase Exposure, CO2 Overpressure

	Pressure in Container, psig					Pressure in Container, psig			
Time, days	Cont. 25	Cont. 26	Cont. 27	Cont. 28	Time, days	Cont. 29	Cont. 30	Cont. 31	Cont. 32
0	137	135	178(a)	180(a)	0	136	136	135	135
5	142	141	166	164	3	140	140	135	135
12	143	142	176	175	10	141	141	135	136
19	144	143	181	180	17	141	141	135	135
26	146	144	186	184	24	141	141	135	135
33	147	145	190	188	31	141	141	135	135
40	148	146	192	191	38	141	141	135	135
54	151	148	197	197	52	141	141	135	135
68	153	150	200	199	66	141	141	135	135
85	157	154	201	202	83	141	141	135	135
96	160	156	202	203	94	141	141	135	135
110	163	159	202	203	108	141	141	135	134
125	167	162	202	204	123	141	141	134	134
139	169	164	202	204	137	141	141	134	134
152	172	167	202	204	150	141	141	135	134
173	175	170	202	204	171	141	141	134	134
194	178	173	202	204	192	141	141	134	134
215	181	176	202	204	213	141	140	134	134
236	184	180	202	204	234	141	140	134	134
257	188	182	202	204	255	141	140	134	134
278	191	185	202	204	276	141	140	134	134
299	195	188	202	204	297	141	140	134	134
320	197	192	202	204	318	142	141	134	134
338	200	194	(pressure before venting containers 25 and 26)						
338	166	165	(pressure after venting containers 25 and 26)						
341	168	167	202	204	339	142	140	134	134
362	170	169	202	204	360	142	140	134	134
383	172	172	202	204	381	142	140	134	134
404	175	174	202	204	402	141	140	134	134
425	177	176	202	204	423	142	140	134	134

(a) 155 psig can be used as the hypothetical starting pressure for these tests.

	Pressure in Container, psig					Pressure in Container, psig			
Time, days	Cont. 25	Cont. 26	Cont. 27	Cont. 28	Time, days	Cont. 29	Cont. 30	Cont. 31	Cont. 32
446	180	179	202	204	444	142	140	134	134
467	182	181	202	204	465	142	140	134	134
488	184	183	202	204	486	142	140	134	134
502	186	184	202	204	500	142	140	133	134
523	188	186	202	204	521	142	140	133	134
551	190	188	202	204	549	142	140	133	134
572	192	190	202	204	570	142	140	133	134
593	194	193	202	204	591	142	140	133	134
614	195	194	202	204	612	142	140	133	134
635	198	197	203	205	633	142	140	133	134
656	199	198	203	205	654	141	140	133	134
677	201	200	203	205	675	142	140	133	134
698	203	202	203	205	696	141	140	133	134
719	204	203	202	204	717	141	140	133	133
728	206	204	203	205	726	141	140	133	134

A-7

APPENDIX A. TABLE A-5
Pressure History. Controlled-CO2 Addition Seal-Welded Container Tests

Summary of Container Environments:

All specimens are completely immersed in Brine A in each container
Container 33: 0.32 mol CO2/m2 steel
Container 34: 0.16 mol CO2/m2 steel
Container 35: 0.063 mol CO2/m2 steel
Container 36: 0.032 mol CO2/m2 steel + N2
Container 37: 0.016 mol CO2/m2 steel + N2
Container 38: 0.00 mol CO2/m2 steel (N2 only)

	Pressure in Container, psig				Pressure in Container, psig		
Time, days	Cont. 33	Cont. 34	Cont. 35	Time, days	Cont. 36	Cont. 37	Cont. 38
0	59	21	-2 (est.)	0	22	19	31
8	69	30	0	6	25	20	34
14	73	33	4	12	27	21	34
22	77	37	6	20	28	23	35
29	80	38	8	27	30	24	36
36	82	40	10	34	31	25	37
43	84	42	10	41	31	26	38
50	85	43	10	48	32	27	39
71	88	44	12	69	34	30	42
85	89	45	13	83	34	31	44
99	90	46	14	97	36	34	46
113	92	46	15	111	38	35	49
127	93	46	17	125	41	39	52
141	94	47	19	139	44	41	56
155	94	47	21	153	46	43	58
162	94	47	22	160	48	44	60
176	94	48	24	174	51	47	63
190	94	48	26	188	53	50	65
212	95	48	30	210	57	53	70
225	95	49	32	223	60	56	72
239	95	49	34	237	62	58	75
253	96	49	36	251	64	61	79
267	95	50	38	265	67	63	81
281	95	50	40	279	69	65	83
295	95	50	42	293	72	67	86
309	95	50	44	307	74	70	88

APPENDIX B-1: INDIVIDUAL SPECIMEN CORROSION-RATE DATA, ANOXIC BRINE (N2/IMMERSED) ENVIRONMENT, SEAL-WELDED-CONTAINER TEST METHOD

Test No.: 1
Test Type: Immersion
Test Environment: Simulated WIPP Brine A, N2 Overpressure (10 atm)
Test Temperature: 30 ±5°C
Test Exposure: 3 Months

Specimen	Material Type	Length, mm	Width, mm	Thickness, mm	Top Hole ID, mm	Bot. Hole ID, mm	Area, dm2	Initial Wt., g	Final Wt., g	Corrosion Rate, mpy	Corrosion Rate, µm/yr
J1	Low-Carbon Steel, Lot J	190.81	86.46	0.695	8.00	8.00	3.321	87.6936	87.5674	0.072	1.834
J2	Low-Carbon Steel, Lot J	190.70	86.41	0.704	8.00	8.00	3.318	89.1819	89.0488	0.076	1.936
J3	Low-Carbon Steel, Lot J	191.42	86.51	0.689	7.99	7.99	3.334	88.0226	87.8895	0.076	1.927
J201	Low-Carbon Steel, Lot J	190.63	51.43	0.712	7.99	8.00	1.979	52.7773	52.7083	0.066	1.683
J202	Low-Carbon Steel, Lot J	190.76	51.36	0.711	8.06	7.99	1.977	52.7223	52.6498	0.070	1.770
J203	Low-Carbon Steel, Lot J	190.72	51.44	0.712	8.02	8.06	1.980	52.7432	SA*	SA	SA
K1	Low-Carbon Steel, Lot K	190.63	86.26	0.878	7.96	7.97	3.322	110.9676	110.8360	0.075	1.912
K2	Low-Carbon Steel, Lot K	190.76	86.42	0.884	7.99	7.96	3.331	111.6249	111.4954	0.074	1.876
K3	Low-Carbon Steel, Lot K	190.46	86.34	0.882	7.96	7.96	3.322	111.2495	111.1130	0.078	1.983
K201	Low-Carbon Steel, Lot K	190.36	51.33	0.877	7.97	7.97	1.981	64.9559	64.8842	0.069	1.747
K202	Low-Carbon Steel, Lot K	190.30	51.39	0.874	7.98	7.98	1.983	65.0662	64.9946	0.069	1.743
K203	Low-Carbon Steel, Lot K	190.31	51.49	0.879	7.98	7.98	1.987	65.6125	SA	SA	SA
L1	Low-Carbon Steel, Lot L	190.83	86.32	1.536	7.94	7.94	3.367	195.4656	195.3277	0.078	1.976
L2	Low-Carbon Steel, Lot L	190.86	86.47	1.549	7.94	7.93	3.375	196.6869	196.5469	0.079	2.002
L3	Low-Carbon Steel, Lot L	190.82	86.37	1.545	7.95	7.94	3.370	196.8227	196.6862	0.077	1.955
L201	Low-Carbon Steel, Lot L	190.84	51.36	1.537	7.96	7.95	2.023	115.3703	115.2924	0.073	1.859
L202	Low-Carbon Steel, Lot L	190.98	51.44	1.506	7.95	7.95	2.025	112.5495	112.4681	0.076	1.939
L203	Low-Carbon Steel, Lot L	190.96	51.43	1.508	7.96	7.95	2.025	112.0076	SA	SA	SA
M1	Low-Carbon Steel, Lot M	189.75	83.66	1.605	7.96	7.96	3.251	197.7103	197.5857	0.073	1.850
M2	Low-Carbon Steel, Lot M	189.91	84.32	1.615	7.99	7.99	3.279	200.2593	200.1577	0.059	1.495
M3	Low-Carbon Steel, Lot M	189.76	84.32	1.597	7.98	7.97	3.276	197.5366	197.4064	0.076	1.918
M201	Low-Carbon Steel, Lot M	190.31	51.48	1.610	7.98	7.98	2.025	121.0624	120.9845	0.073	1.856
M202	Low-Carbon Steel, Lot M	190.55	51.38	1.630	7.98	7.98	2.025	121.8096	121.7324	0.072	1.840
M203	Low-Carbon Steel, Lot M	190.33	51.33	1.583	7.98	7.96	2.018	117.6252	SA	SA	SA

* SA = Specimen was retained for surface analysis.

Test No.: 2
Test Type: Immersion
Test Environment: Simulated WIPP Brine A, N2 Overpressure (10 atm)
Test Temperature: 30 ±5°C
Test Exposure: 3 Months

Specimen	Material Type	Length, mm	Width, mm	Thickness, mm	Top Hole ID, mm	Bot. Hole ID, mm	Area, dm2	Initial Wt., g	Final Wt., g	Corrosion Rate, mpy	Corrosion Rate, μm/yr
J4	Low-Carbon Steel, Lot J	191.06	86.53	0.705	7.96	7.95	3.329	89.0290	88.8927	0.078	1.976
J5	Low-Carbon Steel, Lot J	190.92	86.59	0.715	7.95	7.95	3.330	90.1033	89.9545	0.085	2.157
J6	Low-Carbon Steel, Lot J	190.94	86.63	0.700	7.95	7.94	3.331	88.1796	88.0323	0.084	2.134
J204	Low-Carbon Steel, Lot J	189.68	51.26	0.717	7.95	7.95	1.963	52.3102	52.2325	0.075	1.910
J205	Low-Carbon Steel, Lot J	190.95	51.46	0.711	7.95	7.95	1.983	52.4953	52.4071	0.084	2.146
J206	Low-Carbon Steel, Lot J	190.63	51.37	0.705	7.95	7.95	1.976	52.2646	SA*	SA	SA
K4	Low-Carbon Steel, Lot K	190.38	86.29	0.877	7.96	7.96	3.319	111.1520	110.9998	0.087	2.213
K5	Low-Carbon Steel, Lot K	190.26	86.30	0.878	7.97	7.97	3.317	111.2736	111.1244	0.085	2.171
K6	Low-Carbon Steel, Lot K	190.45	86.33	0.871	7.96	7.96	3.321	110.2407	110.0600	0.103	2.626
K204	Low-Carbon Steel, Lot K	190.24	51.42	0.885	7.96	7.97	1.984	66.3359	66.2520	0.080	2.041
K205	Low-Carbon Steel, Lot K	190.11	51.36	0.874	7.97	7.97	1.979	64.8904	64.8103	0.077	1.953
K206	Low-Carbon Steel, Lot K	190.14	51.42	0.887	7.97	7.96	1.983	66.3186	SA	SA	SA
L4	Low-Carbon Steel, Lot L	190.91	86.43	1.556	7.97	7.96	3.374	197.5401	197.3664	0.098	2.484
L5	Low-Carbon Steel, Lot L	190.96	86.13	1.544	7.96	7.96	3.363	196.3888	196.2330	0.088	2.236
L6	Low-Carbon Steel, Lot L	190.90	86.35	1.551	7.98	7.97	3.371	197.1904	197.0352	0.087	2.222
L204	Low-Carbon Steel, Lot L	191.07	51.48	1.503	7.96	7.96	2.028	112.3139	112.2253	0.083	2.109
L205	Low-Carbon Steel, Lot L	190.79	51.47	1.551	7.97	7.97	2.027	115.6739	SA	SA	SA
L206	Low-Carbon Steel, Lot L	190.75	51.53	1.539	7.97	7.97	2.028	115.0275	114.9364	0.085	2.168
M4	Low-Carbon Steel, Lot M	190.01	84.38	1.594	7.96	7.96	3.282	198.2676	198.1661	0.059	1.492
M5	Low-Carbon Steel, Lot M	190.12	84.39	1.607	7.96	7.96	3.285	199.5875	199.4617	0.073	1.848
M6	Low-Carbon Steel, Lot M	190.02	84.39	1.605	7.97	7.96	3.283	199.4802	199.3576	0.071	1.802
M204	Low-Carbon Steel, Lot M	190.50	51.16	1.612	7.97	7.97	2.015	120.5647	120.4844	0.076	1.923
M205	Low-Carbon Steel, Lot M	190.51	51.19	1.628	7.96	7.96	2.017	121.5140	121.4350	0.074	1.890
M206	Low-Carbon Steel, Lot M	190.48	51.23	1.582	7.97	7.96	2.016	118.7620	SA	SA	SA

* SA = Specimen was retained for surface analysis.

B-3

Test No: 9
Test Type: Immersion
Test Environment: Simulated WIPP Brine A, N2 Overpressure (10 atm)
Test Temperature: 30 ±5°C
Test Exposure: 6 Months

Specimen	Material Type	Length, mm	Width, mm	Thickness, mm	Top Hole ID, mm	Bot. Hole ID, mm	Area, dm2	Initial Wt., g	Final Wt., g	Corrosion Rate, mpy	Corrosion Rate, μm/yr
J25	Low-Carbon Steel, Lot J	188.90	80.04	0.702	7.92	7.93	3.045	80.9667	80.7737	0.0614	1.559
J26	Low-Carbon Steel, Lot J	188.90	80.05	0.704	7.97	7.95	3.046	80.8076	80.5991	0.0663	1.684
J26	Low-Carbon Steel, Lot J	188.90	80.06	0.704	7.96	7.95	3.046	80.7470	80.5377	0.0666	1.691
J225	Low-Carbon Steel, Lot J	188.83	50.76	0.694	7.97	7.60	1.935	50.3613	SA*	SA	SA
J226	Low-Carbon Steel, Lot J	188.82	50.77	0.697	7.70	8.01	1.935	50.3302	50.1976	0.0664	1.686
J227	Low-Carbon Steel, Lot J	188.83	50.77	0.712	7.93	7.90	1.935	51.5671	51.4323	0.0675	1.714
K25	Low-Carbon Steel, Lot K	188.90	80.05	0.882	7.97	7.98	3.056	102.9565	102.7551	0.0638	1.622
K26	Low-Carbon Steel, Lot K	188.89	80.06	0.845	7.98	7.97	3.054	98.7986	98.5901	0.0661	1.680
K27	Low-Carbon Steel, Lot K	188.90	80.06	0.875	7.98	7.98	3.056	101.7641	101.5616	0.0642	1.630
K225	Low-Carbon Steel, Lot K	188.83	50.65	0.856	7.97	7.97	1.938	62.3278	SA	SA	SA
K226	Low-Carbon Steel, Lot K	188.84	50.70	0.882	7.97	7.97	1.942	64.3067	64.1754	0.0655	1.664
K227	Low-Carbon Steel, Lot K	188.83	50.72	0.870	7.97	7.97	1.942	63.6805	63.5473	0.0665	1.688
L25	Low-Carbon Steel, Lot L	188.89	79.98	1.501	7.98	7.98	3.090	175.5799	175.3297	0.0784	1.993
L26	Low-Carbon Steel, Lot L	188.91	79.99	1.510	7.98	7.98	3.091	175.0349	174.8040	0.0724	1.838
L27	Low-Carbon Steel, Lot L	188.92	80.00	1.496	7.97	7.97	3.091	175.1505	174.9067	0.0764	1.941
L225	Low-Carbon Steel, Lot L	188.92	50.80	1.516	7.98	7.98	1.980	110.7318	110.5803	0.0741	1.883
L226	Low-Carbon Steel, Lot L	188.92	50.80	1.510	7.98	7.98	1.979	110.8363	110.6818	0.0756	1.921
L227	Low-Carbon Steel, Lot L	188.93	50.78	1.503	7.98	7.98	1.978	110.1434	SA	SA	SA
M25	Low-Carbon Steel, Lot M	188.87	80.03	1.592	7.97	7.98	3.097	186.8781	186.6534	0.0703	1.785
M26	Low-Carbon Steel, Lot M	188.89	80.03	1.624	7.98	7.98	3.099	189.3488	189.1299	0.0684	1.738
M27	Low-Carbon Steel, Lot M	188.89	80.05	1.585	7.98	7.98	3.097	185.2336	185.0096	0.0701	1.780
M225	Low-Carbon Steel, Lot M	188.97	50.45	1.615	7.99	7.99	1.972	118.7449	118.6025	0.0700	1.777
M226	Low-Carbon Steel, Lot M	188.97	50.56	1.593	7.98	7.98	1.975	116.9096	SA	SA	SA
M227	Low-Carbon Steel, Lot M	188.96	50.60	1.590	7.99	7.98	1.976	116.5333	116.3875	0.0715	1.815

* SA = Specimen was retained for surface analysis.

B-4

Test No: 10
Test Type: Immersion
Test Environment: Simulated WIPP Brine A, N2 Overpressure (10 atm)
Test Temperature: 30 ±5°C
Test Exposure: 6 Months

Specimen	Material Type	Length, mm	Width, mm	Thickness, mm	Top Hole ID, mm	Bot. Hole ID, mm	Area, dm2	Initial Wt., g	Final Wt., g	Corrosion Rate, mpy	Corrosion Rate, µm/yr
J28	Low-Carbon Steel, Lot J	188.89	80.06	0.697	7.95	7.95	3.046	80.0200	79.8289	0.0605	1.537
J29	Low-Carbon Steel, Lot J	188.90	80.07	0.694	7.99	7.99	3.046	79.8873	79.6907	0.0623	1.581
J30	Low-Carbon Steel, Lot J	188.90	80.08	0.689	7.98	7.95	3.046	78.2569	78.0661	0.0604	1.535
J228	Low-Carbon Steel, Lot J	188.82	50.77	0.708	7.98	7.89	1.935	51.1553	SA*	SA	SA
J229	Low-Carbon Steel, Lot J	188.82	50.78	0.696	7.89	7.95	1.935	50.3692	50.2458	0.0615	1.562
J230	Low-Carbon Steel, Lot J	188.82	50.79	0.716	7.89	7.91	1.936	51.6435	51.5210	0.0610	1.550
K28	Low-Carbon Steel, Lot K	188.88	80.06	0.868	8.00	7.98	3.055	101.0222	100.8198	0.0639	1.623
K29	Low-Carbon Steel, Lot K	188.89	80.06	0.872	7.99	7.99	3.056	101.4461	101.2481	0.0625	1.587
K30	Low-Carbon Steel, Lot K	188.89	80.07	0.873	7.99	7.99	3.056	102.0831	101.8812	0.0637	1.618
K228	Low-Carbon Steel, Lot K	188.82	50.76	0.881	7.99	7.99	1.943	64.3251	64.1936	0.0653	1.658
K229	Low-Carbon Steel, Lot K	188.82	50.75	0.872	7.99	7.99	1.943	63.6800	SA	SA	SA
K230	Low-Carbon Steel, Lot K	188.82	50.70	0.870	7.99	7.99	1.941	63.6278	63.4930	0.0670	1.702
L28	Low-Carbon Steel, Lot L	188.91	80.01	1.562	8.00	8.00	3.095	182.4419	182.2019	0.0748	1.900
L29	Low-Carbon Steel, Lot L	188.91	80.02	1.557	8.00	8.00	3.095	180.9204	180.6789	0.0753	1.912
L30	Low-Carbon Steel, Lot L	188.91	80.01	1.509	8.00	8.00	3.092	175.5258	175.2851	0.0751	1.907
L228	Low-Carbon Steel, Lot L	188.91	50.79	1.515	8.00	8.00	1.979	110.3849	SA	SA	SA
L229	Low-Carbon Steel, Lot L	188.91	50.78	1.572	8.01	8.00	1.982	115.3170	115.1635	0.0747	1.898
L230	Low-Carbon Steel, Lot L	188.90	50.80	1.549	8.00	8.00	1.981	113.1697	113.0134	0.0761	1.933
M28	Low-Carbon Steel, Lot M	188.39	80.05	1.612	7.99	8.00	3.091	188.3112	188.1011	0.0656	1.665
M29	Low-Carbon Steel, Lot M	188.90	80.05	1.630	8.00	8.00	3.100	191.1087	190.9019	0.0643	1.634
M30	Low-Carbon Steel, Lot M	188.91	80.04	1.576	8.00	8.00	3.097	183.1318	182.9269	0.0638	1.621
M228	Low-Carbon Steel, Lot M	188.96	50.70	1.596	8.00	7.99	1.980	117.1475	117.0186	0.0628	1.594
M229	Low-Carbon Steel, Lot M	188.89	50.66	1.601	8.00	8.00	1.978	117.3251	SA	SA	SA
M230	Low-Carbon Steel, Lot M	188.96	50.80	1.587	8.00	8.00	1.984	117.2574	117.1245	0.0646	1.641

* SA = Specimen was retained for surface analysis.

B-5

Test No: 17
Test Type: Immersion
Test Environment: Simulated WIPP Brine A, N2 Overpressure (10 atm)
Test Temperature: 30 ±5°C
Test Exposure: 12 Months

Specimen	Material Type	Length, mm	Width, mm	Thickness, mm	Top Hole ID, mm	Bot. Hole ID, mm	Area, dm2	Initial Wt., g	Final Wt., g	Corrosion Rate, mpy	Corrosion Rate, μm/yr
J49	Low-Carbon Steel, Lot J	189.09	79.94	0.701	8.00	7.96	3.044	80.8697	80.6038	0.0423	1.075
J50	Low-Carbon Steel, Lot J	189.08	79.96	0.710	8.00	7.99	3.045	81.8711	81.6146	0.0408	1.037
J51	Low-Carbon Steel, Lot J	189.08	79.95	0.711	7.99	7.97	3.045	82.2706	81.9798	0.0463	1.176
J249	Low-Carbon Steel, Lot J	189.05	50.71	0.713	7.95	7.88	1.935	51.6008	51.4386	0.0406	1.032
J250	Low-Carbon Steel, Lot J	189.05	50.73	0.709	7.96	8.00	1.936	51.3007	SA*	SA	SA
J251	Low-Carbon Steel, Lot J	189.05	50.62	0.717	7.98	7.98	1.932	51.3406	51.1739	0.0418	1.062
K49	Low-Carbon Steel, Lot K	189.08	79.95	0.885	7.89	7.92	3.056	102.3283	102.0000	0.0521	1.323
K50	Low-Carbon Steel, Lot K	189.09	79.96	0.884	7.86	7.88	3.056	102.3078	101.9911	0.0502	1.276
K51	Low-Carbon Steel, Lot K	189.08	79.95	0.886	7.92	7.81	3.056	102.6056	102.2900	0.0500	1.271
K249	Low-Carbon Steel, Lot K	189.05	50.71	0.878	7.90	7.88	1.944	64.2702	64.0744	0.0488	1.240
K250	Low-Carbon Steel, Lot K	189.05	50.71	0.867	7.93	7.92	1.944	63.8434	63.6375	0.0513	1.304
K251	Low-Carbon Steel, Lot K	189.06	50.70	0.886	7.93	7.93	1.944	64.7405	SA	SA	SA
L49	Low-Carbon Steel, Lot L	189.22	80.02	1.511	7.93	7.93	3.097	175.6488	175.3203	0.0514	1.306
L50	Low-Carbon Steel, Lot L	189.21	80.03	1.492	7.94	7.95	3.096	174.8962	174.5729	0.0506	1.285
L51	Low-Carbon Steel, Lot L	189.21	80.02	1.555	7.94	7.93	3.100	181.6679	181.3421	0.0509	1.294
L249	Low-Carbon Steel, Lot L	189.19	50.72	1.511	7.95	7.93	1.979	110.2186	110.0169	0.0494	1.254
L250	Low-Carbon Steel, Lot L	189.20	50.73	1.528	8.00	8.00	1.981	111.5012	111.2935	0.0508	1.291
L251	Low-Carbon Steel, Lot L	189.20	50.73	1.525	8.02	7.98	1.980	111.2591	SA	SA	SA
M49	Low-Carbon Steel, Lot M	189.33	80.15	1.599	7.98	7.98	3.109	186.2713	185.9466	0.0506	1.286
M50	Low-Carbon Steel, Lot M	189.33	80.17	1.551	8.00	8.00	3.107	182.8244	182.4943	0.0515	1.308
M51	Low-Carbon Steel, Lot M	189.34	80.17	1.557	7.99	8.00	3.108	182.4878	182.1446	0.0535	1.360
M249	Low-Carbon Steel, Lot M	189.06	50.59	1.607	8.01	7.98	1.978	117.4947	117.2953	0.0489	1.241
M250	Low-Carbon Steel, Lot M	189.07	50.63	1.592	7.98	7.97	1.979	116.7827	SA	SA	SA
M251	Low-Carbon Steel, Lot M	189.08	50.60	1.610	7.99	7.98	1.979	117.6595	117.4538	0.0504	1.280

* SA = Specimen was retained for surface analysis.

B-6

Test No: 18
Test Type: Immersion
Test Environment: Simulated WIPP Brine A, N2 Overpressure (10 atm)
Test Temperature: 30 ±5°C
Test Exposure: 12 Months

Specimen	Material Type	Length, mm	Width, mm	Thickness, mm	Top Hole ID, mm	Bot. Hole ID, mm	Area, dm2	Initial Wt., g	Final Wt., g	Corrosion Rate, mpy	Corrosion Rate, μm/yr
J52	Low-Carbon Steel, Lot J	189.03	79.97	0.710	7.90	7.94	3.045	81.9938	81.7411	0.0402	1.021
J53	Low-Carbon Steel, Lot J	189.03	79.97	0.703	7.91	7.92	3.045	81.7066	81.4348	0.0433	1.099
J54	Low-Carbon Steel, Lot J	189.09	80.00	0.707	7.95	7.94	3.047	81.8526	81.5930	0.0413	1.049
J252	Low-Carbon Steel, Lot J	189.07	50.68	0.709	7.93	7.88	1.934	51.5550	51.3992	0.0390	0.992
J253	Low-Carbon Steel, Lot J	189.06	50.73	0.712	7.94	7.91	1.936	52.0054	51.8393	0.0416	1.056
J254	Low-Carbon Steel, Lot J	189.07	50.73	0.714	7.93	7.90	1.936	51.7604	SA*	SA	SA
K52	Low-Carbon Steel, Lot K	189.09	79.99	0.879	7.85	7.89	3.057	102.0543	101.7510	0.0481	1.221
K53	Low-Carbon Steel, Lot K	189.10	79.97	0.872	7.92	7.84	3.056	101.7205	101.4067	0.0498	1.264
K54	Low-Carbon Steel, Lot K	189.09	79.97	0.874	7.85	7.88	3.056	101.4722	101.1585	0.0497	1.264
K252	Low-Carbon Steel, Lot K	189.06	50.77	0.885	7.93	7.90	1.947	64.8092	64.6186	0.0474	1.205
K253	Low-Carbon Steel, Lot K	189.08	50.79	0.885	7.95	7.89	1.948	64.9056	64.7110	0.0484	1.230
K254	Low-Carbon Steel, Lot K	189.07	50.74	0.885	7.95	7.93	1.946	65.0250	SA	SA	SA
L52	Low-Carbon Steel, Lot L	189.21	80.02	1.534	7.95	7.96	3.099	179.1034	178.7480	0.0556	1.412
L53	Low-Carbon Steel, Lot L	189.23	80.04	1.551	7.96	7.95	3.101	180.9391	180.6093	0.0515	1.309
L54	Low-Carbon Steel, Lot L	189.21	80.03	1.552	7.94	7.93	3.100	181.8081	181.4741	0.0522	1.326
L252	Low-Carbon Steel, Lot L	189.21	50.75	1.544	7.97	7.95	1.982	112.8618	SA	SA	SA
L253	Low-Carbon Steel, Lot L	189.20	50.73	1.499	7.97	7.93	1.979	109.7198	109.5079	0.0519	1.318
L254	Low-Carbon Steel, Lot L	189.19	50.72	1.545	7.96	7.95	1.981	112.0234	111.8130	0.0515	1.307
M52	Low-Carbon Steel, Lot M	189.36	80.20	1.544	7.93	7.93	3.109	182.6694	182.3404	0.0513	1.303
M53	Low-Carbon Steel, Lot M	189.35	80.24	1.555	7.93	7.93	3.111	182.9135	182.5880	0.0507	1.288
M54	Low-Carbon Steel, Lot M	189.38	80.18	1.557	7.93	7.94	3.109	182.9513	182.6276	0.0505	1.282
M252	Low-Carbon Steel, Lot M	189.11	50.67	1.606	7.94	7.95	1.982	117.3912	SA	SA	SA
M253	Low-Carbon Steel, Lot M	189.11	50.69	1.591	7.95	7.94	1.982	116.5208	116.3211	0.0488	1.241
M254	Low-Carbon Steel, Lot M	189.12	50.62	1.596	7.96	7.95	1.979	116.7564	116.5523	0.0500	1.269

* SA = Specimen was retained for surface analysis.

Test No.: 25
Test Type: Immersion
Test Environment: Simulated WIPP Brine A, N2 Overpressure (10 atm)
Test Temperature: 30 ±5°C
Test Exposure: 24 Months

Specimen	Material Type	Length, mm	Width, mm	Thickness, mm	Top Hole ID, mm	Bot. Hole ID, mm	Area, dm2	Initial Wt., g	Final Wt., g	Corrosion Rate, mpy	Corrosion Rate, μm/yr
J73	Low-Carbon Steel, Lot J	188.86	79.90	0.709	7.89	7.92	3.040	81.9915	81.5206	0.0381	0.967
J74	Low-Carbon Steel, Lot J	188.89	79.92	0.718	7.89	7.88	3.042	82.8456	82.3799	0.0376	0.956
J75	Low-Carbon Steel, Lot J	188.86	79.89	0.703	7.89	7.89	3.039	81.6919	81.2330	0.0371	0.943
J273	Low-Carbon Steel, Lot J	189.04	50.83	0.709	7.86	7.85	1.940	51.7868	51.4873	0.0380	0.964
J274	Low-Carbon Steel, Lot J	189.06	50.84	0.692	7.87	7.87	1.940	50.6111	SA*	SA	SA
J275	Low-Carbon Steel, Lot J	189.09	50.85	0.717	7.89	7.88	1.941	52.2689	51.9801	0.0366	0.929
K73	Low-Carbon Steel, Lot K	188.89	79.94	0.858	7.88	7.88	3.051	99.8946	99.2461	0.0523	1.327
K74	Low-Carbon Steel, Lot K	188.86	79.89	0.858	7.89	7.88	3.048	99.8410	99.2438	0.0482	1.223
K75	Low-Carbon Steel, Lot K	188.90	79.94	0.870	7.94	7.94	3.051	101.1830	100.6200	0.0454	1.152
K273	Low-Carbon Steel, Lot K	189.04	50.82	0.877	7.91	7.92	1.948	64.3493	63.9994	0.0442	1.121
K274	Low-Carbon Steel, Lot K	189.05	50.84	0.867	7.93	7.94	1.948	63.4702	63.1022	0.0464	1.179
K275	Low-Carbon Steel, Lot K	189.04	50.82	0.864	7.91	7.92	1.947	63.4661	SA	SA	SA
L73	Low-Carbon Steel, Lot L	188.91	79.96	1.559	7.92	7.96	3.093	180.6934	180.2229	0.0374	0.950
L74	Low-Carbon Steel, Lot L	188.96	80.00	1.568	7.85	7.92	3.096	182.0639	181.5921	0.0375	0.952
L75	Low-Carbon Steel, Lot L	188.97	79.98	1.518	7.90	7.86	3.092	177.1573	176.7111	0.0355	0.901
L273	Low-Carbon Steel, Lot L	189.18	50.79	1.503	7.94	7.88	1.982	109.3805	SA	SA	SA
L274	Low-Carbon Steel, Lot L	189.19	50.82	1.554	7.92	7.88	1.986	113.2251	112.9405	0.0352	0.895
L275	Low-Carbon Steel, Lot L	189.18	50.88	1.558	7.90	7.91	1.988	113.9692	113.6746	0.0364	0.925
M73	Low-Carbon Steel, Lot M	189.04	80.15	1.578	7.90	7.90	3.103	185.8791	185.4481	0.0341	0.867
M74	Low-Carbon Steel, Lot M	189.03	80.10	1.586	7.92	7.91	3.102	186.1507	185.6994	0.0358	0.908
M75	Low-Carbon Steel, Lot M	189.02	80.13	1.601	7.93	7.94	3.104	187.5477	187.0784	0.0372	0.944
M273	Low-Carbon Steel, Lot M	189.09	50.79	1.552	7.92	7.94	1.983	114.4320	114.1137	0.0395	1.002
M274	Low-Carbon Steel, Lot M	189.14	50.81	1.576	7.94	7.91	1.986	115.8318	SA	SA	SA
M275	Low-Carbon Steel, Lot M	189.16	50.98	1.581	7.91	7.89	1.993	116.7991	116.4833	0.0390	0.989

*SA = Specimen was retained for surface analysis.

Test No.: 26
Test Type: Immersion
Test Environment: Simulated WIPP Brine A, N2 Overpressure (10 atm)
Test Temperature: 30 ±5°C
Test Exposure: 24 Months

Specimen	Material Type	Length, mm	Width, mm	Thickness, mm	Top Hole ID, mm	Bot. Hole ID, mm	Area, dm2	Initial Wt., g	Final Wt., g	Corrosion Rate, mpy	Corrosion Rate, µm/yr
J76	Low-Carbon Steel, Lot J	188.95	79.99	0.704	7.93	7.95	3.044	81.5207	81.0630	0.0369	0.938
J77	Low-Carbon Steel, Lot J	188.96	79.99	0.708	7.94	7.94	3.045	82.1630	81.6953	0.0377	0.959
J78	Low-Carbon Steel, Lot J	188.99	79.98	0.706	7.94	7.95	3.045	81.4929	81.0709	0.0341	0.865
J276	Low-Carbon Steel, Lot J	189.15	50.89	0.714	7.95	7.96	1.943	52.1371	51.8144	0.0408	1.037
J277	Low-Carbon Steel, Lot J	189.14	50.90	0.699	7.94	7.94	1.943	51.5245	51.2103	0.0397	1.010
J278	Low-Carbon Steel, Lot J	189.15	50.93	0.712	7.96	7.93	1.945	51.9054	SA*	SA	SA
K76	Low-Carbon Steel, Lot K	188.98	79.97	0.861	7.94	7.96	3.053	100.3056	99.7797	0.0423	1.075
K77	Low-Carbon Steel, Lot K	188.95	79.99	0.872	7.95	7.93	3.054	101.3347	100.7793	0.0447	1.135
K78	Low-Carbon Steel, Lot K	188.95	79.99	0.870	7.95	7.93	3.054	101.0741	100.5218	0.0444	1.129
K276	Low-Carbon Steel, Lot K	189.10	50.90	0.863	7.95	7.95	1.951	63.6048	SA	SA	SA
K277	Low-Carbon Steel, Lot K	189.09	50.86	0.869	7.94	7.95	1.950	63.8011	63.4727	0.0414	1.051
K278	Low-Carbon Steel, Lot K	189.08	50.88	0.877	7.93	7.94	1.951	64.4909	64.1461	0.0434	1.103
L76	Low-Carbon Steel, Lot L	189.01	80.05	1.539	7.92	7.93	3.097	179.1690	178.7389	0.0341	0.867
L77	Low-Carbon Steel, Lot L	189.02	80.05	1.546	7.93	7.91	3.097	180.9903	180.5484	0.0351	0.891
L78	Low-Carbon Steel, Lot L	189.00	80.06	1.539	7.95	7.95	3.097	180.3304	179.9089	0.0334	0.850
L276	Low-Carbon Steel, Lot L	189.25	50.70	1.490	7.95	7.94	1.978	108.9996	108.7177	0.0350	0.890
L277	Low-Carbon Steel, Lot L	189.24	50.69	1.563	7.96	7.94	1.981	113.9647	SA	SA	SA
L278	Low-Carbon Steel, Lot L	189.25	50.73	1.510	7.95	7.96	1.980	110.1100	109.8020	0.0382	0.971
M76	Low-Carbon Steel, Lot M	189.07	80.15	1.592	7.93	7.95	3.105	186.8068	186.3409	0.0369	0.937
M77	Low-Carbon Steel, Lot M	189.05	80.17	1.573	7.93	7.93	3.104	184.7843	184.3148	0.0372	0.944
M78	Low-Carbon Steel, Lot M	189.06	80.18	1.581	7.92	7.93	3.105	186.2283	185.7450	0.0383	0.972
M276	Low-Carbon Steel, Lot M	189.20	50.89	1.598	7.95	7.96	1.991	117.7083	117.3963	0.0385	0.978
M277	Low-Carbon Steel, Lot M	189.21	50.88	1.578	7.96	7.91	1.989	116.8505	SA	SA	SA
M278	Low-Carbon Steel, Lot M	189.22	50.75	1.594	7.96	7.97	1.985	117.3540	117.0425	0.0386	0.979

*SA = Specimen was retained for surface analysis.

APPENDIX B-2: INDIVIDUAL SPECIMEN CORROSION-RATE DATA, ANOXIC BRINE (N2/VAPOR) ENVIRONMENT, SEAL-WELDED-CONTAINER TEST METHOD

Test No.: 5
Test Type: Vapor Phase Exposure
Test Environment: Simulated WIPP Brine A Vapor + N2 (12 atm)
Test Temperature: 30 ±5°C
Test Exposure: 3 Months

Specimen	Material Type	Length, mm	Width, mm	Thickness, mm	Top Hole ID, mm	Bot. Hole ID, mm	Area, dm2	Initial Wt., g	Final Wt., g	Corrosion Rate, mpy	Corrosion Rate, µm/yr
J13	Low-Carbon Steel, Lot J	190.72	86.48	0.721	8.01	8.01	3.322	89.7014	89.6852	0.010	0.246
J14	Low-Carbon Steel, Lot J	190.86	86.15	0.699	8.00	8.00	3.311	88.0915	88.0757	0.009	0.240
J15	Low-Carbon Steel, Lot J	190.48	86.53	0.708	8.01	8.02	3.319	89.0198	89.0032	0.010	0.252
J213	Low-Carbon Steel, Lot J	190.22	51.26	0.710	8.00	8.00	1.968	51.7779	SA*	SA	SA
J214	Low-Carbon Steel, Lot J	189.00	51.18	0.714	8.02	8.01	1.952	51.6697	51.6596	0.010	0.261
J215	Low-Carbon Steel, Lot J	190.78	51.31	0.714	8.01	8.01	1.976	52.5299	52.5174	0.013	0.319
K13	Low-Carbon Steel, Lot K	190.63	86.12	0.877	7.96	7.96	3.316	110.5081	110.4738	0.021	0.521
K14	Low-Carbon Steel, Lot K	189.15	86.02	0.866	7.97	7.96	3.286	108.6067	108.5912	0.009	0.238
K15	Low-Carbon Steel, Lot K	190.69	86.29	0.868	7.98	7.98	3.323	109.8060	109.7874	0.011	0.282
K213	Low-Carbon Steel, Lot K	189.21	51.27	0.881	7.98	7.97	1.967	64.8458	64.8327	0.013	0.336
K214	Low-Carbon Steel, Lot K	189.94	51.19	0.879	7.98	7.97	1.971	64.9311	64.9156	0.016	0.396
K215	Low-Carbon Steel, Lot K	188.87	51.31	0.874	7.98	7.99	1.965	64.4635	SA	SA	SA
L13	Low-Carbon Steel, Lot L	190.72	86.54	1.547	7.97	7.96	3.375	196.6486	196.6070	0.024	0.621
L14	Low-Carbon Steel, Lot L	190.12	86.22	1.528	7.98	7.97	3.351	194.8468	194.8260	0.012	0.313
L15	Low-Carbon Steel, Lot L	190.85	86.54	1.532	7.98	7.97	3.376	196.7299	196.7094	0.012	0.306
L213	Low-Carbon Steel, Lot L	191.75	51.42	1.496	7.97	7.97	2.032	112.0215	SA	SA	SA
L214	Low-Carbon Steel, Lot L	190.77	51.38	1.504	7.98	7.98	2.021	112.0013	111.9888	0.012	0.312
L215	Low-Carbon Steel, Lot L	189.97	51.45	1.551	7.98	7.97	2.017	115.0684	115.0554	0.013	0.325
M13	Low-Carbon Steel, Lot M	189.93	84.29	1.597	7.97	7.97	3.277	197.9004	197.8821	0.011	0.281
M14	Low-Carbon Steel, Lot M	190.37	84.37	1.576	7.97	7.97	3.287	197.9424	197.9222	0.012	0.310
M15	Low-Carbon Steel, Lot M	189.98	84.36	1.576	7.96	7.96	3.280	197.0945	197.0710	0.014	0.361
M213	Low-Carbon Steel, Lot M	190.47	51.49	1.611	7.97	7.96	2.028	121.3102	121.2944	0.015	0.393
M214	Low-Carbon Steel, Lot M	190.45	51.34	1.624	7.97	7.96	2.022	121.8258	SA	SA	SA
M215	Low-Carbon Steel, Lot M	190.45	51.39	1.621	7.98	7.96	2.024	121.4284	121.4114	0.017	0.423

* SA = Specimen was retained for surface analysis.

Test No.: 6
Test Type: Vapor Phase Exposure
Test Environment: Simulated WIPP Brine A Vapor + N2 (10 atm)
Test Temperature: 30 ±5°C
Test Exposure: 3 Months

Specimen	Material Type	Length, mm	Width, mm	Thickness, mm	Top Hole ID, mm	Bot. Hole ID, mm	Area, dm2	Initial Wt., g	Final Wt., g	Corrosion Rate, mpy	Corrosion Rate, μm/yr
J16	Low-Carbon Steel, Lot J	189.13	85.78	0.701	7.96	7.96	3.267	87.5332	87.5126	0.013	0.318
J17	Low-Carbon Steel, Lot J	189.15	85.78	0.706	7.96	7.95	3.268	87.2655	87.2528	0.008	0.196
J18	Low-Carbon Steel, Lot J	189.14	85.78	0.712	7.95	7.95	3.268	88.6485	88.6354	0.008	0.202
J216	Low-Carbon Steel, Lot J	189.60	50.98	0.713	7.96	7.96	1.951	51.6486	51.6404	0.008	0.212
J217	Low-Carbon Steel, Lot J	189.60	50.98	0.702	7.97	7.96	1.951	51.0916	51.0824	0.009	0.238
J218	Low-Carbon Steel, Lot J	189.60	50.98	0.716	7.96	7.96	1.951	52.1835	SA*	SA	SA
K16	Low-Carbon Steel, Lot K	189.13	85.78	0.874	7.96	7.95	3.277	109.1842	109.1557	0.017	0.438
K17	Low-Carbon Steel, Lot K	189.14	85.78	0.871	7.96	7.95	3.277	108.9417	108.9199	0.013	0.335
K18	Low-Carbon Steel, Lot K	189.14	85.78	0.876	7.97	7.96	3.278	109.3402	109.3300	0.006	0.157
K216	Low-Carbon Steel, Lot K	189.60	50.98	0.874	7.97	7.96	1.960	64.4479	64.4418	0.006	0.157
K217	Low-Carbon Steel, Lot K	189.61	50.98	0.885	7.97	7.96	1.960	65.5893	65.5844	0.005	0.126
K218	Low-Carbon Steel, Lot K	189.60	50.98	0.886	7.97	7.97	1.960	65.4429	SA	SA	SA
L16	Low-Carbon Steel, Lot L	189.14	85.80	1.561	7.96	7.95	3.319	195.4773	195.4522	0.015	0.381
L17	Low-Carbon Steel, Lot L	189.14	85.79	1.543	7.97	7.96	3.318	192.9296	192.9102	0.012	0.295
L18	Low-Carbon Steel, Lot L	189.14	85.78	1.536	7.97	7.96	3.317	192.8766	192.8570	0.012	0.298
L216	Low-Carbon Steel, Lot L	189.62	50.98	1.543	7.98	7.97	1.995	115.2451	115.2340	0.011	0.280
L217	Low-Carbon Steel, Lot L	189.61	50.98	1.559	7.98	7.98	1.996	115.3136	115.3033	0.010	0.260
L218	Low-Carbon Steel, Lot L	189.61	50.99	1.546	7.97	7.97	1.996	113.7260	SA	SA	SA
M16	Low-Carbon Steel, Lot M	189.16	84.36	1.600	7.96	7.96	3.267	199.1066	199.0927	0.008	0.214
M17	Low-Carbon Steel, Lot M	189.15	84.31	1.560	7.97	7.96	3.263	193.9453	193.9291	0.010	0.250
M18	Low-Carbon Steel, Lot M	189.15	84.31	1.555	7.97	7.97	3.262	193.5659	193.5514	0.009	0.224
M216	Low-Carbon Steel, Lot M	189.60	50.98	1.560	7.98	7.97	1.996	115.6005	SA	SA	SA
M217	Low-Carbon Steel, Lot M	189.62	50.99	1.595	7.97	7.97	1.999	118.5693	118.5622	0.007	0.179
M218	Low-Carbon Steel, Lot M	189.61	50.98	1.618	7.97	7.97	1.999	119.9987	119.9914	0.007	0.184

* SA = Specimen was retained for surface analysis.

B-13

Test No: 13
Test Type: Vapor Phase Exposure
Test Environment: Simulated WIPP Brine A Vapor + N2 (10 atm)
Test Temperature: 30 ±5°C
Test Exposure: 6 Months

Specimen	Material Type	Length, mm	Width, mm	Thickness, mm	Top Hole ID, mm	Bot. Hole ID, mm	Area, dm2	Initial Wt., g	Final Wt., g	Corrosion Rate, mpy	Corrosion Rate, μm/yr
J37	Low-Carbon Steel, Lot J	188.99	80.14	0.710	7.82	7.80	3.052	80.4475	80.4279	0.0062	0.158
J38	Low-Carbon Steel, Lot J	188.96	80.12	0.706	7.84	7.80	3.050	80.3535	80.3360	0.0056	0.141
J39	Low-Carbon Steel, Lot J	188.98	80.12	0.705	7.86	7.79	3.050	80.5772	80.5568	0.0065	0.165
J237	Low-Carbon Steel, Lot J	188.86	50.79	0.720	7.82	7.81	1.937	51.5181	51.5082	0.0050	0.126
J238	Low-Carbon Steel, Lot J	188.85	50.79	0.720	7.73	7.74	1.938	51.8347	SA*	SA	SA
J239	Low-Carbon Steel, Lot J	188.85	50.79	0.709	7.90	7.60	1.937	51.1926	51.1795	0.0066	0.166
K37	Low-Carbon Steel, Lot K	188.96	80.13	0.890	7.88	7.89	3.061	102.6192	102.5993	0.0063	0.160
K38	Low-Carbon Steel, Lot K	188.95	80.13	0.885	7.89	7.89	3.061	102.3975	102.3796	0.0057	0.144
K39	Low-Carbon Steel, Lot K	188.96	80.12	0.887	7.89	7.80	3.061	102.3473	102.3294	0.0057	0.144
K237	Low-Carbon Steel, Lot K	188.90	50.63	0.873	7.85	7.89	1.939	63.1282	63.1211	0.0035	0.090
K238	Low-Carbon Steel, Lot K	188.90	50.77	0.877	7.86	7.90	1.945	63.4326	63.4181	0.0072	0.183
K239	Low-Carbon Steel, Lot K	188.90	50.70	0.877	7.87	7.89	1.942	63.5664	SA	SA	SA
L37	Low-Carbon Steel, Lot L	188.90	80.00	1.554	7.88	7.89	3.094	179.5847	179.5643	0.0064	0.162
L38	Low-Carbon Steel, Lot L	188.90	80.02	1.499	7.89	7.80	3.092	173.7574	173.7341	0.0073	0.185
L39	Low-Carbon Steel, Lot L	188.91	80.01	1.500	7.81	7.84	3.092	173.4066	173.3820	0.0077	0.196
L237	Low-Carbon Steel, Lot L	188.88	50.75	1.560	7.86	7.89	1.980	113.7850	SA	SA	SA
L238	Low-Carbon Steel, Lot L	188.89	50.78	1.570	7.86	7.88	1.982	114.5543	114.5352	0.0093	0.237
L239	Low-Carbon Steel, Lot L	188.92	50.78	1.564	7.86	7.85	1.982	113.8630	113.8443	0.0091	0.232
M37	Low-Carbon Steel, Lot M	188.87	80.02	1.554	7.78	7.86	3.095	181.2015	181.1747	0.0084	0.213
M38	Low-Carbon Steel, Lot M	188.92	80.04	1.554	7.84	7.85	3.096	181.1371	181.1088	0.0089	0.225
M39	Low-Carbon Steel, Lot M	188.90	80.06	1.608	7.83	7.86	3.100	187.6152	187.5916	0.0074	0.187
M237	Low-Carbon Steel, Lot M	188.93	50.78	1.601	7.89	7.88	1.984	117.4677	117.4507	0.0083	0.211
M238	Low-Carbon Steel, Lot M	188.94	50.77	1.608	7.89	7.89	1.984	117.6713	117.6583	0.0063	0.161
M239	Low-Carbon Steel, Lot M	188.94	50.77	1.602	7.86	7.88	1.984	116.7488	SA	SA	SA

* SA = Specimen was retained for surface analysis.

Test No: 14
Test Type: Vapor Phase Exposure
Test Environment: Simulated WIPP Brine A Vapor + N2 (10 atm)
Test Temperature: 30 ±5°C
Test Exposure: 6 Months

Specimen	Material Type	Length, mm	Width, mm	Thickness, mm	Top Hole ID, mm	Bot. Hole ID, mm	Area, dm2	Initial Wt., g	Final Wt., g	Corrosion Rate, mpy	Corrosion Rate, μm/yr
J40	Low-Carbon Steel, Lot J	188.97	80.09	0.699	7.82	7.84	3.049	80.4540	80.4293	0.0078	0.199
J41	Low-Carbon Steel, Lot J	188.96	80.10	0.706	7.84	7.84	3.049	80.3870	80.3624	0.0078	0.199
J42	Low-Carbon Steel, Lot J	188.95	80.10	0.685	7.82	7.85	3.048	78.4684	78.4421	0.0084	0.212
J240	Low-Carbon Steel, Lot J	188.83	50.75	0.697	7.58	7.84	1.935	50.7707	SA*	SA	SA
J241	Low-Carbon Steel, Lot J	188.83	50.73	0.697	7.76	7.82	1.934	50.7602	50.7460	0.0071	0.181
J242	Low-Carbon Steel, Lot J	188.83	50.75	0.692	7.81	7.82	1.934	50.3101	50.2961	0.0070	0.178
K40	Low-Carbon Steel, Lot K	188.96	80.13	0.884	7.85	7.87	3.061	102.6329	102.6003	0.0103	0.262
K41	Low-Carbon Steel, Lot K	188.95	80.14	0.866	7.88	7.81	3.060	100.0001	99.9826	0.0055	0.141
K42	Low-Carbon Steel, Lot K	188.95	80.13	0.887	7.88	7.86	3.061	102.7006	102.6789	0.0069	0.174
K240	Low-Carbon Steel, Lot K	188.89	50.77	0.879	7.88	7.86	1.945	63.9198	63.9039	0.0079	0.201
K241	Low-Carbon Steel, Lot K	188.90	50.77	0.875	7.87	7.87	1.945	63.6705	SA	SA	SA
K242	Low-Carbon Steel, Lot K	188.90	50.79	0.878	7.88	7.85	1.946	63.5059	63.4963	0.0048	0.121
L40	Low-Carbon Steel, Lot L	188.90	80.01	1.505	7.81	7.85	3.092	174.7145	174.6882	0.0082	0.209
L41	Low-Carbon Steel, Lot L	188.91	80.02	1.524	7.86	7.86	3.093	175.8240	175.7930	0.0097	0.247
L42	Low-Carbon Steel, Lot L	188.94	80.03	1.493	7.84	7.86	3.092	174.3934	174.3593	0.0107	0.271
L240	Low-Carbon Steel, Lot L	188.91	50.80	1.511	7.86	7.90	1.980	110.2232	110.2082	0.0073	0.186
L241	Low-Carbon Steel, Lot L	188.89	50.79	1.560	7.87	7.83	1.982	114.3206	SA	SA	SA
L242	Low-Carbon Steel, Lot L	188.92	50.78	1.552	7.85	7.88	1.981	113.5412	113.5162	0.0122	0.310
M40	Low-Carbon Steel, Lot M	188.91	80.06	1.620	7.88	7.88	3.100	188.5504	188.5181	0.0101	0.256
M41	Low-Carbon Steel, Lot M	188.90	80.07	1.623	7.85	7.83	3.101	187.0956	187.0698	0.0081	0.205
M42	Low-Carbon Steel, Lot M	188.86	80.08	1.611	7.86	7.88	3.100	187.7237	187.6942	0.0092	0.234
M240	Low-Carbon Steel, Lot M	188.94	50.74	1.585	7.87	7.83	1.982	116.4061	116.3939	0.0060	0.151
M241	Low-Carbon Steel, Lot M	188.94	50.76	1.619	7.88	7.86	1.984	119.0870	SA	SA	SA
M242	Low-Carbon Steel, Lot M	188.95	50.76	1.615	7.89	7.87	1.984	119.1614	119.1458	0.0076	0.193

* SA = Specimen was retained for surface analysis.

B-15

Test No: 21
Test Type: Vapor Phase Exposure
Test Environment: Simulated WIPP Brine A Vapor +N2 (10 atm)
Test Temperature: 30 ±5°C
Test Exposure: 12 Months

Specimen	Material Type	Length, mm	Width, mm	Thickness, mm	Top Hole ID, mm	Bot. Hole ID, mm	Area, dm2	Initial Wt., g	Final Wt., g	Corrosion Rate, mpy	Corrosion Rate, μm/yr
J61	Low-Carbon Steel, Lot J	189.10	79.98	0.708	7.88	7.92	3.047	81.9678	81.9551	0.0021	0.053
J62	Low-Carbon Steel, Lot J	189.09	79.99	0.699	7.86	7.89	3.047	81.4793	81.4631	0.0027	0.067
J63	Low-Carbon Steel, Lot J	189.05	80.01	0.700	7.84	7.86	3.047	81.2433	81.2270	0.0027	0.068
J261	Low-Carbon Steel, Lot J	189.09	50.67	0.713	7.90	7.88	1.934	51.9571	51.9463	0.0028	0.071
J262	Low-Carbon Steel, Lot J	189.11	50.75	0.711	7.88	7.91	1.938	51.8130	SA*	SA	SA
J263	Low-Carbon Steel, Lot J	189.14	50.66	0.704	7.91	7.89	1.934	51.0897	51.0800	0.0025	0.064
K61	Low-Carbon Steel, Lot K	189.15	79.98	0.870	7.86	7.92	3.057	101.5718	101.5529	0.0031	0.078
K62	Low-Carbon Steel, Lot K	189.14	80.09	0.869	7.88	7.81	3.061	101.4023	101.3854	0.0028	0.070
K63	Low-Carbon Steel, Lot K	189.16	80.00	0.865	7.85	7.89	3.058	100.5147	100.4987	0.0026	0.066
K261	Low-Carbon Steel, Lot K	189.10	50.67	0.864	7.94	7.87	1.942	63.1254	SA	SA	SA
K262	Low-Carbon Steel, Lot K	189.10	50.68	0.864	7.91	7.92	1.943	63.4264	63.4183	0.0021	0.053
K263	Low-Carbon Steel, Lot K	189.10	50.75	0.871	7.93	7.88	1.946	63.8094	63.7969	0.0032	0.081
L61	Low-Carbon Steel, Lot L	189.15	80.03	1.553	7.94	7.91	3.099	181.1958	181.1687	0.0044	0.111
L62	Low-Carbon Steel, Lot L	189.17	79.98	1.498	7.95	7.92	3.094	176.1699	176.1470	0.0037	0.094
L63	Low-Carbon Steel, Lot L	189.20	80.01	1.504	7.94	7.91	3.096	176.0578	176.0357	0.0036	0.090
L261	Low-Carbon Steel, Lot L	189.15	50.68	1.557	7.94	7.90	1.980	113.9161	113.8993	0.0042	0.108
L262	Low-Carbon Steel, Lot L	189.17	50.70	1.488	7.94	7.93	1.977	109.7299	SA	SA	SA
L263	Low-Carbon Steel, Lot L	189.19	50.72	1.566	7.94	7.94	1.982	114.3665	114.3471	0.0049	0.124
M61	Low-Carbon Steel, Lot M	189.23	80.11	1.612	7.93	7.92	3.107	189.3613	189.3410	0.0033	0.083
M62	Low-Carbon Steel, Lot M	189.27	80.11	1.626	7.91	7.91	3.109	190.4287	190.4079	0.0033	0.085
M63	Low-Carbon Steel, Lot M	189.29	80.16	1.612	7.92	7.93	3.110	189.8820	189.8629	0.0031	0.078
M261	Low-Carbon Steel, Lot M	189.06	50.69	1.604	7.92	7.93	1.982	118.1401	118.1283	0.0030	0.075
M262	Low-Carbon Steel, Lot M	189.05	50.67	1.608	7.93	7.92	1.981	118.0343	SA	SA	SA
M263	Low-Carbon Steel, Lot M	189.06	50.52	1.580	7.92	7.93	1.974	114.3347	114.3188	0.0040	0.102

* SA = Specimen was retained for surface analysis.

Test No: 22
Test Type: Vapor Phase Exposure
Test Environment: Simulated WIPP Brine A Vapor +N2 (10 atm)
Test Temperature: 30 ±5°C
Test Exposure: 12 Months

Specimen	Material Type	Length, mm	Width, mm	Thickness, mm	Top Hole ID, mm	Bot. Hole ID, mm	Area, dm2	Initial Wt., g	Final Wt., g	Corrosion Rate, mpy	Corrosion Rate, µm/yr
J64	Low-Carbon Steel, Lot J	189.11	79.96	0.705	7.86	7.89	3.046	81.5597	81.5417	0.0029	0.075
J65	Low-Carbon Steel, Lot J	189.10	79.95	0.709	7.92	7.83	3.046	81.8360	81.8160	0.0033	0.083
J66	Low-Carbon Steel, Lot J	189.09	79.94	0.705	7.90	7.82	3.045	81.4581	81.4403	0.0029	0.074
J264	Low-Carbon Steel, Lot J	189.13	50.75	0.722	7.85	7.86	1.938	52.4947	52.4859	0.0023	0.058
J265	Low-Carbon Steel, Lot J	189.14	50.75	0.705	7.90	7.91	1.937	50.9732	50.9641	0.0023	0.060
J266	Low-Carbon Steel, Lot J	189.13	50.71	0.702	7.86	7.85	1.936	50.6710	SA*	SA	SA
K64	Low-Carbon Steel, Lot K	189.14	79.98	0.867	7.90	7.85	3.057	100.9647	100.9289	0.0058	0.148
K65	Low-Carbon Steel, Lot K	189.14	79.98	0.896	7.90	7.90	3.059	103.8692	103.8507	0.0030	0.077
K66	Low-Carbon Steel, Lot K	189.14	79.98	0.897	7.90	7.87	3.059	103.1913	103.1758	0.0025	0.064
K264	Low-Carbon Steel, Lot K	189.08	50.74	0.869	7.87	7.91	1.945	63.8704	63.8585	0.0031	0.078
K265	Low-Carbon Steel, Lot K	189.07	50.75	0.873	7.91	7.92	1.946	63.8454	SA	SA	SA
K266	Low-Carbon Steel, Lot K	189.08	50.69	0.873	7.89	7.92	1.943	63.5818	63.5688	0.0033	0.085
L64	Low-Carbon Steel, Lot L	189.17	80.00	1.501	7.95	7.93	3.095	175.2797	175.2388	0.0066	0.168
L65	Low-Carbon Steel, Lot L	189.17	80.00	1.538	7.92	7.93	3.097	179.6310	179.6042	0.0043	0.110
L66	Low-Carbon Steel, Lot L	189.19	80.00	1.534	7.94	7.95	3.097	178.8025	178.7730	0.0048	0.121
L264	Low-Carbon Steel, Lot L	189.19	50.72	1.547	7.96	7.92	1.981	112.9342	112.9185	0.0040	0.100
L265	Low-Carbon Steel, Lot L	189.19	50.74	1.498	7.97	7.93	1.979	109.8000	109.7840	0.0040	0.102
L266	Low-Carbon Steel, Lot L	189.21	50.72	1.541	7.96	7.93	1.981	113.1228	SA	SA	SA
M64	Low-Carbon Steel, Lot M	189.34	80.15	1.548	7.93	7.94	3.106	182.5703	182.5497	0.0033	0.084
M65	Low-Carbon Steel, Lot M	189.36	80.18	1.607	7.93	7.93	3.111	189.1902	189.1695	0.0033	0.084
M66	Low-Carbon Steel, Lot M	189.37	80.19	1.584	7.95	7.92	3.111	185.9014	185.8767	0.0040	0.101
M264	Low-Carbon Steel, Lot M	189.08	50.62	1.567	7.96	7.96	1.977	115.0593	115.0463	0.0033	0.083
M265	Low-Carbon Steel, Lot M	189.11	50.44	1.582	7.96	7.96	1.972	114.8420	114.8296	0.0031	0.080
M266	Low-Carbon Steel, Lot M	189.12	50.60	1.557	7.94	7.93	1.977	114.2275	SA	SA	SA

* SA = Specimen was retained for surface analysis.

B-17

Test No.: 29
Test Type: Vapor Phase Exposure
Test Environment: Simulated WIPP Brine A Vapor + N2 (10 atm)
Test Temperature: 30 ±5°C
Test Exposure: 24 Months

Specimen	Material Type	Length, mm	Width, mm	Thickness, mm	Top Hole ID, mm	Bot. Hole ID, mm	Area, dm2	Initial Wt., g	Final Wt., g	Corrosion Rate, mpy	Corrosion Rate, µm/yr
J85	Low-Carbon Steel, Lot J	188.96	79.97	0.702	7.91	7.91	3.044	81.0579	81.0232	0.0028	0.071
J86	Low-Carbon Steel, Lot J	188.96	79.98	0.709	7.93	7.94	3.045	81.3179	81.2897	0.0023	0.058
J87	Low-Carbon Steel, Lot J	188.95	79.95	0.706	7.92	7.93	3.043	81.1321	81.1059	0.0021	0.054
J285	Low-Carbon Steel, Lot J	189.12	50.88	0.711	7.90	7.90	1.943	51.7369	SA*	SA	SA
J286	Low-Carbon Steel, Lot J	189.10	50.89	0.701	7.92	7.92	1.942	51.5338	51.5150	0.0024	0.061
J287	Low-Carbon Steel, Lot J	189.14	50.88	0.714	7.91	7.93	1.943	52.3371	52.3199	0.0022	0.055
K85	Low-Carbon Steel, Lot K	188.83	79.96	0.873	7.92	7.92	3.051	101.5585	101.5376	0.0017	0.043
K86	Low-Carbon Steel, Lot K	188.91	79.96	0.862	7.94	7.91	3.052	100.3989	100.3758	0.0019	0.047
K87	Low-Carbon Steel, Lot K	189.93	79.95	0.878	7.91	7.94	3.069	102.0867	102.0592	0.0022	0.056
K285	Low-Carbon Steel, Lot K	189.10	50.92	0.864	7.92	7.92	1.952	63.2837	63.2640	0.0025	0.063
K286	Low-Carbon Steel, Lot K	189.11	50.88	0.868	7.91	7.93	1.951	64.0563	SA	SA	SA
K287	Low-Carbon Steel, Lot K	189.12	50.84	0.863	7.91	7.94	1.949	63.6442	63.6221	0.0028	0.071
L85	Low-Carbon Steel, Lot L	188.87	79.92	1.549	7.92	7.93	3.090	179.8499	179.8074	0.0034	0.086
L86	Low-Carbon Steel, Lot L	188.87	79.91	1.509	7.94	7.92	3.087	175.4831	175.4435	0.0032	0.080
L87	Low-Carbon Steel, Lot L	188.87	79.91	1.508	7.95	7.95	3.087	175.2537	175.2074	0.0037	0.094
L285	Low-Carbon Steel, Lot L	189.07	50.83	1.560	7.93	7.91	1.985	113.3798	113.3477	0.0040	0.101
L286	Low-Carbon Steel, Lot L	189.08	50.83	1.522	7.93	7.92	1.983	110.3635	SA	SA	SA
L287	Low-Carbon Steel, Lot L	189.07	50.81	1.555	7.93	7.93	1.984	113.2895	113.2535	0.0045	0.114
M85	Low-Carbon Steel, Lot M	188.89	79.99	1.571	7.91	7.90	3.095	183.9039	183.8634	0.0032	0.082
M86	Low-Carbon Steel, Lot M	188.87	80.00	1.609	7.90	7.90	3.097	188.5787	188.5526	0.0021	0.053
M87	Low-Carbon Steel, Lot M	188.96	80.02	1.585	7.89	7.91	3.098	185.7263	185.7002	0.0021	0.053
M285	Low-Carbon Steel, Lot M	189.03	50.70	1.601	7.91	7.90	1.982	117.4508	117.4300	0.0026	0.066
M286	Low-Carbon Steel, Lot M	189.03	50.67	1.582	7.92	7.90	1.980	115.8337	115.8150	0.0023	0.059
M287	Low-Carbon Steel, Lot M	189.04	50.71	1.559	7.94	7.92	1.980	114.3128	SA	SA	SA

*SA = Specimen was retained for surface analysis.

B-18

Test No.: 30
Test Type: Vapor Phase Exposure
Test Environment: Simulated WIPP Brine A Vapor + N2 (10 atm)
Test Temperature: 30 ±5°C
Test Exposure: 24 Months

Specimen	Material Type	Length, mm	Width, mm	Thickness, mm	Top Hole ID, mm	Bot. Hole ID, mm	Area, dm2	Initial Wt., g	Final Wt., g	Corrosion Rate, mpy	Corrosion Rate, μm/yr
J88	Low-Carbon Steel, Lot J	188.96	79.97	0.702	7.92	7.93	3.044	80.7136	80.6792	0.0028	0.071
J89	Low-Carbon Steel, Lot J	189.00	79.94	0.706	7.92	7.94	3.043	81.3005	81.2809	0.0016	0.040
J90	Low-Carbon Steel, Lot J	189.02	79.96	0.715	7.93	7.93	3.045	81.9655	81.9459	0.0016	0.040
J288	Low-Carbon Steel, Lot J	189.13	50.89	0.711	7.91	7.94	1.943	52.1447	SA*	SA	SA
J289	Low-Carbon Steel, Lot J	189.12	50.91	0.717	7.91	7.90	1.944	52.5598	52.5481	0.0015	0.038
J290	Low-Carbon Steel, Lot J	189.17	50.92	0.721	7.92	7.90	1.945	52.5694	52.5554	0.0018	0.045
K88	Low-Carbon Steel, Lot K	188.90	79.94	0.860	7.93	7.91	3.051	99.9478	99.9259	0.0018	0.045
K89	Low-Carbon Steel, Lot K	188.91	80.03	0.881	7.94	7.92	3.056	102.1515	102.1301	0.0017	0.044
K90	Low-Carbon Steel, Lot K	188.91	79.96	0.875	7.92	7.93	3.053	101.8537	101.8308	0.0018	0.047
K288	Low-Carbon Steel, Lot K	189.14	50.86	0.870	8.36	7.91	1.949	63.8811	SA	SA	SA
K289	Low-Carbon Steel, Lot K	189.13	50.93	0.866	7.93	7.91	1.953	63.9961	63.9851	0.0014	0.035
K290	Low-Carbon Steel, Lot K	189.13	50.85	0.869	7.95	7.91	1.950	63.9998	63.9822	0.0022	0.056
L88	Low-Carbon Steel, Lot L	188.88	79.91	1.500	7.92	7.93	3.087	174.4848	174.4534	0.0025	0.064
L89	Low-Carbon Steel, Lot L	188.87	79.94	1.555	7.93	7.92	3.091	180.0901	180.0611	0.0023	0.059
L90	Low-Carbon Steel, Lot L	188.91	79.94	1.561	7.93	7.94	3.092	180.6883	180.6564	0.0025	0.064
L288	Low-Carbon Steel, Lot L	189.09	50.85	1.562	7.93	7.93	1.986	114.1488	114.1286	0.0025	0.064
L289	Low-Carbon Steel, Lot L	189.13	50.84	1.513	7.93	7.91	1.984	111.2062	SA	SA	SA
L290	Low-Carbon Steel, Lot L	189.14	50.82	1.524	7.92	7.94	1.983	111.1832	111.1619	0.0026	0.067
M88	Low-Carbon Steel, Lot M	188.94	80.06	1.604	7.93	7.92	3.100	187.6189	187.5772	0.0033	0.084
M89	Low-Carbon Steel, Lot M	188.95	80.03	1.614	7.91	7.93	3.099	189.2799	189.2551	0.0020	0.050
M90	Low-Carbon Steel, Lot M	188.95	80.05	1.581	7.92	7.94	3.098	185.6152	185.5892	0.0021	0.052
M288	Low-Carbon Steel, Lot M	189.12	50.69	1.582	7.93	7.94	1.981	115.9691	115.9532	0.0020	0.050
M289	Low-Carbon Steel, Lot M	189.07	50.70	1.585	7.93	7.90	1.981	115.4328	SA	SA	SA
M290	Low-Carbon Steel, Lot M	189.09	50.77	1.549	7.92	7.93	1.982	113.4237	113.4066	0.0021	0.054

*SA = Specimen was retained for surface analysis.

APPENDIX B-3: INDIVIDUAL SPECIMEN CORROSION-RATE DATA, ANOXIC BRINE (CO_2/IMMERSED) ENVIRONMENT, SEAL-WELDED-CONTAINER TEST METHOD

Test No.: 3
Test Type: Immersion
Test Environment: Simulated WIPP Brine A, CO2 Overpressure (12 atm)
Test Temperature: 30 ±5°C
Test Exposure: 3 Months

Specimen	Material Type	Length, mm	Width, mm	Thickness, mm	Top Hole ID, mm	Bot. Hole ID, mm	Area, dm2	Initial Wt., g	Final Wt., g	Corrosion Rate, mpy	Corrosion Rate, μm/yr
J7	Low-Carbon Steel, Lot J	191.14	86.60	0.706	7.96	7.96	3.333	89.6822	88.9643	0.423	10.739
J8	Low-Carbon Steel, Lot J	190.90	86.49	0.703	7.96	7.95	3.325	88.8109	88.0909	0.425	10.798
J9	Low-Carbon Steel, Lot J	191.22	86.56	0.698	7.96	7.97	3.333	88.5780	87.8283	0.442	11.217
J207	Low-Carbon Steel, Lot J	190.82	51.42	0.708	7.94	7.93	1.980	52.9288	SA*	SA	SA
J208	Low-Carbon Steel, Lot J	191.09	51.41	0.715	7.99	8.00	1.983	53.3468	53.0005	0.343	8.708
J209	Low-Carbon Steel, Lot J	190.70	51.42	0.719	8.11	8.10	1.979	52.5722	51.8871	0.680	17.262
K7	Low-Carbon Steel, Lot K	190.59	86.26	0.877	7.97	7.96	3.321	111.2580	110.6618	0.352	8.952
K8	Low-Carbon Steel, Lot K	190.58	86.15	0.868	7.96	7.94	3.316	109.7743	109.2249	0.325	8.261
K9	Low-Carbon Steel, Lot K	190.54	86.32	0.873	7.96	7.96	3.322	110.3311	109.6990	0.374	9.487
K207	Low-Carbon Steel, Lot K	190.38	51.36	0.885	7.96	7.96	1.983	65.9886	65.6516	0.334	8.475
K208	Low-Carbon Steel, Lot K	190.25	51.35	0.869	7.97	7.96	1.980	64.4717	64.1096	0.359	9.118
K209	Low-Carbon Steel, Lot K	190.29	51.30	0.888	7.96	7.96	1.980	65.6494	SA	SA	SA
L7	Low-Carbon Steel, Lot L	190.88	86.35	1.549	7.97	7.96	3.370	197.1697	196.7695	0.233	5.921
L8	Low-Carbon Steel, Lot L	190.82	86.41	1.556	7.97	7.96	3.372	197.3520	197.0446	0.179	4.546
L9	Low-Carbon Steel, Lot L	190.65	86.37	1.556	7.97	7.95	3.367	197.4031	197.0804	0.188	4.779
L207	Low-Carbon Steel, Lot L	190.49	51.31	1.523	7.96	7.96	2.016	113.0462	112.7509	0.288	7.303
L208	Low-Carbon Steel, Lot L	190.59	51.32	1.556	7.97	7.97	2.019	115.4697	SA	SA	SA
L209	Low-Carbon Steel, Lot L	190.69	51.31	1.536	7.97	7.97	2.019	114.5975	114.4094	0.183	4.646
M7	Low-Carbon Steel, Lot M	189.83	84.32	1.588	7.99	8.00	3.276	196.7823	195.8714	0.546	13.864
M8	Low-Carbon Steel, Lot M	189.96	84.34	1.607	8.00	8.00	3.280	199.3454	198.8286	0.309	7.856
M9	Low-Carbon Steel, Lot M	190.92	84.33	1.588	8.00	8.00	3.295	198.0555	197.5907	0.277	7.033
M207	Low-Carbon Steel, Lot M	190.77	51.21	1.591	8.00	8.00	2.019	118.7277	118.4063	0.313	7.939
M208	Low-Carbon Steel, Lot M	190.30	51.21	1.595	8.01	8.00	2.014	120.4206	120.1534	0.260	6.616
M209	Low-Carbon Steel, Lot M	190.71	51.23	1.602	8.01	8.00	2.019	119.8208	SA	SA	SA

* SA = Specimen was retained for surface analysis.

B-22

Test No.: 4
Test Type: Immersion
Test Environment: Simulated WIPP Brine A, CO2 Overpressure (12 atm)
Test Temperature: 30 ±5°C
Test Exposure: 3 Months

Specimen	Material Type	Length, mm	Width, mm	Thickness, mm	Top Hole ID, mm	Bot. Hole ID, mm	Area, dm2	Initial Wt., g	Final Wt., g	Corrosion Rate, mpy	Corrosion Rate, µm/yr
J10	Low-Carbon Steel, Lot J	191.13	86.74	0.701	7.96	7.96	3.338	88.7716	87.8619	0.535	13.588
J11	Low-Carbon Steel, Lot J	190.72	86.78	0.704	7.97	7.96	3.333	89.1730	88.3056	0.511	12.978
J12	Low-Carbon Steel, Lot J	190.61	86.24	0.708	7.95	7.95	3.311	89.4414	88.7932	0.384	9.763
J210	Low-Carbon Steel, Lot J	190.40	51.15	0.716	7.97	7.96	1.966	52.5713	52.0152	0.555	14.104
J211	Low-Carbon Steel, Lot J	190.55	51.47	0.711	7.98	7.97	1.980	52.9630	52.2422	0.715	18.157
J212	Low-Carbon Steel, Lot J	190.68	51.47	0.710	7.96	7.96	1.981	52.6438	SA*	SA	SA
K10	Low-Carbon Steel, Lot K	189.59	86.22	0.866	8.00	7.99	3.301	108.7415	108.0088	0.436	11.067
K11	Low-Carbon Steel, Lot K	190.02	86.15	0.867	8.00	7.99	3.306	108.8873	108.2597	0.373	9.465
K12	Low-Carbon Steel, Lot K	190.23	86.22	0.868	8.01	8.00	3.313	109.3152	108.6920	0.369	9.381
K210	Low-Carbon Steel, Lot K	189.40	51.20	0.875	8.01	8.00	1.966	64.7175	64.3014	0.416	10.555
K211	Low-Carbon Steel, Lot K	189.50	51.30	0.868	8.00	8.00	1.970	64.5583	SA	SA	SA
K212	Low-Carbon Steel, Lot K	188.88	51.17	0.872	8.01	8.00	1.959	64.2470	63.8068	0.441	11.204
L10	Low-Carbon Steel, Lot L	190.53	86.49	1.537	7.95	7.95	3.369	195.4332	195.1021	0.193	4.901
L11	Low-Carbon Steel, Lot L	190.24	86.33	1.540	7.97	7.96	3.358	195.1232	194.8036	0.187	4.746
L12	Low-Carbon Steel, Lot L	190.39	86.37	1.538	7.97	7.95	3.362	195.3679	194.9886	0.222	5.626
L210	Low-Carbon Steel, Lot L	190.44	51.18	1.496	7.97	7.97	2.009	111.1462	110.9507	0.191	4.852
L211	Low-Carbon Steel, Lot L	190.73	51.42	1.492	7.98	7.97	2.021	111.6578	SA	SA	SA
L212	Low-Carbon Steel, Lot L	190.27	51.40	1.552	7.98	7.97	2.019	115.5176	115.2931	0.218	5.545
M10	Low-Carbon Steel, Lot M	190.22	84.31	1.576	8.01	8.00	3.282	197.0038	196.5995	0.242	6.143
M11	Low-Carbon Steel, Lot M	190.08	84.43	1.612	8.00	8.00	3.286	200.1839	199.8368	0.207	5.267
M12	Low-Carbon Steel, Lot M	190.36	84.43	1.550	8.01	8.01	3.287	193.6257	193.2085	0.249	6.329
M210	Low-Carbon Steel, Lot M	190.34	51.41	1.616	8.02	8.01	2.023	121.3934	121.1619	0.225	5.706
M211	Low-Carbon Steel, Lot M	190.85	51.33	1.603	8.03	8.02	2.025	120.0643	SA	SA	SA
M212	Low-Carbon Steel, Lot M	190.60	51.30	1.599	8.03	8.03	2.021	119.5115	119.2148	0.288	7.321

* SA = Specimen was retained for surface analysis.

Test No: 11
Test Type: Immersion
Test Environment: Simulated WIPP Brine A, CO2 Overpressure (12 atm)
Test Temperature: 30 ±5°C
Test Exposure: 6 Months

Specimen	Material Type	Length, mm	Width, mm	Thickness, mm	Top Hole ID, mm	Bot. Hole ID, mm	Area, dm2	Initial Wt., g	Final Wt., g	Corrosion Rate, mpy	Corrosion Rate, μm/yr
J31	Low-Carbon Steel, Lot J	188.93	80.08	0.702	7.95	7.91	3.047	80.0602	78.9040	0.3679	9.344
J32	Low-Carbon Steel, Lot J	188.93	80.09	0.713	7.95	7.96	3.048	81.3335	80.4336	0.2862	7.270
J33	Low-Carbon Steel, Lot J	188.93	80.09	0.708	7.97	7.94	3.048	81.3839	80.3414	0.3316	8.423
J231	Low-Carbon Steel, Lot J	188.83	50.78	0.709	7.95	7.95	1.935	50.9416	SA*	SA	SA
J232	Low-Carbon Steel, Lot J	188.83	50.78	0.715	7.94	7.91	1.936	51.2092	50.4458	0.3824	9.712
J233	Low-Carbon Steel, Lot J	188.83	50.78	0.710	8.05	7.70	1.936	51.2145	50.2643	0.4759	12.089
K31	Low-Carbon Steel, Lot K	188.91	80.09	0.864	7.98	7.97	3.057	100.2633	99.5902	0.2135	5.423
K32	Low-Carbon Steel, Lot K	188.92	80.09	0.884	7.98	7.98	3.058	102.5432	101.8378	0.2237	5.681
K33	Low-Carbon Steel, Lot K	188.91	80.10	0.876	7.98	7.97	3.058	101.6378	100.4497	0.3767	9.569
K231	Low-Carbon Steel, Lot K	188.83	50.74	0.875	7.99	7.97	1.943	63.6236	SA	SA	SA
K232	Low-Carbon Steel, Lot K	188.84	50.73	0.875	7.99	7.98	1.942	63.7375	62.7541	0.4909	12.470
K233	Low-Carbon Steel, Lot K	188.85	50.67	0.869	7.99	7.98	1.940	63.3250	62.6792	0.3228	8.199
L31	Low-Carbon Steel, Lot L	188.91	80.02	1.554	7.99	7.98	3.095	180.6953	180.1964	0.1563	3.970
L32	Low-Carbon Steel, Lot L	188.91	80.02	1.508	7.99	7.97	3.092	173.7476	173.2288	0.1627	4.132
L33	Low-Carbon Steel, Lot L	188.91	80.02	1.503	7.98	7.97	3.092	173.7478	173.2274	0.1632	4.145
L231	Low-Carbon Steel, Lot L	188.90	50.27	1.567	7.98	7.98	1.962	112.5016	112.1628	0.1674	4.253
L232	Low-Carbon Steel, Lot L	188.89	50.76	1.559	7.99	7.98	1.980	113.8185	SA	SA	SA
L233	Low-Carbon Steel, Lot L	188.87	50.78	1.555	7.98	7.98	1.980	113.1084	112.6689	0.2152	5.465
M31	Low-Carbon Steel, Lot M	188.90	80.04	1.606	7.99	7.98	3.098	188.5694	187.7950	0.2423	6.156
M32	Low-Carbon Steel, Lot M	188.88	80.03	1.576	7.98	7.98	3.096	183.0774	182.4466	0.1976	5.018
M33	Low-Carbon Steel, Lot M	188.87	80.01	1.586	7.98	7.98	3.096	184.6954	184.0358	0.2066	5.248
M231	Low-Carbon Steel, Lot M	188.94	50.79	1.619	7.98	7.98	1.985	118.1074	SA	SA	SA
M232	Low-Carbon Steel, Lot M	188.92	50.78	1.586	7.98	7.98	1.983	117.2962	116.8442	0.2210	5.615
M233	Low-Carbon Steel, Lot M	188.91	50.70	1.565	7.99	7.99	1.978	114.3836	113.9568	0.2092	5.313

* SA = Specimen was retained for surface analysis.

B-24

Test No: 12
Test Type: Immersion
Test Environment: Simulated WIPP Brine A, CO2 Overpressure (12 atm)
Test Temperature: 30 ±5°C
Test Exposure: 6 Months

Specimen	Material Type	Length, mm	Width, mm	Thickness, mm	Top Hole ID, mm	Bot. Hole ID, mm	Area, dm2	Initial Wt., g	Final Wt., g	Corrosion Rate, mpy	Corrosion Rate, μm/yr
J34	Low-Carbon Steel, Lot J	188.94	80.10	0.692	8.01	8.00	3.047	80.2577	79.4066	0.2706	6.872
J35	Low-Carbon Steel, Lot J	188.92	80.10	0.689	7.99	7.91	3.047	79.4202	78.7872	0.2012	5.112
J36	Low-Carbon Steel, Lot J	188.95	80.10	0.711	8.01	8.02	3.049	80.9811	80.0300	0.3022	7.676
J234	Low-Carbon Steel, Lot J	188.85	50.79	0.698	7.77	8.03	1.936	50.3958	49.7281	0.3342	8.488
J235	Low-Carbon Steel, Lot J	188.85	50.79	0.713	8.09	7.80	1.936	51.6316	SA*	SA	SA
J236	Low-Carbon Steel, Lot J	188.85	50.73	0.709	7.78	8.05	1.934	51.1730	50.4057	0.3844	9.763
K34	Low-Carbon Steel, Lot K	188.95	80.11	0.883	8.03	8.03	3.059	102.4166	101.3527	0.3369	8.558
K35	Low-Carbon Steel, Lot K	188.95	80.11	0.891	8.04	8.04	3.060	103.6533	102.7167	0.2966	7.533
K36	Low-Carbon Steel, Lot K	188.96	80.11	0.884	8.04	8.03	3.059	102.5319	101.2962	0.3913	9.939
K234	Low-Carbon Steel, Lot K	188.87	50.76	0.882	8.03	8.03	1.944	64.1602	63.8577	0.1508	3.829
K235	Low-Carbon Steel, Lot K	188.87	50.77	0.872	8.04	8.04	1.944	63.5034	62.8671	0.3171	8.055
K236	Low-Carbon Steel, Lot K	188.88	50.77	0.882	8.04	8.04	1.944	64.0895	SA	SA	SA
L34	Low-Carbon Steel, Lot L	188.94	80.03	1.556	8.04	8.04	3.095	180.1520	179.7073	0.1392	3.535
L35	Low-Carbon Steel, Lot L	188.92	80.02	1.553	8.04	8.03	3.095	180.3099	179.9042	0.1270	3.226
L36	Low-Carbon Steel, Lot L	188.92	80.01	1.552	8.05	8.04	3.094	179.5812	179.1778	0.1263	3.208
L234	Low-Carbon Steel, Lot L	188.90	50.75	1.561	8.05	8.04	1.980	113.7402	113.5039	0.1156	2.937
L235	Low-Carbon Steel, Lot L	188.93	50.80	1.559	8.04	8.04	1.982	113.7897	113.5187	0.1325	3.365
L236	Low-Carbon Steel, Lot L	188.89	50.78	1.546	8.04	8.04	1.980	113.1743	SA	SA	SA
M34	Low-Carbon Steel, Lot M	188.87	80.02	1.553	8.04	8.04	3.094	181.5511	180.9146	0.1993	5.062
M35	Low-Carbon Steel, Lot M	188.88	80.00	1.599	8.04	8.04	3.096	185.5557	185.0397	0.1615	4.101
M36	Low-Carbon Steel, Lot M	188.88	80.00	1.589	8.04	8.05	3.095	184.9131	184.1543	0.2375	6.032
M234	Low-Carbon Steel, Lot M	188.92	50.74	1.569	8.05	8.04	1.980	114.8283	SA	SA	SA
M235	Low-Carbon Steel, Lot M	188.92	50.79	1.604	8.05	8.04	1.984	118.3917	118.1223	0.1316	3.342
M236	Low-Carbon Steel, Lot M	188.92	50.79	1.578	8.05	8.03	1.982	115.3701	115.0396	0.1615	4.102

* SA = Specimen was retained for surface analysis.

B-25

Test No: 19
Test Type: Immersion
Test Environment: Simulated WIPP Brine A, CO2 Overpressure (12 atm)
Test Temperature: 30 ±5°C
Test Exposure: 12 Months

Specimen	Material Type	Length, mm	Width, mm	Thickness, mm	Top Hole ID, mm	Bot. Hole ID, mm	Area, dm2	Initial Wt., g	Final Wt., g	Corrosion Rate, mpy	Corrosion Rate, µm/yr
J55	Low-Carbon Steel, Lot J	189.11	79.96	0.706	7.83	7.86	3.046	81.5981	80.7627	0.1329	3.376
J56	Low-Carbon Steel, Lot J	189.09	79.95	0.708	7.84	7.84	3.046	81.8740	81.3033	0.0908	2.307
J57	Low-Carbon Steel, Lot J	189.09	79.96	0.711	7.80	7.85	3.042	81.8164	81.1144	0.1118	2.840
J255	Low-Carbon Steel, Lot J	189.08	50.72	0.719	7.84	7.88	1.937	51.7608	SA*	SA	SA
J256	Low-Carbon Steel, Lot J	189.10	50.60	0.713	7.92	7.88	1.932	51.5461	50.9211	0.1568	3.983
J257	Low-Carbon Steel, Lot J	189.11	50.70	0.709	7.91	7.91	1.935	51.5252	50.8732	0.1633	4.147
K55	Low-Carbon Steel, Lot K	189.10	79.95	0.866	7.78	7.79	3.056	101.0552	100.3553	0.1110	2.820
K56	Low-Carbon Steel, Lot K	189.11	79.95	0.885	7.83	7.83	3.057	103.1937	102.2030	0.1571	3.990
K57	Low-Carbon Steel, Lot K	189.12	79.97	0.854	7.89	7.92	3.055	99.7712	98.6927	0.1711	4.345
K255	Low-Carbon Steel, Lot K	189.09	50.71	0.884	7.91	7.84	1.945	65.1223	64.7259	0.0988	2.509
K256	Low-Carbon Steel, Lot K	189.09	50.74	0.878	7.88	7.80	1.946	64.8900	64.2907	0.1493	3.791
K257	Low-Carbon Steel, Lot K	189.08	50.74	0.876	7.84	7.88	1.946	64.7653	SA	SA	SA
L55	Low-Carbon Steel, Lot L	189.17	80.00	1.562	7.93	7.94	3.099	182.0185	181.5973	0.0659	1.673
L56	Low-Carbon Steel, Lot L	189.15	79.99	1.549	7.94	7.93	3.097	180.2001	179.6670	0.0834	2.119
L57	Low-Carbon Steel, Lot L	189.14	79.98	1.553	7.93	7.95	3.097	181.4972	181.0665	0.0674	1.712
L255	Low-Carbon Steel, Lot L	189.14	50.71	1.569	7.96	7.95	1.981	114.5227	SA	SA	SA
L256	Low-Carbon Steel, Lot L	189.12	50.68	1.511	7.94	7.93	1.977	110.4609	110.2196	0.0591	1.502
L257	Low-Carbon Steel, Lot L	189.12	50.67	1.496	7.94	7.94	1.976	109.6952	109.4363	0.0635	1.613
M55	Low-Carbon Steel, Lot M	189.31	80.12	1.601	7.95	7.95	3.108	187.0912	186.4560	0.0991	2.516
M56	Low-Carbon Steel, Lot M	189.29	80.12	1.548	7.94	7.90	3.105	182.6324	182.0434	0.0919	2.335
M57	Low-Carbon Steel, Lot M	189.25	80.10	1.553	7.92	7.92	3.103	183.5540	182.8145	0.1155	2.933
M255	Low-Carbon Steel, Lot M	189.31	50.62	1.602	7.94	7.92	1.982	117.8308	117.3415	0.1197	3.039
M256	Low-Carbon Steel, Lot M	189.29	50.48	1.583	7.94	7.96	1.975	116.4617	116.1487	0.0768	1.951
M257	Low-Carbon Steel, Lot M	189.26	50.59	1.610	7.95	7.96	1.980	117.9880	SA	SA	SA

* SA = Specimen was retained for surface analysis.

Test No: 20
Test Type: Immersion
Test Environment: Simulated WIPP Brine A, CO2 Overpressure (12 atm)
Test Temperature: 30 ±5°C
Test Exposure: 12 Months

Specimen	Material Type	Length, mm	Width, mm	Thickness, mm	Top Hole ID, mm	Bot. Hole ID, mm	Area, dm2	Initial Wt., g	Final Wt., g	Corrosion Rate, mpy	Corrosion Rate, μm/yr
J58	Low-Carbon Steel, Lot J	189.12	80.01	0.702	7.89	7.86	3.048	80.9211	79.8984	0.1626	4.130
J59	Low-Carbon Steel, Lot J	189.12	79.98	0.704	7.87	7.92	3.047	81.8872	80.8236	0.1692	4.297
J60	Low-Carbon Steel, Lot J	189.11	79.97	0.690	7.85	7.92	3.046	80.5422	79.7011	0.1338	3.400
J258	Low-Carbon Steel, Lot J	189.12	50.66	0.731	7.92	7.90	1.935	52.2297	51.6413	0.1474	3.743
J259	Low-Carbon Steel, Lot J	189.14	50.68	0.726	7.87	7.89	1.936	52.3322	51.6187	0.1786	4.537
J260	Low-Carbon Steel, Lot J	189.13	50.69	0.724	7.92	7.90	1.936	52.3393	SA*	SA	SA
K58	Low-Carbon Steel, Lot K	189.14	79.97	0.860	7.89	7.89	3.056	100.5629	99.3321	0.1952	4.958
K59	Low-Carbon Steel, Lot K	189.14	79.98	0.865	7.89	7.88	3.057	100.9443	99.9581	0.1564	3.971
K60	Low-Carbon Steel, Lot K	189.14	79.98	0.869	7.88	7.90	3.057	102.3157	101.4593	0.1358	3.449
K258	Low-Carbon Steel, Lot K	189.09	50.32	0.889	7.86	7.86	1.931	65.0805	SA	SA	SA
K259	Low-Carbon Steel, Lot K	189.09	50.70	0.886	7.92	7.88	1.945	65.1449	64.6333	0.1275	3.238
K260	Low-Carbon Steel, Lot K	189.10	50.68	0.860	7.90	7.87	1.943	63.1326	62.7096	0.1055	2.680
L58	Low-Carbon Steel, Lot L	189.13	79.98	1.557	7.92	7.90	3.097	180.6159	180.2452	0.0580	1.473
L59	Low-Carbon Steel, Lot L	189.15	79.98	1.548	7.93	7.90	3.097	180.0252	179.6116	0.0647	1.644
L60	Low-Carbon Steel, Lot L	189.16	79.97	1.566	7.93	7.93	3.098	181.7287	181.2482	0.0752	1.909
L258	Low-Carbon Steel, Lot L	189.15	50.69	1.558	7.95	7.90	1.980	113.6880	113.4177	0.0661	1.680
L259	Low-Carbon Steel, Lot L	189.15	50.73	1.486	7.95	7.91	1.978	109.3001	SA	SA	SA
L260	Low-Carbon Steel, Lot L	189.15	50.71	1.551	7.95	7.91	1.981	110.2340	109.9352	0.0731	1.857
M58	Low-Carbon Steel, Lot M	189.27	80.10	1.557	7.90	7.84	3.104	183.3880	182.9589	0.0670	1.702
M59	Low-Carbon Steel, Lot M	189.25	80.09	1.620	7.89	7.89	3.107	188.9110	188.3172	0.0926	2.353
M60	Low-Carbon Steel, Lot M	189.24	80.10	1.616	7.86	7.90	3.107	188.9908	188.1878	0.1252	3.181
M258	Low-Carbon Steel, Lot M	189.09	50.21	1.606	7.93	7.94	1.964	115.8765	SA	SA	SA
M259	Low-Carbon Steel, Lot M	189.10	50.65	1.605	7.91	7.92	1.981	117.7221	117.1470	0.1407	3.574
M260	Low-Carbon Steel, Lot M	189.08	50.68	1.599	7.90	7.86	1.982	117.5165	116.9818	0.1308	3.322

* SA = Specimen was retained for surface analysis.

Test No.: 27
Test Type: Immersion
Test Environment: Simulated WIPP Brine A, CO2 Overpressure (12 atm)
Test Temperature: 30 ±5°C
Test Exposure: 24 Months

Specimen	Material Type	Length, mm	Width, mm	Thickness, mm	Top Hole ID, mm	Bot. Hole ID, mm	Area, dm2	Initial Wt., g	Final Wt., g	Corrosion Rate, mpy	Corrosion Rate, μm/yr
J79	Low-Carbon Steel, Lot J	188.98	80.01	0.714	7.97	7.97	3.046	81.9966	81.0910	0.0731	1.856
J80	Low-Carbon Steel, Lot J	188.99	80.03	0.709	7.96	7.94	3.047	82.0435	81.2813	0.0615	1.562
J81	Low-Carbon Steel, Lot J	189.00	80.01	0.705	7.94	7.96	3.046	81.9907	81.0176	0.0785	1.995
J279	Low-Carbon Steel, Lot J	189.15	50.93	0.719	7.95	7.98	1.945	52.2287	51.7101	0.0655	1.665
J280	Low-Carbon Steel, Lot J	189.17	50.92	0.702	7.96	7.96	1.944	51.3165	50.9371	0.0480	1.219
J281	Low-Carbon Steel, Lot J	189.18	50.89	0.702	7.96	7.95	1.943	51.3331	SA*	SA	SA
K79	Low-Carbon Steel, Lot K	188.94	79.97	0.861	7.98	7.96	3.053	99.9204	99.2529	0.0538	1.365
K80	Low-Carbon Steel, Lot K	188.97	79.98	0.863	7.96	7.94	3.054	100.5006	99.5972	0.0727	1.847
K81	Low-Carbon Steel, Lot K	188.99	79.99	0.855	7.94	7.97	3.054	99.7339	98.9676	0.0617	1.567
K279	Low-Carbon Steel, Lot K	189.08	50.85	0.871	7.95	7.96	1.949	64.4807	SA	SA	SA
K280	Low-Carbon Steel, Lot K	189.10	50.86	0.878	7.96	7.91	1.950	64.7214	64.2372	0.0610	1.550
K281	Low-Carbon Steel, Lot K	189.09	50.86	0.860	7.98	7.96	1.949	63.4749	62.9064	0.0717	1.821
L79	Low-Carbon Steel, Lot L	189.00	80.03	1.499	7.98	7.96	3.093	175.0865	174.6950	0.0311	0.790
L80	Low-Carbon Steel, Lot L	189.00	80.03	1.544	7.96	7.94	3.096	180.8945	180.5277	0.0291	0.740
L81	Low-Carbon Steel, Lot L	188.97	80.02	1.550	7.94	7.93	3.096	181.0917	180.0015	0.0866	2.199
L279	Low-Carbon Steel, Lot L	189.24	50.77	1.566	7.94	7.97	1.985	113.9270	113.6557	0.0336	0.854
L280	Low-Carbon Steel, Lot L	189.25	50.80	1.544	7.84	7.94	1.985	113.2527	112.7035	0.0680	1.728
L281	Low-Carbon Steel, Lot L	189.21	50.73	1.580	7.91	7.96	1.984	115.3752	SA	SA	SA
M79	Low-Carbon Steel, Lot M	189.04	80.16	1.574	7.92	7.94	3.104	185.3045	184.6508	0.0518	1.315
M80	Low-Carbon Steel, Lot M	189.04	80.15	1.583	7.96	7.93	3.104	186.6548	186.1674	0.0386	0.981
M81	Low-Carbon Steel, Lot M	189.03	80.13	1.573	7.95	7.98	3.102	183.0341	182.5454	0.0387	0.984
M279	Low-Carbon Steel, Lot M	189.22	50.92	1.597	7.97	7.96	1.992	118.3555	SA	SA	SA
M280	Low-Carbon Steel, Lot M	189.19	50.92	1.605	7.92	7.92	1.992	118.4153	118.0134	0.0496	1.260
M281	Low-Carbon Steel, Lot M	189.20	50.88	1.598	7.91	7.94	1.990	118.0693	117.7003	0.0456	1.158

*SA = Specimen was retained for surface analysis.

B-28

Test No.: 28
Test Type: Immersion
Test Environment: Simulated WIPP Brine A, CO2 Overpressure (12 atm)
Test Temperature: 30 ±5°C
Test Exposure: 24 Months

Specimen	Material Type	Length, mm	Width, mm	Thickness, mm	Top Hole ID, mm	Bot. Hole ID, mm	Area, dm2	Initial Wt., g	Final Wt., g	Corrosion Rate, mpy	Corrosion Rate, µm/yr
J82	Low-Carbon Steel, Lot J	189.04	80.06	0.702	7.99	7.97	3.048	82.0773	81.3106	0.0617	1.568
J83	Low-Carbon Steel, Lot J	189.04	80.05	0.694	7.97	7.97	3.047	80.3571	79.3098	0.0844	2.143
J84	Low-Carbon Steel, Lot J	189.05	80.05	0.701	7.96	7.97	3.048	81.1452	80.2389	0.0730	1.854
J282	Low-Carbon Steel, Lot J	189.23	50.95	0.713	7.98	7.98	1.946	52.0976	SA*	SA	SA
J283	Low-Carbon Steel, Lot J	189.22	50.96	0.699	7.96	7.96	1.946	51.0211	50.6394	0.0482	1.223
J284	Low-Carbon Steel, Lot J	189.22	50.96	0.703	7.99	7.96	1.946	51.3464	50.9825	0.0459	1.166
K82	Low-Carbon Steel, Lot K	188.99	80.03	0.860	7.97	7.95	3.056	100.4228	99.4067	0.0816	2.073
K83	Low-Carbon Steel, Lot K	189.00	80.02	0.877	7.97	7.96	3.056	101.9646	100.6979	0.1017	2.584
K84	Low-Carbon Steel, Lot K	189.01	80.05	0.870	7.95	7.96	3.057	101.3292	100.4551	0.0702	1.783
K282	Low-Carbon Steel, Lot K	189.18	50.90	0.865	7.96	7.98	1.952	63.8153	SA	SA	SA
K283	Low-Carbon Steel, Lot K	189.18	50.93	0.859	7.95	7.96	1.953	63.3199	62.8758	0.0558	1.418
K284	Low-Carbon Steel, Lot K	189.21	50.94	0.859	7.95	7.94	1.953	63.2987	62.5052	0.0997	2.533
L82	Low-Carbon Steel, Lot L	188.98	80.02	1.565	8.00	7.98	3.096	182.3109	181.8291	0.0382	0.970
L83	Low-Carbon Steel, Lot L	188.94	79.98	1.552	7.98	7.96	3.094	181.0362	180.7109	0.0258	0.656
L84	Low-Carbon Steel, Lot L	188.94	79.98	1.571	7.97	7.98	3.095	182.1545	181.7372	0.0331	0.841
L282	Low-Carbon Steel, Lot L	189.22	50.89	1.567	7.95	7.93	1.989	115.4343	115.0263	0.0504	1.279
L283	Low-Carbon Steel, Lot L	189.18	50.81	1.497	7.95	7.95	1.982	109.6492	109.3121	0.0418	1.061
L284	Low-Carbon Steel, Lot L	189.17	50.80	1.508	7.96	7.96	1.982	110.1402	SA	SA	SA
M82	Low-Carbon Steel, Lot M	189.00	80.12	1.584	7.96	7.98	3.102	186.4713	185.6583	0.0643	1.634
M83	Low-Carbon Steel, Lot M	188.97	80.10	1.545	7.96	8.01	3.098	181.7548	181.1451	0.0483	1.227
M84	Low-Carbon Steel, Lot M	188.98	80.08	1.588	7.99	7.97	3.100	186.5229	185.7996	0.0573	1.455
M282	Low-Carbon Steel, Lot M	189.19	50.83	1.569	7.96	7.96	1.987	116.1085	SA	SA	SA
M283	Low-Carbon Steel, Lot M	189.16	50.84	1.601	7.96	7.95	1.988	118.8486	118.4332	0.0513	1.303
M284	Low-Carbon Steel, Lot M	189.14	50.81	1.535	7.96	7.94	1.984	113.8922	113.4784	0.0512	1.301

*SA = Specimen was retained for surface analysis.

APPENDIX B-4: INDIVIDUAL SPECIMEN CORROSION-RATE DATA, ANOXIC BRINE (CO2/VAPOR) ENVIRONMENT, SEAL-WELDED-CONTAINER TEST METHOD

Test No.: 7
Test Type: Vapor Phase Exposure
Test Environment: Simulated WIPP Brine A Vapor + CO2 (10 atm)
Test Temperature: 30 ±5°C
Test Exposure: 3 Months

Specimen	Material Type	Length, mm	Width, mm	Thickness, mm	Top Hole ID, mm	Bot. Hole ID, mm	Area, dm2	Initial Wt., g	Final Wt., g	Corrosion Rate, mpy	Corrosion Rate, μm/yr
J19	Low-Carbon Steel, Lot J	189.13	85.78	0.701	8.09	8.10	3.266	87.4959	87.4712	0.015	0.373
J20	Low-Carbon Steel, Lot J	189.13	85.78	0.711	8.01	8.00	3.267	88.4081	88.3855	0.013	0.341
J21	Low-Carbon Steel, Lot J	189.13	85.78	0.710	8.01	8.01	3.267	87.8460	87.8149	0.018	0.470
J219	Low-Carbon Steel, Lot J	189.58	50.98	0.720	8.01	8.01	1.951	52.7502	52.7276	0.022	0.571
J220	Low-Carbon Steel, Lot J	189.59	50.98	0.720	8.02	8.01	1.951	52.6166	SA*	SA	SA
J221	Low-Carbon Steel, Lot J	189.59	50.98	0.682	8.03	8.02	1.949	50.7769	50.7373	0.039	1.002
K19	Low-Carbon Steel, Lot K	189.11	85.77	0.862	7.99	8.00	3.276	108.7068	108.6909	0.009	0.239
K20	Low-Carbon Steel, Lot K	189.11	85.77	0.867	8.00	8.00	3.276	109.4164	109.4028	0.008	0.205
K21	Low-Carbon Steel, Lot K	189.11	85.78	0.875	8.00	8.00	3.277	109.3517	109.3401	0.007	0.175
K219	Low-Carbon Steel, Lot K	189.58	50.97	0.889	8.00	8.00	1.960	65.5730	65.5643	0.009	0.219
K220	Low-Carbon Steel, Lot K	189.58	50.97	0.888	8.00	8.00	1.960	65.5550	65.5480	0.007	0.176
K221	Low-Carbon Steel, Lot K	189.58	50.97	0.877	8.01	8.00	1.959	64.7891	SA	SA	SA
L19	Low-Carbon Steel, Lot L	189.13	85.80	1.490	7.98	7.97	3.315	187.2841	187.2598	0.014	0.362
L20	Low-Carbon Steel, Lot L	189.13	85.80	1.532	7.97	7.96	3.317	192.5109	192.4857	0.015	0.375
L21	Low-Carbon Steel, Lot L	189.13	85.80	1.490	7.98	7.97	3.315	187.9035	187.8749	0.017	0.426
L219	Low-Carbon Steel, Lot L	189.60	50.99	1.538	7.97	7.98	1.995	113.3141	113.2979	0.016	0.401
L220	Low-Carbon Steel, Lot L	189.60	50.99	1.544	7.99	7.99	1.996	113.9537	113.9315	0.022	0.549
L221	Low-Carbon Steel, Lot L	189.60	50.98	1.559	7.99	7.98	1.996	115.4085	SA	SA	SA
M19	Low-Carbon Steel, Lot M	189.12	84.35	1.613	7.97	7.97	3.267	200.1505	200.1297	0.012	0.314
M20	Low-Carbon Steel, Lot M	189.12	84.35	1.620	7.98	7.98	3.267	200.4969	200.4733	0.014	0.356
M21	Low-Carbon Steel, Lot M	189.13	85.81	1.575	7.98	7.98	3.320	198.1883	198.1654	0.013	0.340
M219	Low-Carbon Steel, Lot M	189.61	50.98	1.552	7.98	7.98	1.996	115.2150	115.2049	0.010	0.250
M220	Low-Carbon Steel, Lot M	189.60	50.98	1.592	7.99	7.98	1.998	118.3897	SA	SA	SA
M221	Low-Carbon Steel, Lot M	189.60	50.98	1.579	7.98	7.98	1.997	117.9729	117.9509	0.021	0.543

* SA = Specimen was retained for surface analysis.

Test No.: 8
Test Type: Vapor Phase Exposure
Test Environment: Simulated WIPP Brine A Vapor + CO2 (10 atm)
Test Temperature: 30 ±5°C
Test Exposure: 3 Months

Specimen	Material Type	Length, mm	Width, mm	Thickness, mm	Top Hole ID, mm	Bot. Hole ID, mm	Area, dm2	Initial Wt., g	Final Wt., g	Corrosion Rate, mpy	Corrosion Rate, µm/yr
J22	Low-Carbon Steel, Lot J	189.14	85.79	0.718	7.99	7.99	3.268	88.1511	88.1247	0.016	0.398
J23	Low-Carbon Steel, Lot J	189.14	85.78	0.709	7.99	7.99	3.267	88.5012	88.4797	0.013	0.325
J24	Low-Carbon Steel, Lot J	189.14	85.79	0.705	7.99	7.99	3.268	87.4136	87.3831	0.018	0.460
J222	Low-Carbon Steel, Lot J	189.62	50.98	0.685	7.99	7.99	1.950	50.6810	SA*	SA	SA
J223	Low-Carbon Steel, Lot J	189.63	50.99	0.692	8.00	8.00	1.951	50.7238	50.7028	0.021	0.531
J224	Low-Carbon Steel, Lot J	189.61	50.98	0.695	8.00	7.99	1.950	51.3646	51.3354	0.029	0.739
K22	Low-Carbon Steel, Lot K	189.15	85.78	0.872	7.97	7.97	3.277	109.1905	109.1701	0.012	0.307
K23	Low-Carbon Steel, Lot K	189.14	85.79	0.872	7.97	7.96	3.278	109.0113	108.9867	0.015	0.370
K24	Low-Carbon Steel, Lot K	189.14	85.78	0.875	7.97	7.96	3.277	109.4165	109.3997	0.010	0.253
K222	Low-Carbon Steel, Lot K	189.60	50.98	0.886	7.97	7.97	1.960	65.5292	65.5115	0.018	0.445
K223	Low-Carbon Steel, Lot K	189.59	50.98	0.884	7.98	7.97	1.960	65.4462	65.4335	0.013	0.320
K224	Low-Carbon Steel, Lot K	189.59	50.98	0.870	7.98	7.98	1.959	64.5470	SA	SA	SA
L22	Low-Carbon Steel, Lot L	189.14	85.79	1.484	7.98	7.97	3.314	185.6642	185.6345	0.017	0.442
L23	Low-Carbon Steel, Lot L	189.14	85.79	1.543	7.98	7.97	3.318	194.4421	194.4154	0.016	0.397
L24	Low-Carbon Steel, Lot L	189.15	85.79	1.539	7.99	7.98	3.318	192.8785	192.8516	0.016	0.400
L222	Low-Carbon Steel, Lot L	189.59	50.99	1.545	7.98	7.99	1.996	114.0443	SA	SA	SA
L223	Low-Carbon Steel, Lot L	189.59	50.98	1.552	7.98	7.98	1.996	115.1881	115.1557	0.032	0.801
L224	Low-Carbon Steel, Lot L	189.58	50.99	1.513	7.99	7.99	1.994	112.1181	112.0915	0.026	0.658
M22	Low-Carbon Steel, Lot M	189.14	84.39	1.587	7.98	7.98	3.267	196.0964	196.0682	0.017	0.426
M23	Low-Carbon Steel, Lot M	189.14	84.39	1.580	7.99	7.98	3.267	194.8490	194.8226	0.016	0.399
M24	Low-Carbon Steel, Lot M	189.15	84.39	1.626	7.98	7.98	3.270	200.8466	200.8174	0.017	0.441
M222	Low-Carbon Steel, Lot M	189.58	50.99	1.614	7.99	7.98	1.999	120.0831	SA	SA	SA
M223	Low-Carbon Steel, Lot M	189.59	50.99	1.609	8.00	7.99	1.999	120.3188	120.3062	0.012	0.311
M224	Low-Carbon Steel, Lot M	189.58	50.99	1.587	8.00	7.98	1.998	118.2353	118.2107	0.024	0.608

* SA = Specimen was retained for surface analysis.

Test No: 15
Test Type: Vapor Phase Exposure
Test Environment: Simulated WIPP Brine A Vapor + CO_2 (10 atm)
Test Temperature: 30 ±5°C
Test Exposure: 6 Months

Specimen	Material Type	Length, mm	Width, mm	Thickness, mm	Top Hole ID, mm	Bot. Hole ID, mm	Area, dm2	Initial Wt., g	Final Wt., g	Corrosion Rate, mpy	Corrosion Rate, µm/yr
J43	Low-Carbon Steel, Lot J	188.94	80.09	0.711	8.00	7.98	3.048	81.6922	81.6774	0.0047	0.119
J44	Low-Carbon Steel, Lot J	188.95	80.08	0.704	8.00	7.95	3.048	81.1870	81.1682	0.0060	0.152
J45	Low-Carbon Steel, Lot J	188.94	80.07	0.702	8.02	7.99	3.047	80.4568	80.4208	0.0114	0.291
J243	Low-Carbon Steel, Lot J	188.80	50.74	0.710	8.02	7.98	1.933	51.2853	51.2567	0.0143	0.364
J244	Low-Carbon Steel, Lot J	188.80	50.73	0.712	8.08	7.88	1.933	51.5502	SA*	SA	SA
J245	Low-Carbon Steel, Lot J	188.77	50.72	0.714	7.95	8.05	1.933	51.4095	51.3405	0.0346	0.879
K43	Low-Carbon Steel, Lot K	188.91	80.09	0.864	8.01	8.01	3.057	100.0602	99.9801	0.0254	0.645
K44	Low-Carbon Steel, Lot K	188.91	80.09	0.868	8.01	8.01	3.057	100.7607	100.6312	0.0410	1.042
K45	Low-Carbon Steel, Lot K	188.91	80.08	0.866	8.01	8.00	3.056	100.2789	100.2519	0.0086	0.217
K243	Low-Carbon Steel, Lot K	188.88	50.78	0.879	8.01	8.01	1.945	64.1399	64.1197	0.0101	0.256
K244	Low-Carbon Steel, Lot K	188.89	50.71	0.885	8.01	8.01	1.942	64.5459	64.4956	0.0251	0.637
K245	Low-Carbon Steel, Lot K	188.89	50.20	0.874	8.02	8.02	1.922	63.0785	SA	SA	SA
L43	Low-Carbon Steel, Lot L	188.90	80.01	1.501	8.02	8.01	3.091	175.6515	175.5875	0.0201	0.509
L44	Low-Carbon Steel, Lot L	188.90	80.02	1.507	8.02	8.01	3.092	176.2958	176.2439	0.0163	0.413
L45	Low-Carbon Steel, Lot L	188.91	80.02	1.509	8.01	8.01	3.092	175.1453	175.1023	0.0135	0.342
L243	Low-Carbon Steel, Lot L	188.87	50.77	1.548	8.02	8.02	1.980	113.2535	SA	SA	SA
L244	Low-Carbon Steel, Lot L	188.87	50.75	1.506	8.02	8.01	1.977	109.3093	109.2521	0.0280	0.712
L245	Low-Carbon Steel, Lot L	188.87	50.27	1.543	8.02	8.02	1.960	111.7084	111.6328	0.0374	0.949
M43	Low-Carbon Steel, Lot M	188.89	80.05	1.608	8.02	8.01	3.099	188.2269	188.1949	0.0100	0.254
M44	Low-Carbon Steel, Lot M	188.90	80.04	1.584	8.02	8.01	3.097	184.9015	184.8665	0.0109	0.278
M45	Low-Carbon Steel, Lot M	188.89	80.05	1.619	8.01	8.01	3.099	189.3780	189.3368	0.0129	0.327
M243	Low-Carbon Steel, Lot M	188.91	50.77	1.559	8.02	8.01	1.981	114.0451	114.0240	0.0103	0.262
M244	Low-Carbon Steel, Lot M	188.89	50.76	1.558	8.02	8.02	1.980	114.1413	114.0999	0.0203	0.515
M245	Low-Carbon Steel, Lot M	188.90	50.76	1.562	8.01	8.01	1.980	113.7145	SA	SA	SA

* SA = Specimen was retained for surface analysis.

Test No: 16
Test Type: Vapor Phase Exposure
Test Environment: Simulated WIPP Brine A Vapor + CO2 (10 atm)
Test Temperature: 30 ±5°C
Test Exposure: 6 Months

Specimen	Material Type	Length, mm	Width, mm	Thickness, mm	Top Hole ID, mm	Bot. Hole ID, mm	Area, dm2	Initial Wt., g	Final Wt., g	Corrosion Rate, mpy	Corrosion Rate, μm/yr
J46	Low-Carbon Steel, Lot J	188.95	80.07	0.704	8.00	8.00	3.047	80.5476	80.5206	0.0086	0.218
J47	Low-Carbon Steel, Lot J	188.95	80.07	0.708	7.98	7.94	3.048	81.2328	81.1523	0.0256	0.650
J48	Low-Carbon Steel, Lot J	188.94	80.06	0.713	7.98	7.98	3.047	81.5028	81.4719	0.0098	0.250
J246	Low-Carbon Steel, Lot J	188.78	50.72	0.711	8.00	8.00	1.933	51.5578	51.5449	0.0065	0.164
J247	Low-Carbon Steel, Lot J	188.78	50.72	0.706	8.00	8.00	1.932	50.9101	SA*	SA	SA
J248	Low-Carbon Steel, Lot J	188.78	50.68	0.710	7.95	8.03	1.931	51.4672	51.4508	0.0082	0.209
K46	Low-Carbon Steel, Lot K	188.89	80.07	0.863	8.02	8.02	3.055	100.1253	100.0712	0.0172	0.436
K47	Low-Carbon Steel, Lot K	188.86	80.04	0.885	8.02	8.02	3.055	102.7517	102.6885	0.0200	0.509
K48	Low-Carbon Steel, Lot K	188.85	80.03	0.882	8.02	8.02	3.054	102.1519	102.0891	0.0199	0.506
K246	Low-Carbon Steel, Lot K	188.90	50.66	0.865	8.02	8.01	1.940	63.1837	63.0895	0.0470	1.195
K247	Low-Carbon Steel, Lot K	188.91	50.70	0.877	8.02	8.02	1.942	63.4839	SA	SA	SA
K248	Low-Carbon Steel, Lot K	188.91	50.76	0.869	8.02	8.01	1.944	63.0387	63.0012	0.0187	0.475
L46	Low-Carbon Steel, Lot L	188.91	80.03	1.512	8.02	8.02	3.092	176.3947	176.3588	0.0112	0.286
L47	Low-Carbon Steel, Lot L	188.91	80.02	1.509	8.03	8.02	3.092	175.6374	175.5947	0.0134	0.340
L48	Low-Carbon Steel, Lot L	188.92	80.01	1.509	8.02	8.02	3.092	175.4664	175.4066	0.0187	0.476
L246	Low-Carbon Steel, Lot L	188.88	50.49	1.562	8.03	8.02	1.970	112.9453	112.8699	0.0371	0.942
L247	Low-Carbon Steel, Lot L	188.84	50.75	1.500	8.03	8.03	1.976	109.7192	109.6457	0.0360	0.915
L248	Low-Carbon Steel, Lot L	188.84	50.75	1.555	8.04	8.03	1.979	113.1176	SA	SA	SA
M46	Low-Carbon Steel, Lot M	188.89	80.03	1.582	8.03	8.02	3.096	185.4076	185.3686	0.0122	0.310
M47	Low-Carbon Steel, Lot M	188.86	80.00	1.590	8.02	8.02	3.095	186.6108	186.5414	0.0217	0.552
M48	Low-Carbon Steel, Lot M	188.83	79.98	1.590	8.02	8.02	3.094	185.7308	185.6967	0.0107	0.271
M246	Low-Carbon Steel, Lot M	188.90	50.76	1.604	8.03	8.02	1.982	117.9382	117.9264	0.0058	0.146
M247	Low-Carbon Steel, Lot M	188.87	50.74	1.611	8.02	8.02	1.982	117.2196	SA	SA	SA
M248	Low-Carbon Steel, Lot M	188.87	50.73	1.609	8.03	8.02	1.981	118.2908	118.2547	0.0177	0.448

* SA = Specimen was retained for surface analysis.

Test No: 23
Test Type: Vapor Phase Exposure
Test Environment: Simulated WIPP Brine A Vapor +CO2 (10 atm)
Test Temperature: 30 ±5°C
Test Exposure: 12 Months

Specimen	Material Type	Length, mm	Width, mm	Thickness, mm	Top Hole ID, mm	Bot. Hole ID, mm	Area, dm2	Initial Wt., g	Final Wt., g	Corrosion Rate, mpy	Corrosion Rate, μm/yr
J67	Low-Carbon Steel, Lot J	189.08	79.96	0.701	7.88	7.93	3.045	81.3418	81.3227	0.0031	0.080
J68	Low-Carbon Steel, Lot J	189.09	79.98	0.710	7.86	7.88	3.047	81.9931	81.9693	0.0039	0.099
J69	Low-Carbon Steel, Lot J	189.08	79.96	0.705	7.90	7.88	3.046	81.7696	81.7274	0.0069	0.176
J267	Low-Carbon Steel, Lot J	189.15	50.67	0.720	7.92	7.89	1.935	51.7629	51.7503	0.0032	0.083
J268	Low-Carbon Steel, Lot J	189.14	50.65	0.731	7.89	7.90	1.935	52.1323	52.1189	0.0035	0.088
J269	Low-Carbon Steel, Lot J	189.14	50.74	0.708	7.86	7.90	1.937	51.1253	SA*	SA	SA
K67	Low-Carbon Steel, Lot K	189.13	80.01	0.866	7.91	7.92	3.058	100.4655	100.4378	0.0045	0.115
K68	Low-Carbon Steel, Lot K	189.14	80.00	0.879	7.89	7.90	3.058	102.1231	102.1036	0.0032	0.081
K69	Low-Carbon Steel, Lot K	189.14	80.00	0.871	7.91	7.93	3.058	101.5011	101.4825	0.0030	0.077
K267	Low-Carbon Steel, Lot K	189.08	50.63	0.871	7.92	7.89	1.941	63.5558	SA	SA	SA
K268	Low-Carbon Steel, Lot K	189.08	50.77	0.881	7.83	7.86	1.947	64.0648	64.0547	0.0026	0.066
K269	Low-Carbon Steel, Lot K	189.08	50.60	0.874	7.89	7.89	1.940	63.6321	63.6177	0.0037	0.094
L67	Low-Carbon Steel, Lot L	189.18	80.02	1.496	7.94	7.93	3.096	174.6833	174.6585	0.0040	0.102
L68	Low-Carbon Steel, Lot L	189.18	80.02	1.498	7.95	7.95	3.096	174.8022	174.7669	0.0057	0.145
L69	Low-Carbon Steel, Lot L	189.18	80.02	1.544	7.97	7.96	3.099	179.6399	179.5993	0.0065	0.166
L267	Low-Carbon Steel, Lot L	189.18	50.75	1.493	7.99	7.98	1.979	109.5154	109.4940	0.0054	0.137
L268	Low-Carbon Steel, Lot L	189.17	50.76	1.531	7.96	7.97	1.982	112.6513	112.6285	0.0057	0.146
L269	Low-Carbon Steel, Lot L	189.19	50.79	1.561	7.98	7.98	1.985	114.6015	SA	SA	SA
M67	Low-Carbon Steel, Lot M	189.35	80.19	1.576	7.97	7.96	3.110	185.1187	185.1020	0.0027	0.068
M68	Low-Carbon Steel, Lot M	189.38	80.20	1.608	7.95	7.96	3.113	189.0036	188.9802	0.0038	0.095
M69	Low-Carbon Steel, Lot M	189.37	80.21	1.557	7.98	7.98	3.110	182.6606	182.6320	0.0046	0.117
M267	Low-Carbon Steel, Lot M	189.12	50.68	1.565	7.95	7.97	1.980	113.6987	113.6856	0.0033	0.084
M268	Low-Carbon Steel, Lot M	189.12	50.35	1.551	8.00	7.99	1.966	112.6640	112.6483	0.0040	0.101
M269	Low-Carbon Steel, Lot M	189.13	50.29	1.546	7.99	8.00	1.964	112.4100	SA	SA	SA

* SA = Specimen was retained for surface analysis.

Test No: 24
Test Type: Vapor Phase Exposure
Test Environment: Simulated WIPP Brine A Vapor +CO2 (10 atm)
Test Temperature: 30 ±5°C
Test Exposure: 12 Months

Specimen	Material Type	Length, mm	Width, mm	Thickness, mm	Top Hole ID, mm	Bot. Hole ID, mm	Area, dm2	Initial Wt., g	Final Wt., g	Corrosion Rate, mpy	Corrosion Rate, μm/yr
J70	Low-Carbon Steel, Lot J	189.10	79.98	0.703	7.91	7.92	3.046	81.6353	81.6148	0.0034	0.085
J71	Low-Carbon Steel, Lot J	189.11	80.00	0.700	7.94	7.90	3.047	81.6443	81.6218	0.0037	0.094
J72	Low-Carbon Steel, Lot J	189.10	79.98	0.708	7.93	7.92	3.047	81.4066	81.3738	0.0054	0.136
J270	Low-Carbon Steel, Lot J	189.18	50.76	0.729	7.92	7.96	1.939	51.2001	51.1890	0.0029	0.073
J271	Low-Carbon Steel, Lot J	189.20	50.47	0.703	7.89	7.92	1.927	50.2557	50.2402	0.0040	0.102
J272	Low-Carbon Steel, Lot J	189.21	50.78	0.710	7.88	7.93	1.940	51.4334	SA*	SA	SA
K70	Low-Carbon Steel, Lot K	189.18	80.02	0.884	7.93	7.96	3.060	101.7218	101.6887	0.0054	0.137
K71	Low-Carbon Steel, Lot K	189.17	80.09	0.875	7.90	7.88	3.062	101.5879	101.5657	0.0036	0.092
K72	Low-Carbon Steel, Lot K	189.18	80.04	0.869	7.90	7.90	3.060	101.1717	101.1494	0.0036	0.092
K270	Low-Carbon Steel, Lot K	189.09	50.77	0.865	7.90	7.89	1.946	63.2157	SA	SA	SA
K271	Low-Carbon Steel, Lot K	189.10	50.79	0.856	7.98	7.96	1.946	62.7625	62.7484	0.0036	0.092
K272	Low-Carbon Steel, Lot K	189.07	50.70	0.870	7.94	7.95	1.943	63.1447	63.1213	0.0060	0.153
L70	Low-Carbon Steel, Lot L	189.21	80.02	1.556	7.96	7.94	3.100	181.4153	181.3846	0.0049	0.126
L71	Low-Carbon Steel, Lot L	189.20	80.03	1.533	7.93	7.94	3.099	178.5215	178.4916	0.0048	0.122
L72	Low-Carbon Steel, Lot L	189.19	80.03	1.559	7.94	7.95	3.100	181.3424	181.2958	0.0075	0.191
L270	Low-Carbon Steel, Lot L	189.21	50.81	1.550	7.96	7.94	1.985	113.4394	113.4151	0.0061	0.155
L271	Low-Carbon Steel, Lot L	189.20	50.76	1.501	7.95	7.95	1.980	110.3922	110.3708	0.0054	0.137
L272	Low-Carbon Steel, Lot L	189.18	50.75	1.545	7.97	7.96	1.982	112.9268	SA	SA	SA
M70	Low-Carbon Steel, Lot M	189.35	80.16	1.573	7.95	7.94	3.108	184.6148	184.5301	0.0136	0.345
M71	Low-Carbon Steel, Lot M	189.32	80.16	1.602	7.96	7.96	3.110	187.4471	187.4000	0.0076	0.192
M72	Low-Carbon Steel, Lot M	189.30	80.13	1.601	7.94	7.94	3.108	187.0564	187.0282	0.0045	0.115
M270	Low-Carbon Steel, Lot M	189.12	50.38	1.545	7.94	7.94	1.967	112.9702	SA	SA	SA
M271	Low-Carbon Steel, Lot M	189.13	50.47	1.550	7.95	7.95	1.971	113.1766	113.1569	0.0050	0.127
M272	Low-Carbon Steel, Lot M	189.13	50.29	1.608	7.95	7.94	1.967	116.7650	116.7324	0.0083	0.210

* SA = Specimen was retained for surface analysis.

Test No.: 31
Test Type: Vapor Phase Exposure
Test Environment: Simulated WIPP Brine A Vapor + CO2 (10 atm)
Test Temperature: 30 ±5°C
Test Exposure: 24 Months

Specimen	Material Type	Length, mm	Width, mm	Thickness, mm	Top Hole ID, mm	Bot. Hole ID, mm	Area, dm2	Initial Wt., g	Final Wt., g	Corrosion Rate, mpy	Corrosion Rate, μm/yr
J91	Low-Carbon Steel, Lot J	189.00	79.96	0.690	7.93	7.93	3.043	80.2830	80.2563	0.0022	0.055
J92	Low-Carbon Steel, Lot J	189.02	79.96	0.701	7.93	7.93	3.044	81.7406	81.7196	0.0017	0.043
J93	Low-Carbon Steel, Lot J	189.02	79.94	0.701	7.91	7.94	3.044	80.9974	80.9676	0.0024	0.061
J291	Low-Carbon Steel, Lot J	189.16	50.90	0.718	7.93	7.90	1.944	52.7647	SA*	SA	SA
J292	Low-Carbon Steel, Lot J	189.12	50.87	0.717	7.91	7.92	1.942	52.8664	52.8493	0.0022	0.055
J293	Low-Carbon Steel, Lot J	189.11	50.87	0.712	7.93	7.91	1.942	51.8954	51.8661	0.0037	0.094
K91	Low-Carbon Steel, Lot K	188.91	79.97	0.856	7.92	7.92	3.052	99.7789	99.7595	0.0016	0.040
K92	Low-Carbon Steel, Lot K	188.92	79.97	0.881	7.93	7.93	3.054	101.8044	101.7821	0.0018	0.046
K93	Low-Carbon Steel, Lot K	188.91	79.95	0.887	7.92	7.94	3.053	103.4581	103.4119	0.0037	0.095
K291	Low-Carbon Steel, Lot K	189.14	50.84	0.870	7.95	7.92	1.949	64.1470	64.1277	0.0024	0.062
K292	Low-Carbon Steel, Lot K	189.10	50.84	0.865	7.94	7.90	1.949	63.8962	SA	SA	SA
K293	Low-Carbon Steel, Lot K	189.16	50.82	0.874	7.94	7.92	1.949	64.5834	64.5633	0.0025	0.065
L91	Low-Carbon Steel, Lot L	188.92	79.94	1.571	7.92	7.93	3.093	181.4198	181.3852	0.0028	0.070
L92	Low-Carbon Steel, Lot L	188.91	79.94	1.556	7.93	7.94	3.092	180.3477	180.3136	0.0027	0.069
L93	Low-Carbon Steel, Lot L	188.89	79.93	1.563	7.93	7.92	3.092	181.6635	181.6275	0.0029	0.073
L291	Low-Carbon Steel, Lot L	189.15	50.82	1.506	7.94	7.92	1.983	110.2253	SA	SA	SA
L292	Low-Carbon Steel, Lot L	189.16	50.84	1.535	7.94	7.93	1.985	112.9923	112.9612	0.0039	0.098
L293	Low-Carbon Steel, Lot L	189.16	50.80	1.567	7.94	7.93	1.985	114.4277	114.3849	0.0053	0.135
M91	Low-Carbon Steel, Lot M	188.89	80.06	1.579	7.93	7.92	3.098	185.8753	185.8465	0.0023	0.058
M92	Low-Carbon Steel, Lot M	188.91	80.05	1.595	7.93	7.93	3.098	185.6871	185.6585	0.0023	0.058
M93	Low-Carbon Steel, Lot M	188.89	80.05	1.597	7.92	7.92	3.098	186.3069	186.2770	0.0024	0.060
M291	Low-Carbon Steel, Lot M	189.08	50.75	1.601	7.94	7.92	1.984	117.9399	117.9213	0.0023	0.059
M292	Low-Carbon Steel, Lot M	189.11	50.79	1.609	7.93	7.93	1.986	118.5022	SA	SA	SA
M293	Low-Carbon Steel, Lot M	189.13	50.79	1.608	7.93	7.92	1.987	118.4315	118.4123	0.0024	0.061

*SA = Specimen was retained for surface analysis.

B-38

Test No.: 32
Test Type: Vapor Phase Exposure
Test Environment: Simulated WIPP Brine A Vapor + CO2 (10 atm)
Test Temperature: 30 ±5°C
Test Exposure: 24 Months

Specimen	Material Type	Length, mm	Width, mm	Thickness, mm	Top Hole ID, mm	Bot. Hole ID, mm	Area, dm2	Initial Wt., g	Final Wt., g	Corrosion Rate, mpy	Corrosion Rate, μm/yr
J94	Low-Carbon Steel, Lot J	189.02	79.97	0.697	7.91	7.95	3.044	80.8992	80.8710	0.0023	0.058
J95	Low-Carbon Steel, Lot J	189.04	79.95	0.709	7.94	7.94	3.045	82.5590	82.5361	0.0019	0.047
J96	Low-Carbon Steel, Lot J	189.07	79.93	0.696	7.94	7.92	3.044	80.5701	80.5428	0.0022	0.056
J294	Low-Carbon Steel, Lot J	189.11	50.85	0.711	7.93	7.93	1.941	51.3962	SA*	SA	SA
J295	Low-Carbon Steel, Lot J	189.00	50.86	0.702	7.92	7.90	1.940	51.6423	51.6307	0.0015	0.037
J296	Low-Carbon Steel, Lot J	189.03	50.85	0.706	7.93	7.92	1.940	51.5334	51.5161	0.0022	0.056
K94	Low-Carbon Steel, Lot K	188.91	80.00	0.863	7.91	7.94	3.054	100.8548	100.8176	0.0030	0.076
K95	Low-Carbon Steel, Lot K	188.93	79.95	0.872	7.92	7.94	3.052	101.1040	101.0148	0.0072	0.183
K96	Low-Carbon Steel, Lot K	188.91	79.95	0.864	7.91	7.92	3.052	100.6818	100.5488	0.0107	0.272
K294	Low-Carbon Steel, Lot K	189.18	50.83	0.866	7.92	7.92	1.949	64.1060	SA	SA	SA
K295	Low-Carbon Steel, Lot K	189.13	50.84	0.862	7.92	7.93	1.949	63.6030	63.5816	0.0027	0.069
K296	Low-Carbon Steel, Lot K	189.12	50.81	0.878	7.93	7.90	1.949	64.2733	64.2490	0.0031	0.078
L94	Low-Carbon Steel, Lot L	188.94	79.94	1.557	7.93	7.93	3.093	180.8542	180.8178	0.0029	0.074
L95	Low-Carbon Steel, Lot L	188.90	79.94	1.557	7.95	7.93	3.092	181.5524	181.5187	0.0027	0.068
L96	Low-Carbon Steel, Lot L	188.92	79.96	1.573	7.94	7.92	3.094	181.8120	181.7717	0.0032	0.081
L294	Low-Carbon Steel, Lot L	189.17	50.79	1.559	7.94	7.94	1.984	113.6946	113.6669	0.0034	0.087
L295	Low-Carbon Steel, Lot L	189.20	50.89	1.549	7.93	7.95	1.988	113.6312	113.6047	0.0033	0.083
L296	Low-Carbon Steel, Lot L	189.16	50.85	1.546	7.93	7.95	1.986	113.3702	SA	SA	SA
M94	Low-Carbon Steel, Lot M	188.94	80.05	1.595	7.93	7.93	3.099	187.1926	SA	SA	SA
M95	Low-Carbon Steel, Lot M	188.94	80.03	1.592	7.91	7.90	3.098	186.8385	186.5938	0.0194	0.494
M96	Low-Carbon Steel, Lot M	188.91	79.99	1.610	7.93	7.92	3.097	189.2964	189.2558	0.0032	0.082
M294	Low-Carbon Steel, Lot M	189.12	50.79	1.607	7.95	7.96	1.986	118.3168	118.2919	0.0031	0.078
M295	Low-Carbon Steel, Lot M	189.12	50.74	1.568	7.94	7.93	1.982	115.7260	SA	SA	SA
M296	Low-Carbon Steel, Lot M	189.11	50.76	1.606	7.94	7.94	1.985	118.4649	118.4357	0.0036	0.092

*SA = Specimen was retained for surface analysis.

APPENDIX B-5: INDIVIDUAL SPECIMEN CORROSION-RATE DATA, AUTOCLAVE TEST AUT-1

APPENDIX B-5
Individual Specimen Corrosion-Rate Data, Autoclave Test AUT-1

Test No.: AUT-1
Test Type: Immersion
Test Environment: Simulated WIPP Brine A, H2 Overpressure (70 atm)
Test Temperature: 30 ±5°C
Test Exposure: 6 Months

Specimen	Material Type	Length, mm	Width, mm	Thickness, mm	Top Hole ID, mm	Bot. Hole ID, mm	Area, dm2	Initial Wt., g	Final Wt., g	Corrosion Rate, mpy	Corrosion Rate, μm/yr
J297	Low-Carbon Steel, Lot J	191.05	51.49	0.677	7.98	7.97	1.984	49.8704	49.8447	0.013	0.331
J298	Low-Carbon Steel, Lot J	191.30	51.50	0.671	7.98	7.98	1.986	50.1519	50.1270	0.013	0.320
J299	Low-Carbon Steel, Lot J	191.24	51.38	0.690	7.98	7.98	1.982	51.2650	51.2408	0.012	0.312
J300	Low-Carbon Steel, Lot J	190.93	51.50	0.700	7.98	7.98	1.984	51.9040	51.8808	0.012	0.299
J301	Low-Carbon Steel, Lot J	192.91	51.57	0.710	7.98	7.98	2.008	52.7437	52.7189	0.012	0.316
K297	Low-Carbon Steel, Lot K	190.31	51.41	0.876	7.97	7.96	1.984	64.4697	64.4349	0.018	0.448
K298	Low-Carbon Steel, Lot K	190.44	51.34	0.862	7.98	7.97	1.981	63.9087	63.8803	0.014	0.366
K299	Low-Carbon Steel, Lot K	190.52	51.38	0.863	7.98	7.97	1.984	64.4015	64.3738	0.014	0.357
K300	Low-Carbon Steel, Lot K	190.53	51.33	0.854	7.99	7.97	1.982	62.8801	62.8484	0.016	0.409
K301	Low-Carbon Steel, Lot K	190.39	51.38	0.837	7.98	7.98	1.981	61.1923	61.1603	0.016	0.413

APPENDIX B-6: INDIVIDUAL SPECIMEN CORROSION-RATE DATA, AUTOCLAVE TEST AUT-3

Test No.: AUT-3
Test Type: Immersion
Test Environment: Simulated WIPP Brine A, H2 Overpressure (36 atm)
Test Temperature: 30 ±5°C
Test Exposure: 12 Months

Specimen	Material Type	Length, mm	Width, mm	Thickness, mm	Top Hole ID, mm	Bot. Hole ID, mm	Area, dm2	Initial Wt., g	Final Wt., g	Corrosion Rate, mpy	Corrosion Rate, μm/yr
J307	Low-Carbon Steel, Lot J	191.26	51.48	0.679	7.96	7.96	1.986	50.5868	50.5549	0.008	0.204
J308	Low-Carbon Steel, Lot J	191.43	51.41	0.683	7.97	7.96	1.985	50.8966	50.8672	0.007	0.188
J309	Low-Carbon Steel, Lot J	191.24	51.44	0.672	7.98	7.97	1.983	50.4018	50.3710	0.008	0.197
J310	Low-Carbon Steel, Lot J	191.10	51.47	0.674	7.96	7.96	1.983	50.3097	50.2783	0.008	0.201
J311	Low-Carbon Steel, Lot J	190.95	51.49	0.704	7.97	7.97	1.984	51.8678	51.8360	0.008	0.203
K307	Low-Carbon Steel, Lot K	190.32	51.31	0.870	7.98	7.98	1.979	64.5367	64.5000	0.009	0.235
K308	Low-Carbon Steel, Lot K	190.52	51.32	0.864	7.98	7.97	1.982	64.4370	64.3978	0.010	0.251
K309	Low-Carbon Steel, Lot K	190.35	51.33	0.862	7.99	7.98	1.980	64.1058	64.0708	0.009	0.224
K310	Low-Carbon Steel, Lot K	190.39	51.32	0.862	7.99	7.97	1.980	63.8059	63.7624	0.011	0.278
K311	Low-Carbon Steel, Lot K	190.48	51.32	0.855	8.00	7.98	1.981	62.8852	62.8440	0.010	0.264

APPENDIX B-7: INDIVIDUAL SPECIMEN CORROSION-RATE DATA, AUTOCLAVE TEST AUT-4

Test No.: AUT-4
Test Type: Immersion
Test Environment: Simulated WIPP Brine A, H2 Overpressure (70 atm)
Test Temperature: 30 ±5°C
Test Exposure: 12 Months

Specimen	Material Type	Length, mm	Width, mm	Thickness, mm	Top Hole ID, mm	Bot. Hole ID, mm	Area, dm2	Initial Wt., g	Final Wt., g	Corrosion Rate, mpy	Corrosion Rate, μm/yr
J312	Low-Carbon Steel, Lot J	191.24	51.44	0.689	7.96	7.97	1.984	50.9004	50.8725	0.007	0.178
J313	Low-Carbon Steel, Lot J	190.97	51.51	0.711	7.99	7.97	1.985	52.4448	52.4148	0.008	0.191
J314	Low-Carbon Steel, Lot J	190.96	51.49	0.694	7.98	7.97	1.984	51.4439	51.4127	0.008	0.199
J315	Low-Carbon Steel, Lot J	191.00	51.49	0.699	7.97	7.96	1.984	52.1348	52.1020	0.008	0.209
J316	Low-Carbon Steel, Lot J	191.04	51.45	0.694	7.96	7.96	1.983	51.4726	51.4402	0.008	0.207
K312	Low-Carbon Steel, Lot K	190.54	51.06	0.863	7.98	7.98	1.972	63.4063	63.3721	0.009	0.220
K313	Low-Carbon Steel, Lot K	190.38	51.35	0.865	7.99	7.98	1.981	63.2425	63.1963	0.012	0.295
K314	Low-Carbon Steel, Lot K	190.57	51.07	0.860	7.97	7.97	1.972	63.6838	63.6391	0.011	0.287
K315	Low-Carbon Steel, Lot K	190.46	51.32	0.865	7.99	7.98	1.981	64.0279	63.9831	0.011	0.287
K316	Low-Carbon Steel, Lot K	190.50	51.42	0.873	7.98	7.97	1.986	64.4769	64.4353	0.010	0.265

APPENDIX B-8: INDIVIDUAL SPECIMEN CORROSION-RATE DATA, AUTOCLAVE TEST AUT-2

Test No.: AUT-2
Test Type: Immersion
Test Environment: Simulated WIPP Brine A, N2 Overpressure (73 atm)
Test Temperature: 30 ±5°C
Test Exposure: 6 Months

Specimen	Material Type	Length, mm	Width, mm	Thickness, mm	Top Hole ID, mm	Bot. Hole ID, mm	Area, dm2	Initial Wt., g	Final Wt., g	Corrosion Rate, mpy	Corrosion Rate, μm/yr
J302	Low-Carbon Steel, Lot J	191.14	51.49	0.679	7.98	7.98	1.985	50.8021	50.5661	0.120	3.038
J303	Low-Carbon Steel, Lot J	191.19	51.50	0.691	7.98	7.97	1.986	51.9241	51.6993	0.114	2.892
J304	Low-Carbon Steel, Lot J	191.92	51.50	0.704	7.98	7.97	1.995	52.5896	52.3900	0.101	2.557
J305	Low-Carbon Steel, Lot J	191.27	51.47	0.719	7.98	7.98	1.987	53.9753	53.7833	0.097	2.468
J306	Low-Carbon Steel, Lot J	191.22	51.47	0.692	7.99	7.97	1.985	51.3828	51.1608	0.112	2.857
K302	Low-Carbon Steel, Lot K	190.55	51.37	0.846	7.98	7.97	1.983	62.0946	61.8530	0.123	3.113
K303	Low-Carbon Steel, Lot K	190.48	51.35	0.849	7.97	7.96	1.982	62.5359	62.2916	0.124	3.150
K304	Low-Carbon Steel, Lot K	190.44	51.39	0.853	7.97	7.96	1.983	62.9778	62.7334	0.124	3.149
K305	Low-Carbon Steel, Lot K	190.51	51.36	0.851	7.97	7.96	1.982	63.1314	62.8827	0.126	3.206
K306	Low-Carbon Steel, Lot K	190.48	51.37	0.855	7.99	7.97	1.983	62.9294	62.6801	0.126	3.213

APPENDIX B-9: INDIVIDUAL SPECIMEN CORROSION-RATE DATA, AUTOCLAVE TEST AUT-7

Test No.: AUT-7
Test Type: Immersion
Test Environment: Simulated WIPP Brine A, CO2 Overpressure (36 atm)
Test Temperature: 30 ±5°C
Test Exposure: 6 Months

Specimen	Material Type	Length, mm	Width, mm	Thickness, mm	Top Hole ID, mm	Bot. Hole ID, mm	Area, dm2	Initial Wt., g	Final Wt., g	Corrosion Rate, mpy	Corrosion Rate, μm/yr
J7 1	Low-Carbon Steel, Lot J	76.49	37.93	0.702	8.01	0.00	0.588	15.4834	14.9355	0.933	23.705
J7 2	Low-Carbon Steel, Lot J	76.48	37.94	0.699	8.01	0.00	0.588	15.4601	SA*	SA	SA
J7 3	Low-Carbon Steel, Lot J	76.21	36.99	0.691	8.00	0.00	0.571	14.8239	14.3717	0.793	20.143
J7 4	Low-Carbon Steel, Lot J	76.06	37.69	0.702	7.99	0.00	0.581	15.1808	14.6658	0.888	22.549
K7 1	Low-Carbon Steel, Lot K	76.31	37.27	0.849	7.94	0.00	0.580	18.1103	17.5727	0.928	23.568
K7 2	Low-Carbon Steel, Lot K	75.91	37.64	0.851	7.92	0.00	0.583	18.3776	17.7992	0.994	25.238
K7 3	Low-Carbon Steel, Lot K	76.13	37.77	0.842	8.00	0.00	0.586	18.1748	17.5995	0.983	24.962
K7 4	Low-Carbon Steel, Lot K	76.10	37.89	0.842	7.94	0.00	0.588	18.3229	17.7267	1.015	25.792
L7 1	Low-Carbon Steel, Lot L	76.11	37.64	1.485	7.97	0.00	0.600	31.5138	30.7021	1.354	34.389
L7 2	Low-Carbon Steel, Lot L	76.26	37.93	1.474	7.93	0.00	0.606	32.3544	31.4590	1.480	37.592
L7 3	Low-Carbon Steel, Lot L	76.09	37.99	1.450	7.98	0.00	0.605	31.7096	30.8561	1.413	35.899
L7 4	Low-Carbon Steel, Lot L	76.00	37.69	1.474	7.99	0.00	0.600	31.7864	30.9307	1.428	36.278
M7 1	Low-Carbon Steel, Lot M	76.42	37.93	1.541	7.93	0.00	0.609	34.1713	33.2661	1.489	37.819
M7 2	Low-Carbon Steel, Lot M	76.21	36.80	1.545	7.98	0.00	0.590	33.1634	32.3331	1.410	35.821
M7 3	Low-Carbon Steel, Lot M	76.38	37.71	1.565	7.96	0.00	0.606	34.5017	33.6498	1.409	35.780
M7 4	Low-Carbon Steel, Lot M	76.02	37.81	1.542	7.96	0.00	0.604	33.9293	33.1291	1.327	33.712

* SA = Specimen was retained for surface analysis.

APPENDIX B-10: INDIVIDUAL SPECIMEN CORROSION-RATE DATA, AUTOCLAVE TEST AUT-5

Test No.: AUT-5
Test Type: Wicking
Test Environment: Specimens were in contact with coarse particulate WIPP salt. The salt was held in a mesh basket contacting WIPP Brine A, permitting some degree of wicking
of the liquid. The autoclave had a N2 overpressure of 10 atm.
Test Temperature: 30 ±5°C
Test Exposure: 3 Months

Specimen	Material Type	Length, mm	Width, mm	Thickness, mm	Top Hole ID*, mm	Bot. Hole ID*, mm	Area, dm2	Initial Wt., g	Final Wt., g	Corrosion Rate, mpy	Corrosion Rate, μm/yr
JW1	Low-Carbon Steel, Lot J	49.73	25.41	0.717	0.00	0.00	0.264	7.0397	7.0342	0.041	1.049
JW2	Low-Carbon Steel, Lot J	49.97	25.70	0.706	0.00	0.00	0.268	6.9837	6.9774	0.047	1.184
JW3	Low-Carbon Steel, Lot J	50.00	23.95	0.707	0.00	0.00	0.250	6.5473	6.5407	0.052	1.327
JW4	Low-Carbon Steel, Lot J	50.57	25.18	0.711	0.00	0.00	0.265	6.9600	6.9560	0.030	0.758
JW5	Low-Carbon Steel, Lot J	52.62	25.34	0.697	0.00	0.00	0.278	7.1422	7.1352	0.050	1.268
JW6	Low-Carbon Steel, Lot J	49.91	26.82	0.709	0.00	0.00	0.279	7.3286	7.3214	0.051	1.299
JW7	Low-Carbon Steel, Lot J	51.29	25.97	0.705	0.00	0.00	0.277	7.2698	7.2573	0.089	2.266
JW8	Low-Carbon Steel, Lot J	52.28	27.46	0.717	0.00	0.00	0.299	7.9249	7.9101	0.098	2.492
JW9	Low-Carbon Steel, Lot J	52.33	23.44	0.714	0.00	0.00	0.256	6.7602	6.7538	0.049	1.256
JW10	Low-Carbon Steel, Lot J	51.01	25.06	0.708	0.00	0.00	0.266	6.9991	6.9881	0.082	2.075
JW11	Low-Carbon Steel, Lot J	51.50	25.16	0.704	0.00	0.00	0.270	7.0981	7.0894	0.064	1.620
JW12	Low-Carbon Steel, Lot J	52.16	25.44	0.709	0.00	0.00	0.276	7.3294	7.3196	0.070	1.782

* = Specimens were simple rectangular coupons without holes.

B-52

APPENDIX B-11: INDIVIDUAL SPECIMEN CORROSION-RATE DATA, AUTOCLAVE TEST AUT-6

APPENDIX B-11
Individual Specimen Corrosion-Rate Data, Autoclave Test AUT-6

Test No.: AUT-6
Test Type: Vapor
Test Environment: Specimens were in contact with coarse particulate WIPP salt. The salt was held in a mesh basket above the level of the simulated WIPP Brine A in the autoclave.
Condensing water dripped onto the salt. The autoclave had a N2 overpressure of 10 atm.
Test Temperature: 30 ±5°C
Test Exposure: 3 Months

Specimen	Material Type	Length, mm	Width, mm	Thickness, mm	Top Hole ID*, mm	Bot. Hole ID*, mm	Area, dm2	Initial Wt., g	Final Wt., g	Corrosion Rate, mpy	Corrosion Rate, µm/yr
JV1	Low-Carbon Steel, Lot J	50.60	25.69	0.704	0.00	0.00	0.271	7.0583	7.0543	0.029	0.743
JV2	Low-Carbon Steel, Lot J	50.34	25.45	0.705	0.00	0.00	0.267	7.0030	6.9989	0.030	0.772
JV3	Low-Carbon Steel, Lot J	50.27	25.30	0.724	0.00	0.00	0.265	6.8805	6.8761	0.033	0.834
JV4	Low-Carbon Steel, Lot J	50.66	25.78	0.708	0.00	0.00	0.272	7.0851	7.0809	0.031	0.776
JV5	Low-Carbon Steel, Lot J	50.76	26.00	0.693	0.00	0.00	0.275	7.1300	7.1255	0.032	0.824
JV6	Low-Carbon Steel, Lot J	51.08	25.09	0.704	0.00	0.00	0.267	6.9594	6.9553	0.030	0.772
JV7	Low-Carbon Steel, Lot J	51.80	25.73	0.706	0.00	0.00	0.278	7.2946	7.2902	0.031	0.797
JV8	Low-Carbon Steel, Lot J	51.84	25.35	0.712	0.00	0.00	0.274	7.2510	7.2475	0.025	0.643
JV9	Low-Carbon Steel, Lot J	49.64	25.31	0.702	0.00	0.00	0.262	6.7814	6.7785	0.022	0.557
JV10	Low-Carbon Steel, Lot J	51.26	25.73	0.708	0.00	0.00	0.275	7.2437	7.2403	0.024	0.622
JV11	Low-Carbon Steel, Lot J	51.59	25.30	0.698	0.00	0.00	0.272	7.0797	7.0766	0.023	0.573
JV12	Low-Carbon Steel, Lot J	51.98	25.79	0.710	0.00	0.00	0.279	7.3686	7.3650	0.026	0.648

* = Specimens were simple retangular coupons without holes.

APPENDIX B-12: INDIVIDUAL SPECIMEN CORROSION-RATE DATA, COPPER-BASE MATERIALS, ANOXIC BRINE ENVIRONMENT, SEAL-WELDED-CONTAINER TEST 7A

Test No: 7A
Test Type: Immersion
Test Environment: Simulated WIPP Brine A, N2 Overpressure (10 atm)
Test Temperature: 30 ±5°C
Test Exposure: 15 Months

These specimens were considered essentially free of attack during the corrosion test, based on (a) absence of reaction-product gas and (b) post-test appearance of specimens (clean, shiny).

Specimen	Material Type	Outer Diameter, mm	Hole ID, mm	Thickness, mm	Area, dm2	Initial Wt., g	Final Wt.*, g	Wt. Loss, g
C25	Unalloyed copper	38.01	7.84	1.522	0.239	14.4214	14.4214	0.0000
C26	Unalloyed copper	38.01	7.85	1.536	0.239	14.5758	--	--
C27	Unalloyed copper	38.01	7.79	1.513	0.239	14.3556	--	--
C28	Unalloyed copper	38.01	7.83	1.516	0.239	14.3839	--	--
C29	Unalloyed copper	38.01	7.81	1.526	0.239	14.4894	--	--
C30	Unalloyed copper	38.01	7.74	1.523	0.239	14.4357	--	--
C31	Unalloyed copper	38.03	7.81	1.535	0.240	14.5734	14.5733	0.0001
C32	Unalloyed copper	38.01	7.86	1.549	0.239	14.7899	14.7896	0.0003
CN25	Cupronickel 90-10	37.71	7.87	1.512	0.235	14.1479	--	--
CN26	Cupronickel 90-10	38.14	7.88	1.514	0.241	14.5297	--	--
CN27	Cupronickel 90-10	38.09	7.86	1.515	0.240	14.4596	14.4597	-0.0001
CN28	Cupronickel 90-10	37.74	7.86	1.507	0.235	14.1334	14.1336	-0.0002
CN29	Cupronickel 90-10	38.16	7.89	1.512	0.241	14.5506	--	--
CN30	Cupronickel 90-10	37.97	7.86	1.521	0.239	14.4965	--	--
CN31	Cupronickel 90-10	37.66	7.88	1.480	0.234	13.7473	--	--
CN32	Cupronickel 90-10	37.70	7.88	1.507	0.235	14.0880	14.0878	0.0002

* Final weight was determined after rinsing specimen in deionized water and denatured alcohol.
  No chemical etching of specimen was performed.

Test No: 7A
Test Type: Immersion
Test Environment: Simulated WIPP Brine A, N2 Overpressure (10 atm)
Test Temperature: 30 ±5°C
Test Exposure: 15 Months

These specimens were considered essentially free of attack during the corrosion test, based on (a) absence of reaction-product gas and (b) post-test appearance of specimens (clean, shiny).

Specimen	Material Type	Length, mm	Width, mm	Thickness, mm	Top Hole ID, mm	Bot. Hole ID, mm	Area, dm2	Initial Wt., g	Final Wt.*, g	Wt. Loss, g
C225	Unalloyed copper	190.25	63.31	1.574	7.95	7.96	2.477	165.1700	165.1694	0.0006
C226	Unalloyed copper	190.26	63.36	1.575	7.85	7.82	2.479	165.1703	165.1713	-0.0010
C227	Unalloyed copper	190.08	63.13	1.577	7.76	7.85	2.468	165.2828	--	--
C228	Unalloyed copper	190.39	63.33	1.574	7.98	7.94	2.479	165.1163	--	--
C229	Unalloyed copper	190.21	63.24	1.580	7.85	7.84	2.474	166.1690	--	--
C230	Unalloyed copper	190.09	63.22	1.566	7.81	7.88	2.471	165.0357	--	--
C231	Unalloyed copper	190.19	63.20	1.576	7.86	7.85	2.472	165.5649	--	--
C232	Unalloyed copper	190.19	63.19	1.573	7.87	7.86	2.472	164.5055	164.5064	-0.0009
CN225	Cupronickel 90-10	190.25	63.13	1.561	7.91	7.86	2.469	163.7170	--	--
CN226	Cupronickel 90-10	190.36	63.16	1.570	7.98	7.94	2.472	164.8880	--	--
CN227	Cupronickel 90-10	190.27	63.17	1.533	7.94	7.95	2.469	160.8346	160.8397	-0.0051
CN228	Cupronickel 90-10	190.18	63.14	1.554	7.93	7.97	2.468	162.9847	--	--
CN229	Cupronickel 90-10	190.20	63.16	1.557	7.95	7.93	2.469	162.8367	162.8385	-0.0018
CN230	Cupronickel 90-10	190.26	63.35	1.562	7.93	7.96	2.478	163.1214	--	--
CN231	Cupronickel 90-10	190.21	63.15	1.551	7.96	7.98	2.469	161.1034	161.1151	-0.0117
CN232	Cupronickel 90-10	190.26	63.20	1.564	7.99	7.96	2.472	162.9246	--	--

* Final weight was determined after rinsing specimen in deionized water and denatured alcohol.
No chemical etching of specimen was performed.

APPENDIX B-13: INDIVIDUAL SPECIMEN CORROSION-RATE DATA, COPPER-BASE MATERIALS, BRINE/CO2 ENVIRONMENT, SEAL-WELDED-CONTAINER TEST 8A

Test No: 8A
Test Type: Immersion
Test Environment: Simulated WIPP Brine A, CO2 Overpressure (10 atm)
Test Temperature: 30 ±5°C
Test Exposure: 15 Months

These specimens were considered essentially free of attack during the corrosion test, based on (a) absence of reaction-product gas and (b) post-test appearance of specimens (clean, shiny).

Specimen	Material Type	Outer Diameter, mm	Hole ID, mm	Thickness, mm	Area, dm2	Initial Wt., g	Final Wt.*, g	Wt. Loss, g
C33	Unalloyed copper	38.02	7.82	1.537	0.239	14.6355	--	--
C34	Unalloyed copper	38.02	7.81	1.550	0.240	14.7608	--	--
C35	Unalloyed copper	37.99	7.84	1.553	0.239	14.7727	--	--
C36	Unalloyed copper	38.00	7.82	1.551	0.239	14.7803	14.7798	0.0005
C37	Unalloyed copper	38.00	7.85	1.541	0.239	14.6795	--	--
C38	Unalloyed copper	38.03	7.82	1.531	0.240	14.5731	14.5724	0.0007
C39	Unalloyed copper	38.01	7.86	1.540	0.239	14.6600	14.6595	0.0005
C40	Unalloyed copper	38.07	7.82	1.536	0.240	14.5996	--	--
CN33	Cupronickel 90-10	38.16	7.86	1.516	0.241	14.5368	14.5362	0.0006
CN34	Cupronickel 90-10	38.11	7.85	1.527	0.240	14.5600	--	--
CN35	Cupronickel 90-10	37.70	7.85	1.521	0.235	14.2382	--	--
CN36	Cupronickel 90-10	38.06	7.88	1.465	0.239	13.9062	13.9057	0.0005
CN37	Cupronickel 90-10	38.11	7.87	1.537	0.240	14.7243	14.7236	0.0007
CN38	Cupronickel 90-10	38.05	7.87	1.536	0.240	14.7037	--	--
CN39	Cupronickel 90-10	38.09	7.86	1.533	0.240	14.6807	--	--
CN40	Cupronickel 90-10	37.66	7.93	1.532	0.235	14.3520	--	--

* Final weight was determined after rinsing specimen in deionized water and denatured alcohol.

No chemical etching of specimen was performed.

Test No: 8A
Test Type: Immersion
Test Environment: Simulated WIPP Brine A, CO2 Overpressure (10 atm)
Test Temperature: 30 ±5°C
Test Exposure:15 Months

These specimens were considered essentially free of attack during the corrosion test, based on (a) absence of reaction-product gas and (b) post-test appearance of specimens (clean, shiny).

Specimen	Material Type	Length, mm	Width, mm	Thickness, mm	Top Hole ID, mm	Bot. Hole ID, mm	Area, dm2	Initial Wt, g	Final Wt.*, g	Wt. Loss, g
C233	Unalloyed copper	190.34	63.18	1.592	7.88	7.82	2.474	166.2625	166.2527	0.0098
C234	Unalloyed copper	190.32	63.14	1.595	7.84	7.84	2.473	166.2143	--	--
C235	Unalloyed copper	190.30	63.17	1.588	7.86	7.76	2.473	165.5987	--	--
C236	Unalloyed copper	190.22	63.23	1.593	7.85	7.88	2.475	165.3475	165.3406	0.0069
C237	Unalloyed copper	190.16	63.14	1.583	7.87	7.78	2.470	165.0830	--	--
C238	Unalloyed copper	190.18	63.12	1.584	7.90	7.83	2.469	165.1274	--	--
C239	Unalloyed copper	190.17	63.29	1.591	7.87	7.90	2.476	166.9182	--	--
C240	Unalloyed copper	190.11	63.26	1.579	7.88	7.79	2.474	166.1039	166.0932	0.0107
CN233	Cupronickel 90-10	190.17	63.21	1.565	7.95	7.93	2.471	162.7382	162.7287	0.0095
CN234	Cupronickel 90-10	190.23	63.13	1.534	7.94	7.96	2.467	161.0609	161.0555	0.0054
CN235	Cupronickel 90-10	190.35	63.18	1.564	7.95	7.96	2.473	162.9677	162.9616	0.0061
CN236	Cupronickel 90-10	190.19	63.10	1.516	7.97	7.92	2.465	157.6580	--	--
CN237	Cupronickel 90-10	190.20	63.30	1.559	7.91	7.98	2.475	162.8907	--	--
CN238	Cupronickel 90-10	190.25	63.17	1.550	7.98	7.95	2.470	162.8537	--	--
CN239	Cupronickel 90-10	190.26	63.30	1.563	7.92	7.95	2.476	164.3112	--	--
CN240	Cupronickel 90-10	190.31	63.20	1.527	7.55	7.94	2.472	159.7624	--	--

r rinsing specimen in deionized water and denatured alcohol.
al etching of specimen was performed.

APPENDIX B-14: INDIVIDUAL SPECIMEN CORROSION-RATE DATA, COPPER-BASE MATERIALS, BRINE/H2S ENVIRONMENT, SEAL-WELDED-CONTAINER TEST 3A and 9A

Test No: 3A
Test Type: Immersion
Test Environment: Simulated WIPP Brine A, H2S Overpressure (5 atm)
Test Temperature: 30 ±5°C
Test Exposure: 9 Months

Specimen	Material Type	Outer Diameter, mm	Hole ID, mm	Thickness, mm	Area, dm2	Initial Wt., g	Final Wt., g	Corrosion Rate, mpy	Corrosion Rate, μm/yr
C17	Unalloyed copper	38.03	7.81	1.539	0.240	14.6381	--	--	--
C18	Unalloyed copper	38.02	7.79	1.544	0.240	14.6917	14.5120	0.421	10.689
C19	Unalloyed copper	38.03	7.80	1.547	0.240	14.7740	--	--	--
C20	Unalloyed copper	38.04	7.78	1.534	0.240	14.6482	--	--	--
C21	Unalloyed copper	38.01	7.81	1.539	0.239	14.6511	14.4760	0.410	10.426
C22	Unalloyed copper	38.01	7.78	1.536	0.239	14.6423	--	--	--
C23	Unalloyed copper	38.02	7.80	1.538	0.240	14.6244	14.4410	0.430	10.914
C24	Unalloyed copper	38.01	7.84	1.534	0.239	14.5921	14.3980	0.455	11.563
CN17	Cupronickel 90-10	37.67	7.88	1.468	0.234	13.6371	--	--	--
CN18	Cupronickel 90-10	38.16	7.81	1.500	0.241	14.3909	14.2200	0.396	10.063
CN19	Cupronickel 90-10	38.11	7.86	1.452	0.239	13.8900	13.7170	0.403	10.247
CN20	Cupronickel 90-10	37.70	7.87	1.509	0.235	14.0748	--	--	--
CN21	Cupronickel 90-10	38.17	7.85	1.497	0.241	14.3535	--	--	--
CN22	Cupronickel 90-10	37.73	7.87	1.501	0.235	14.0362	--	--	--
CN23	Cupronickel 90-10	38.09	7.87	1.462	0.239	13.9145	--	--	--
CN24	Cupronickel 90-10	38.17	7.86	1.508	0.241	14.4819	--	--	--

Test No: 3A
Test Type: Immersion
Test Environment: Simulated WIPP Brine A, H2S Overpressure (5 atm)
Test Temperature: 30 ±5°C
Test Exposure: 9 Months

Specimen	Material Type	Length, mm	Width, mm	Thickness, mm	Top Hole ID, mm	Bot. Hole ID, mm	Area, dm2	Initial Wt., g	Final Wt., g	Corrosion Rate, mpy	Corrosion Rate, μm/yr
C217	Unalloyed copper	190.23	63.10	1.557	7.89	7.79	2.468	164.1836	--	--	--
C218	Unalloyed copper	190.15	63.17	1.560	7.91	7.90	2.470	163.8577	--	--	--
C219	Unalloyed copper	190.33	63.43	1.567	7.88	7.90	2.482	166.7513	--	--	--
C220	Unalloyed copper	190.43	63.34	1.557	7.90	7.86	2.480	164.4625	--	--	--
C221	Unalloyed copper	190.19	63.31	1.553	7.88	7.87	2.475	163.2704	--	--	--
C222	Unalloyed copper	190.33	63.35	1.554	7.98	7.99	2.478	163.1701	--	--	--
C223	Unalloyed copper	190.25	63.11	1.568	7.86	7.85	2.469	164.8691	162.4500	0.550	13.965
C224	Unalloyed copper	190.05	63.55	1.569	7.88	7.81	2.484	165.5393	162.9500	0.585	14.861
CN217	Cupronickel 90-10	190.33	63.05	1.554	7.98	7.97	2.467	161.4721	--	--	--
CN218	Cupronickel 90-10	190.18	63.09	1.534	7.95	7.97	2.465	160.9541	--	--	--
CN219	Cupronickel 90-10	190.16	63.23	1.526	7.97	7.95	2.470	158.7918	--	--	--
CN220	Cupronickel 90-10	190.31	63.22	1.553	7.82	7.92	2.473	161.7179	--	--	--
CN221	Cupronickel 90-10	190.27	63.20	1.551	7.93	7.95	2.472	163.5478	--	--	--
CN222	Cupronickel 90-10	190.26	63.17	1.540	7.95	7.96	2.470	162.6259	--	--	--
CN223	Cupronickel 90-10	190.24	63.20	1.550	7.95	7.96	2.471	162.6998	159.1500	0.802	20.360
CN224	Cupronickel 90-10	190.32	63.19	1.551	7.94	7.78	2.472	162.8219	159.2000	0.818	20.765

Test No: 9A
Test Type: Immersion
Test Environment: Simulated WIPP Brine A, H2S Overpressure (5 atm)
Test Temperature: 30 ±5°C
Test Exposure: 15 Months

Specimen	Material Type	Outer Diameter, mm	Hole ID, mm	Thickness, mm	Area, dm2	Initial Wt., g	Final Wt., g	Corrosion Rate, mpy	Corrosion Rate, μm/yr
C41	Unalloyed copper	38.03	7.84	1.545	0.240	14.6777	--	--	--
C42	Unalloyed copper	38.03	7.82	1.536	0.240	14.6333	14.4135	0.330	8.376
C43	Unalloyed copper	38.01	7.81	1.544	0.239	14.7425	14.5598	0.274	6.965
C44	Unalloyed copper	38.02	7.85	1.542	0.239	14.7385	14.5364	0.303	7.704
C45	Unalloyed copper	37.99	7.86	1.535	0.239	14.6024	--	--	--
C46	Unalloyed copper	37.98	7.82	1.530	0.239	14.5370	--	--	--
C47	Unalloyed copper	37.98	7.82	1.524	0.239	14.4762	--	--	--
C48	Unalloyed copper	38.00	7.85	1.512	0.239	14.4013	--	--	--
CN41	Cupronickel 90-10	37.62	7.89	1.531	0.234	14.2846	--	--	--
CN42	Cupronickel 90-10	37.60	7.86	1.517	0.234	14.0981	--	--	--
CN43	Cupronickel 90-10	37.74	7.87	1.523	0.236	14.3340	--	--	--
CN44	Cupronickel 90-10	37.67	7.89	1.535	0.235	14.3814	--	--	--
CN45	Cupronickel 90-10	38.10	7.89	1.538	0.240	14.7412	14.5416	0.297	7.539
CN46	Cupronickel 90-10	38.09	7.86	1.524	0.240	14.6116	14.4270	0.275	6.980
CN47	Cupronickel 90-10	38.11	7.89	1.540	0.240	14.7696	--	--	--
CN48	Cupronickel 90-10	38.07	7.88	1.540	0.240	14.7513	--	--	--

Test No: 9A
Test Type: Immersion
Test Environment: Simulated WIPP Brine A, H2S Overpressure (5 atm)
Test Temperature: 30 ±5°C
Test Exposure: 15 Months

Specimen	Material Type	Length, mm	Width, mm	Thickness, mm	Top Hole ID, mm	Bot. Hole ID, mm	Area, dm2	Initial Wt., g	Final Wt., g	Corrosion Rate, mpy	Corrosion Rate, μm/yr
C241	Unalloyed copper	190.27	63.13	1.544	7.86	7.86	2.469	162.8408	_ _	_ _	_ _
C242	Unalloyed copper	190.25	63.26	1.563	7.90	7.84	2.475	165.6610	_ _	_ _	_ _
C243	Unalloyed copper	190.15	63.24	1.554	7.89	7.83	2.472	164.6624	_ _	_ _	_ _
C244	Unalloyed copper	190.10	63.33	1.551	7.86	7.88	2.475	164.2470	_ _	_ _	_ _
C245	Unalloyed copper	190.42	63.25	1.560	7.86	7.79	2.476	164.2390	_ _	_ _	_ _
C246	Unalloyed copper	190.04	63.25	1.576	7.87	7.86	2.472	165.2658	_ _	_ _	_ _
C247	Unalloyed copper	190.14	63.19	1.570	7.85	7.86	2.471	165.3727	159.3332	0.879	22.314
C248	Unalloyed copper	190.00	63.25	1.570	7.85	7.86	2.471	165.4518	159.1513	0.916	23.274
CN241	Cupronickel 90-10	190.26	63.25	1.522	7.99	7.96	2.472	160.9265	_ _	_ _	_ _
CN242	Cupronickel 90-10	190.20	63.25	1.524	7.97	7.94	2.471	160.0673	_ _	_ _	_ _
CN243	Cupronickel 90-10	190.34	63.28	1.570	7.94	7.94	2.477	163.8679	_ _	_ _	_ _
CN244	Cupronickel 90-10	190.35	63.33	1.549	7.92	7.93	2.478	162.2167	_ _	_ _	_ _
CN245	Cupronickel 90-10	190.35	63.16	1.423	7.90	7.92	2.464	149.3230	_ _	_ _	_ _
CN246	Cupronickel 90-10	190.29	63.21	1.555	7.95	7.96	2.472	162.2631	_ _	_ _	_ _
CN247	Cupronickel 90-10	190.16	63.17	1.517	7.96	7.94	2.467	158.4790	152.9509	0.801	20.341
CN248	Cupronickel 90-10	190.25	63.16	1.501	7.94	7.96	2.467	158.7949	152.8068	0.868	22.035

APPENDIX B-15: INDIVIDUAL SPECIMEN CORROSION-RATE DATA, TITANIUM-BASE MATERIALS, ANOXIC BRINE ENVIRONMENT, SEAL-WELDED-CONTAINER TEST 10A

Test No: 10A
Test Type: Immersion
Test Environment: Simulated WIPP Brine A, N2 Overpressure (10 atm)
Test Temperature: 30 ±5°C
Test Exposure: 15 Months

These specimens were considered essentially free of attack during the corrosion test, based on (a) absence of reaction-product gas and (b) post-test appearance of specimens (clean, shiny).

Specimen	Material Type	Outer Diameter, mm	Hole ID, mm	Thickness, mm	Area, dm2	Initial Wt., g	Final Wt.*, g	Wt. Loss, g
T25	Titanium, Gr 2	38.23	7.77	1.562	0.243	7.6314	7.6320	-0.0006
T26	Titanium, Gr 2	38.24	7.74	1.568	0.243	7.6317	7.6319	-0.0002
T27	Titanium, Gr 2	38.30	7.73	1.535	0.243	7.4539	--	--
T28	Titanium, Gr 2	38.25	7.72	1.517	0.242	7.3115	7.3127	-0.0012
T29	Titanium, Gr 2	38.26	7.77	1.575	0.243	7.6711	--	--
T30	Titanium, Gr 2	38.20	7.81	1.558	0.242	7.5792	--	--
T31	Titanium, Gr 2	38.22	7.76	1.567	0.243	7.5611	--	--
T32	Titanium, Gr 2	38.25	7.78	1.567	0.243	7.6222	--	--
TN25	Titanium, Gr 12	38.12	7.73	1.553	0.241	7.4928	--	--
TN26	Titanium, Gr 12	38.17	7.76	1.478	0.241	7.1120	7.1125	-0.0005
TN27	Titanium, Gr 12	38.16	7.81	1.591	0.242	7.6496	7.6498	-0.0002
TN28	Titanium, Gr 12	38.16	7.77	1.539	0.241	7.4599	--	--
TN29	Titanium, Gr 12	38.10	7.84	1.552	0.241	7.4932	--	--
TN30	Titanium, Gr 12	38.14	7.86	1.532	0.241	7.4409	--	--
TN31	Titanium, Gr 12	38.13	7.84	1.568	0.241	7.6198	7.6205	-0.0007
TN32	Titanium, Gr 12	38.16	7.84	1.551	0.241	7.4843	--	--

* Final weight was determined after rinsing specimen in deionized water and denatured alcohol.
  No chemical etching of specimen was performed.

Test No: 10A
Test Type: Immersion
Test Environment: Simulated WIPP Brine A, N2 Overpressure (10 atm)
Test Temperature: 30 ±5°C
Test Exposure: 15 Months

These specimens were considered essentially free of attack during the corrosion test, based on (a) absence of reaction-product gas and (b) post-test appearance of specimens (clean, shiny).

Specimen	Material Type	Length, mm	Width, mm	Thickness, mm	ID, mm	ID, mm	Area, dm2	Initial Wt., g	Final Wt.*, g	Wt. Loss, g
T225	Titanium, Gr 2	190.45	63.38	1.569	7.95	7.94	2.482	83.9200	83.9203	-0.0003
T226	Titanium, Gr 2	190.44	63.47	1.609	8.00	7.98	2.487	86.4833	86.4851	-0.0018
T227	Titanium, Gr 2	190.40	63.46	1.591	7.97	8.00	2.485	84.9097	--	--
T228	Titanium, Gr 2	190.50	63.46	1.570	7.98	7.98	2.485	84.4365	--	--
T229	Titanium, Gr 2	190.52	63.43	1.606	7.98	7.98	2.487	86.1846	--	--
T230	Titanium, Gr 2	190.42	63.38	1.445	8.00	7.99	2.474	77.1828	77.1852	-0.0024
T231	Titanium, Gr 2	190.48	63.49	1.584	7.96	8.00	2.487	85.0025	--	--
T232	Titanium, Gr 2	190.42	63.42	1.591	8.00	7.98	2.484	85.0660	--	--
TN225	Titanium, Gr 12	190.62	63.45	1.533	7.86	7.86	2.485	83.7261	--	--
TN226	Titanium, Gr 12	190.66	63.47	1.487	7.90	7.90	2.484	80.9096	80.9107	-0.0011
TN227	Titanium, Gr 12	190.65	63.42	1.493	7.87	7.88	2.482	80.7866	80.7873	-0.0007
TN228	Titanium, Gr 12	190.43	63.32	1.558	7.86	7.84	2.479	84.3618	84.3612	0.0006
TN229	Titanium, Gr 12	190.38	63.20	1.558	7.83	7.83	2.474	83.5710	--	--
TN230	Titanium, Gr 12	190.59	63.27	1.533	7.83	7.82	2.478	82.6462	--	--
TN231	Titanium, Gr 12	190.25	63.23	1.508	7.80	7.81	2.471	79.5766	--	--
TN232	Titanium, Gr 12	190.59	63.43	1.564	7.88	7.89	2.486	84.0623	--	--

* Final weight was determined after rinsing specimen in deionized water and denatured alcohol.
No chemical etching of specimen was performed.

APPENDIX B-16: INDIVIDUAL SPECIMEN CORROSION-RATE DATA, TITANIUM-BASE MATERIALS, BRINE/CO2 ENVIRONMENT, SEAL-WELDED-CONTAINER TEST 11A

Test No: 11A
Test Type: Immersion
Test Environment: Simulated WIPP Brine A, CO2 Overpressure (10 atm)
Test Temperature: 30 ±5°C
Test Exposure: 15 Months

These specimens were considered essentially free of attack during the corrosion test, based on (a) absence of reaction-product gas and (b) post-test appearance of specimens (clean, shiny).

Specimen	Material Type	Outer Diameter, mm	Hole ID, mm	Thickness, mm	Area, dm2	Initial Wt., g	Final Wt.*, g	Wt. Loss, g
T33	Titanium, Gr 2	38.27	7.73	1.545	0.243	7.4816	--	--
T34	Titanium, Gr 2	38.30	7.75	1.552	0.243	7.5228	--	--
T35	Titanium, Gr 2	38.25	7.79	1.556	0.243	7.5527	--	--
T36	Titanium, Gr 2	38.27	7.73	1.561	0.243	7.5981	--	--
T37	Titanium, Gr 2	38.26	7.78	1.528	0.242	7.4339	7.4338	0.0001
T38	Titanium, Gr 2	38.22	7.75	1.555	0.242	7.5714	7.5713	0.0001
T39	Titanium, Gr 2	38.25	7.74	1.560	0.243	7.6052	7.6052	0.0000
T40	Titanium, Gr 2	38.26	7.72	1.556	0.243	7.5716	--	--
TN33	Titanium, Gr 12	38.22	7.88	1.570	0.242	7.6008	--	--
TN34	Titanium, Gr 12	38.16	7.89	1.566	0.241	7.5923	--	--
TN35	Titanium, Gr 12	38.15	7.89	1.503	0.240	7.2845	--	--
TN36	Titanium, Gr 12	38.15	7.87	1.576	0.242	7.6427	7.6426	0.0001
TN37	Titanium, Gr 12	38.17	7.87	1.499	0.241	7.2705	--	--
TN38	Titanium, Gr 12	38.13	7.85	1.491	0.240	7.2341	--	--
TN39	Titanium, Gr 12	38.14	7.84	1.450	0.240	6.9732	6.9732	0.0000
TN40	Titanium, Gr 12	38.15	7.83	1.505	0.241	7.2528	7.2528	0.0000

* Final weight was determined after rinsing specimen in deionized water and denatured alcohol.
No chemical etching of specimen was performed.

Test No: 11A
Test Type: Immersion
Test Environment: Simulated WIPP Brine A, CO_2 Overpressure (10 atm)
Test Temperature: 30 ±5°C
Test Exposure: 15 Months

These specimens were considered essentially free of attack during the corrosion test, based on (a) absence of reaction-product gas and (b) post-test appearance of specimens (clean, shiny).

Specimen	Material Type	Length, mm	Width, mm	Thickness, mm	ID, mm	ID, mm	Area, dm2	Initial Wt., g	Final Wt.*, g	Wt. Loss, g
T233	Titanium, Gr 2	190.44	63.35	1.608	7.88	7.96	2.483	85.5785	--	--
T234	Titanium, Gr 2	190.45	63.44	1.600	8.00	7.99	2.486	85.8362	--	--
T235	Titanium, Gr 2	190.47	63.44	1.608	7.99	7.98	2.486	86.2818	86.2805	0.0013
T236	Titanium, Gr 2	190.56	63.46	1.609	7.97	7.98	2.488	86.0296	--	--
T237	Titanium, Gr 2	190.42	63.42	1.604	7.98	8.02	2.485	86.0700	86.0686	0.0014
T238	Titanium, Gr 2	190.49	63.52	1.593	8.01	8.04	2.489	85.3463	85.3456	0.0007
T239	Titanium, Gr 2	190.36	63.42	1.597	7.99	7.98	2.484	85.3794	--	--
T240	Titanium, Gr 2	190.45	63.38	1.594	8.01	7.96	2.483	85.3181	--	--
TN233	Titanium, Gr 12	190.57	63.41	1.557	7.88	7.88	2.484	83.7172	--	--
TN234	Titanium, Gr 12	190.39	63.43	1.554	7.86	7.86	2.482	83.3396	--	--
TN235	Titanium, Gr 12	190.40	63.62	1.527	7.86	7.87	2.488	81.8190	--	--
TN236	Titanium, Gr 12	190.61	63.67	1.547	7.86	7.86	2.494	84.3176	84.3172	0.0004
TN237	Titanium, Gr 12	190.81	63.32	1.569	7.85	7.86	2.485	84.0329	84.0321	0.0008
TN238	Titanium, Gr 12	190.47	63.29	1.508	7.85	7.86	2.476	80.0610	--	--
TN239	Titanium, Gr 12	190.48	63.58	1.509	7.86	7.87	2.487	81.1324	--	--
TN240	Titanium, Gr 12	190.63	63.44	1.484	7.86	7.89	2.482	80.6646	80.6639	0.0007

* Final weight was determined after rinsing specimen in deionized water and denatured alcohol.
No chemical etching of specimen was performed.

APPENDIX B-17: INDIVIDUAL SPECIMEN CORROSION-RATE DATA, TITANIUM-BASE MATERIALS, BRINE/H2S ENVIRONMENT, SEAL-WELDED-CONTAINER TEST 12A

Test No: 12A
Test Type: Immersion
Test Environment: Simulated WIPP Brine A, H2S Overpressure (5 atm)
Test Temperature: 30 ±5°C
Test Exposure: 15 Months

These specimens were considered essentially free of attack during the corrosion test, based on (a) absence of reaction-product gas and (b) post-test appearance of specimens (clean, shiny).

Specimen	Material Type	Outer Diameter, mm	Hole ID, mm	Thickness, mm	Area, dm2	Initial Wt., g	Final Wt.*, g	Wt. Loss, g
T41	Titanium, Gr 2	38.24	7.77	1.557	0.243	7.5548	--	--
T42	Titanium, Gr 2	38.23	7.76	1.542	0.242	7.4892	--	--
T43	Titanium, Gr 2	38.24	7.73	1.573	0.243	7.6494	7.6493	0.0001
T44	Titanium, Gr 2	38.24	7.78	1.543	0.242	7.4582	--	--
T45	Titanium, Gr 2	38.20	7.79	1.512	0.241	7.3003	7.3001	0.0002
T46	Titanium, Gr 2	38.20	7.79	1.528	0.242	7.3614	--	--
T47	Titanium, Gr 2	38.20	7.79	1.535	0.242	7.4042	7.4043	-0.0001
T48	Titanium, Gr 2	38.25	7.76	1.547	0.243	7.5067	--	--
TN41	Titanium, Gr 12	38.10	7.82	1.539	0.240	7.3482	--	--
TN42	Titanium, Gr 12	38.10	7.89	1.540	0.240	7.3484	7.3485	-0.0001
TN43	Titanium, Gr 12	38.10	7.91	1.557	0.241	7.4566	7.4566	0.0000
TN44	Titanium, Gr 12	38.09	7.90	1.516	0.240	7.2560	--	--
TN45	Titanium, Gr 12	38.10	7.83	1.564	0.241	7.5030	--	--
TN46	Titanium, Gr 12	38.12	7.85	1.526	0.240	7.3176	--	--
TN47	Titanium, Gr 12	38.16	7.81	1.506	0.241	7.3057	--	--
TN48	Titanium, Gr 12	38.12	7.87	1.477	0.240	7.1354	7.1354	0.0000

* Final weight was determined after rinsing specimen in deionized water and denatured alcohol.
  No chemical etching of specimen was performed.

Test No: 12A
Test Type: Immersion
Test Environment: Simulated WIPP Brine A, H2S Overpressure (5 atm)
Test Temperature: 30 ±5°C
Test Exposure: 15 Months

These specimens were considered essentially free of attack during the corrosion test, based on (a) absence of reaction-product gas and (b) post-test appearance of specimens (clean, shiny).

Specimen	Material Type	Length, mm	Width, mm	Thickness, mm	Top Hole ID, mm	Bot. Hole ID, mm	Area, dm2	Initial Wt., g	Final Wt.*, g	Wt. Loss, g
T241	Titanium, Gr 2	190.46	63.36	1.560	7.97	7.97	2.481	83.7408	83.7397	0.0011
T242	Titanium, Gr 2	190.45	63.37	1.603	7.99	7.98	2.483	85.7788	85.7784	0.0004
T243	Titanium, Gr 2	190.48	63.37	1.576	7.99	7.96	2.482	84.0563	--	--
T244	Titanium, Gr 2	190.42	63.29	1.593	7.97	7.97	2.479	85.4843	--	--
T245	Titanium, Gr 2	190.45	63.34	1.598	7.98	8.00	2.482	85.4462	85.4457	0.0005
T246	Titanium, Gr 2	190.55	63.39	1.600	7.96	7.98	2.485	85.6183	--	--
T247	Titanium, Gr 2	190.43	63.38	1.596	7.97	7.96	2.483	85.2410	--	--
T248	Titanium, Gr 2	190.50	63.46	1.604	7.98	7.99	2.487	86.1754	--	--
TN241	Titanium, Gr 12	190.53	63.61	1.568	7.86	7.86	2.492	83.7340	83.7328	0.0012
TN242	Titanium, Gr 12	190.76	63.39	1.443	7.85	7.85	2.480	77.6584	--	--
TN243	Titanium, Gr 12	190.62	63.45	1.555	7.85	7.61	2.487	83.4980	--	--
TN244	Titanium, Gr 12	190.55	63.41	1.544	7.83	7.83	2.483	83.3203	83.3195	0.0008
TN245	Titanium, Gr 12	190.83	63.37	1.526	7.84	7.84	2.484	83.0038	83.0030	0.0008
TN246	Titanium, Gr 12	190.46	63.52	1.560	7.84	7.83	2.487	83.0839	--	--
TN247	Titanium, Gr 12	190.29	63.27	1.428	7.86	7.87	2.468	77.6856	--	--
TN248	Titanium, Gr 12	190.54	63.39	1.554	7.86	7.87	2.483	84.3729	--	--

* Final weight was determined after rinsing specimen in deionized water and denatured alcohol.
  No chemical etching of specimen was performed.

.

APPENDIX C: METHOD OF DETERMINING DEGREE OF MOLAR EQUIVALENCE BETWEEN H_2 FORMED AND FE REACTED IN ANOXIC BRINE (BRINE/N_2) AND BRINE/CO_2 SEAL-WELDED-CONTAINER TESTS

APPENDIX C: METHOD OF DETERMINING DEGREE OF MOLAR EQUIVALENCE BETWEEN H_2 FORMED AND Fe REACTED IN ANOXIC BRINE (BRINE/N_2) AND BRINE/CO_2 SEAL-WELDED-CONTAINER TESTS

The method of determining the degree of molar equivolence between H_2 formed and Fe reacted in the anoxic brine (brine/N_2) and the brine/CO_2 seal-welded-container tests is presented here. The results of the calculations are shown here and in Tables 6.4 and 6.7. The "Average Corrosion" rates are the mean value rates for all steel lots from Tables 6.2 and 6.6. The "Final P (P_f)" values are from either the pressure history curves or the raw data summations of Appendix A. The "Fraction H_2" values are from Tables 6.1 and 6.5.

The corrosion rate of steel in μm/yr is converted to mol/m^2-yr of Fe by the conversion factor 0.141 mol/μm-m$_2$, as 0.141 mol Fe is contained in a piece of Fe (steel) having an area of 1 m^2 and a thickness of 1 μm.

Moles Fe Consumed by the Corrosion Reaction (Gravimetric Analysis)

	Test Duration, months	Containers	Average Corrosion Rate, μm/yr	Fe Reacted, mol/m^2-yr
Brine/N_2	3	1,2	1.96	0.276
	6	9,10	1.72	0.243
	12	17,18	1.23	0.173
	24	25,26	0.99	0.140
Brine/CO_2	3	3,4	8.76	1.24
	6	11,12	6.31	0.890
	12	19,20	2.91	0.410
	24	27,28	1.46	0.206

Moles H$_2$ Formed by the Corrosion Reaction (Gas Pressure and Compositon)

	Test Duration, months	Final P (P$_f$)		Fraction H$_2$	Atm H$_2$	H$_2$,[a] mol/m^2-yr	moles H$_2$ / moles Fe
		psig	psia				
Brine/N$_2$	3	155	170	0.103	1.19	0.190	0.69
	6	175	190	0.191	2.47	0.209	0.86
	12	193	208	0.262	3.71	0.156	0.90
	24	236	251	0.391	6.68	0.141	1.0
Brine/CO$_2$	3	198	213	0.478	6.94	1.11	0.89
	6	212	227	0.673	10.4	0.877	0.98
	12	203	218	0.617	9.18	0.386	0.94
	24	204	219	0.595	8.84	0.186	0.90

[a]

$$\text{moles } H_2 = \frac{PV}{RT} = \frac{P_f \, \text{atm} \cdot 0.634L}{0.0821 \frac{\text{atm-L}}{\text{mole-}^\circ K} \cdot 303^\circ K} \cdot \frac{12 \text{ months/yr}}{\Delta t \text{ months}} \cdot \frac{1}{Am^2}$$

where 0.634L = plenum volume of container
       Δt = test duration, months
       A = area of steel in test (from Appendix D)

APPENDIX D: TOTAL STEEL SPECIMEN AREA, SEAL-WELDED-CONTAINER TESTS

APPENDIX D: TOTAL STEEL SPECIMEN AREA, SEAL-WELDED-CONTAINER TESTS

Low-Carbon Steel

Test Container	Area, m²	Test Container	Area, m²	Test Container	Area, m²
1	0.639	15	0.603	29	0.604
2	0.639	16	0.604	30	0.604
3	0.639	17	0.604	31	0.604
4	0.638	18	0.605	32	0.604
5	0.638	19	0.604	33	0.630
6	0.631	20	0.604	34	0.629
7	0.631	21	0.604	35	0.629
8	0.631	22	0.604	36	0.629
9	0.604	23	0.604	37	0.630
10	0.604	24	0.604	38	0.629
11	0.604	25	0.604	40	0.497
12	0.604	26	0.605	41	0.498
13	0.604	27	0.605	42	0.497
14	0.604	28	0.605	43	0.498

Alternative Materials

Test Container	Area, m²	Test Container	Area, m²
1A	0.434	10A	0.436
2A	0.433	11A	0.436
3A	0.434	12A	0.436
4A	0.436	13A	0.434
5A	0.436	14A	0.434
6A	0.436	15A	0.434
7A	0.433	16A	0.436
8A	0.434	17A	0.436
9A	0.434	18A	0.436

DISTRIBUTION

Federal Agencies

US Department of Energy (6)
Office of Civilian Radioactive Waste
  Management
Attn: Deputy Director, RW-2
         Associate Director, RW-10/50
         Office of Program and Resources
         Management
         Office of Contract Business
         Management
         Director, Analysis and Verification
         Division, RW-22
         Associate Director, RW-30
         Office of Systems and Compliance
         Associate Director, RW-40
         Office of Storage and
         Transportation
         Director, RW-4/5
         Office of Strategic Planning and
         International Programs
         Office of External Relations
Forrestal Building
Washington, DC 20585

US Department of Energy
Albuquerque Operations Office
Attn: National Atomic Museum Library
PO Box 5400
Albuquerque, NM 87185-5400

US Department of Energy (4)
WIPP Project Integration Office
Attn: W.J. Arthur III
         L.W. Gage
         P.J. Higgins
         D.A. Olona
PO Box 5400
Albuquerque, NM 87115-5400

US Department of Energy (2)
WIPP Project Integration Satellite   Office
Attn: R. Batra
         R. Becker
PO Box 3090, Mail Stop 525
Carlsbad, NM 88221-3090

US Department of Energy (3)
WIPP Project Site Office (Carlsbad)
Attn: V. Daub
         J. Lippis
         J.A. Mewhinney
PO Box 3090
Carlsbad, NM 88221-3090

US Department of Energy
Research & Waste Management Division
Attn: Director
PO Box E
Oak Ridge, TN 37831

US Department of Energy
Attn: E. Young
Room E-178
GAO/RCED/GTN
Washington, DC 20545

US Department of Energy
Office of Environmental Restoration
  and Waste Management
Attn: J. Lytle, EM-30,
         Trevion II
Washington, DC 20585-0002

US Department of Energy (3)
Office of Environmental Restoration
  and Waste Management
Attn: M. Frei, EM-34,
         Trevion II
Washington, DC 20585-0002

US Department of Energy
Office of Environmental Restoration
  and Waste Management
Attn: S. Schneider, EM-342,
         Trevion II
Washington, DC 20585-0002

US Department of Energy (2)
Office of Environment, Safety
  and Health
Attn: C. Borgstrom, EH-25
         R. Pelletier, EH-231
Washington, DC 20585

US Department of Energy (2)
Idaho Operations Office
Fuel Processing and Waste
  Management Division
785 DOE Place
Idaho Falls, ID 83402

US Environmental Protection
  Agency (2)
Radiation Programs (ANR-460)
Attn: M. Oge
        r. Guimond
Washington, DC 20460

US Geological Survey (2)
Water Resources Division
Attn: R. Livingston
4501 Indian School NE
Suite 200
Albuquerque, NM 87110

US Nuclear Regulatory Commission
Division of Waste Management
Attn: H. Marson
Mail Stop 623SS
Washington, DC 20555

Boards

Defense Nuclear Facilities Safety Board
Attn: D. Winters
625 Indiana Ave. NW, Suite 700
Washington, DC 20004

Nuclear Waste Technical Review
Board (2)
Attn: D.A. Deere
        S.J.S. Parry
1100 Wilson Blvd., Suite 910
Arlington, VA 22209-2297

Advisory Committee on Nuclear   Waste
Nuclear Regulatory Commission
Attn: R. Major
7920 Norfolk Ave.
Bethesda, MD 20814

State Agencies

Environmental Evaluation Group (3)
Attn: Library
7007 Wyoming NE
Suite F-2
Albuquerque, NM 87109

NM Bureau of Mines and Mineral
  Resources
Socorro, NM 87801

NM Energy, Minerals, and Natural
  Resources Department
Attn: Library
2040 S. Pacheco
Santa Fe, NM 87505

NM Environment Department (3)
Secretary of the Environment
Attn: J. Espinosa
1190 St. Francis Drive
Santa Fe, NM 87503-0968

NM Environment Department
WIPP Project Site
Attn: P. McCasland
PO Box 3090
Carlsbad, NM 88221

Laboratories/Corporations

Battelle Pacific Northwest Laboratories (36)
Attn: S.M.Bruemmer, P8-16
        H.C. Burkholder, P7-41
        P.G. Doctor, K6-96
        R.E. Einziger, P7-14
        P.W. Eslinger, K6-96
        W.W. Laity, K2-50
        G.L. McVay, K2-45
        K.H. Pool, P8-44
        R.L. Skaggs, K6-77
        P. Silva, P8-44
        M.T. Smith, P8-35
        M.R. Telander, P8-44 (10)
        R.E. Westerman, P8-44 (10)
        Publishing Coordination Technical
        Report Files (5)
Battelle Blvd.
Richland, WA 99352

INTERA Inc.
Attn: J.F. Pickens
6850 Austin Center Blvd.
Suite 300
Austin, TX 78731

INTERA Inc.
Attn: W. Stensrud
PO Box 2123
Carlsbad, NM 88221

IT Corporation
Attn: R.F. McKinney
Regional Office
5301 Central NE
Suite 700
Albuquerque, NM 87108

Los Alamos National Laboratory
Attn: B. Erdal, CNC-11
PO Box 1663
Los Alamos, NM 87544

RE/SPEC, Inc.
Attn: W. Coons
4775 Indian School NE
Suite 300
Albuquerque, NM 87110-3927

RE/SPEC, Inc.
Attn: J.L. Ratigan
PO Box 725
Rapid City, SD 57709

Southwest Research Institute (2)
Center for Nuclear Waste
  Regulatory Analysis
Attn: P.K. Nair
6220 Culebra Road
San Antonio, TX 78228-0510

SAIC
Attn: D.C. Royer
101 Convention Center Dr.
Las Vegas, NV 89109

SAIC
Attn: H.R. Pratt
10260 Campus Point Dr.
San Diego, CA 92121

SAIC (2)
Attn: M. Davis
      J. Tollison
2109 Air Park Rd. SE
Albuquerque, NM 87106

Tech Reps Inc. (3)
Attn: J. Chapman
      C. Crawford
      T. Peterson
5000 Marble NE
Suite 222
Albuquerque, NM 87110

TRW Environmental Safety Systems
Attn: L. Wildman
2650 Park Tower Dr., Suite 1300
Vienna, VA 22180-7306

Westinghouse Electric Corporation (5)
Attn: Library
      C. Cox
      L. Fitch
      B.A. Howard
      R. Kehrman
PO Box 2078
Carlsbad, NM 88221

Westinghouse–Savannah River Technology
Center (4)
Attn: N. Bibler
      J.R. Harbour
      M.J. Plodinec
      G.G. Wicks
Aiken, SC 29802

National Academy of Sciences, WIPP Panel

Howard Adler
Oak Ridge Associated Universities
Medical Sciences Division
PO Box 117
Oak Ridge, TN 37831-0117

Ina Alterman
Board on Radioactive
  Waste Management, GF456
2101 Constitution Ave.
Washington, DC 20418

John D. Bredehoeft
Western Region Hydrologist
Water Resources Division
US Geological Survey (M/S 439)
345 Middlefield Road
Menlo Park, CA 94025

Fred M. Ernsberger
250 Old Mill Road
Pittsburgh, PA 15238

Rodney C. Ewing
Department of Geology
University of New Mexico
Albuquerque, NM 87131

Charles Fairhurst, Chairman
Department of Civil and
   Mineral Engineering
University of Minnesota
500 Pillsbury Dr. SE
Minneapolis, MN 55455-0220

B. John Garrick
PLG Incorporated
4590 MacArthur Blvd., Suite 400
Newport Beach, CA 92660-2027

Leonard F. Konikow
US Geological Survey
431 National Center
Reston, VA 22092

Peter B. Myers
National Academy of Sciences
Board on Radioactive
   Waste Management
2101 Constitution Ave.
Washington, DC 20418

Jeremiah O'Driscoll
Jody Incorporated
505 Valley Hill Drive
Atlanta, GA 30350

Christopher G. Whipple
Clement International
160 Spear St., Suite 1380
San Francisco, CA 94105

Individuals

P. Drez
8816 Cherry Hills Rd. NE
Albuquerque, NM 87111

D.W. Powers
Star Route Box 87
Anthony, TX 79821

Universities

University of New Mexico
Geology Department
Attn: Library
Albuquerque, NM 87131

University of Washington
College of Ocean
   and Fishery Sciences
Attn: G.R.Heath
583 Henderson Hall
Seattle, WA 98195

Libraries

Thomas Brannigan Library
Attn: D. Dresp
106 W. Hadley St.
Las Cruces, NM 88001

Government Publications Department
Zimmerman Library
University of New Mexico
Albuquerque, NM 87131

New Mexico Junior College
Pannell Library
Attn: R. Hill
Lovington Highway
Hobbs, NM 88240

New Mexico State Library
Attn: N. McCallan
325 Don Gaspar
Santa Fe, NM 87503

New Mexico Tech
Martin Speere Memorial Library
Campus Street
Socorro, NM 87810

WIPP Public Reading Room
Carlsbad Public Library
Attn: Director
101 S. Halagueno St.
Carlsbad, NM 88220

Foreign Addresses

Studiecentrum Voor Kernenergie
Centre D'Energie Nucleaire
Attn: A. Bonne
SCK/CEN   Boeretang 200
B-2400 Mol, BELGIUM

Atomic Energy of Canada, Ltd. (3)
Whiteshell Research Estab.
Attn: B. Goodwin
         M. Stevens
         D. Wushke
Pinewa, Manitoba, CANADA R0E 1L0

Francois Chenevier (2)
ANDRA
Route du Panorama Robert Schumann
B.P. 38
92266 Fontenay-aux-Roses, Cedex
FRANCE

Jean-Pierre Olivier
OECD Nuclear Energy Agency
Division of Radiation Protection
 and Waste Management
38, Boulevard Suchet
75016 Paris, FRANCE

Claude Sombret
Centre D'Etudes Nucleaires
 De La Vallee Rhone
CEN/VALRHO
S.D.H.A.   B.P. 171
30205 Bagnols-Sur-Ceze, FRANCE

Gesellschaft fur Reaktorsicherheit   (GRS)
(2)
Attn: B. Baltes
      W. Muller
Schwertnergasse 1
D-5000 Cologne, GERMANY

Bundesanstalt fur Geowissenschaften
 und Rohstoffe
Attn: M. Langer
Postfach 510 153
3000 Hanover 51, GERMANY

Bundesministerium fur Forschung und
 Technologie
Postfach 200 706
5300 Bonn 2, GERMANY

Institut fur Tieflagerung (2)
Attn: K. Kuhn
Theodor-Heuss-Strasse 4
D-3300 Braunschweig, GERMANY

Kerforschungszentrum Karlsruhe GmbH
Institut fur Nukleare Entsorgungstechnik (2)
Attn: W. Lutze
         E. Smailos
Postfach 3640
D-7500 Karlsruhe 1
GERMANY

Physikalisch-Technische Bundesanstalt
Attn: P. Brenneke
Postfach 3345
D-3300 Braunschweig, GERMANY

Shingo Tashiro
Japan Atomic Energy Research Inst.
Tokai-Mura, Ibaraki-Ken, 319-11
JAPAN

Netherlands Energy Research Foundation
ECN
Attn: L.H. Vons
3 Westerduinweg
PO Box 1
1755 ZG Petten, THE NETHERLANDS

Svensk Karnbransleforsorjning AB
Attn: F. Karlsson
Project KBS
Karnbranslesakerhet
Box 5864
10248 Stockholm, SWEDEN

Nationale Genossenschaft für die   Lagerung
Radioaktiver Abfälle (2)
Attn: S. Vomvoris
      P. Zuidema
Hardstrasse 73
CH-5430 Wettingen, SWITZERLAND

AEA Technology
Attn: J.H. Rees
D5W/29 Culham Laboratory
Abington, Oxfordshire OX14 3DB
UNITED KINGDOM

AEA Technology
Attn: W.R. Rodwell
044/A31 Winfrith Technical Centre
Dorchester, Dorset DT2 8DH
UNITED KINGDOM

AEA Technology
Attn: J.E. Tinson
B4244 Harwell Laboratory
Didcot, Oxfordshire OX11 0RA
UNITED KINGDOM

D.R. Knowles
British Nuclear Fuels, plc
Risley, Warrington, Cheshire WA3 6AS
1002607 UNITED KINGDOM

Internal

1502	J.C. Cummings
6000	D.L. Hartley
6100	R.W. Lynch
6101	P.J. Hommert
6119	E.D. Gorham
6119	S.W. Webb (10)
6119	Staff (14)
6121	J.R. Tillerson
6121	Staff (7)
6300	D.E. Ellis
6302	L.E. Shephard
6303	S.Y. Pickering
6303	W.D. Weart
6305	S.A. Goldstein
6305	A.R. Lappin
6306	A.L. Stevens
6342	D.R. Anderson
6342	Staff (20)
6343	V. Harper-Slaboszewicz
6343	Staff (2)
6345	R.C. Lincoln
6345	Staff (9)
6347	D.R. Schafer
6348	J.T. Holmes
6348	Staff (4)
6348	M.A. Molecke (10)
6348	L.H. Brush
6351	R.E. Thompson
6352	D.P. Garber
6352	S.E. Sharpton
6352	WIPP Central Files (RC/AC, 1.1.1.1.3) (10)
7141	Technical Library (5)
7151	Technical Publications
7613-2	Document Processing for DOE/OSTI (10)
8523-2	Central Technical Files